ISSN 2413-5577

№ 4 Октябрь – Декабрь 2025

# Экологическая безопасность прибрежной и шельфовой зон моря

# Ecological Safety of Coastal and Shelf Zones of Sea

No. 4 October – December 2025

ecological-safety.ru

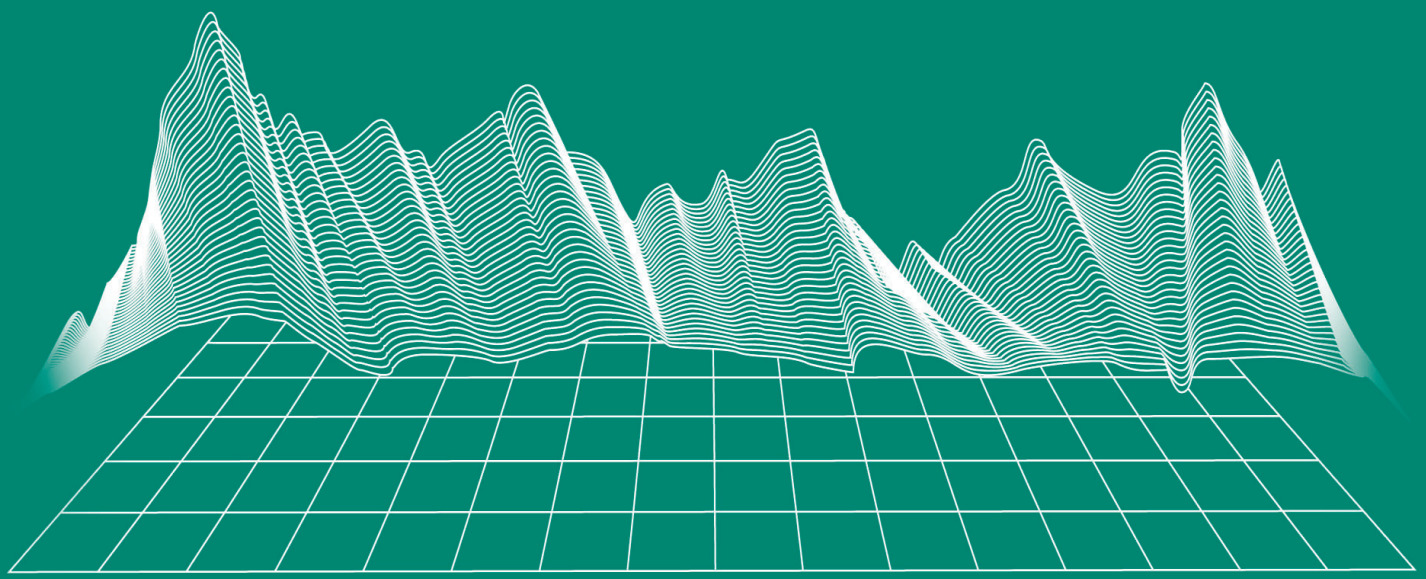

**No. 4, 2025**
**October – December**

Publication frequency:
Quarterly

**16+**

# ECOLOGICAL SAFETY OF COASTAL AND SHELF ZONES OF SEA

Scientific and theoretical journal

FOUNDER AND PUBLISHER:
Federal State Budget Scientific Institution
Federal Research Centre
"Marine Hydrophysical Institute of RAS"

Journal is on the list of peer reviewed academic journals of the Higher Attestation Commission of the Russian Federation, where one may publish main research results of a Ph.D. thesis in the following field:

1.6.14 – Geomorphology and paleography (geographical sciences),
1.6.17 – Oceanology (geographical sciences, physical and mathematical sciences, technical sciences),
1.6.18 – Atmosphere and climate sciences (geographical, physical and mathematical sciences),
1.6.20 – Geoinformatics and cartography (geographical sciences),
1.6.21 – Geoecology (geographical sciences),
1.5.16 – Hydrobiology (biological sciences).

Journal is under the scientific and methodological guidance of the Earth Sciences Department of the Russian Academy of Sciences.

Journal is registered by the Federal Service for Supervision of Communications, Information Technology, and Mass Media (registration number ПИ № ФС77-73714 of 21 September 2018 and Эл № ФС77-82679 of 21 January 2022).

Journal coverage: The Russian Federation, other countries.

The Journal is indexed in and reposited at Russian Science Citation Index (RSCI), International Interactive Information and Bibliography System EBSCO.

Journal is in the catalog of scientific periodicals of the RSCI on the platform of the scientific electronic library eLibrary.ru, Cyberleninka.

There is no fee for publishing articles.

**e-mail:** ecology-safety@mhi-ras.ru

**website:** http://ecological-safety.ru

**Founder, Publisher and Editorial Office address:**

2, Kapitanskaya St.,
Sevastopol, 299011, Russia

**Phone, fax:** + 7 (8692) 54-57-16

## РЕДАКЦИОННАЯ КОЛЛЕГИЯ

CONTENTS

№ 4. 2025 October – December, 2025

СОДЕРЖАНИЕ

№ 4. 2025 Октябрь – Декабрь, 2025

ISSN 2413-5577, Ecological Safety of Coastal and Shelf Zones of Sea, 2025, No. 4, pp. 6–32.

Original paper

# Current State and Dynamics of the Western Crimean Bay-Bars

**Yu. N. Goryachkin** [1, 2]

[1] *Marine Hydrophysical Institute of RAS, Sevastopol, Russia*

[2] *Shirshov Institute of Oceanology of RAS, Moscow, Russia*

*e-mail: yngor@mhi-ras.ru*

**Abstract**

The bay-bars of Crimean salt lakes are unique natural formations of significant recreational value. Since 2015, the bay-bars have undergone intensive development, with construction projects being planned. This paper analyses and characterizes the current state of the bay-bars in Western Crimea and assesses their dynamics over the past 150 years, based on long-term field monitoring data from Marine Hydrophysical Institute of the Russian Academy of Sciences, satellite imagery, cartographic materials, official reports, and published literature. It was revealed that the condition and dynamics of these bay-bars are determined by the aggregate effect of natural and anthropogenic factors. Key natural processes include storm-induced sediment redistribution along the bay-bar and adjacent coastline, sediment transport from the coastal slope into the lakes across the bay-bars, and aeolian processes. Nevertheless, human activity constitutes the dominant forcing factor. Sand mining was widespread across nearly all bay-bar sites, with industrial-scale extraction occurring at Lakes Sasyk-Sivash, Donuzlav, Sakskoye and Kyzyl-Yar. Consequently, the sediment volume of the bay-bars has been severely diminished, with a reduction in both width and height. This has, in turn, increased the vulnerability of structures to storm damage. Additional anthropogenic pressures include artificial breaching of the bars, extensive construction, removal of dunes and vegetation and beach grading. Collectively, these interventions have degraded the natural landscape and led to loss of the lakes' therapeutic qualities. The intensive development, which entails the physical destruction and transformation of the bay-bars, poses a significant threat to the survival of these unique ecosystems and the vital recreational and ecological services they provide. An urgent shift in management strategy, prioritizing conservation and restoration of the bay-bars, is therefore imperative.

**Keywords**: Black Sea, Western Crimea, bay-bar, coastal dynamic, anthropogenic impact, coastal area

**Acknowledgments**: The work with remote sensing data and the assessment of the current state of accumulative forms were supported by Russian Science Foundation grant no. 25-17-00104, https://rscf.ru/project/25-17-00104/, and the analysis of the results of long-term monitoring field work and archival reports of the Marine Hydrophysical Institute was carried out as part of the state assignment of MHI RAS no. FNNN-2024-0016.

**For citation**: Goryachkin, Yu.N., 2025. Current State and Dynamics of the Western Crimean Bay-Bars. *Ecological Safety of Coastal and Shelf Zones of Sea*, (4), pp. 6–32.

# Текущее состояние и динамика пересыпей Западного Крыма

**Ю. Н. Горячкин** [1, 2]

[1] *Морской гидрофизический институт РАН, Севастополь, Россия*

[2] *Институт океанологии им. П.П. Ширшова РАН, Москва, Россия*

*e-mail: yngor@mhi-ras.ru*

**Аннотация**

Пересыпи соленых озер Крыма – это уникальные природные объекты, представляющие собой ценный рекреационный ресурс. С 2015 г. началось их интенсивное освоение, разрабатываются проекты застройки. В статье на основе материалов многолетних мониторинговых полевых работ Морского гидрофизического института РАН, спутниковых снимков, картографических материалов, ведомственных отчетов и литературных источников проанализировано и охарактеризовано современное состояние пересыпей Западного Крыма и дана оценка их динамике за последние 150 лет. Установлено, что состояние и динамика пересыпей Западного Крыма определяются совместным влиянием природных и антропогенных факторов. К природным относятся перераспределение наносов между отдельными участками пересыпи и соседними участками берега при штормовом волнении, перенос наносов с берегового склона в озера через пересыпи и эоловые процессы. Однако доминирующую роль играет антропогенное воздействие. Почти повсеместно на пересыпях добывали песок. В промышленных масштабах отбор проводился на пересыпях озер Сасык-Сиваш, Донузлав, Сакского, Кызыл-Яр. Как результат, объем пересыпей значительно сократился: уменьшилась их ширина и высота, что повысило уязвимость строений на них при штормовом воздействии. Отмечены и другие виды антропогенного воздействия: прорытие пересыпей, капитальное строительство, уничтожение дюн и растительности, планировка пляжей, приведшие к деградации естественных ландшафтов и утрате озерами лечебных свойств. Интенсивное освоение пересыпей, сопровождающееся их физическим уничтожением и трансформацией, создает реальную угрозу для сохранения этих уникальных природных объектов, выполняющих важные рекреационные и экологические функции. Необходим пересмотр подходов к их хозяйственному использованию в сторону сохранения и восстановления.

**Ключевые слова**: Черное море, Западный Крым, пересыпь, динамика берегов, антропогенное воздействие, береговая зона

**Благодарности:** работа с данными дистанционного зондирования и оценка современного состояния аккумулятивных форм выполнены за счет гранта Российского научного фонда № 25-17-00104, https://rscf.ru/project/25-17-00104/, анализ результатов многолетних мониторинговых полевых работ и архивных отчетов Морского гидрофизического института выполнен в рамках государственного задания ФГБУН ФИЦ МГИ FNNN-2024-0016.

**Для цитирования**: *Горячкин Ю. Н.* Текущее состояние и динамика пересыпей Западного Крыма // Экологическая безопасность прибрежной и шельфовой зон моря. 2025. № 4. С. 6–32. EDN UVGARW.

## Introduction

According to generally accepted terminology, a bay-bar is a strip of land formed by sediment accumulation, which separates a lagoon or bay entrance from the open sea. Bay-bars are formed by wave action and wave-driven currents resulting from longshore or cross-shore sediment transport. They are composed of sand, gravel, pebbles or shells [1), 2)]. Morphologically, bay-bars belong to the closing coastal landforms, which are of the accumulative and barrier-type variety [3)]. A coastal bar is what they are genetically. During its growth, an accumulative spit can attach its distal end to the opposite shore of the bay, transforming into a bay-bar. More complex bay-bars also exist, consisting of several systems of coastal ridges of different ages which can include relics of former lagoons. Such bay-bars are typical of Western Crimea.

While accumulative beaches are subject to considerable variability, bay-bars are a relatively stable component of coastal dynamics. Only during rare, extreme storms can waves overtop narrow bay-bars, transferring sediments from the seaward side to the lake side and forming washover channels which are, however, rapidly filled in again [1, 2]. Bay-bars of various lithological compositions, like other large accumulative landforms, shape the typical landscapes of the north-western Black Sea coast, including Western Crimea. These accumulative forms are a result of the Quaternary history of the Black Sea, during which tectonic movements and changes in sea level formed the shallow shelf in the north-west of the sea. The most distinctive features of the Black Sea coastline are lagoons, formed when the lower reaches of gullies and river valleys flooded. Most coastal depressions are currently separated from the open sea by continuous bay-bars formed by sediment transport.

In Western Crimea, bay-bars are typical of the North-Western, Tarkhankut and Evpatoriya sectors [3]. In the North-Western sector, they occupy ~ 10 km of the coastline; in the Tarkhankut sector, they are localised to three bays; and in the Evpatoriya sector, they account for around half of the entire 42 km coastline (Fig. 1).

Just a century ago, the study of marine-origin bay-bars was considered important from both scientific and practical perspectives, since their formation was associated with the genesis of valuable minerals such as salt, therapeutic muds and construction materials like gravel, sand and silt [4]. Understanding the formation and structure of bay-bars was also emphasised as important for beach management and grading, afforestation, dune stabilisation, road construction, creating marine canals,

---

1) Zenkovich, V.P. and Popov, B.A., eds., 1980. [*Marine Geomorphology. Terminology Reference Book. Coastal Zone: Processes, Concepts, Definitions*]. Moscow: Mysl, 280 p. (in Russian).

2) Akhromeev, V.N., 2002. [*Geomorphological Reference Dictionary*]. Bryansk: Izdatelstvo BGU, 320 p. (in Russian).

3) Zenkovich, V.P., 1960. [*Morphology and Dynamics of the Soviet Black Sea Coast, Vol. I*]. Moscow: AS USSR Publ., 187 p. (in Russian).

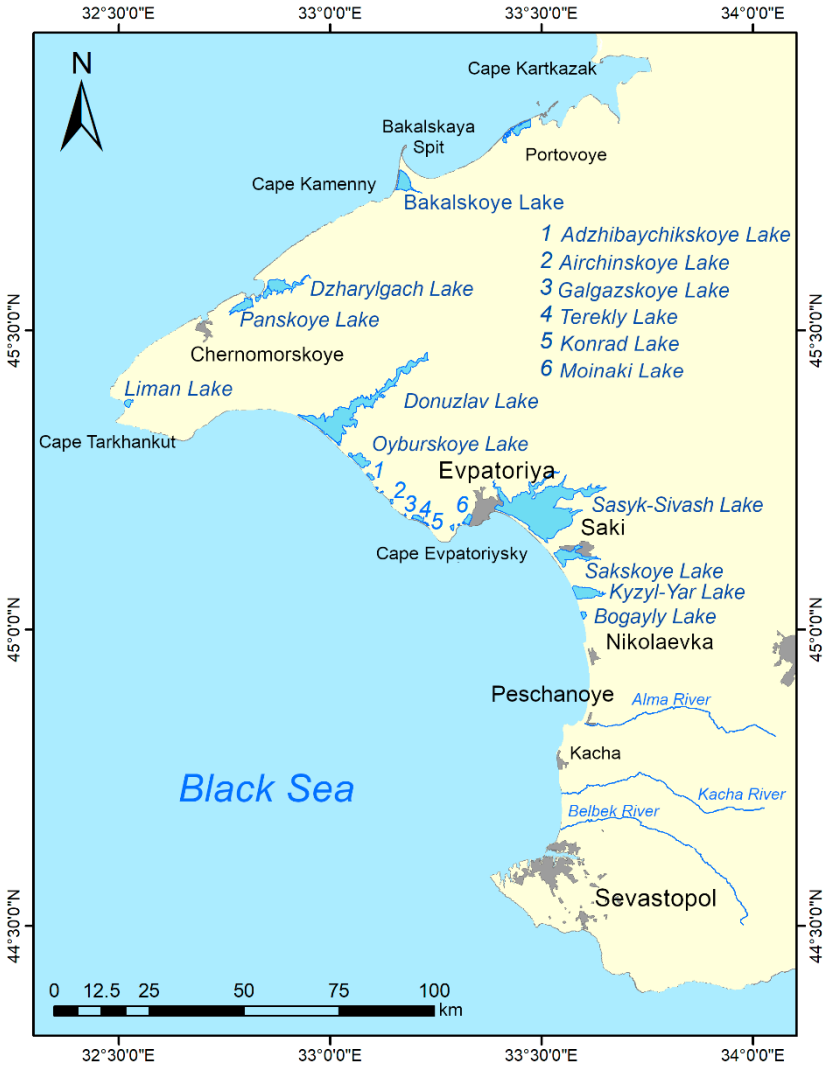


F i g . 1 . Major salt lakes of Western Crimea and their bay-bars

and constructing structures [4]. Study [4)] states that, in the 1920s and 1930s, sand mining was carried out directly on the beaches of bay-bars and in river channels in Crimea where the reserves of this material were considered inexhaustible.

Currently, bay-bars are primarily regarded as valuable recreational resources. These unique natural formations support biodiversity and play an important role in coastal ecosystems. Much of the coastline of Western Crimea still consists of wide, sandy beaches that are ideal for recreation. However, they have been subjected to

[4)] Pavlov, I.S., ed., 1932. [*Reference Book for Construction Materials Industry. Iss. 1. Ukraine and Crimea*]. Moscow, 119 p. (in Russian).

intensive development over the past decade. Construction projects are underway or planned on the bay-bars of lakes Bakalskoye and Karadzha. Plans have been made to build a new city with a population of around 30,000 people on the bay-bars of several lakes between the villages of Shtormovoye and Zaozernoye. The large-scale project "Golden Sands of Russia" is being actively developed and promoted. This involves extensive construction on the bay-bar of Lake Sasyk-Sivash with the aim of accommodating around one million tourists per year. Construction on the bay-bar of Lake Sakskoye is almost complete. Insufficient understanding of coastal dynamics by project developers can lead to unjustified decisions. Such decisions are already having a negative impact on the environment and carry the risk of unnecessary financial costs [5].

The earliest references to the bay-bars in salt lakes, including those in Western Crimea, appear in works primarily devoted to salt lakes and salt extraction [5), 6), 7)]. These studies are valuable because they describe the characteristics of the bay-bars as they were in the last quarter of the 19th century. The first studies to focus specifically on the origin and structure of the Crimean bay-bars were published in the early 1930s by the renowned Soviet geologist A. I. Dzens-Litovsky [4), 8)] [6]. These publications were the outcome of expeditions conducted as part of an extensive study of the hydrogeological features of Crimean salt lakes, undertaken by the Institute of Hydrogeology and Engineering Geology of the All-Union Geological Survey.

The next stage in the study of Crimean bay-bars is associated with V. P. Zenkovich, the founder of Soviet coastal geomorphology. In his generalising monograph [3)], he used the Northern Black Sea region as an example to explain the formation and development of accumulative landforms, including bay-bars. The regional volume of monograph [9)] contains specific data on the bay-bars of Western Crimea, reflecting their state in the late 1940s. More recent information on certain bay-bars from the late 20th century is presented in the works of Yu. D. Shuisky [7–9]. Notable recent studies of the bay-bars of Western Crimea include [1, 2, 10–12].

This study aims to characterise the current state of the bay-bars in Western Crimea and assess their dynamics over the past 150 years. This will be achieved by analysing satellite imagery, cartographic materials and archival data.

---

5) Pershke, L., 1882. [*Salt Lakes of the Northern Black Sea Coast and the Basis for their Rational Development*]. Saint Petersburg: Tipografiya i Khromolitografiya A. Transhelya, 89 p. (in Russian).

6) Mushketov, I.V., 1895. [A Note on the Origin of the Crimean Salt Lakes]. *Gorny Zhurnal*, 2(6), pp. 344–393 (in Russian).

7) Konrady, A.V., 1896. [*Saki Salt Industry of Master of the Hunt I. P. Balashev in Crimea*]. Saint Petersburg: Tip. Trenke i Fyusno, 31 p. (in Russian).

8) Dzens-Litovsky, A.I., Pastak, A.I. and Meyer, R.F., 1934. [*The Resort of Saki and its Suburbs*]. Moscow: Fizkultura i Turizm, 78 p. (in Russian).

9) Zenkovich, V.P., 1960. [*Morphology and Dynamics of the Soviet Black Sea Coast, Vol. 2*]. Moscow: AS USSR Publ., 216 p. (in Russian).

## Materials and methods

This study is based on long-term field monitoring data from Marine Hydrophysical Institute of the Russian Academy of Sciences (MHI RAS), as well as satellite imagery, cartographic materials, official reports and published literature. The electronic archive of coastal photographs of the Crimean Peninsula, created at the MHI RAS, was also used. General geographical and cartographic methods were employed, as well as analysis of satellite imagery of the Earth's surface.

## Results and discussion

*North-Western sector*

The sector extends 105 km from the northern border of Crimea to Cape Kamennyy, to the west of the Bakalskaya Spit. The coastline is formed by Quaternary marine and continental deposits, comprising both abrasive and accumulative segments. Some capes and protrusions have eastward-oriented spits, while small attached terraces are found on the side facing away from them. Accumulative landforms have primarily been created as a result of the longshore transport of sand and shell material from west to east. The sector is characterised by sustained land subsidence, as evidenced by drowned ravine mouths, lagoons, and silty deposits in the nearshore zone. According to map [10)] dated 1941, spits in the stage of attachment and bay-bar formation existed in the northern part of the sector at that time. These features currently appear as bay-bars; the area has undergone anthropogenic transformation, with former lakes and lagoons being converted into rice paddies and fish-breeding ponds. Only one segment remains: a complexly configured bay-bar, ~ 1.5 km long, located 2 km north of Cape Kartkazak. Map [10)] dated 1941 shows this bay-bar as a spit in the stage of attachment.

To the southwest of the Lebyazhyi Islands, the coast is low-lying and accumulative, of lagoon type. These accumulative landforms are predominantly composed of whole and fragmented shell material. This coastal segment is characterized by both cross-shore and longshore (northeastward) transport of detrital-shell sediments. The most notable recent event in this area is the formation of a new bay-bar. Historical maps dating back to 1817 clearly show the progressive separation of small lagoons, formation of bar-bays, an increase in the number of Kondzhalayskie islets and the growth of the Sergeevskaya Spit. This spit eventually transformed a marine bay into the Andreevsky Lagoon [11), 12), 13), 14), 15), 16)] (Fig. 2).

---

[10)] RKKA, 1941. *Northern Crimea*, 1:25000. Moscow: Generalny Shtab RKKA.

[11)] Mukhin, S.A., 1817. *Ordnance Topographic Map of the Crimean Peninsula*, 1:168000. Saint Petersburg: Voenno-Topograficheskoe Depo.

[12)] Kozlovsky, A.N., 1842. *Topographic Map of the Crimean Peninsula*, 1:210000. Saint Petersburg: Voenno-Topograficheskoe Depo.

[13)] VTD, 1865–1876. *Map of Taurida Governorate*, 1:126000. Saint Petersburg: Voenno-Topograficheskoe Depo.

[14)] KSU, 1922. *Map of Crimea*, 1:420000. Krymskoe Statisticheskoe Upravlenie.

[15)] RKKA, 1938. *Map by General Staff of RKKA*, 1:50000, L-36-5234.


F i g . 2 . Andreevsky Lagoon and Sergeevskaya Spit (bay-bar) on a map of 1842 [12] (*top*) and a satellite image (July 2024) (*bottom*)

The growth of the Sergeevskaya Spit was particularly significant during the last two decades of the 20th century. During this period, a new spit, the Zapovednaya Spit, began to grow from the village of Portovoye towards the Lebyazhyi Islands. It is currently attaching itself to one of the islands.

In 1989, the Andreevsky Lagoon had not yet been completely separated from the sea [16]. According to [13], the breach was still ~ 15 m wide in 1998.

The 2006 map shows a fully formed bay-bar [17]. However, analysis of satellite imagery revealed that breaches periodically appeared in the bay-bar until 2017. Since 2018, such breaches have not been recorded (Fig. 2). The current length of the Sergeevskaya Bay-Bar is ~ 10 km, with a width ranging from 5 to 80 m. Its narrowest section is in the east.

---

[16] General Staff, 1993. *Map by General Staff of Armed Forces of the USSR, State of the Territory as of 1989*, 1:100000, L-36-79.

[17] Soyuzkarta, 2006. *Topographic Guide Map of Crimea*, 1:50 000. Simferopol: NPP Soyuzkarta.


Fig. 3. Disappeared villages of Sergeevka and Andreevka on the map [18)]

It is also important to note that the coastline is retreating at a rate of up to 3 m per year, according to work [13]. The former village of Sergeevka, located 15 km northeast of the present-day village of Steregushcheye, has consequently been completely submerged. Although the sea engulfed it at the end of the 1940s, it was still shown on the shoreline on map [18)] (Fig. 3). In the 1980s, the village of Andreevka, situated on the spit separating the lagoon from the sea, was also submerged (Fig. 2). Indeed, modern toponyms such as Andreevsky Lagoon and Sergeevskaya Bay-Bar originate from the names of these vanished settlements. The coastal dynamics of this area are examined in greater detail in [3, 14].

*Tarkhankut sector*

The Tarkhankut sector extends 138 km from Cape Kamennyy to Lake Donuzlav. Tectonically, it corresponds to the Tarkhankut Rise, which is a raised area dissected by a network of ravines. The largest of these ravines form the wide bays of Yarylgachskaya, Uzkaya (also known as Ak-Mechetskaya) and Karadzhinskaya. Large accumulative landforms known as bay-bars separate the salt lakes in the heads of these ravines. Smaller ravines create concavities along the coastline, in which minor bay-bars also develop. Behind these are topographic depressions. Most of the coastline consists of cliffs formed by abrasion, with Sarmatian and Pontian limestones and clays predominantly exposed. Beaches are formed from abrasion material in coastal concavities and bays, which act as natural sediment traps. More detailed information on the coasts of the sector is presented in work [3] and monograph [9)].

[18)] Ministry of Defense of the USSR, 1947. [*Atlas of Black Sea Soils*]. Ministerstvo Oborony SSSR, 30 p. (in Russian).

Yarylgachskaya Bay has the most complex configuration of marine accumulative landforms, with a shoreline length of ~ 9 km. Here, a sandy bay-bar separates three salt lakes, Dzharylgach, Yarylgach (Karlav) and Panskoye (Sasyk), and the Karlav Lagoon (Maloye Solenoye) from the sea (Fig. 4).

The Dzharylgach and Yarylgach lakes, as well as the Karlav Lagoon, are separated from the sea by a wide, curved bay-bar reaching up to 600 m in width near Lake Dzharylgach and 150 m near the lagoon. The village of Mezhvodnoye (formerly Yarylgach) is located in the northern part of the bay-bar. Lakes Yarylgach and Dzharylgach are divided by a narrow (10–15 m wide) secondary bay-bar, which was reinforced when a road was constructed across it. Secondary accumulative features (spits and bay-bars) are attached to both bay-bars. The Karlav Lagoon still has a connection to the bay through a wide (~ 150 m), though shallow, breach.

According to radiocarbon dating, a marine bay existed at the site of present-day Lake Dzharylgach 5000–5400 years ago, with free water exchange with the sea. Later, during the Black Sea transgression and intensification of abrasion processes, a lagoon formed. The lagoon connection with the sea became increasingly restricted, finally becoming completely separated ~ 4600 years ago [15].

Lake Panskoye, known as Sasyk until the 1940s, lies in the western part of Yarylgachskaya Bay. In 1978, an artificial breach 130 m wide was cut through the bay-bar, dividing the bay into two parts. Between 1979 and 1991, the new port of Chernomorskoye was built on the northern shore of the lake with a quay line extending 1 km. Two concrete groynes (75 m and 150 m long) were constructed at either end of the breach to minimise siltation in the fairway. Consequently, the brine and therapeutic muds of the lake underwent desalination (from 100% to 18%), resulting in the loss of their therapeutic properties. In effect, Lake Panskoye has been transformed into a man-made technogenic bay.

The Yarylgach Bay-Bar is predominantly composed of fine- to medium-grained sands (0.25–0.5 mm), which account for 70–90% of its mass. It also contains admixtures of fragmented and whole shell material (10–30%), as well as oolitic limestone grains. According to drilling data, the vertical thickness of the sands ranges from 3 to 7 m [16]. Coarser sediments are found in the north-eastern part of


Fig. 4. Yarylgachskaya Bay. The numbers denote salt lakes: Panskoye (*1*), Karlav Lagoon (*2*), Yarylgach (*3*) and Dzharylgach (*4*)

the bay-bar, which is most exposed to wave action. In some places, dunes are preserved but they are subject to displacement, particularly in areas without vegetation.

The beach width reaches 40–60 m in the northern part, decreasing to 20 m in the south. A significant portion of the beach is occupied by an oil storage facility and other structures. As it was noted in [9], the volume of sand far exceeds what could have been produced by the erosion of local rocks or the remains of organisms that have lived here. Therefore, it is most probable that the sand was delivered from the open sea during severe storms.

A comparative analysis of cartographic materials from various historical periods, alongside modern satellite imagery, reveals that the configuration of four primary salt lakes has undergone minimal change. According to satellite imagery, the shoreline has remained relatively stable, shifting by 2–5 m depending on the season and severe storm activity. The accumulation of sediment against the eastern groyne of Lake Panskoye suggests that predominant longshore sediment transport in the bay occurs in a clockwise direction. Unfortunately, traces of illegal sand mining are still periodically observed on the bay-bar, which has currently been significantly altered due to defensive works carried out as part of the Special Military Operation.

*Uzkaya Bay* (also known as Ak-Mechetskaya Bay) is located 10 km southwest of Yarylgachskaya Bay. It was formed by the confluence of two large, wide ravines. From the south, the bay could formerly be approached via a flat interfluve area but this is now densely built up. To the east of this development lies salt Lake Ak-Mechetskoye, which often dries out completely. Over the past decade, the lake has progressively been filled in to make way for residential construction projects. The entire low-lying coastal area is bordered by a 1 km long, 20–50 m wide strip of sandy beach. This beach consists of light grey, medium- to coarse-grained sand containing detritus, whole shells and limestone fragments. According to satellite imagery, the eastern part of the beach eroded by 10–15 m between 2009 and 2018. Immediately behind the entrance cape on the western side of the bay lies small salt Lake Mayakskoye, which is separated from the bay by a sand-and-shingle bay-bar. Unlike Yarylgachskaya Bay, there is probably low-intensity, near-bottom sediment flow along the open coast of Uzkaya Bay, which replenishes the sediment volume [9]. The ruins of the ancient settlement of Kalos Limen, which are located close to the water edge, demonstrate clearly the gradual retreat of the shoreline from ancient times until now.

*Karadzhinskaya Bay* is located at the westernmost tip of the Crimean Peninsula, between Cape Tarkhankut and Cape Priboynyy (also known as Kara-Mrun). The bay extends inland as salt Lake Liman (Karadzha), which has a wide ravine that extends several kilometres into the land. The southwestern part of the lake is divided by two secondary bay-bars (10–60 m wide), creating small lakes Bolshoy Kipchak and Maly Kipchak, which dry out in summer (Fig. 5). The main bay-bar is ~ 2 km long and up to 200 m wide. Breaches occasionally form in it after severe storms. The width of the bay-bars is highly dependent on the water level of the lakes.

The bay-bar is composed of shell-oolitic sands and gravel sized between 10 and 50 mm. Fractions sized 0.1–1.0 mm (up to 95%) are predominant. Like other bay-bars in the area, it is primarily fed by comminuted limestone fragments resulting from the erosion of the bay cliffs and submarine slopes. The shell content is low at no more than 12%. Drilling has shown that the upper layer is up to 6 m thick and overlies a 2.4 m thick lens of mud containing marine shells. These muds are underlain by Upper Sarmatian limestone, and a layer of lithified sand has been identified at a depth of 3 m [17]. Fragments of this lithified layer are sometimes visible on the surface of the bay-bar, possibly originating from the nearshore bench. The material of the secondary bay-bars is of marine origin.

According to the authors of study [17], as the bay-bar migrated towards the head of the bay, it overrode the muds, which became buried beneath the bay-bar sands. The presence of a dead cliff on the segment adjoining the bay-bar can also suggest that its body was previously more advanced seawards. In [18], the authors propose that the lake was separated from the sea by a sandy bay-bar during the Dzhemetinian phase of the Black Sea transgression (i.e. around 1000 years ago) based on a paleogeographic reconstruction of the ancient shoreline.

Satellite imagery from the last twenty years shows that, despite seasonal fluctuations, the shoreline of the bay-bar has remained stable. This finding is corroborated by direct observations conducted between 1960 and 1994 [19)]. Unlike two bays previously discussed, the sandy dunes on the Karadzhinskaya Bay-Bar remained in relatively good condition until recently. However, under the current intensive development project for the bay, the dunes are scheduled for removal and replacement with tiles. Overall, only one-third (55,000 $m^2$) of the existing 165,000 $m^2$ beach

F i g . 5 . Lake Liman (Karadhza) on a quadcopter image

[19)] Shuysky, Yu.D. and Vykhovanets, G.V., 2006. [A Map of Average Rate of Erosion and Accumulation. 1960–1994]. In: L. I. Mitin, 2006. [*Atlas of Nature Protection of the Black Sea and the Sea of Azov*]. Saint Petersburg: GUNiO MO RF, p. 44 (in Russian).

area extending to the foredune line is proposed to be preserved. Local residents of Olenyovka, a village located within the bay, oppose these plans strongly. Notably, they successfully halted a project involving the artificial breaching of the bay-bar and the construction of a yacht marina in Lake Liman in 2012.

*Evpatoriya sector*

The Evpatoriya coastal sector extends 76 km from the bay-bar of Lake Donuzlav to the bay-bar of Lake Kyzyl-Yar. The coast is low-lying and predominantly accumulative. The typical landscape consists of saline lagoons (waterlogged areas), which are separated from the sea by sand and shell bay-bars. Lagoonal silty deposits usually lie beneath these spits. A continuous strip of beaches runs along the coastline, backed by an undisturbed low coastal ridge that transitions into modest sand dunes or waterlogged areas. The land is weakly dissected by broad, gentle ravines. Morphologically, the coast belongs to the lagoon-estuary type. A significant proportion of the sand on the beaches consists of crushed shell, particularly in the Evpatoriya area. To the east of the city, the proportion of shingle on the beaches increases. Wind processes play an important role in the dynamics of the bay-bars, particularly in areas lacking coastal vegetation. Much of the coastline has already been developed and continues to be built up. In these areas, the original natural landscapes have disappeared. More detailed information on the characteristics of the sector can be found in [3].

*Lake Donuzlav* extends 30 km inland. Originally, it was separated from the sea by a bay-bar ~ 10 km long and between 200 and 400 m wide. In [5)], the authors report a width of 0.5 versts (~ 500 m) in 1876 while in [19], a width of 200–400 m is indicated (1930). The bay-bar continues underwater towards the lake as a submarine extension, dropping off steeply. The steepness of this slope suggests that the bay-bar migrated towards the lake during its early formation stages. The lake, which is now a man-made bay, can be classified as a tectonic-erosional trough or a ria-type bay, as evidenced by the structure of its basin, its considerable depth of up to 27 m, and other characteristic features.

The bay-bar is composed of medium-grained, well-sorted sand with a significant admixture of quartz. Accumulations of whole shells are commonly found throughout the area, and intact shells and shell detritus (broken-up shell fragments) are present in all samples, often accounting for 100% of their composition. The rock-forming components of the sediments include quartz, feldspar and carbonates.

The submarine slope in front of the bay-bar extends down to a depth of 15 m and is composed of a mixture of sand and shell material. Several underwater shore-parallel bars have been formed in this area. Below this sandy area, the seabed is made up of limestone. At depths greater than 20 m, the seabed transitions to silted shelly sediment. The large sand reserve on the seabed is evidently linked to the main unloading zone for longshore sediment transport being located at the bay-bar of Lake Donuzlav. A substantial volume of material (primarily from seabed abrasion) is supplied from the shallow-water area between the bay-bar and Cape Evpatoriysky. It is also suggested that the accumulation of sediments was facilitated by the historical landward retreat of the bay-bar itself [9].

According to [9], the bay-bar was completely closed off relatively recently, in 1874. Prior to this, a passageway was observed there, which subsequently became blocked by silt. However, other sources [20] state that the inlet was formed in 1874 as a result of a catastrophic storm.

At the end of 1961, a 200 m wide canal was excavated through the bay-bar and two protective groynes were built to guard the entrance. This divided the bay-bar into two spits: a southern one and a northern one (Fig. 6).

The lake was originally intended for use as a civilian port but a small naval base was instead built there and has operated ever since. In the years immediately following the construction of the canal (1961–1966), the shoreline of the bay retreated by 25–60 m in certain exposed sections. By the 1980s, the shoreline had stabilised. Between 1982 and 1987, certain sections of the bay-bar experienced changes to the shoreline involving both advance and retreat as well as vertical deformation of the beach and underwater profiles relative to the mean position. Our analysis of ultra-high-resolution satellite imagery revealed areas of both progradation and retreat of the shoreline between 2003 and 2020. Average rates for this period indicate that retreat predominates: the northern spit retreated at an average rate of 0.2 m per year,

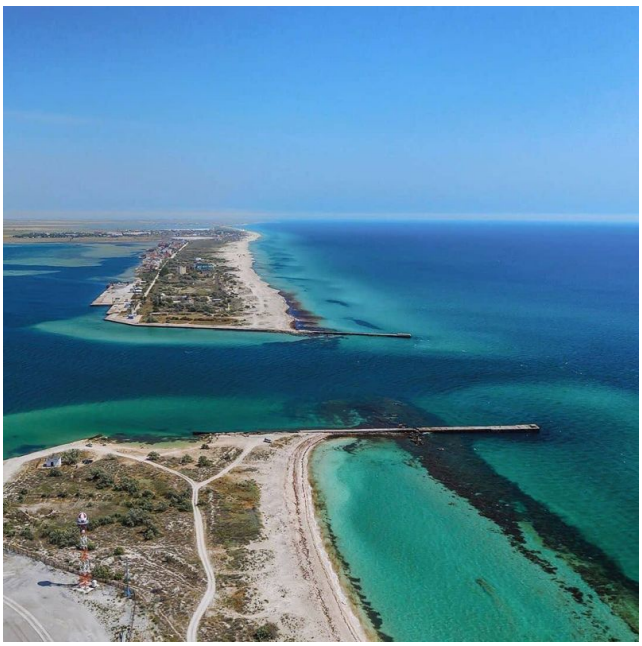

Fig. 6. Quadcopter view of the northern (at the foreground) and southern spits of the Donuzlav Bay-Bar

[20] Kurnakov, N.S., Kuznetsov, V.G., Dzens-Litovsky, A.I. and Ravich, M.I., 1936. [*Saline Lakes of Crimea*]. Moscow, Leningrad: Izdarelstvo AN SSSR, 278 p. (in Russian).

whereas the retreat rate of the southern one was 0.5 m per year. According to an earlier study [21)], the shoreline of the Donuzlav Bay-Bar had slowly retreated at a rate of up to 0.2 m per year over the previous 100 years.

A sand quarry has been operating on the lake, directly adjacent to the bay-bar, for the past 60 years. Additionally, the navigation channel on the seaward side of the bay-bar has been periodically dredged. Between 1963 and 1992, 11.5 million tonnes (5.5 million $m^3$) of sand were removed from the channel during these operations. Approximately 350,000 tonnes (165,000 $m^3$) of sand were extracted in a single dredging campaign. According to official data, up to 7.7 million tonnes of sand were mined from the lakeshore immediately adjacent to the bay-bar between 1992 and 2014, with extraction ongoing.

The northern spit remains largely undeveloped for recreational purposes due to its remote location and lack of infrastructure. Nevertheless, a project has been developed to create a world-class resort called the "Crimean Maldives" in the Belyaus area. The southern spit has been intensively developed since the end of the last century. The lakeside is completely built up with cottages, while the seafront is partially developed. During construction, bulldozers have levelled the natural beach relief and destroyed the coastal dunes, removing the shrubs and trees that stabilised them.

A chain of salt lakes stretches along the coast from *Lake Donuzlav to Cape Evpatoriysky*: Oyburskoye, Adzhibaychikskoye, Airchinskoye, Galgaz, Konrad and Terekly, as well as several smaller lakes located between them. A strip of waterlogged areas lies between the bay-bars of the lakes, separated from the sea by a sandy barrier. In spring, these areas fill with water to form shallow ponds. All the lakes lie below sea level. The typical width of the bay-bars separating the salt lakes ranges from 70 to 150 m. The width of the bay-bar decreases where the limestone surface is slightly elevated. Breaches often form in such locations as a result of storm surges. The lakes basins are mostly elongated and run parallel to the seashore, representing lagoons rather than estuarine lakes. Where wide, shallow valleys approach the lakes directly, the bodies of water exhibit features of both types. Examples include lakes Oyburskoye and Konrad.

The profiles of all the bay-bars slope relatively steeply towards the sea while the slope towards the lakes is gentle. These bay-bars extend along almost half the length of the coastline and are typically 1–1.5 m high although study [9] shows heights of up to 2.5 m. The beaches of this coastal section consist of medium-grained sand made up of oolite grains with shell fragments mixed in. Large limestone fragments are also prevalent, particularly after storms. The shoreline is typically marked by beach cusps, or festoons, with their shape and size depending on the characteristics of the preceding wave action.

On this section of coastline, sediments cover not only the beaches, but also the upper part of the underwater slope. This creates an accumulation zone where longshore sediment transport is largely saturated. In the southern part of the section, this zone extends to a depth of 2 m; in the northern part, it widens and extends to

---

[21)] Dolotov, Yu.S., Shadrin, I.F. and Yurkevich, M.G., 1971. [On Dynamics of Relief of a Submerged Coastal Slope Formed by Shells]. In: V. P. Zenkovich, 1971. [*New Studies of Coastal Processes*]. Moscow: Nauka, pp. 110–119 (in Russian).

the 8 m isobath. The offshore extent of sandy bottom deposits is typically 300 m from the waterline near the village of Popovka, compared to just 10–20 m near Cape Evpatoriysky. At the sandbars of the salt lakes, the seaward boundary of the sands increases abruptly to 1.5 km, and satellite images show that this changes very little over time [19]. Beyond the accumulation zone, sediments only accumulate in depressions in the limestone bedrock, controlled by the seabed slope. At slopes of 0.003–0.007 (typical for the section in question), sediments are thrown onto the shore, with accumulation occurring only within a narrow nearshore strip [9]. The same factor explains why the accumulation zone widens near the salt lakes, where depressions in the landscape extend to the seabed.

The shoreline in this area is relatively stable, with a slight overall tendency towards retreat. Typically, retreating segments correspond to headlands while advancing segments correspond to embayments. At the same time, however, the waterline exhibits significant annual and interannual shifts due to fluctuations in sea level and bidirectional sand migration. According to survey data from fixed transects between 2006 and 2017, as well as analysis of satellite imagery, these shifts reach 34 m near Popovka and 18 m near Shtormovoye. After storms, temporary spits and beach ridges can form either parallel or perpendicular to the shore but they are quickly eroded. Assuming the accuracy of data from [9, 20], the width of the bay-bars separating lakes Adzhi-Baychi and Oyburskoye has significantly decreased since 1933, while the width of the bay-bars separating lakes Airchinskoye and Konrad has increased. However, it should be noted that the widths of the bay-bars of all these lakes are currently approximately the same.

We investigated lithodynamic processes in this area based on a statistical analysis of retrospective calculations of wind waves for 1979–2018 and numerical modelling performed in [19]. The study showed that the most intense longshore sediment flows were generated by wave action caused by winds blowing from the west, southwest and south. Under these conditions, longshore sediment transport is directed clockwise towards the northern spit of Lake Donuzlav, where it meets an opposing flow coming from the opposite direction. Along the south-eastern coast, longshore flows diverge, forming convergence zones in the concave embayments of the bay-bars. An increase in the rate of sediment transport on the underwater slope opposite coastal headlands and a decrease opposite embayments result in the redistribution of material and its deposition in the coastal zone of the bay-bars.

The largest lake in this area is *Lake Oyburskoye*. The length of the bay-bar that separates it is ~ 4 km, its height is ~ 1.5 m and its width ranges from 100 to 220 m (according to [20], widths are up to 300 m). Inside the lake, five smaller lakes have been cut off by bay-bars and two artificial dams. Another small lake is being closed off by spits. According to [9], the lake is bordered by extensive waterlogged areas, which are now mostly built up. The bay-bar, which still contains sections of sandy dunes, is used as a recreational area by local residents. However, it is also the subject of ongoing disputes between the residents and commercial entities.

In the 1970s, a canal was dug through the bay-bar to create a mullet farm on the lake. However, it was quickly filled in with sand and the project was abandoned. A similar situation occurred in 2019, when mass protests by local residents ultimately led to the cancellation of a planned shrimp farm.

The pits resulting from illegal sand extraction are visible on the bay-bar; however, this problem affects all bay-bars in the area. One positive development was the creation of a recreational landscape park on the Oyburskaya bay-bar in 2022, achieved through public pressure. Thanks to this, the bay-bars in the area have generally retained their natural state, despite undergoing some localised alterations. Thus, during the construction of a boarding house, the western part of the bay-bar of Lake Airchinskoye was artificially widened by around 50 m with fill material.

Particular concern is raised by the increasing anthropogenic impact on the bay-bar beaches, especially the practice of levelling the beach relief for the purpose of beautification, which involves the destruction of dunes. This results in adverse changes in the composition of the beach sediment and its reduction, which is clearly seen in Fig. 7.

F i g . 7 . A beach near the village of Shtormovoye after grading its natural relief (*top*), the same beach before a storm (*bottom left*) and after the storm (*bottom right*)

Beyond Cape Evpatoriysky, there is small Moinakskaya Bay. A bay-bar forms its shore and separates the lagoon-type lakes known as Bolshoy and Malyy Otar-Moinak (the larger of which is usually simply called Moinaki) and Yaly-Moinak from the sea. The bay-bar is ~ 4 km long, with ~ 1 km of this directly facing Lake Moinaki. According to [20], the sandy bar of Lake Moinaki had a minimum width of ~ 160 m in 1933 and reached 580 m at its widest point. The highest part of the bar rises approximately 1.5 m above the sea level (according to [20], 2.3 m). These parameters remain roughly the same to this day. Originally, smaller secondary lakes were cut off in the inner corners formed by the bay-bar and the shores of the main lakes. However, during the construction of a pioneer camp on the bay-bar in the last quarter of the 20th century, some of these smaller lakes were filled in. The remaining lakes currently accumulate domestic wastewater and floodwater, which has led to strong freshening and loss of their therapeutic value. Currently, only ~ 20% of the bay-bar remains undeveloped and locates temporary structures.

The upper layer of the bay-bar sands is 6–8 m thick. This is underlain by a 3 m thick layer of dense grey silt, beneath which lies another 10 m thick layer of sand. The grey silt extends towards the lake, forming the lake bed beneath a thin layer of black lagoon mud. The presence of an interlayer of grey lagoon silts indicates that the final stage in the bay-bar development was its retreat into the bay and overthrust onto lagoon deposits. Prior to this, during the transgression period, the Otar-Moinakskaya Bay-Bar alternately extended beyond the modern shoreline and occupied its current position [9)]. Work [20] gives slightly different thickness values, based on borehole data but the sequence of layers remains the same.

The Moinakskaya Bay-Bar is made up of oolitic sand mixed with whole and broken shell fragments, as well as small amounts of gravel and limestone clasts. The latter are particularly abundant after storms. The dominant grain size in the samples is 0.25–0.5 mm, while the subordinate fraction is 0.5–1 mm. Together, these two fractions account for 55–90% of the sediment mass.

According to the 1933 survey, the crest of the beach ridge, which was 6–7 m wide, consisted of fine windblown sand [20)]. Newsreel footage from 1943 shows a rather steep beach scarp here. This morphology persisted until the 1970s, as can clearly be seen in photographs from that period. Eyewitness accounts, including the author hereof, also confirm this. Today, the intensively used beach has a significantly gentler slope. Until the mid-1960s, a channel that connected to Lake Moinaki and flooded during storms crossed the eastern end of the bay-bar in the form of a wet log. This feature no longer exists.

It is noted in [20] that in Moinakskaya Bay, limestone is exposed on the seabed at depths of 1–1.5 m, and the rocks underwater are abundantly overgrown with brown branched algae from the Cystoseira genus. However, our observations indicate that the seabed immediately adjacent to the bay-bar consists predominantly of sand, with increasing amounts of gravel, silt and shell fragments present the further one goes out to sea. The description in [20] most likely refers to the seabed to the east and west

of Moinakskaya Bay-Bar (i.e. the bay-bar of Lake Yaly-Moinak). The reason for this discrepancy is unclear but it can reflect multi-decadal changes or, more likely, the limitations of underwater observations conducted over a century ago.

Lake Yaly-Moinak is located next to the sea and is elongated, running parallel to the shoreline. Unlike Lake Moinaki, which is situated in a ravine, Lake Yaly-Moinak occupies a lagoon along a concave stretch of coastline. The lagoon is separated from the sea by a continuous bay-bar, which is ~ 1 km wide. The bay-bar is currently fully developed with recreational facilities. However, construction waste is being dumped into Lake Yaly-Moinak from the east, with buildings then being erected on top of it. Notably, a Greco-Scythian settlement existed on the bay-bar near the lake from the 4th to 1st centuries BC. This was discovered in 1959 during sand extraction.

The shoreline of Moinakskaya Bay-Bar has remained relatively stable, as can be seen by comparing aerial photographs from 1941 with satellite images taken between 2005 and 2020. Direct measurements conducted by us between 2010 and 2015 revealed that the shoreline there exhibited seasonal and inter-annual variability of up to 12 m. Typically, the area of the beach is at its maximum in autumn and at its minimum in early summer, due to seasonal fluctuations in sea level. The shoreline of the bay-bar of Lake Yaly-Moinak has undergone significant modification. Currently, despite an overall slight retreat, it experiences significant inter-annual and seasonal variations due to the presence of cross-shore hydraulic structures. Additionally, a reduction in the vertical thickness of beach sediments has been observed [21].

Old maps show that Lake Karantinnoye was located where central Evpatoriya (Gogolya Street) is today, but it was filled in at some point in the early 20th century. The sandbar that separated the lake from the bay was 150–200 m wide. From the early 5th century BC to the end of the 2nd century BC, the ancient Greek settlement of Kerkinitis was located on this bay-bar.

The coastline *from Evpatoriya to Lake Kyzyl-Yar* consists of a continuous bay-bar. Although it is known by different names in its different areas, it is one unbroken bay-bar in terms of structure and position. Spanning 25 km, the bar separates the largest lake in Crimea, Sasyk-Sivash, as well as lakes Sakskoye and Kyzyl-Yar, from the sea.

The Lake Sasyk-Sivash basin is genetically an estuarine widening of five ravines flowing into the Black Sea, meaning the lake has a lagoon-like origin. Its highly indented shoreline features numerous secondary bays and accumulative landforms.

In 1933, the width of *the bay-bar of Lake Sasyk-Sivash* ranged from 400 m in the narrowest places to 1500 m in the widest places, with elevations above sea level of 1–5 m [20]. The width ranges from 0.9 to 1.62 km in [5]. Currently, the minimum width of the bay-bar is 140 m. Determining the maximum width is almost impossible, as the northern (lake-side) part of the bay-bar has undergone significant alteration due to salt extraction operations, sand mining and filling of certain lake sections with construction waste. Until the early 20th century, a second bay-bar existed alongside the outer one in the west, but it disappeared subsequently due to the construction of salt evaporation ponds.

The upper layer of the bay-bar currently consists of sand, gravel, pebbles and a small quantity of shell fragments. These deposits slope away from the shore towards the lake at an angle of 5–10° beneath the lakebed silt cover where erosion occurs. Drilling into the bay-bar deposits reveals that at a depth of 4 m, the sand transforms into oolitic one, followed by a thick layer of finer-grained sand. At a depth of 16 m, this is replaced by a thick layer of greenish clay of marine origin [20]. Drilling and trenching on the bay-bar indicate that the deposits, across their entire thickness (up to 31 m to the bedrock), are characterised by extreme mottling and compositional variability, both vertically and horizontally.

As noted in [22], the bay-bar is dominated by the 0.1–0.25 mm fraction, reaching up to 45% at most, with boulder-pebble fractions reaching 40% at most. Previously, the surf zone was littered with the shells of modern mollusks. After storms, layers of shells up to 30 cm thick formed in places, mainly consisting of scallops (Pecten) [4]. Currently, the amount of shell material has decreased significantly. Recent studies by MHI RAS [23] have shown that the 0.25–0.5 mm fraction predominates on the bay-bar (39%), with coarse and fine sand inclusions accounting for 24% and 28%, respectively. The proportion of gravel material in beach sediments has significantly reduced (9%), which can indicate weakening of the intensity of the alongshore sediment flow directed from the south. At the water edge, the percentage of the gravel-pebble fraction increases when moving southwards. The decrease in the proportion of fine-grained fractions can be due to material being transported from the beach zone to the sea by wind and then redeposited on the submarine coastal slope.

Aeolian sand deflation plays a significant role in the formation of the bay-bar of Lake Sasyk-Sivash, as strong land-based winds frequently occur here during the winter. Direct studies of the bay-bar have shown that at a wind speed of ~ 15 m per second, ~ 50 kg of sand per hour are transported through a 1 m wide cross-section [24]. The most intensive aeolian transport occurs in the middle part of the beach. Transport is considerably less in the nearshore zone due to the high moisture content of the particles. Vegetation also has a significant impact: experiments have demonstrated that dense herbaceous cover can reduce the movement of sand particles by a factor of 5–10.

As shown in [4], the surf zone and the bay-bar have a similar granulometric composition of pebbles, gravel and sand of the same grain size. Currently, pebbles are primarily found in the swash zone. The same study notes that during storms, a ridge of sand, gravel and pebbles up to 1 m high and 5–10 m wide at the base forms along the shoreline from Lake Kyzyl-Yar to Evpatoriya, extending ~ 20 km. On average, up to 3 $m^3$ of gravel is deposited per linear metre of shoreline, totalling 30–50 thousand $m^3$ along the entire coast. No processes of such scale have been observed in the last hundred years.

Following [6], the authors of [20] consider that the bay-bar of Lake Sasyk-Sivash became fully separated at the end of the 19th century. This conclusion is supported by the fact that the sea overflowed into the lake across the lowest and narrowest part of the bay-bar near the city of Evpatoriya during that period and under strong winds. It should be noted that the bay-bar in this area is only ~ 900 m wide and 1.5 m high, and that the crest of the bay-bar is not yet as distinctly pronounced here as it is further east [20].

We find this statement doubtful because, as is the case today, the width of the bay-bar at this location was ~ 150 m at that time [22], and a road had run along the bay-bar since the Greek colonisation period. Additionally, during the Crimean War, the Turks dug a defensive ditch in this location, connecting the sea with the lake. Subsequently, this site was used for sand extraction as it was the closest area to the city.

It should be noted that the bay-bar of Lake Sasyk-Sivash has been subject to significant man-made impact. In addition to the existing highway, the 20th century saw the addition of a railway, gas and water pipelines, and communication lines.

A workers' settlement called "Dneprostroy" was built on the bay near the village of Kara-Tobe (now Pribrezhnoye) in 1929. A 1934 publication reported: "During the intense days of the First Five-Year Plan, thousands of workers laboured day and night in gravel pits here, extracting gravel and sand for the concrete structures of the giant [Dnieper Hydroelectric Station – *Yu. G.*] under construction... Around the workers' settlement, vast and deep excavations now extend, the layered structure of the bay-bar clearly visible in their walls" [23]. Later, high dunes were replaced by waterlogged areas, which fill with seawater during storms. They are currently gradually being built over.

Work [24] states that the Evpatoriya deposit encompasses the beaches and adjacent bay-bars of lakes Sasyk, Sakskoye and Kyzyl-Yar. It also states that the sand from this deposit is the best on the peninsula for concrete production.

In the second half of the 20th century, the bay was used by unorganised tourists for car camping. By the end of the century, temporary recreational infrastructure had been built there. Gradual development of the bay-bar began in the 21st century, and the western and eastern parts are currently under development. Built-up areas now extend 3 km along the shoreline to the west and slightly further to the east. A project is now being implemented to develop the entire bay, creating a world-class resort called "Golden Sands of Russia". However, the construction volumes envisaged by the project threaten the preservation of the bay unique beaches, which are currently among the cleanest and best preserved in Crimea. An additional threat comes from beach leaseholders levelling and destroying dunes and vegetation that were previously planted to protect against wind erosion (Fig. 8).

Analysis of data from contact measurements, aerial and satellite imagery indicates that, despite interannual and seasonal fluctuations, most of the coastline has remained relatively stable in recent decades. Study [25] shows that the maximum range of interannual fluctuations is ~ 7 m, whereas seasonal fluctuations can reach 26 m. At the same time, signs of coastline retreat have been noted in the east,

---

[22] Totleben, E.I., 1863. [*Sheet IX of Evpatoriya Case as of 5(17) February 1855. Atlas of Plans and Blueprints to Description of Defence of Sevastopol*]. Voenno-Topograficheskoe Depo.

[23] Dzens-Litovsky, A.I., Pastak, A.I. and Meyer, R.F., 1934. [*The Resort of Saki and its Suburbs*]. Moscow: Fizkultura i Turizm, p. 61–62 (in Russian).

[24] Muratov, N.V. and Oginsky, I.M., 1938. [*Resources of Mineral Construction Materials of the USSR*]. Moscow, Leningrad: GONTI NKTP SSSR, 76 p. Vol. 2: Crimean ASSR (in Russian).


Fig. 8. Grading of the full-profile beach relief at the Sasyk-Sivash Lake's bay-bar

in areas of intensive construction and beach exploitation. This is evident in satellite images and in the erosion of the coastal scarp, which consists of sandy loam deposits containing gravel and pebbles. Currently, undeveloped sections of the bay-bar are occupied by anti-landing obstacles.

*The bay-bar of Lake Sakskoye* is narrower (~ 500 m wide) than that of Lake Sasyk-Sivash, which is 500–600 m wide according to [8]. Lake Sakskoye was once a single body of water but it has now been divided into a series of small and large basins as a result of economic activity. Its bay-bar is characterised by a coarser sediment composition than that of Sasyk-Sivash; its deposits consist of sand mixed with gravel and pebbles. Overall, sand is the dominant component of the bay-bar deposits while gravel and pebbles play a subordinate role.

The bay-bar was previously dominated by limestone and green Cretaceous sandstone pebbles, as well as clay shales, granites, diabases, porphyrites and andesites according to [20]. The same study noted that the seaward slopes of the bar descend steeply into the water and are 10–20 m wide, and that the surf zone is littered with the shells of modern mollusks. However, this description no longer corresponds to reality, as the bay-bar is now completely built up, the beaches have been flattened and mollusk shells are extremely scarce.

The bay-bar deposits are up to 31 m thick throughout their entire depth (down to bedrock), with sands accounting for ~ 24 m of this. These deposits are underlain by a 8 m thick layer of grey silt, with red-brown clays forming the lake shores below that [9]. However, these data are not confirmed by [20], which reports a 9.5 m thick layer of sand underlain by 3 m of grey silt, with red-brown clays beneath.

Data from individual boreholes and test pits generally indicate significant variation in the structure of the bay-bar, both vertically and horizontally. Currently, the beach sediments are predominantly medium-grained sand (0.5–0.25 mm in size). A notable trend is the decrease in the proportion of medium-grained sand and the increase in fine-grained material from the south to the north [23]. In cross-sections, sands typically alternate with gravel and pebble interlayers. The main source of sediment is alongshore flow originating from the south, where an active conglomerate cliff is being eroded between lakes Kyzyl-Yar and Bogayly.

Dating and lithostratigraphic analysis of bottom sediments in Lake Sakskoye revealed a transition from marine to lacustrine conditions 5430–4960 years ago, indicating that the bay-bar of Lake Sakskoye is approximately of the same age as the bay-bar of Lake Dzharylgach [15].

Of all the bay-bars in Crimea, the bay-bar of Lake Sakskoye has been subjected to the longest period of intensive man-made impact.

In 1885, a canal was dug through the bay-bar of Lake Sakskoye, connecting the sea and the lake. Between 1950 and 1964, a sand and gravel deposit on the bay-bar was exploited. During this time, the barrier separating the quarry from the sea narrowed and deformed towards the quarry due to storms. During this period, a reduction in the width of the beach was observed in areas adjacent to the barrier. The quarry was closed due to concerns that it would alter the salinity of the brine in Lake Sakskoye. However, shortly thereafter, underwater sand extraction began in the same area. During operation of the quarry, almost all alongshore sediment flows were intercepted, resulting in a sediment deficit and subsequent coastline retreat. Once the negative impact of the quarry had become apparent, it was closed by the Crimean Region Executive Committee. The shoreline remained stabilised until the early 1980s.

In 1982, a hydraulic structure perpendicular to the shore was constructed to the south of the bay-bar of Lake Sakskoye. This structure intercepted the sediment flow coming from the south along the coast. A classic case of downdrift erosion, intensive coastline retreat, began north of the structure, reaching 18–33 m in some areas. Subsequently, the rate of erosion decreased. To protect the resort facilities from destruction, considerable financial resources were invested in the construction of groins designed to retain the beach, seawalls with wave-dissipating chambers, PVC structures, and other protective measures.

In 2016, a project was developed to build a 5600 m long promenade along the bay and expand the beach by adding material to create a 35 m wide stretch of sand. This would replace the existing sand-pebble mixture with a gravel and boulder mixture (70–80 mm), significantly reducing the recreational value of the beach. Despite criticism of the design solutions by MHI RAS (see [5]), construction was started. The negative consequences soon became apparent. Between 2020 and 2021, the beach almost completely disappeared in some areas, while in others, its width decreased and its elevation marks dropped. Construction was therefore suspended, with MHI RAS commissioned to revise the project. Following recommendations of the institute's experts, any structures that could cause significant negative changes to the morphodynamics of the coastal zone were removed from the project. Construction remains frozen at present.

*The bay-bar of Lake Kyzyl-Yar* is located to the south of the bay-bar of Lake Sakskoye. Genetically, the lake basin forms part of the Kyzyl-Yar ravine, which was flooded by the sea before becoming cut off by a sand and gravel bar. According to drilling data, the spit and the entire lake basin consist of red-brown clays which occur at a depth of 17 m in the middle part of the bay-bar [20)].

According to historical data, the width of the bay-bar was 180–200 sazhens (414–460 m) in 1880 [5)]. By 1934, the minimum width of the bay-bar had decreased to 170 m in the south and 380 m in the centre [8)]. Report [25)] by Institute of Mineral Resources dated 1986 indicated a width of 200–300 m, which is approximately of the same value as that determined from a satellite image taken in 1985. However, a more detailed analysis reveals that the width of the bay-bar is closely related to the water level in the lake. Currently, the bay-bar is 2.5 km long and ranges in width from 100 m at the northern end to 30 m at the southern end, excluding the reed overgrowth on the lakeside.

The southern end of the bay-bar is adjacent to a ~ 20 m high steep bank known as Krasnaya Gorka. An actively retreating cliff composed of red-brown clays and gravel-pebble conglomerates extends southwards from there for 2.5 km. The erosion of this cliff provides material that replenishes the beaches to the north. Previously, the bay-bar was the highest of the surrounding ones at 3.1 m, a height explained by the huge accumulation of pebbles near Krasnaya Gorka [8)]. Currently, the height of the bay-bar is 1–2 m.

Previous studies reported that the bay-bar of Lake Kyzyl-Yar was predominantly composed of pebbles with interlayers of sand [9)]. In [22], the dominant fraction is shown to be 0.25–0.5 mm (~ 40%), with significant gravel content (up to 39%). Investigations by MHI RAS revealed that, except for the waterline zone, most of the beach surface consisted of medium-grained (54.9%) and fine-grained (27.7%) sands. At the waterline, fine gravel predominates (39.1%), with inclusions of coarse- and medium-grained sand (28.8%) [23]. After storms, bands of a thin layer of fine- to medium-sized pebbles are observed on the surface.

At the end of the 19th century, a canal was dug through the bay-bar to facilitate salt extraction, but it was swiftly replenished by the sea [8)]. In the early 1980s, seepage losses from the Mezhgornoye Reservoir resulted in a permanent stream flowing into the lake. Consequently, the lake water level rose sharply, causing the width of the bay-bar to decrease. The lake itself became significantly desalinated and the therapeutic properties of the bottom muds were lost.

The aforementioned cross-shore structure at the northern edge of the bay-bar of Lake Kyzyl-Yar caused the shoreline to advance 30 m seawards over a distance of about 1 km between 1984 and 2017. In contrast, the southern part retreated by 30–40 m towards the lake. At present, the bay-bar is popular with tourists travelling by car.

*The bay-bar of Lake Bogayly* (also known as Kaptugan or Kichik-Bel) lies 2.5 km south of Lake Kyzyl-Yar, beyond Krasnaya Gorka. It is the southernmost lake of the Evpatoriya group. The lake is a lagoon formed at the confluence of two ravines.

---

[25)] Romanyuk, O.S., 1988. [*Report on Topic "To Draw Up the Cadastral Register of the Above-Water Part of the Crimean Coasts with Regard to 1:200 000 Scale"*]. Simferopol, 497 p.

The bay-bar is 1.4 km long and 50–70 m wide, with a full-profile beach crest reaching heights of 1.2–1.5 m. According to [19], the bay-bar was formerly 150 m wide and 3.2 m high, due to the accumulation of large quantities of pebbles.

Unlike the neighbouring bay-bars described above, the beach here consists of pebbles for the first 10–15 m from the shoreline, with medium-grained sand mixed with pebbles found farther out to sea. At the waterline, the dominant fraction is fine gravel (up to 40%), with inclusions of coarse- and medium-grained sand (up to 30%) [23]. Granulometric analysis of samples from the seabed shows that the zone of migration of beach-forming sediments near the bay-bar of Lake Bogayly is limited to the 2–2.5 m isobaths. Deeper than that, fine-grained silty fractions predominate.

The two ends of the bay-bar are both supported by abrasive cliffs composed of red-brown and yellowish-brown clays interbedded with layers of sandstone and conglomerate. These conglomerates occur as cemented pebble beds or lenses exposed at elevations ranging from 2 to 6 m. The typical height of the cliffs is 8–10 m.

The dynamics of the bay-bar are largely controlled by those of the adjacent cliffs. According to our data, the cliff adjoining the bay-bar from the west has receded by 45 m between 1975 and 2014, which corresponds to an average retreat rate of 1.2 m per year. The highest rate was observed between 1980 and 1985 (up to 2.2 m per year). Most of our benchmark markers were destroyed by the retreating shoreline. Analysis of satellite imagery showed that the cliff retreated 42 m between 1984 and 2016. According to satellite data from 1984 to 2018, the bay-bar itself retreated 30–35 m landward. Higher-resolution satellite imagery indicated an average retreat of 8–10 m between 2005 and 2016. The retreating shoreline has completely destroyed the promenade, boat shed and hangar at the western end of the bay-bar, and the buildings of the nearby recreation facility are now at risk.

It should be noted that during strong storms, water overflows the bay-bar and sediments are transported into the lake via topographic lows, forming overflow cones that are clearly visible on modern satellite images. Further information on the structure and dynamics of the bay-bar of Lake Bogayly can be found in [2]. Currently, the western end of the bay-bar is primarily used for recreational purposes.

In [20], the presence of the Kherson group of nine lakes was reported in the Sevastopol area of Western Crimea. Currently, only one of these lakes remains (Mayachnoye). The lakes have either been filled in or their bay-bars dismantled to extract sand (e. g. Kamyshovoye, Krugloye). This is discussed in detail in [26].

**Conclusion**

Based on the above, it can be concluded that the state and development of the bay-bars in Western Crimea have been influenced by a combination of natural and man-made factors since the late 19th century.

The most obvious manifestation of natural factors is the increase in the number of Kondzhalayskie islets and the formation of the Sergeevskaya Spit in the northwestern area. This led to the Andreevsky lagoon being closed off by the Sergeevskaya Bay-Bar. This process is noteworthy for being well documented. Growth of spits has also been observed in the same area.

In the remaining areas, the primary influence of natural factors is the redistribution of sediments between the individual segments of the bay-bar and the adjacent shoreline, caused by storm waves. As beach width can vary significantly (by up to 30 m), measurements taken at a single point in time can lead to erroneous conclusions about long-term dynamics. For this reason, it is preferable to use high-resolution satellite imagery with precise georeferencing, for which data has been collected for most areas over at least two decades.

It is also necessary to take into account the transfer of sediments from the foreshore to the lakes via the bay-bars during strong storms (e.g. lakes Karadzha and Bogayly), as well as aeolian transport. These processes are occurring against the backdrop of the current rise in the level of the Black Sea.

The impact of man-made activity on bay-bars is of greater importance. Material has been extracted from bay-bars in varying volumes almost everywhere. Large-scale industrial sand mining has taken place on the bay-bars of lakes Sasyk-Sivash, Donuzlav, Sakskoye and Kyzyl-Yar.

In the 1950s, V. P. Zenkovich observed that large-scale extraction of beach sediments was only occurring on the bay-bars of lakes Kyzyl-Yar and Sakskoye. However, these are constantly replenished by longshore sediment transport from the south. Meanwhile, removals in the lower reaches of the Belbek and Kacha rivers are compensated for during floods and do not endanger shoreline stability.

However, the rivers were later regulated, and the natural erosion of the cliffs, which supplied material to the beaches, was protected by various structures. Together with the construction of structures perpendicular to the shore, this resulted in a significant decrease in the supply of sediment along the coast. Consequently, the volume of beaches, including bay-bars, has decreased significantly. This is evident in the changes to the width and height of the bay-bars, which makes them far more susceptible to wave action. Lower-than-natural elevations therefore result in the flooding of buildings on the bay-bars of lakes Sasyk-Sivash and Sakskoye. The composition of the sediment on the bay-bars has also changed.

The following forms of man-made impact should be noted: cutting of channels through bay-bars (lakes Panskoye, Donuzlav, Oyburskoye, Sasyk-Sivash and Kyzyl-Yar); beach surface levelling, which has resulted in the destruction of dunes and vegetation; infilling of lakes; use of bay-bars as sources of construction material in the Sevastopol and Evpatoriya areas at different times. The use of bay-bars as roads has decreased (Donuzlav, Kyzyl-Yar and Bogayly). Most of the lakes have lost their therapeutic value, which is an irreparable loss, particularly given the development of the resort industry in Western Crimea.

Almost all of the bay-bars in Western Crimea are currently used for recreational purposes. Plans are in place for the full development of the bay-bars of lakes Sasyk-Sivash and Karadzha, and the bay-bar of Lake Sakskoye has already been developed. Currently, only the bay-bar of Lake Oyburskoye has low-level protected status. In view of this situation, preserving the natural uniqueness of the bay-bars is of the utmost importance, as is preventing the loss of unique ecosystems and landscapes, reducing the decline in biodiversity and minimising the risk of flooding in coastal areas.

## REFERENCES


1. Krylenko, V.V., Goryachkin, Yu.N., Krylenko, M.V. and Divinsky, B.V., 2025. Transformation of the Western Branch of the Bakalskaya Spit (Northwestern Crimea) as a Result of the Storm on 26–27 November 2023. *Ecological Safety of Coastal and Shelf Zones of Sea*, (1), pp. 51–71.
2. Krylenko, V.V., Goryachkin, Yu.N., Krylenko, M.V. and Divinsky, B.V., 2024. Transformation of the Lake Bogaily Barrier Beach (Western Crimea) under the Influence of an Extreme Storm. *Ecological Safety of Coastal and Shelf Zones of Sea*, (3), pp. 59–78.
3. Goryachkin, Yu.N. and Dolotov, V.V., 2019. *Sea Coasts of Crimea*. Sevastopol: Colorit, 256 p. (in Russian).
4. Dzens-Litovskij, A.I., 1933. [The Bay-Bars and Spits of the Crimean Salt Lakes]. *Izvestiia Gosudarstvennogo Geograficheskogo Obshchestva = Izvestia de la Société Russe de Géographie*, 65(6), pp. 585–595 (in Russian).
5. Fomin, V.V. and Goryachkin, Yu.N., 2022. Accounting for the Local Wave and Morphodynamic Processes in Coastal Hydraulic Engineering. *Physical Oceanography*, 29(3), pp. 271–290.
6. Dzens-Litovski, A.I., 1938. “Peresyps” (Bars) and “Limans” (Estuaries) of the Azof-Black Sea Coast and the Steppe Crimea. *Priroda*, (6), pp. 22–36 (in Russian).
7. Shuysky, Yu.D., 2002. [Main Patterns in Sediment Distribution at the Underwater Slope of the Donuzlav Bay-Bar]. In: SCSEIO, 2002. *The Black Sea Ecological Problems: Collected Papers* / SCSEIO. Odessa: SCSEIO, pp. 287–295 (in Russian).
8. Shuisky, Yu.D., 2005. Basic Peculiarities of Morphology and Dynamic of the Western Crimea Peninsula Coast. *Ekologicheskaya Bezopasnost' Pribrezhnykh i Shel'fovykh Zon i Kompleksnoe Ispol'zovanie Resursov Shel'fa* [Ecological Safety of Coastal and Shelf Zones and Comprehensive Use of Shelf Resources]. Sevastopol: ECOSI-Gidrofizika. Iss. 13, pp. 62–72 (in Russian).
9. Shuisky, Yu.D., 2007. Mechanical Composition of Beach Alluvium on West Coast of the Crimea. *Ekologicheskaya Bezopasnost' Pribrezhnykh i Shel'fovykh Zon i Kompleksnoe Ispol'zovanie Resursov Shel'fa* [Ecological Safety of Coastal and Shelf Zones and Comprehensive Use of Shelf Resources]. Sevastopol: ECOSI-Gidrofizika. Iss. 15, pp. 370–385 (in Russian).
10. Agarkova, I.V., 1999. [Economic Activity Influence on the Dynamics of the Saki Coast]. *Scientific Notes of Taurida National V. I. Vernadsky University. Series: Geography*, 12(1), pp. 35–38 (in Russian).
11. Goryachkin, Yu.N. and Kosyan, R.D., 2018. The Bakalskaya Spit is a Unique Natural Object of the Crimean Peninsula (Review). *Ecological Safety of Coastal and Shelf Zones of Sea*, (4), pp. 5–14. https://doi.org/10.22449/2413-5577-2018-4-5-14 (in Russian).
12. Rudnev, V.I., Divinskiy, B.V. and Kosyan, R.D., 2020. Changes in Topography of the Coastal Zone of the Bakalskaya Spit from 2018 to 2019. *Ecological Safety of Coastal and Shelf Zones of Sea*, (1), pp. 22–35. https://doi.org/10.22449/2413-5577-2020-1-22-35 (in Russian).
13. Klyukin, A.A., 2005. Extreme Manifestations of the Unfavourable and Dangerous Exogenous Processes in the XX Century in Crimea. *Geopolitics and Ecogeodynamics of regions*, 1(1), pp. 27–38 (in Russian).
14. Goryachkin, Y.N. and Kosyan, R.D., 2020. Formation of a New Island of the Coast of Crimea. *Oceanology*, 60(2), pp. 286–292. https://doi.org/10.1134/S0001437020020034

15. Subetto, D.A., Sapelko, T.V., Stolba, V.F., Kuznetsov, D.D., Ludikova, A.V. and Neustrueva, I.Yu., 2023. Paleolimnology of Lakes of Western Crimea. *Doklady Earth Sciences*, 510(1), pp. 329–334. https://doi.org/10.1134/S1028334X23600184
16. Longinov, V.V., 1955. [Yarylgach Bay]. In: V. V. Longinov, ed., 1955. [*Dynamics and Morphology of Marine Coasts*]. Collection of Papers of Academy of Sciences of the USSR, Institute of Oceanology, Vol. 4. Moscow: AN SSSR, pp. 152–166 (in Russian).
17. Zenkovich, V.P., 1955. [Karadzhinskaya Bay]. In: V. V. Longinov, ed., 1955. [*Dynamics and Morphology of Marine Coasts*]. Collection of Papers of Academy of Sciences of the USSR, Institute of Oceanology, Vol. 4. Moscow: AN SSSR, pp. 100–109 (in Russian).
18. Pospelov, D.V., 2013. The Black Sea Coastline in the Classical Period and the Middle Ages as the Navigation Factor. *Science Prospects*, (10), pp. 118–120 (in Russian).
19. Goryachkin, Yu.N. and Fomin, V.V., 2020. Wave Regime and Lithodynamics in the Region of the Western Crimea Accumulative Coasts. *Physical Oceanography*, 27(4), pp. 415-429. https://doi.org/10.22449/1573-160X-2020-4-415-429
20. Ilinsky, V.P., ed., 1936. Moinakskoye Lake and its Muds. In: V. P. Ilinsky, ed., 1936. *Trudy Solyanoy Laboratorii*. Moscow, Leningrad: Izdatelstvo AN SSSR, 213 p. Iss. VIII (in Russian).
21. Goryachkin, Yu.N., 2020. Changes in the Yevpatoria Coastal Zone in the Last 100 Years. *Ecological Safety of Coastal and Shelf Zones of Sea*, (1), pp. 5–21. https://doi.org/10.22449/2413-5577-2020-1-5-21 (in Russian).
22. Shuisky, Yu.D., 2007. Mechanical Composition of Beach Alluvium on West Coast of the Crimea. *Ekologicheskaya Bezopasnost' Pribrezhnykh i Shel'fovykh Zon i Kompleksnoe Ispol'zovanie Resursov Shel'fa* [Ecological Safety of Coastal and Shelf Zones and Comprehensive Use of Shelf Resources]. Sevastopol: ECOSI-Gidrofizika. Iss. 15, pp. 370–385 (in Russian).
23. Gurov, K.I., 2018. Results of Sediment Granulometric Composition Monitoring in Coastal Zone of the Kalamitsky Bay. *Ecological Safety of Coastal and Shelf Zones of Sea*, (3), pp. 56–63. https://doi.org/10.22449/2413-5577-2018-3-56-63 (in Russian).
24. Vykhovanets, G.V., 2003. [*Aeolian Process on the Sea Shore*]. Odessa: Astroprint, 368 p. (in Russian).
25. Goryachkin, Yu.N., Lazorenko, D.I. and Fomin, V.V., 2024. Dynamics of Accumulative Coast under the Influence of Transverse Hydraulic Structure. *Physical Oceanography*, 31(4), pp. 486–506.
26. Efremova, T.V. and Goryachkin, Yu.N., 2023. Morphodynamics of the Sevastopol Bays under Anthropogenic Impact. *Ecological Safety of Coastal and Shelf Zones of Sea*, (1), pp. 31–47.

Submitted 08.08.2025; accepted after review 02.09.2025;
revised 17.09.2025; published 30.12.2025

*About the author:*

**Yuri N. Goryachkin**, Chief Research Associate, Marine Hydrophysical Institute of RAS (2 Kapitanskaya St., Sevastopol, 299011, Russian Federation), DSc (Geogr.), **ORCID ID: 0000-0002-2807-201X, ResearcherID: I-3062-2015**, *yngor@mhi-ras.ru*

*The author has read and approved the final manuscript.*

ISSN 2413-5577, Ecological Safety of Coastal and Shelf Zones of Sea, 2025, No. 4, pp. 33–52.

Original paper

# Hydro- and Lithodynamic Processes in the Area near the Kerch Strait (the Black Sea) During the Oil Spill Following the Tanker Accident (December 2024)

**V. V. Fomin, L. V. Kharitonova *, D. V. Alekseev, D. I. Lazorenko, A. Yu. Belokon, M. V. Shokurov, V. S. Barabanov, K. I. Gurov, E. V. Ivancha, A. A. Polozok**

*Marine Hydrophysical Institute of RAS, Sevastopol, Russia*
* *e-mail:kharitonova.dntmm@gmail.com*

**Abstract**
The expansion of maritime energy transport in the Kerch Strait may lead to accidental oil spills, with mazut posing a particularly severe ecological threat. The study aims to develop a methodological framework for investigating the dynamics of mazut-polluted bottom sediments under various wind-wave conditions, using the area near the Kerch Strait (the Black Sea) as a case study. We applied numerical modeling of hydro- and lithodynamic processes for 13–27 December 2024 to conduct an integrated analysis of wave fields, currents, bottom sediment transport, and mobility ratio for sand and oil agglomerates (ranging in size from 0.03 to 10 cm) formed by sunken mazut. Atmospheric circulation, wave fields and currents were calculated using the WRF and ADCIRC+SWAN models. We analysed the spatial variability of the agglomerate mobility ratio, defined as the ratio of the shear stress induced by waves and currents to its critical value for a given agglomerate size class. To calculate the bottom sediment transport, we used a modified Soulsby method considering the size of sand and oil agglomerates and the density of the sand-mazut mixture. The results indicate that on the first days following the spill, most of petroleum products were transported towards the Anapa Bay-Bar and into the Kerch Strait. After a shift in wind direction, mazut entered the coastal zone of Southeastern Crimea. The key areas of the possible agglomerate transport and deposition included the coastal zone from Cape Chauda to Cape Takil, the waters of the Kerch Strait and areas along the Anapa Bay-Bar. The study established that agglomerates up to 1 cm could be transported in the coastal zone at depths of up to 10 meters, while larger agglomerates (5 cm and above) remained immobile. Zones of sediment transport convergence were identified near Cape Zhelezny Rog and the southern part of the Anapa Bay-Bar, where the accumulation of sand and oil agglomerates is likely to occur. The developed methodological framework enables the reconstruction and forecasting of the transport and accumulation of contaminated sediments. This is crucial for planning effective oil spill response measures and for providing recommendations in case of emergency situations.

**Keywords**: Black Sea, petroleum products spill, mazut spill, sediments, waves, currents, lithodynamics, numerical modelling, *ADCIRC+SWAN*, mobility ratio

**Acknowledgements**: The work was performed under state assignment no. FNNN-2025-0002 of MHI RAS.

**For citation**: Fomin, V.V., Kharitonova, L.V., Alekseev, D.V., Lazorenko, D.I., Belokon, A.Yu., Shokurov, M.V., Barabanov, V.S., Gurov, K.I., Ivancha, E.V. and Polozok, A.A., 2025. Hydro- and Lithodynamic Processes in the Area near the Kerch Strait (Black Sea) During the Oil Spill Following the Tanker Accident (December 2024). *Ecological Safety of Coastal and Shelf Zones of Sea*, (4), pp. 33–52.

# Гидро- и литодинамические процессы в Прикерченском районе Черного моря в период разлива мазута после крушения танкеров (декабрь 2024 года)

**В. В. Фомин, Л. В. Харитонова *, Д. В. Алексеев, Д. И. Лазоренко, А. Ю. Белоконь, М. В. Шокуров, В. С. Барабанов, К. И. Гуров, Е. В. Иванча, А. А. Полозок**

*Морской гидрофизический институт РАН, Севастополь, Россия*
** e-mail: kharitonova.dntmm@gmail.com*

**Аннотация**

Интенсификация транспортировки энергоносителей в Керченском проливе приводит к аварийным разливам нефтепродуктов, наиболее экологически опасным из которых является мазут. Цель работы – развитие методических подходов к исследованию динамики донных отложений, загрязненных мазутом, под влиянием ветро-волновых условий на примере Прикерченского района Черного моря. На основе численного моделирования гидро- и литодинамических процессов за период 13–27 декабря 2024 г. проведен совместный анализ полей волнения, течений, потоков донных наносов и индексов подвижности для песчано-нефтяных агломератов (размер от 0.03 до 10 см), образованных осевшим на дно мазутом. Атмосферная циркуляция, поля волнения и течений рассчитаны с помощью моделей *WRF* и *ADCIRC+SWAN*. Проанализирована пространственная изменчивость индекса подвижности агломератов, определяемого как отношение сдвигового напряжения, вызванного волнами и течениями, к его критическому значению для заданного класса агломератов. Для расчета потока донных наносов использована модифицированная методика Солсби, учитывающая размер песчано-нефтяных агломератов и плотность смеси песка и мазута. Установлено, что в первые дни после аварии бóльшая часть нефтепродуктов была перемещена к Анапской пересыпи и в Керченский пролив. После смены направления ветра мазут попал в береговую зону Юго-Восточного Крыма. Выявлены основные районы потенциального перемещения и оседания песчано-нефтяных агломератов: прибрежная зона от м. Чауда до м. Такиль, акватория Керченского пролива, а также участки вдоль Анапской пересыпи. Установлено, что песчано-нефтяные агломераты размером до 1 см могли перемещаться в береговой зоне на глубинах до 10 м, тогда как более крупные агломераты (5 см и более) оставались неподвижными. Определены зоны конвергенции потока наносов в районе м. Железный Рог и южной части Анапской пересыпи, где возможно накопление песчано-нефтяных агломератов. Разработанные методические подходы позволяют реконструировать и прогнозировать перемещение и накопление загрязненных донных отложений, что важно при планировании работ по ликвидации последствий загрязнения, а также в качестве рекомендаций при возможных аварийных ситуациях.

**Ключевые слова**: Черное море, разлив нефтепродуктов, разлив мазута, донные наносы, волны, течения, литодинамика, численное моделирование, *ADCIRC+SWAN*, индекс подвижности

**Благодарности**: работа выполнена в рамках темы государственного задания ФГБУН ФИЦ МГИ FNNN-2025-0002.

**Для цитирования**: Гидро- и литодинамические процессы в Прикерченском районе Черного моря в период разлива мазута после крушения танкеров (декабрь 2024 года) / В. В. Фомин [и др.] // Экологическая безопасность прибрежной и шельфовой зон моря. 2025. № 4. С. 33–52. EDN TUWYZA.

## Introduction

Due to increase in the energy carrier transportation via sea routes in the Kerch Strait, there are occasional emergency spills of petroleum products, leading to disastrous consequences for the Azov-Black Sea basin [1]. These spills primarily result from the wreckage of river/sea class tankers. Thus, on 11 November 2007, tankers *Volgoneft-123* and *Volgoneft-139* were damaged in the strait. One of the tankers broke apart and sank, which caused a release of petroleum products into the marine environment. Another, much more severe accident took place on 15 December 2024. In the southern part of the strait, the tankers *Volgoneft-212* and *Volgoneft-239* were wrecked. The tankers broke in half and three sections sank at depths of 19–22 m, while the stern part of *Volgoneft-239* was towed to the coast of the Taman Peninsula near Cape Panagia (Fig. 1). According to official commission findings, the accidents were caused by non-compliance with seasonal navigation restrictions in the Sea of Azov and the Kerch Strait for river/sea class vessels.

The tankers were carrying about 9.2 thousand tonnes of M100 grade mazut, some of which leaked out. Various estimates show that 3 to 5 thousand tonnes of petroleum products entered the water, with the major part entering the Kerch Strait waters on the first days after the accident. The tanker wreckage remained sources of active petroleum product release into the Black Sea waters for several months post-accident. In late January 2025, the mazut-polluted site near Cape Panagia was isolated from the sea by constructing an earthen wall.

Various mazut fractions were transported by currents over significant distances from the accident site, reaching the coasts of Crimea and Krasnodar Krai. The coastal zone near the Kerch Strait, from Cape Chauda (Leninsky Region, Republic of Crimea) to Cape Anapsky (Anapa, Krasnodar Krai), was the most severely affected. Pollution was also found along the southeastern, southern and western coasts of Crimea, with some mazut having entered the Sea of Azov.

During its spreading, the mazut was adsorbed on suspended particles, mixed with bottom sediments in the surf zone and formed heavier-than-water sand and oil agglomerates (SOAs), which settled to the bottom [2]. Despite massive efforts taken

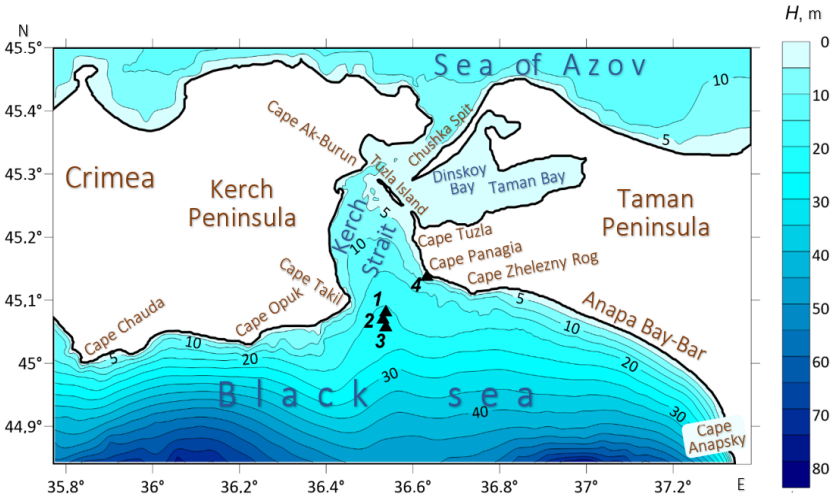


Fig. 1. Bathymetric map of the area near the Kerch Strait. The black triangles indicate the location of tanker wreckage

by the authorities to clean the seabed, many SOAs still remain in the coastal zone near the Kerch Strait, and under certain conditions, they can cause secondary coastal pollution.

Various consequences of petroleum product spills in the Kerch Strait have been studied in papers [1, 3–13]. However, studies on mechanisms of formation, transport and deposition of mazut-containing sediments are scarce. Therefore, existing methods and technologies have proven insufficient to soundly ground any response measures and make decisions on cleaning the coastal zones of Crimea and Krasnodar Krai from the pollution.

To date, the literature lacks mathematical models that allow comprehensive studying of the dynamics of mazut-polluted bottom sediments in coastal waters. The main problem is that SOAs are extremely heterogeneous in size, shape, spatial distribution and average density due to their dependence on local characteristics of the sediment particle-size distribution and the rheological properties of mazut.

In this situation, to study the dynamics of mazut-polluted bottom sediments, it is reasonable to use known mathematical models that consider the presence of oil pollution in a parametric form. This approach was implemented for the northern coast of the Gulf of Mexico, which was severely polluted after the Deepwater Horizon platform accident [14, 15]. In the report [1)] and work [16], numerical modelling of coastal currents, potential transport of SOAs and their interaction with the bottom

[1)] Plant, N.G., Long, J.W., Dalyander, P.S., Thompson, D.M. and Raabe, E.A., 2013. *Application of a Hydrodynamic and Sediment Transport Model for Guidance of Response Efforts Related to the Deepwater Horizon Oil Spill in the Northern Gulf of Mexico Along the Coast of Alabama and Florida*. 2013 (2012–1234). US Geological Survey, 47 p. https://doi.org/10.3133/ofr20121234

was conducted. The potential for movement of oil-containing bottom sediments was also assessed using mobility ratios by comparing modelled shear stress induced by waves and currents with threshold shear stress values for SOAs of various sizes. A statistical analysis of SOA distribution, based on data obtained during the cleanup of the gulf's coastal zone, showed general agreement with the numerical modelling results [16]. The above approach, with some modifications, is applied in this work.

The aim of this work is to develop methodological approaches for studying the dynamics of mazut-polluted bottom sediments under wind-wave conditions using the area near the Kerch Strait in the Black Sea as a case study.

The objectives of the work are:

– to modify the Soulsby [17] algorithm for calculating the bedload flux by including SOA sizes and the density of the sand-mazut mixture;

– to perform a joint analysis of wave fields, currents, bedload fluxes, and mobility ratios for sand and oil agglomerates of different sizes in the area near the Kerch Strait in December 2024;

– to identify zones with high mobility ratio values, where potential SOA movement is possible;

– to identify zones of convergence and reduced bedload flux capacity, where SOA accumulation is likely.

**Materials and Methods**

The study area is the region near the Kerch Strait, spanning the Black Sea waters adjacent to the coastline from Cape Chauda in the west to Cape Anapsky in the southeast, including the Kerch Strait (Fig. 1).

Mathematical modelling was performed for the entire Azov-Black Sea basin. The calculations covered the period of the accident’s onset and development, from 13 to 27 December 2024.

*Near-surface atmosphere modelling.* To reproduce near-surface wind and atmospheric pressure fields over the Azov-Black Sea basin, the mesoscale WRF-ARW model v. 4.5 with a spatial resolution of 5 km was used [2)]. The input data were taken from the Global Data Assimilation System (GDAS) dataset with a horizontal resolution of 0.25° and a temporal discretisation of 6 h. Meteorological fields were output with a temporal resolution of 1 h. The calculations were performed on the MHI computing cluster in a parallel calculation mode.

*Wave and current modelling.* Hydrodynamic processes were modelled on an unstructured computational grid refined in the coastal zone of the study area, which increased modelling accuracy along the coast. For the entire Azov-Black Sea basin, the coastline configuration and bathymetric dataset were obtained by digitising high-resolution satellite images and all available navigation maps, respectively. Grid nodes (~76,000 nodes) were generated based on the distance between the coastline

[2)] Available at: www.mmm.ucar.edu/wrf [Accessed: 21 November 2025].

points, and depths were interpolated for these nodes. The minimum finite element size in the coastal area near the Kerch Strait was about 200 m. A fragment of the unstructured computational grid used for modelling hydro- and lithodynamic processes in the area near the Kerch Strait is shown in Fig. 2.

We used the coupled numerical model ADCIRC+SWAN [18, 19], which integrates two models: the Advanced Circulation Model for Shelves, Coasts and Estuaries (ADCIRC) [3), 4)] and the Simulation Waves Nearshore (SWAN) model [3)]. The input data for the coupled model were the bathymetric field, near-surface wind and atmospheric pressure fields over the study area.

We used the depth-averaged version of the ADCIRC model. Wind shear stress and bottom friction were approximated by square dependencies on velocity. To calculate the bottom friction coefficient, we applied the Manning bottom roughness coefficient n = 0.02 s/m$^{1/3}$. The horizontal turbulent viscosity coefficient was set to 5 m²/s. The time integration step was 1 s. The model results were a depth-averaged current velocity field and a sea level field.

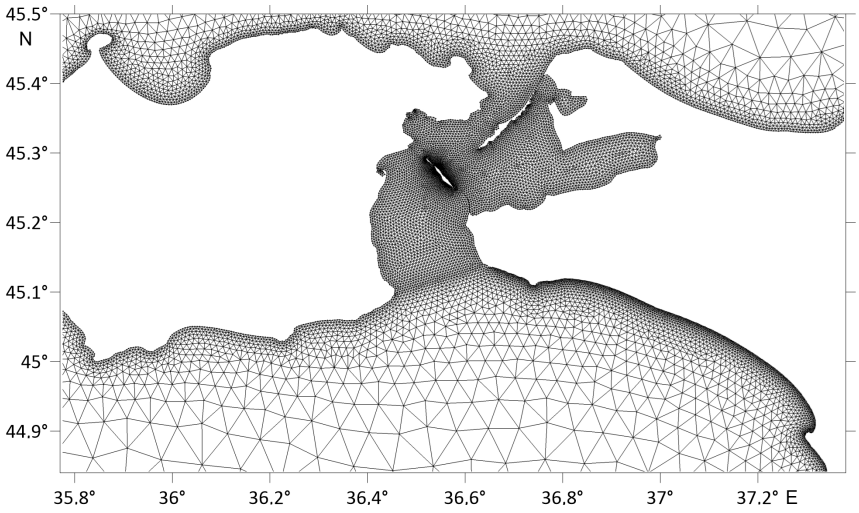


Fig. 2. Fragment of an unstructured computational grid for modelling hydro- and lithodynamic processes in the area near the Kerch Strait

---

[3)] Luettich, R.A., Westerink, J.J. and Scheffner, N.W., 1992. *ADCIRC: An Advanced Three-Dimensional Circulation Model for Shelves Coasts and Estuaries. Report 1: Theory and Methodology of ADCIRC2DDI and ADCIRC-3DL*. Vicksburg: U.S. Army Engineers Waterways Experiment Station, 137 p.

[4)] Luettich, R.A. and Westerink, J.J., 2004. Formulation and Numerical Implementation of the 2D/3D ADCIRC. Finite Element Model Version 44.XX. 74 p. Available at: https://adcirc.org/wp-content/uploads/ sites/2255/2018/11/adcirc_theory_2004_12_08.pdf [Accessed: 19 August 2025].

In the SWAN model, the angular resolution was 10°. Along the frequency coordinate, a non-structured grid with 40 nodes in the frequency range of 0.03–1.4 Hz was used. The main model settings were chosen considering the recommendations for SWAN v. 3.31 (swanmodel.sourceforge.io/settings), which is part of the coupled model. The temporal integration step was 20 min. The calculation results were fields of significant wave heights, mean wave direction, wave periods and near-bottom orbital movement velocity.

The coupling interval for the ADCIRC and SWAN models was 20 minutes. On this interval, the current and sea level fields were first determined using the ADCIRC model, then wave fields were calculated using the SWAN model. In this process, ADCIRC used the wave-induced stresses from SWAN, while SWAN used the current velocities and sea level from ADCIRC. The coupled model algorithm is detailed in paper [18]. Calculations with the coupled model were performed on the MHI computing cluster in parallel processing mode. Model data were output with a temporal resolution of 1 h.

*Near-bottom stresses induced by waves and currents.* We used hydrodynamic modelling data to calculate combined near-bottom shear stresses $\tau_{wc}$, $\tau_m$, induced by waves and currents, using the Soulsby method [17] ($\tau_{wc}$ corresponds to the mean shear stress for a wave period [17] and is used to assess sediment mobility; $\tau_m$ represents the maximum shear stress for a wave period and is used to determine bedload flux):

$$\tau_{wc} = \sqrt{(\tau_m + \tau_w \cdot \cos\varphi)^2 + (\tau_w \cdot \sin\varphi)^2},$$

$$\tau_m = \tau_c \left[ 1 + 1.2 \cdot \left( \frac{\tau_w}{\tau_c + \tau_w} \right)^{3.2} \right],$$

where $\tau_w$, $\tau_c$ are the shear stresses induced by waves and currents, respectively, kg/(m·s²); φ is the angle between the directions of currents and waves. To determine $\tau_w$ and $\tau_c$, the depth-averaged current velocity, amplitude of near-bottom wave orbital movement velocity and peak wave period are used [20, 21].

*Properties of bottom sediments including SOAs.* For numerical modelling of sand and SOA transport, we need to know their physical properties. For sandy sediments (without mazut), the median sand diameter in the study area was assumed to be 0.3 mm. To depths of 3–5 m, sediments in this area are mostly quartz with bioclastic varieties [5), 6)] [22, 23] with a density of about 2650 kg/m³.

---

[5)] Shnyukov, E.F. and Palansky, M.G., 1979. [Geological Significance of Some Geochemical Studies of Modern Bottom Sediments of the Kerch Strait]. In: E. F. Shnyukov, ed., 1979. *Lithological and Geochemical Conditions for the Formation of Bottom Sediments*. Kiev: Naukova Dumka, pp. 3–17 (in Russian).

[6)] Makarenko, D.E., ed., 1981. [*Geology of the Ukrainian SSR Shelf*]. Kiev: Naukova Dumka, 158 p. (in Russian).

Paper [7] proposes a formula for estimating the density of a mixture of bottom sediments consisting of sand, water and mazut

$$\rho SOA = \left[ \frac{\alpha_w}{\rho} + \frac{(1-\alpha_w)\times\alpha_m}{\rho_m} + \frac{1-\alpha_w-(1-\alpha_w)\times\alpha_m}{\rho_s} \right]^{-1}, \qquad (1)$$

where $\rho_{SOA}$, $\rho$, $\rho_m$, $\rho_s$ are the density of the mixture, water, mazut and sand, kg/m³, respectively; $\alpha_w$, $\alpha_m$ are the percentage content of water and mazut, respectively.

Some results of laboratory studies of mazut samples and its mixture with sand from the tanker wreckage area are presented in an unpublished report by A. V.Topchiev Institute of Petrochemical Synthesis, RAS. According to their information, within the water temperature range of 8–40°C, the density of the spilled mazut varies from 985 to 962 kg/m³. The mean percentage of mazut in sand $\alpha_m$ = 13%. The percentage of water in sand is unknown.

Substituting these values into formula (1) at $\alpha_w$ = 0, $\rho$ = 1012 kg/m³, $\rho_m$ = 985 kg/m³ and $\rho_s$ = 2650 kg/m³ gives $\rho_{SOA}$ = 2173 kg/m³. This estimate of the mixture density is rather approximate, since it is based on a very limited dataset. The main errors in determining the density of the sediment mixture are related to assigning the weight coefficients $\alpha_w$, $\alpha_m$. The calculations show that varying $\alpha_m$ within 10–15% leads to an increase in $\rho_{SOA}$ by 7%, while varying $\alpha_w$ within 0–5% leads to a decrease in $\rho_{SOA}$ by 5.5%.

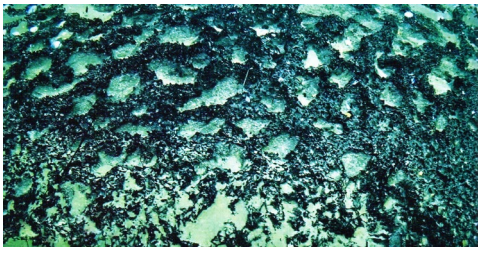

***a***

***b***

Fig. 3. Sand and oil mats [24, p. 92] (*a*); agglomerates in the form of pebble (*b*) on the bottom near the Anapskaya Bay-Bar [24, p. 90]

In the area near the Kerch Strait, no observations were conducted on the size distribution of SOAs. An analysis of available open-source photo and video materials showed that in the coastal zone, SOAs varied greatly in sizes and configurations. Larger agglomerates were spread on the bottom as mazut mats accumulating in bottom depressions (Fig. 3, *a*). Such formations could be up to 100 m long and several centimetres thick [8] [24]. Part of the mazut was

[7] Plant, N.G., Long, J.W., Dalyander, P.S., Thompson, D.M. and Raabe, E.A., 2013. *Application of a Hydrodynamic and Sediment Transport Model for Guidance of Response Efforts Related to the Deepwater Horizon Oil Spill in the Northern Gulf of Mexico Along the Coast of Alabama and Florida. 2013 (2012–1234)*. US Geological Survey, p. 45. https://doi.org/10.3133/ofr20121234

[8] Matishov, G.G., Grigorenko, K.S., Kulygin, V.V. and Sushko, K.S., 2025. [*SSC RAS Expedition to the Anapskaya Spit 9–15 June 2025: Information Bulletin*]. Rostov-on-Don: Izdatelstvo YUNTS RAN, 104 p. (in Russian).

Characteristics of sand and oil agglomerates and their corresponding critical shear stresses

| Class | $d_{SOA}$, cm | $\rho_{SOA}$, kg/m$^3$ | Critical stress $\tau_{cr}$, Pa | | |
|---|---|---|---|---|---|
| | | | high $\tau_{crh}$ | moderate $\tau_{crm}$ | low $\tau_{crl}$ |
| *S*1 | 0.03 | 2173 | 0.95 | 0.32 | 0.16 |
| *S*2 | 0.5 | 2173 | 7.77 | 2.59 | 1.30 |
| *S*3 | 1 | 2173 | 10.21 | 3.40 | 1.70 |
| *S*4 | 2.5 | 2173 | 13.58 | 4.53 | 2.26 |
| *S*5 | 5 | 2173 | 18.71 | 6.24 | 3.12 |
| *S*6 | 10 | 2173 | 34.29 | 11.43 | 5.72 |

mixed with sand and submerged vegetation. In a slight sea, the mazut mats remained stable, but the sand became suspended and transported, gradually covering the mazut on the bottom (Fig. 3, *a*).

Some mazut agglomerates, formed on site or separated from mazut mats by waves, were pebble-shaped with a diameter of 2–10 cm (Fig. 3, *b*). According to work [25], such formations consist of a weathered oil core coated with a thin layer of sand or shell fragments. They can be transported along the bottom by waves and washed ashore [26, 27].

In consideration of the above, to study the mobility properties of bottom sediments in the area near the Kerch Strait, we selected a number of SOA size classes with dimensions $d_{SOA}$ from 0.03 to 10 cm to cover the presumed variability in SOA sizes. The selected agglomerate classes are presented in the table.

*Critical shear stresses for different SOA classes.* The critical shear stress for each SOA class was determined by the expression [2]

$$\tau_{cr} = \theta_{cr}\, g\, \rho\, \Delta d_{SOA}, \tag{2}$$

where $\theta_{cr}$ is the Shields parameter [9]; g is gravitational acceleration; $\Delta = \rho_{SOA}/\rho - 1$. This is the classic formula for calculating shear stresses, where the mean sediment diameter $d_{50}$ and sand density are replaced by the size and density of the SOA, respectively.

The Shields parameter in formula (2) was estimated using the empirical relationship [28]

$$\theta_{cr} = \frac{0.3}{1+1.2d_*} + 0.055 \cdot [1 - \exp(-0.02d_*)], \tag{3}$$

[9] Shields, A., 1936. Anwendung der Ähnlichkeits-Mechanik und der Turbulenzforschung auf die Geschiebebewegung. In: Preußischen Versuchsanstalt für Wasserbau, 1936. *Mitteilungen der Preußischen Versuchsanstalt für Wasserbau*. Berlin: Preussishe Versuchsanstalt für Wasserbrau und Schiffbau, 26, S. 26 (in German).

$$d_* = d_{SOA}\left[\frac{g\,\Delta}{\nu^2}\right]^{1/3}, \qquad (4)$$

where $d_*$ is the non-dimensional particle diameter; $\nu = 1.36 \cdot 10^{-6}$ m²/s is the kinematic viscosity of water.

*In situ* experiments demonstrate that the critical stress value can decrease depending on the extent to which an individual particle protrudes from the sediment layer (this can also be expected for an individual SOA) [29–31]. Since individual SOAs may have different positions relative to the bottom surface, three types of critical stress were considered [1)]: high (strong) ($\tau_{crh}$) – the agglomerate is within the sediment layer; medium ($\tau_{crm}$) – the agglomerate partially protrudes from the sediment layer; low (weak) ($\tau_{crl}$) – the agglomerate is entirely on the surface of the sediment layer. High critical stress values were calculated using formulas (2)–(4). Medium and low critical stress values were estimated as one-third and one-sixth of the high critical stress value, respectively.

*SOA mobility ratios.* Sediment mobility ratios are widely used to classify the mobility properties of bottom sediments and to predict bottom erosion and sediment deposition processes in specific water areas [32–34].

In this paper, the SOA mobility ratio is defined as the ratio of the shear stress, induced by waves and currents, to the critical shear stress for a given agglomerate class:

$$MI_{SOA} = \tau_{wc} / \tau_{cr,SOA}.$$

The fulfilment of condition $MI_{SOA} \geq 1$ in a certain area indicates that agglomerates of the specified class can start to move. The probability of this movement depends on the duration of the condition.

*Bedload fluxes.* As another indicator for identifying probable regularities of SOA redistribution along the coast, the capacity and direction of the bedload flux $q_b = (q_{bx}, q_{by})$ are used, where $q_{bx}$, $q_{by}$ are the zonal and meridional components of the flux. Calculations of $q_b$ were performed using the Soulsby method [17, 20], modified by including SOA sizes and the density of the sand and mazut sediment mixture based on formulas (1) and (4).

**Discussion of the results**

Let us consider the results of numerical modelling of atmospheric circulation, waves, currents and bedload fluxes in the area near the Kerch Strait during the occurrence and development of the accident. Time in the text is given in UTC (Coordinated Universal Time), and wave heights refer to significant wave height.

*Atmospheric circulation.* On 15–17 December 2024, atmospheric circulation over the Azov-Black Sea basin was determined by the passage of a cold front of a large mid-latitude cyclone centred near Saint Petersburg. On the first day of observations, 15 December, the cold front manifested as a jet of strong south-westerly wind,

stretching from south-west of Istanbul to the north-east towards the Kerch Strait. The maximum wind speed reached 15 m/s. This wind field configuration was favourable for the development of wind waves along the jet from the south-west to the north-east, since it provided a considerable fetch (over 1000 km), which is almost the maximum possible for the Black Sea.

Over time, the front advanced south-eastward, and this favourable fetch configuration was of short duration. After 16:00 on 15 December, the front had shifted to the south-east, and a moderate north-westerly wind (speed up to 10 m/s) from the cyclone's cold sector settled along the entire favourable fetch line from the Bosporus Strait to the Kerch Strait. This wind did not generate wind waves in the Kerch Strait. Swell generated earlier along the favourable fetch line continued to enter the Kerch Strait area for some time thereafter (from 16:00 on 15 December until 02:00 on 16 December, providing that wave generation started around 09:00).

*Wind waves.* The storm of 15–17 December 2024 was preceded by north-westerly waves with heights of about 0.5 m. The storm began during the night of 15 December when the wave direction shifted to southerly and wave heights started to increase. According to available information [10)], the tanker wreckage took place at 06:00 on 15 December, when modelled wave heights at the accident site reached 2.5 m (Fig. 4, *a*).

Further, the storm evolved as follows. Between 14:00 and 19:00, the wave direction shifted from southerly to south-westerly, with wave heights about 2 m. For the next 2.5 days, waves with heights of 1.7–2.8 m arrived from the sector between south-west and west-south-west. Maximum wave heights were registered at 22:00 on 16 December (Fig. 4, *b*).

From 18 December, the storm intensity decreased, and westerly waves with heights of 1–1.5 m settled for about a day. Further, on 19 December, the wave direction began shifting through the southern sector to the south-east: by 05:00 waves were from the south-west, and by 22:00 they were southerly, with heights of 0.5–0.6 m. For the following two days (20–22 December), waves from the south-south-east to south-east sector, with heights of ~0.8 m, arrived in the study area (Fig. 4, *c*).

From 05:00 to 14:00 on 22 December, the wave direction shifted to the south-west. Thereafter, until the end of the modelling period (00:00 on 23 December), wave heights increased to 2 m (Fig. 4, *d*).

*Wind- and wave-induced currents.* Fig. 5 shows depth-averaged wind- and wave-induced current fields for four time instances. At the moment of the accident (Fig. 5, *a*), currents in the study area were characterised by velocities of ~0.2 m/s in the offshore part. Along the coast of Krasnodar Krai and from Cape Takil (the Crimean Peninsula), currents with velocities up to 0.3–0.4 m/s were directed into the Kerch Strait, and from the strait into the Sea of Azov, where their velocities exceeded 0.8 m/s in some areas.

---

[10)] Available at: https://ngs.ru/text/incidents/2025/01/15/74987513/ [Accessed: 10 July 2025].

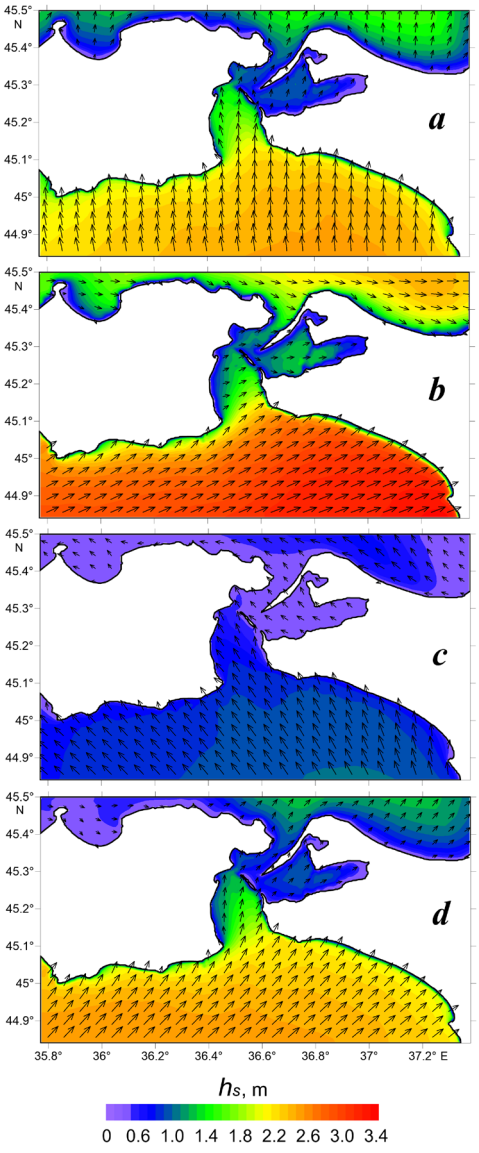


Fig. 4. Significant wave height $h_s$ and average direction of waves in the area near the Kerch Strait: on 15 December 2024 at 06:00 (*a*), 16 December 2024 at 22:00 (*b*); 21 December 2024 at 20:00 (*c*); 22 December 2024 at 23:00 (*d*)

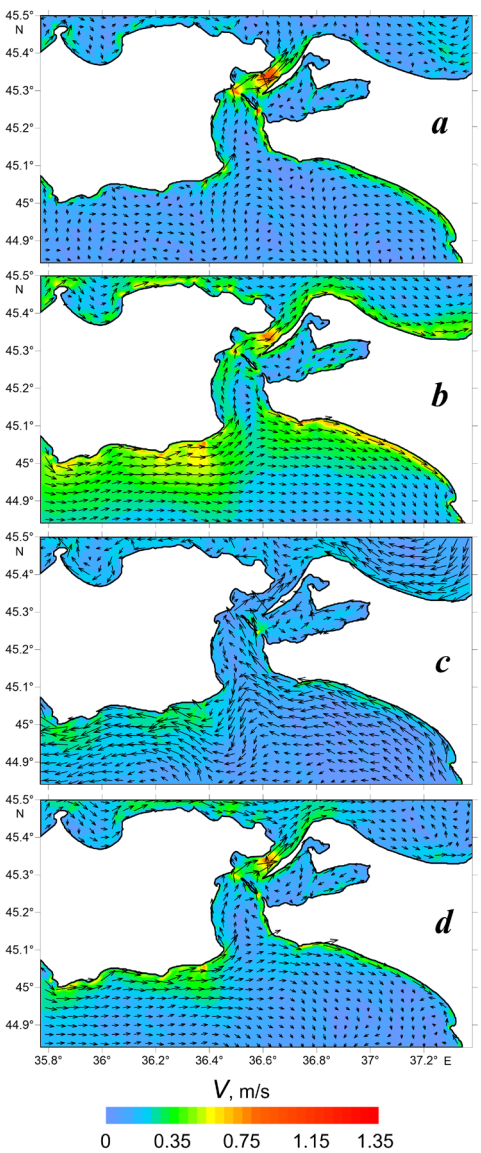


Fig. 5. Velocity $V$ and direction of currents in the area near the Kerch Strait: on 15 December 2024 at 06:00 (*a*), 16 December 2024 at 22:00 (*b*); 21 December 2024 at 20:00 (*c*); 22 December 2024 at 23:00 (*d*)

From 14:00 to 21:00 on 15 December, the currents restructured. Along the south-eastern coast of Crimea, the current directed from west to east. From Cape Takil, water was partly directed into the Kerch Strait and further along its western coast into the Sea of Azov. Along the Taman Peninsula and the Anapa Bay-Bar, currents were oriented to the south-east. Current velocities reached their maximum by 22:00 on 16 December, measuring 0.3–0.4 m/s across most of the study area, with velocities of 0.6–0.7 m/s in the alongshore jet (Fig. 5, *b*), followed by their decrease. This spatial structure of currents, with minor variations, remained for three days and favoured the transport of petroleum products from the tanker wreckage to the Anapa Bay-Bar and further to the south-east.

On 19 December, the current direction changed north of Cape Panagia, and by 19:00, currents along the Anapa Bay-Bar and Taman Peninsula were directed into the Kerch Strait. From the accident site, currents flowed south-westward, and offshore they moved towards Cape Opuk (Fig. 5, *c*), transporting pollution to the Crimean Peninsula. Current velocities were 0.1–0.3 m/s.

From 08:00 to 18:00 on 22 December, the current field restructured again. Along the Crimean coast, the current flowed eastwards, and further from Cape Takil, it was directed into the Kerch Strait. From the accident site, water masses spread towards Cape Panagia, which became a zone of divergence: south of the cape, the currents were directed south-eastward, while north of the cape they flowed into the Kerch Strait. The currents from Cape Zhelezny Rog flowed south-eastward, and those from Cape Anapsky moved in the opposite direction, forming a convergence zone in the southern part of the Anapa Bay-Bar (Fig. 5, *d*).

*Mobility ratios*. The studied situation of potential SOA movement on the first days after the release of petroleum products into the marine environment implies that the formed agglomerates were located on the surface of the sediment layer. Thus, the analysis focused on calculation results for low critical stress values ($\tau_{crl}$).

Fig. 6 shows the spatial distribution of the maximum calculated mobility ratios ($MI_{SOA}$) over the period for sand with a median diameter of 0.03 cm and for three SOA size classes: 1, 2.5 and 5 cm. The areas with $MI_{SOA} \geq 1$ (shown in pink) indicate exceedance of the mobility threshold value.

As seen in Fig. 6, *a*, *b*, the calculated areas of potential transport for sand and 1-cm SOAs are nearly the same. Thus, where there are such sediments on the bottom, movement is likely down to depths of 10 m in the coastal zone from Cape Chauda to Cape Takil and from Cape Panagia to Cape Anapsky and no deeper than 5 m in the Kerch Strait and along the Sea of Azov coasts.

SOAs sized 2.5 cm could only be moved in very limited areas, up to the 5 m isobath (Fig. 6, *c*). Along the Crimean coast, movement of such agglomerates may occur near capes, while in the Kerch Strait it may take place on both sides of Tuzla Island and between the Chushka Spit and the Kerch Peninsula. Along the Anapa Bay-Bar, such areas can be seen as fragments in its northern, central, and southern parts. The largest areas of potential agglomerate movement are located between Cape Tuzla and Cape Zhelezny Rog. For SOAs sized 5 cm and larger, no areas with a mobility ratio exceeding unity are observed (Fig. 6, *d*).

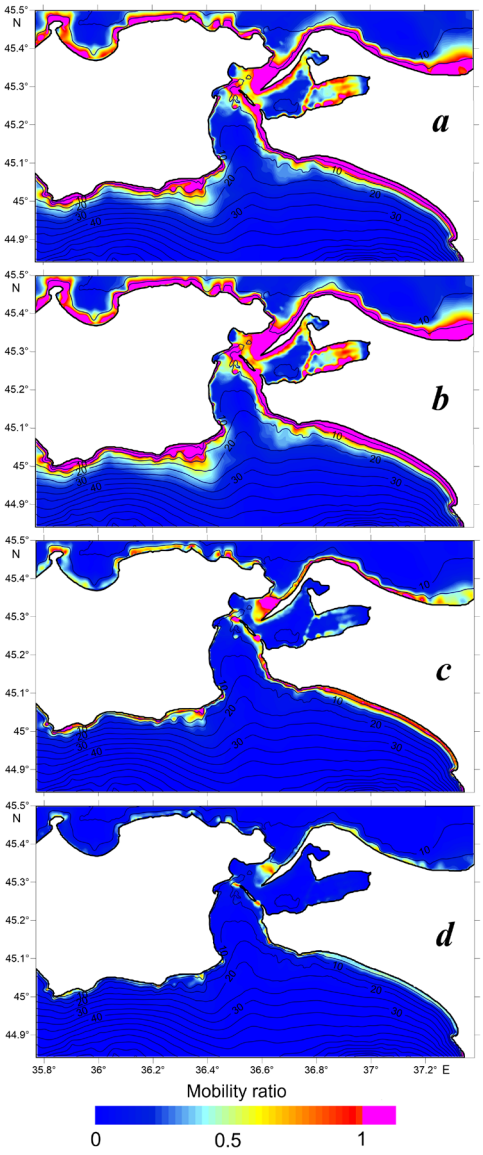


Fig. 6. Mobility ratio for bottom sediments in the area near the Kerch Strait for sand (*a*) and sand and oil agglomerates 1 cm (*b*), 2.5 cm (*c*) and 5 cm (*d*) in size on 13–22 December 2024. The bathymetric contour interval is 5 m

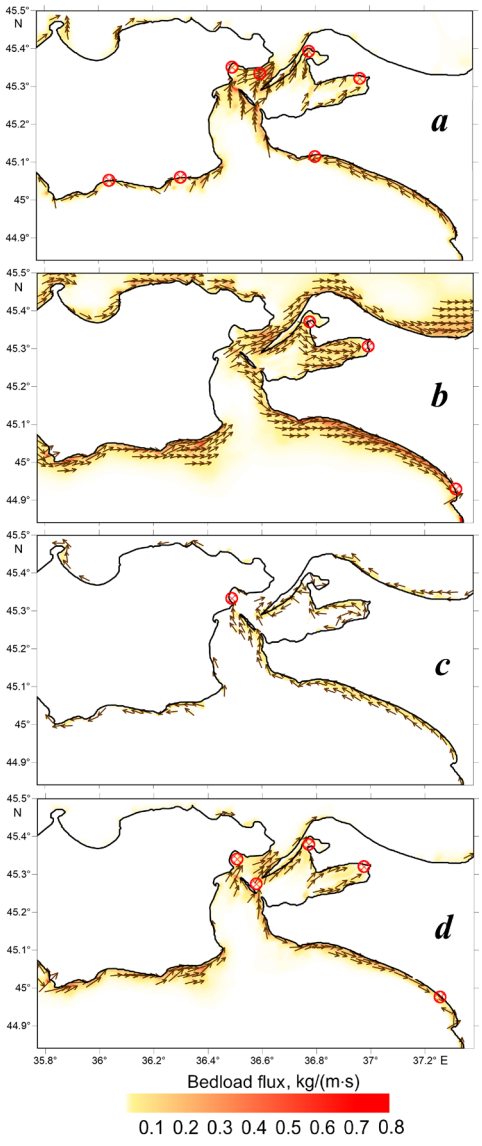


Fig. 7. Potential volume and direction of sediment flows in the area near the Kerch Strait: on 15 December 2024 at 06:00 (*a*), 16 December 2024 at 22:00 (*b*); 21 December 2024 at 20:00 (*c*); 22 December 2024 at 23:00 (*d*). The red circles indicate zones of convergence and velocity deceleration of sediment flows

In the areas, where sand is mobile but SOAs are not, it is more likely that SOAs will be buried under sand. In such cases, mobility ratio will need to be calculated at high critical stress values.

*Bedload fluxes*. At the next study stage, parameters of potential bedload fluxes were calculated. Fig. 7 shows the spatial distribution and directions of these fluxes in the area near the Kerch Strait for sand sized 0.03 cm. The flux field reveals zones of convergence (opposing directions of two fluxes) or zones of reduced capacity, which can be interpreted as areas of potential accumulation for sand and SOAs. The areas with divergence or increased flux capacity are, on the contrary, less prone to sediment accumulation.

Under southerly waves with heights of ~2.5 m (Fig. 7, *a*), a south-east-to-north-west bedload flux occurs along the Anapa Bay-Bar, with a convergence zone forming in the northern part of the bay-bar (near Cape Zhelezny Rog). Farther north (from Capes Zhelezny Rog and Panagia), the bedload flux is directed into the Kerch Strait. There are multidirectional fluxes along Crimea, which form convergence zones in coastline indentations; from Cape Takil, sediments move into the strait. Potential sediment deposition areas in the Kerch Strait are located north of Cape Ak-Burun and in the top parts of Taman and Dinskoy Bays.

Fig. 7, *b* presents the situation at the peak of the storm on 15–17 December 2024, when waves of 2.5–2.8 m height arrived from the south-west. Along the Crimean coast, sediments moved eastwards. In the northern part of the Kerch Strait, the material moved to the Sea of Azov. Along the Black Sea coasts of Krasnodar Krai, there was a persistent south-eastward bedload flux, which, according to calculations, had a deposition zone in the southern part of the Anapa Bay-Bar near Cape Anapsky.

Waves from the south-east with heights of ~0.8 m generated a bedload flux from Cape Anapsky north-westward into the Kerch Strait, along Tuzla Island towards Cape Ak-Burun (Fig. 7, *c*). A divergence zone formed in the Crimean coastal area near Cape Takil, from where the material moved into the Kerch Strait and along the southeastern coast of Crimea. Under these conditions, the potential flux capacities were relatively low. Therefore, sand particles and SOAs could have been moved only over short distances. However, with the intensification of the disturbing wind-wave impact of the south-eastern sector, the sediments will be able to move along calculated trajectories over longer distances.

Under south-westerly waves (Fig. 7, *d*), there is a unidirectional eastward flux along the south-eastern Crimean coast. Along the Krasnodar Krai coasts, a divergence zone is evident in the flux field near Cape Panagia. From this zone, the material will spread south-eastward to the southern part of the Anapa Bay-Bar (where it will deposit) and north-westward through the strait between Tuzla Island and its namesake cape. Under such wind-wave conditions, the bottom sediments near Cape Panagia, polluted by mazut leakage from the stern section of *Volgoneft-239* prior to the construction of the wall in late January 2025, will be a source for SOA transport towards the Kerch Strait and the Anapa Bay-Bar.

**Conclusion**

A numerical algorithm was developed to calculate the dynamic characteristics of mazut-polluted bottom sediments. The algorithm includes several blocks:

– modelling of wave and current fields;

– calculation of bottom shear stress induced by waves and currents;

– determination of critical shear stress based on specified SOA characteristics;

– calculation of bottom sediment mobility ratios; determination of bedload fluxes;

– identification of possible areas of polluted sediments accumulation in the coastal zone.

Based on numerical modelling of the hydrodynamic and lithodynamic processes during the onset and evolution of the accident in December 2024, an integrated analysis of wave fields, currents, bedload fluxes, and mobility ratios for SOAs of different sizes was conducted for the area near the Kerch Strait in the Black Sea.

The modelling results showed that during the storm of 15–17 December 2024, wind-induced waves from the south and south-west were up to 2.8 m high. In the following four days after the storm, waves with heights of 0.8–1.5 m from the south-west–south-east sector persisted in the study area. From 22 December until the end of the modelling period, the wave direction shifted to south-westerly, with wave heights increasing to 2 m.

Calculations showed that during the period under study, the structure of the current field changed three times. At the moment of the tanker wreckage, the currents along the coast of Crimea and Krasnodar Krai had a velocity of 0.3–0.8 m/s and were directed towards the Kerch Strait. During the active phase of the storm and in the following days, the direction of the currents changed: the flow started to move from the tanker wreckage towards the Anapa Bay-Bar. This flow carried the spilled mazut during the first three days.

From 19 to 22 December, the current velocities decreased to 0.1–0.3 m/s. Along the coast of Krasnodar Krai, the flow was directed to the north-west, with pollution from the accident site moving towards the Crimean Peninsula. Until the end of the calculation period, petroleum products were carried from the area where the tanker wreckage was located to the Kerch Strait and the Anapa Bay-Bar.

An analysis of the mobility ratios revealed that, during the time interval under study, sand and SOAs sized 1 cm could be transported within the same areas of the coastal zone, down to depths of 10 m. As for 2.5-cm SOAs, they could move over very confined areas, reaching only the 5-m isobath. Under those wind-wave conditions, SOAs sized 5 cm and larger remained immobile.

The spatial distribution of bedload fluxes under various wave scenarios was determined. During the storm, a fairly stable south-easterly bedload flux formed along the coast of the Taman Peninsula, with a deposition area in the southern Anapa Bay-Bar. As waves moved from the south-east along the Black Sea coast of

the Krasnodar Krai, sediments were transported to the Kerch Strait. Under south-westerly winds, a zone of divergence of two flows directed to the north-west and south-east formed near Cape Panagia.

The results of the obtained estimates can be used in planning and implementing measures to eliminate the consequences of pollution, as well as recommendations for possible emergency situations in the area under study.

## REFERENCES


1. Matishov, G.G., Stepanyan, O.V., Kharkovsky, V.M. and Soyer, V.G., 2016. Oil Pollution of Azov and Black Seas Increases. *Priroda*, (5), pp. 64–69 (in Russian).
2. Dalyander, P.S., Plant, N.G., Long, J.W. and McLaughlin, M., 2015. Nearshore Dynamics of Artificial Sand and Oil Agglomerates. *Marine Pollution Bulletin*, 96(1–2), pp. 344–355. https://doi.org/10.1016/j.marpolbul.2015.04.049
3. Ovsienko, S.N., Fashchuck, D.Ja., Zatsepa, S.I., Ivchenko, A.A. and Petrenko, O.A., 2008. Storm of 11 November, 2007, in Strait of Kerch: Chronology of Events, Mathematical Modeling and Geographic/Ecological Analysis of Oil Spill. In: E. V. Borisov, ed., 2008. *Proceedings of SOI*. Moscow. Iss. 211, pp. 307–339 (in Russian).
4. Ivanov, A.Yu., Litovchenko, K.Ts., Zatyagalova, V.V., 2008. Emergency Oil Spill in the Kerch Strait: Radar Monitoring and Numerical Modeling. *Issledovanie Zemli iz Kosmosa*, (4), pp. 62–76 (in Russian).
5. Matishov, G.G., Berdnikov, S.V. and Savitsky, R.M., 2008. [*Ecosystem Monitoring and Assessment of the Impact of Oil Spills in the Kerch Strait. Ship Accidents in November 2007*]. Rostov-on-Don: Yuzhny Nauchny Zentr RAN, 80 p. (in Russian).
6. Kuznetsov, A.N. and Fyodorov, Yu.A., 2010. Regularities of Distribution and Transformation of Oily Pollution in the Region of Technogenic Catastrophe in Kerch Strait. *Proceedings of the Russian Geographical Society*, 142(2), pp. 53–59.
7. Lyubartseva, S.P. and Ryabtsev, Yu.N., 2010. Modeling the Oil Pollution in Kerch Strait. In: MHI, 2010. *Ekologicheskaya Bezopasnost' Pribrezhnykh i Shel'fovykh Zon i Kompleksnoe Ispol'zovanie Resursov Shel'fa* [Ecological Safety of Coastal and Shelf Zones and Comprehensive Use of Shelf Resources]. Sevastopol: ECOSI-Gidrofizika. Iss. 22, pp. 245–252 (in Russian).
8. Fashchuk, D.Ya., Flint, M.V., Ivanova, A.A. and Tkachenko, Yu.Yu., 2010. Kerch Strait Oil Pollution by the Results of 2007-2009 Researches. *Izvestiya Rossiiskoi Akademii Nauk. Seriya Geograficheskaya*, (4), pp. 86–97 (in Russian).
9. Fashchuk, D.J., Flint, M.V., Koluchkina, G.A. and Panov, B.N., 2010. Interagency Field Research of the Consequences of the Wreck of the Tanker Volgoneft-139 in the Kerchenskii Strait. *Oceanology*, 50(3), pp. 435–438. https://doi.org/10.1134/S0001437010030124
10. Klenkin, A.A. and Agapov, S.A., 2011. Dynamics of Oil Product Distributions in Water and Bottom Sediments of the Sea of Azov and the Black Sea after Ship Accidents in the Kerch Strait. *Water Resources*, 38(2), pp. 220–228. https://doi.org/10.1134/S0097807811020060
11. Shybaeva, S.A., Ryabinin, A.I., Ilyin, Y.P. and Lomakin, P.D., 2011. Kerch Strait Hydrochemistry Regime and Pollution in 1979–2009. *Morskoy Ecologicheskiy Zhurnal*, 10(4), pp. 77–87 (in Russian).
12. Matishov, G.G., Inzhebeikin, Y.I. and Savitskii, R.M., 2013. The Environmental and Biotic Impact of the Oil Spill in Kerch Strait in November 2007. *Water Resources*, 40(3), pp. 271–284. https://doi.org/10.1134/S0097807813020048

13. Zavialov, P.O., Zavialov, I.B., Izhitskiy, A.S., Izhitskaya, E.S., Konovalov, B.V., Krementskiy, V.V., Nemirovskaya, I.A. and Chasovnikov, V.K., 2022. Assessment of Pollution of the Kerch Strait and Adjacent Black Sea Area Based on Field Measurements of 2019–2020. *Oceanology*, 62(2), pp. 162–170. https://doi.org/10.1134/S0001437022020175
14. McNutt, M.K., Camilli, R., Crone, T.J., Guthrie, G.D., Hsieh, P.A., Ryerson, T.B., Savas, O. and Shaffer, F., 2011. Review of Flow Rate Estimates of the Deepwater Horizon Oil Spill. *Proceedings of the National Academy of Sciences USA*, 109(50), pp. 20260–20267. https://doi.org/10.1073/PNAS.1112139108
15. Reddy, C.M., Arey, J.S., Seewald, J.S., Sylva, S.P., Lemkau, K.L., Nelson, R.K., Carmichael, C.A., McIntyre, C.P., Fenwick, J. [et al.], 2012. Composition and Fate of Gas and Oil Released to the Water Column During the Deepwater Horizon Oil Spill. *Proceedings of the National Academy of Sciences USA*, 109(50), pp. 20229–20234. https://doi.org/10.1073/pnas.1101242108
16. Dalyander, P.S., Long, J.W., Plant, N.G. and Thompson, D.M., 2014. Assessing Mobility and Redistribution Patterns of Sand and Oil Agglomerates in the Surf Zone. *Marine Pollution Bulletin*, 80, pp. 200–209. http://doi.org/10.1016/j.marpolbul.2014.01.004
17. Soulsby, R., 1997. *Dynamics of Marine Sands: A Manual for Practical Applications*. London: Thomas Telford, 249 p.
18. Dietrich, J.C., Zijlema, M., Westerink, J.J., Holthuijsen, L.H., Dawson, C., Luettich, R.A., Jensen, R.E., Smith, J.M., G.S. Stelling [et al.], 2011. Modeling Hurricane Waves and Storm Surge using Integrally-Coupled, Scalable Computations. *Coastal Engineering*, 58, pp. 45–65. https://doi.org/10.1016/j.coastaleng.2010.08.001
19. Fomin, V.V., 2017. Numerical Modeling of Wind Waves in the Black Sea Generated by Atmospheric Cyclones. *Journal of Physics: Conference Series*, 899(5), 052005 https://doi.org/10.1088/1742-6596/899/5/052005
20. Ivanov, V.A. and Fomin, V.V., 2010. *Mathematical Modeling of Dynamical Processes in the Sea – Land Area*. Kiev: Akademperiodika, 286 p.
21. Fomin, V.V., Ivancha, E.V. and Polozok, A.A., 2024. Resuspension of Bottom Sediments in a Shallow Lagoon by Currents and Waves Based on the Numerical Modeling Data (Using the Example of Sivash Bay, the Sea of Azov). *Physical Oceanography*, 31(3), pp. 427–445.
22. Fashchuk, D.Ya., Kovalchuk, S.K., Terentiev, A.S., Dubinets, G.A. and Kriskevich, L.V., 2013. Changes in Coastal Zone of Kerch Strait and their Environmental Effects. *Izvestiya Rossiiskoi Akademii Nauk. Seriya Geograficheskaya*, (5), pp. 125–138 (in Russian).
23. Ovsyanyi, E.I., Konovalov, S.K., Kotel'yanets, E.A. and Mitropol'skii, A.Y., 2015. Organic Carbon and Carbonates in the Recent Bottom Sediments of the Kerch Strait. *Geochemistry International*, 53(12), pp. 1123–1133. https://doi.org/10.1134/S0016702915120071
24. Matishov, G., Kleshchenkov, A., Kulygin, V., Berdnikov, S., 2025. [*Accidents and Consequences of Tanker Transport of Mazut (the Kerch Strait 2007, Anapa 2024)*]. Rostov-on-Don: Izdatelstvo YuNTs RAN, 152 p. (in Russian).
25. Michel, J., Owens, E.H., Zengel, S., Graham, A., Nixon, Z., Allard, T., Holton, W., Reimer, P.D., Lamarche, A. [et al.], 2013. Extent and Degree of Shoreline Oiling: Deepwater Horizon Oil Spill, Gulf of Mexico, USA. *PLOS ONE*, 8(6), e65087. https://doi.org/10.1371/journal.pone.0065087
26. Gabche, C.E., Folack, J. and Yongbi, G.C., 1998. Tar Ball Levels on Some Beaches in Cameroon. *Marine Pollution Bulletin*, 36(7), pp. 535–539. https://doi.org/10.1016/S0025-326X(97)00200-2

27. Del Sontro, T.S., Leifer, I., Luyendyk, B.P. and Broitman, B.R., 2007. Beach Tar Accumulation, Transport Mechanisms, and Sources of Variability at Coal Oil Point, California. *Marine Pollution Bulletin*, 54(9), pp. 1461–1471. https://doi.org/10.1016/j.marpolbul.2007.04.022

28. Soulsby, R.L. and Whitehouse, R.J.S., 1997. Threshold of Sediment Motion in Coastal Environments. In: CAE, 1997. *Pacific coasts and ports '97: Proceedings of the 13th Australasian Coastal and Ocean Engineering Conference and the 6th Australasian Port and Harbour Conference, Christchurch, New Zealand, 7–11 September 1997*. Christchurch, N.Z.: Centre for Advanced Engineering, University of Canterbury, Vol. 1, pp. 145–154.

29. Fenton, J.D. and Abbott, J.E., 1977. Initial Movement of Grains on a Stream Bed: the Effect of Relative Protrusion. *Proceedings of the Royal Society of London, Series A, Mathematical and Physical Sciences*, 352(1671), pp. 523–537. https://doi.org/10.1098/rspa.1977.0014

30. Wiberg, P.L. and Smith, J.D., 1987. Calculations of the Critical Shear Stress for Motion of Uniform and Heterogeneous Sediments. *Water Resources Research*, 23(8), pp. 1471–1480. https://doi.org/10.1029/WR023i008p01471

31. Bottacin-Busolin, A., Tait, S.J., Marion, A., Chegini, A. and Tregnaghi, M., 2008. Probabilistic Description of Grain Resistance from Simultaneous Flow Field and Grain Motion Measurements. *Water Resources Research*, 44(9), pp. 1–12. https://doi.org/10.1029/2007WR006224

32. Hemer, M., 2006. The Magnitude and Frequency of Combined Flow Bed Shear Stress as a Measure of Exposure on the Australian Continental Shelf. *Continental Shelf Research*, 26(11), pp. 1258–1280. https://doi.org/10.1016/j.csr.2006.03.011

33. Li, M.Z., Hannah, C.G., Perrie, W.A., Tang, C.C.L., Prescott, R.H. and Greenberg, D.A. 2015. Modelling Seabed Shear Stress, Sediment Mobility, and Sediment Transport in the Bay of Fundy. *Canadian Journal of Earth Sciences*, 52(9), pp. 757–775. https://doi.org/10.1139/cjes-2014-0211

34. Coughlan, M., Guerrini, M., Creane, S., O'Shea, M., Ward, S.L., Van Landeghem, K.J.J., Murphy, J. and Doherty, P., 2021. A New Seabed Mobility Index for the Irish Sea: Modelling Seabed Shear Stress and Classifying Sediment Mobilisation to Help Predict Erosion, Deposition, and Sediment Distribution. *Continental Shelf Research*, 229, 104574. https://doi.org/10.1016/j.csr.2021.104574

Submitted 03.08.2025; accepted after review 21.08.2025;
revised 17.09.2025; published 30.12.2025

*About the authors:*

**Vladimir V. Fomin**, Chief Research Associate, Marine Hydrophysical Institute of RAS (2 Kapitanskaya St., Sevastopol, 299011, Russian Federation), DSc (Phys.-Math.), **ResearcherID: H-8185-2015**, **ORCID ID: 0000-0002-9070-4460**, *fomin.dntmm@gmail.com*

**Ludmila V. Kharitonova**, Senior Research Associate, Marine Hydrophysical Institute of RAS (2 Kapitanskaya St., Sevastopol, 299011, Russian Federation), PhD (Geogr.), **ResearcherID: Y-17802018**, **ORCID ID: 0000-0003-0705-0812**, *l.kharitonova@mhi-ras.ru*

**Dmitry V. Alekseev**, Scientific Secretary, Marine Hydrophysical Institute of RAS (2 Kapitanskaya St., Sevastopol, 299011, Russian Federation), PhD (Phys.-Math.), **ResearcherID: I-3548-2017, ORCID ID: 0000-0003-4006-0967, Scopus Author ID: 8284177400**, *dalexeev@rambler.ru*

**Dmitry I. Lazorenko**, Research Associate, Marine Hydrophysical Institute of RAS (2 Kapitanskaya St., Sevastopol, 299011, Russian Federation), PhD (Tech.), **ResearcherID: J-1925-2015**, **ORCID ID: 0000-0001-7524-565X**, *d.lazorenko.dntmm@gmail.com*

**Aleksandra Yu. Belokon**, Senior Research Associate, Marine Hydrophysical Institute of RAS (2 Kapitanskaya St., Sevastopol, 299011, Russian Federation), PhD (Phys.-Math.), **ResearcherID: M-6839-2018**, **ORCID ID: 0000-0002-1299-0983**, *a.bazykina@mhi-ras.ru*

**Mikhail V. Shokurov,** Leading Research Associate, Marine Hydrophysical Institute of RAS (2 Kapitanskaya Str., Sevastopol, 299011, Russian Federation), DSc (Phys.-Math.), **ResearcherID: V-7160-2017, ORCID ID: 0000-0003-1595-8281,** *shokurov.m@gmail.com*

**Vladislav S. Barabanov**, Senior Research Associate, Marine Hydrophysical Institute of RAS (2 Kapitanskaya St., Sevastopol, 299011, Russian Federation), PhD (Phys.-Math.), **ResearcherID: C-6007-2013**, **ORCID ID: 0000-0002-2689-161X**, *wbarbs@gmail.com*

**Konstantin I. Gurov**, Research Associate, Marine Hydrophysical Institute of RAS (2 Kapitanskaya Str., Sevastopol, 299011, Russian Federation), PhD (Geogr.) **ResearcherID: L-7895-2017**, **ORCID ID: 0000-0003-3460-9650**, **Scopus Author ID: 57200248245**, *gurovki@gmail.com*

**Elena V. Ivancha,** Junior Research Associate, Marine Hydrophysical Institute of RAS (2 Kapitanskaya Str., Sevastopol, 299011, Russian Federation), **ResearcherID: AAG-9265-2020**, **ORCID ID: 0000-0001-8328-4915,** *ev_ivancha@rambler.ru*

**Anton A. Polozok**, Senior Engineer-Programmer, Marine Hydrophysical Institute of RAS (2 Kapitanskaya St., Sevastopol, 299011, Russian Federation), **ResearcherID: ADJ-1790-2022**, **ORCID ID: 0000-0002-0825-8669,** *polozok.umi@gmail.com*

*Contribution of the authors:*

**Vladimir V. Fomin** – task statement, developing a numerical algorithm for calculating the dynamic characteristics of bottom sediments contaminated with mazut, performing numerical experiments, processing simulation results, preparing and editing the article text

**Ludmila V. Kharitonova** – review of literature on the study topic, visualisation of the results of calculations of the mobility ratio and bedload fluxes, analysis and interpretation of modelling results, preparation of illustrations and article text

**Dmitry V. Alekseev** – task statement, reviewing the literature on the study problem, preparing and editing the article text

**Dmitry I. Lazorenko** – creation of an unstructured calculation grid and mathematical modelling of currents, visualisation of calculation results, preparation of illustrations

**Aleksandra Yu. Belokon** – visualisation and analysis of calculation results of wave and current fields, preparation of illustrations, preparation of the article text

**Mikhail V. Shokurov** – modelling of above-surface wind and atmospheric pressure fields, interpretation of results

**Vladislav S. Barabanov** – modelling of above-surface wind and atmospheric pressure fields, visualisation of calculation results

**Konstantin I. Gurov** – analysis of the granulometric composition of bottom sediments in the study area

**Elena V. Ivancha** – collecting material for review, editing the text and formatting the article

**Anton A. Polozok** – visualisation of wave characteristic calculation results

*All the authors have read and approved the final manuscript.*

ISSN 2413-5577, Ecological Safety of Coastal and Shelf Zones of Sea, 2025, No. 4, pp. 53–63.

Original paper

# Black Sea Crimean Shelf Zoning by Temporal Variability of Sea Surface Temperature

**O. A. Lukashova, V. N. Belokopytov** *

*Marine Hydrophysical Institute RAS, Sevastopol, Russia*
* *e-mail: belokopytov.vn@mhi-ras.ru*

**Abstract**
This study analyzes the daily sea surface temperature from the Copernicus database on a grid with a spatial resolution of 0.05° × 0.05°. It calculates the characteristics of total sea surface temperature variability and seasonal variations across multiple temporal scales. A regional synthesis of these characteristics was performed for four areas along the Black Sea coast of the Crimean Peninsula over the 1991–2020 climate period. Characteristics of seasonal and interannual/decadal variability were evaluated using monthly averages, the main part of the synoptic range was evaluated with 10-day averages and the low-frequency part of the mesoscale band was analysed using daily averages. The results show distinct regional patterns. Karkinit Bay differed significantly from the other regions, exhibiting the largest seasonal range and the highest intensity of variability across all bands during winter. The Western region demonstrated the lowest level of temporal variability in all parameters. The Kerch-Feodosia shelf exhibited the highest variability across all bands in autumn. The Southern Coast of Crimea held an intermediate position in terms of temporal variability characteristics between the Western and Kerch-Feodosia regions. Overall, the shelf zone of the Crimean Peninsula shows enhanced regional contrast in sea surface temperature variability across different temporal scales compared to the open Black Sea. One of the primary drivers of these intense water temperature fluctuations is the occurrence of upwelling and downwelling events, which are linked to the variability of wind fields over the region.

**Keywords**: Crimean shelf, sea surface temperature, seasonal variability, interannual variability, mesoscale variability, sub-mesoscale variability

**Acknowledgments**: The work was funded by the state assignment no. FNNN-2024-0014 “Fundamental studies of interaction processes in the sea–air system that form the physical state variability of the marine environment at various spatial and temporal scales”.

**For citation**: Lukashova, O.A. and Belokopytov, V.N., 2025. Black Sea Crimean Shelf Zoning by Temporal Varia bility of Sea Surface Temperature. *Ecological Safety of Coastal and Shelf Zones of Sea*, (4), pp. 53–63.

# Районирование черноморского шельфа Крыма по характеристикам временной изменчивости температуры воды поверхностного слоя

**О. А. Лукашова, В. Н. Белокопытов** *

*Морской гидрофизический институт РАН, Севастополь, Россия*
* *e-mail: belokopytov.vn@mhi-ras.ru*

**Аннотация**
На основе массива ежесуточных спутниковых данных *Copernicus* о температуре поверхности моря на сетке с пространственным разрешением 0.05° × 0.05° рассчитаны характеристики общей интенсивности изменчивости температуры поверхности моря и сезонных вариаций температуры на различных временны́х масштабах. Проведено региональное обобщение этих характеристик по четырем районам черноморского побережья Крымского полуострова за климатический период 1991–2020 гг. Характеристики сезонного хода и межгодовой/десятилетней изменчивости оценивались по среднемесячным значениям, основной части синоптического диапазона – по среднедекадным значениям, а низкочастотной части мезомасштабного диапазона – по среднесуточным значениям. Существенно отличается от остальных районов Каркинитский залив, с максимальным размахом сезонного хода и наибольшей интенсивностью во всех диапазонах изменчивости в зимний период. Западный район по всем параметрам имеет самый низкий уровень временно́й изменчивости. Для Керченско-Феодосийского шельфа осенью характерна наибольшая интенсивность изменчивости во всех диапазонах. Южный берег Крыма по характеристикам временно́й изменчивости занимает промежуточное положение между Западным и Керченско-Феодосийским районами. В целом шельфовая зона Крымского полуострова, в сравнении с открытой частью Черного моря, демонстрирует повышенную региональную контрастность в изменчивости поверхностной температуры воды на различных временны́х масштабах. Одной из причин интенсивных колебаний температуры воды являются апвеллинги и даунвеллинги, связанные с изменчивостью полей ветра в рассматриваемом регионе.

**Ключевые слова**: шельф Крыма, температура поверхности моря, сезонный ход, межгодовая изменчивость, синоптическая изменчивость, мезомасштабная изменчивость

**Благодарности**: работа выполнена в рамках государственного задания ФГБУН ФИЦ МГИ по теме FNNN-2024-0014 «Фундаментальные исследования процессов взаимодействия в системе океан-атмосфера, формирующих изменчивость физического состояния морской среды на различных пространственно-временных масштабах».

**Для цитирования**: *Лукашова О. А., Белокопытов В. Н.* Районирование черноморского шельфа Крыма по характеристикам временной изменчивости температуры воды поверхностного слоя // Экологическая безопасность прибрежной и шельфовой зон моря. 2025. № 4. С. 53–63. EDN XGKJBD.

## Introduction

The distribution of sea surface temperature (SST) fluctuation energy across different bands of temporal variability in seas and oceans exhibits distinct regional characteristics. The most distinct regional differences are observed in the characteristics of seasonal variability, which are governed by the seasonal cycle of the sea surface heat balance. The contribution of other bands of temporal variability to the total variance of SST fluctuations has received much less attention than estimates of the mean seasonal cycle. This is due to the requirement for longer SST data series at fixed locations with greater temporal resolution. However, such data are now becoming available thanks to the development of remote sensing methods that use satellite radiometers operating in the infrared and microwave bands as the primary measurement tools.

Comprehensive monographs based primarily on the data analysis from contact observations provide general information on the intensity of sea water temperature variability across different temporal scales in the Black Sea basin [1–4]. With the advent of satellite data, in addition to seasonal variability, interannual fluctuations and long-term SST trends began to be investigated [4–11]. The improvement of spatial and temporal resolution of satellite measurement tools has made it possible to study higher-frequency processes, such as synoptic variability [12] and the diurnal cycle [13–15]. Results of 20 years of research with the use of remote methods confirmed patterns previously identified from contact observations, showing that the intensity of SST variability decreases in the following order of scales: seasonal, interannual, synoptic, mesoscale. The northwestern and northeastern parts of the Black Sea, where both seasonal and interannual SST variability reach their maximum, stand out from other Black Sea parts.

Assessments of the intensity of sea water temperature variability across different temporal bands have been extremely limited for coastal areas. Only a few coastal marine meteorological stations met the necessary requirements for data series, while the reliability and spatial resolution of satellite data near the shore were insufficient. The emergence of digital datasets for individual seas with a resolution of 0.05° enables to perform more detailed assessments of the distribution of fluctuation energy in the coastal zone across various temporal bands.

This study aims to evaluate regional characteristics of overall intensity of SST variability across different temporal scales in coastal and shelf areas of the Crimean shelf, using a satellite dataset with a high spatial resolution.

## Materials and methods of research

The study used the Black Sea High Resolution L4 Sea Surface Temperature Reprocessed dataset [1)] from the Copernicus Marine Service. This dataset provides daily night-time SST averages referenced to a depth of 20 cm, with a spatial resolution of 0.05° × 0.05°, from 1 January 1982 to the present day [16]. This product

[1)] *Black Sea – High Resolution L4 Sea Surface Temperature Reprocessed* [online]. Available at: https://data.marine.copernicus.eu/product/SST_BS_SST_L4_REP_OBSERVATIONS_010_022/description [Accessed: 15 February 2024]. http://doi.org/10.48670/moi-00160

forms part of the global digital SST dataset created for climate research within the following European projects: the ESA Climate Change Initiative and the Copernicus Climate Change Service. It is based on measurements processed from 22 satellite platforms equipped with infrared (AVHRR, ATSR and SLSTR) and microwave (AMSR) radiometers.

Temporal variability in SST was assessed in four areas of the shelf adjacent to the Black Sea coast of Crimea (Fig. 1):

1) Karkinit Bay, which is a constituent part of the extensive northwestern shelf with its own specific hydrological regime;

2) the Western Crimea shelf, which extends from Cape Tarkhankut to Cape Chersonesus and represents a transitional zone between the northwestern shelf and the deep-water part of the Black Sea;

3) the Southern Coast of Crimea, which is characterised by conditions similar to those in the central part of the sea and is directly influenced by the Rim Current (Main Black Sea Current);

4) the Eastern Crimea shelf (Kerch-Feodosia shelf), which extends from Cape Meganom to Anapa and is affected by water exchange with the Sea of Azov, as well as by the Rim Current, which changes direction along the Caucasian coast towards the Crimean Peninsula.

The period from 1991 to 2020 was selected for the calculations as it corresponds to the most recent climate period defined by the World Meteorological Organization (WMO). It is also used as the climate norm when processing this SST dataset.

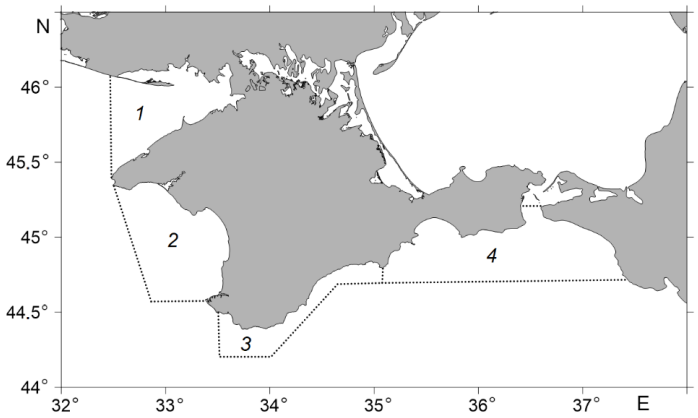


Fig. 1. Crimean shelf regions division by oceanographic conditions: *1* – Karkinit Bay, *2* – Western Region, *3* – Southern Coast of Crimea, *4* – Kerch-Feodosia Region

Ten-day and monthly averages were calculated for each year from daily data for each grid node. Then, using selected time series, the following variances were calculated:

– variance of daily averages for 365 calendar days;

– variance of 10-day averages for 370 calendar days;

– variance of monthly averages for 12 calendar months.

The overall level of interannual and decadal variability corresponded to the variance of the monthly averages, which were then averaged over the year. The variances of 10-day averages, which characterise synoptic variability to a certain extent (periods ranging from days to a month), were averaged over 12 months and for the full year. Similarly, the variances of daily averages, representing the low-frequency part of the mesoscale band (periods ranging from hours to days), were averaged over 12 months and for the full year. Seasonal variability was assessed from the mean seasonal cycle, namely mean standard deviation and range of the monthly averages, averaged over the selected 30-year period. All resulting mean fields of the calculated temporal variability characteristics were smoothed using a Gaussian filter with a radius of five grid nodes.

The results were compared with those from other studies [11, 12], which used an earlier version of the Black Sea High Resolution L4 Sea Surface Temperature Reprocessed dataset with a spatial resolution of 0.04° × 0.04° [17]. This dataset was based on AVHRR Pathfinder Version 5.2 (PFV52) and covered the periods 1982–2014 and 1982–2018.

**Results and discussion**

The Black Sea, including its shelf zone, is characterised by a large amplitude of seasonal variability in SST, which exceeds temporal variability on other scales significantly [1–12]. The range of the seasonal cycle increases sharply in the shallow northern areas of the sea that are prone to freezing, reaching a maximum of 22°C in Karkinit Bay (Fig. 2). Conversely, the minimum seasonal range in the Black Sea, which is less than 17°C, is observed in the Kerch-Feodosia region and near the south-western tip of Crimea. This is connected with the warming effect of the Rim Current during winter. Another example of a minimum in the seasonal range in the Black Sea is found off the Sinop Peninsula, where persistent summer upwelling causes the lowest values.

Quantitative values and spatial distribution of mean standard deviation of seasonal variability are in good agreement with the results of [11], despite differences in the averaging period, set of satellite platforms, reference depth of SST and L4 processing algorithms.

As previously noted in [3, 11], the next most intense component after seasonal variability is interannual variability. Its mean standard deviation is much smaller than that of the seasonal component. Using this calculation method, the contribution of lower-frequency fluctuations, such as decadal (10-year) and interdecadal variability, increases as the averaging period increases within this range. The next most significant components, in order of decreasing intensity, are 10-day variability (conditionally synoptic) and daily variability (conditionally mesoscale),

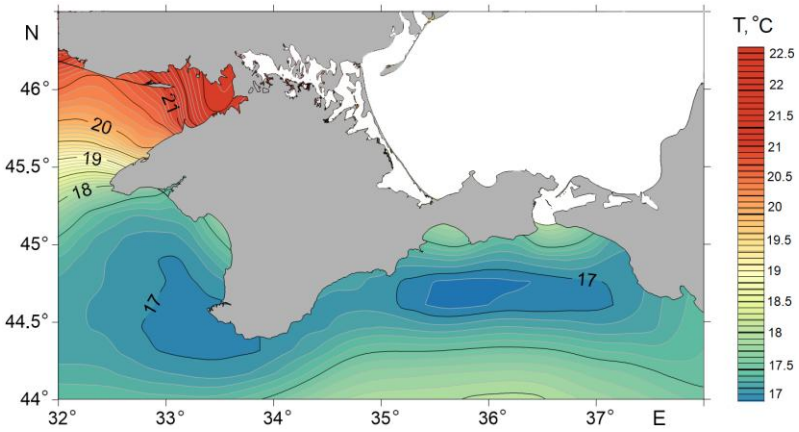


Fig. 2. Mean season range of the sea surface temperature in the Black Sea near the Crimean coast in 1991–2020

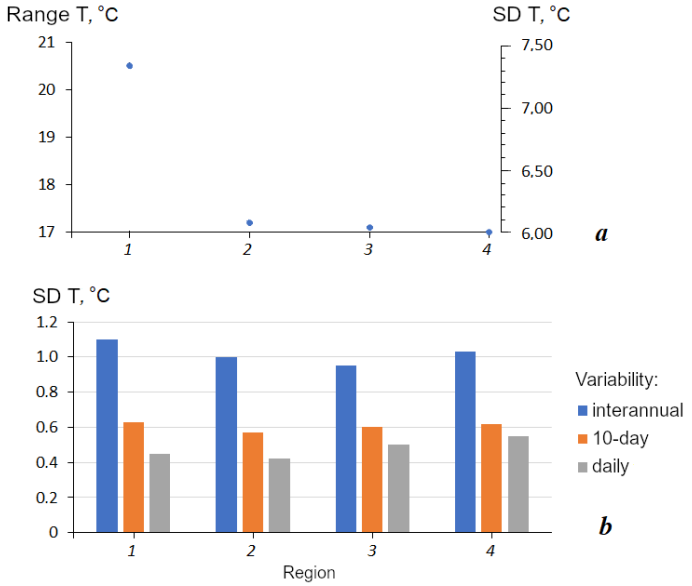


Fig. 3. Mean standard deviations of seasonal, interannual, 10-day and daily variability of sea surface temperature for four Crimean shelf regions in 1991–2020. Digits stand for region numbers (see Fig.1)

which are twice and four times weaker than interannual variability, respectively. The ratio of different SST variability bands exhibits its own regional characteristics in each of the studied areas (Fig. 3).

The spatial distributions of interannual and 10-day variability exhibit a qualitatively similar pattern (Fig. 4). The main difference from the seasonal cycle spatial distribution is the emergence of a new maximum in the Kerch Strait area and the reduction of the zone of maximum values in Karkinit Bay. When considering the higher-frequency part of the spectrum (i. e. daily variability), a minimum appears in the southwestern region (i. e. Kalamita Bay) (Fig. 5).

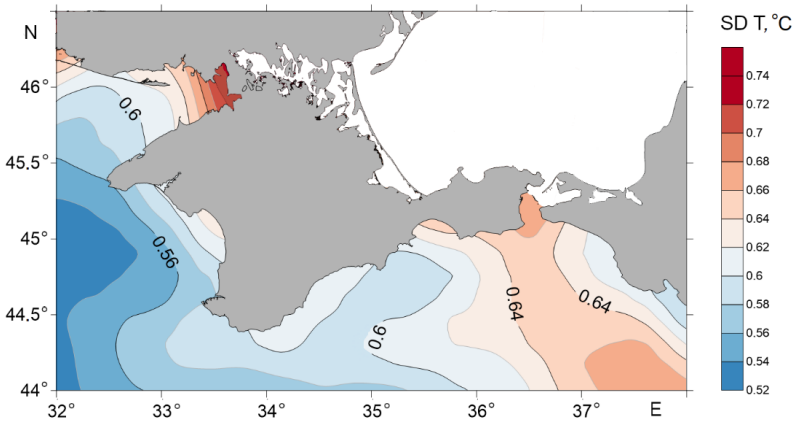


Fig. 4. Mean standard deviation of 10-day variability of sea surface temperature near the Crimean coast in 1991–2020

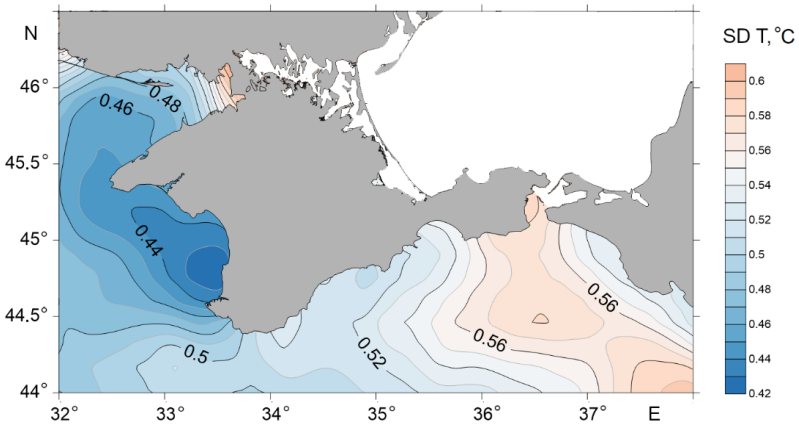


Fig. 5. Mean standard deviation of daily SST variability near the Crimean coast in 1991–2020

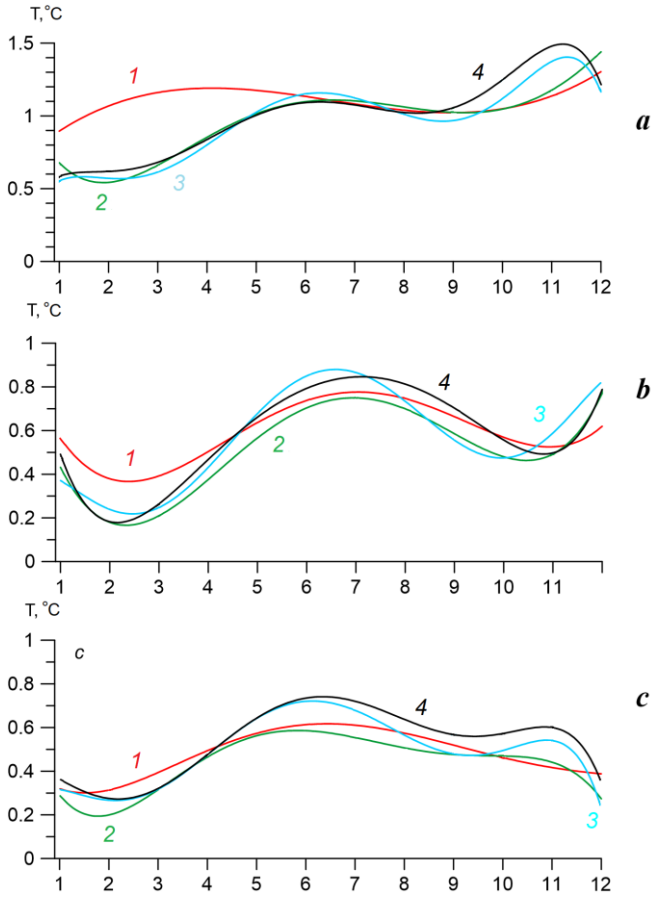


Fig. 6. Seasonal variability of mean standard deviations for sea surface temperature: interannual (*a*), 10-day (*b*) and daily (*c*) in 1991–2020. Digits stand for region numbers (see Fig. 1)

The spatial distribution of mean standard deviation of interannual SST variability is qualitatively consistent with the results of [11], but the quantitative estimates in this study are, on average, 10% lower. These differences are due not only to the use of different SST datasets, but also to discrepancies in the methods employed to evaluate variability across various time periods. Direct quantitative comparison with data from [12], which is dedicated to synoptic SST variability, is not feasible. In that study, variability was estimated over intramonthly intervals, thereby including fluctuation contribution from a broader frequency range. Consequently, the total variance for the 10-day and daily bands combined (Figs. 4 and 5) is 1.5–2 times lower than the values reported in [12]. However, the spatial patterns of 10-day variability remain qualitatively similar (Fig. 4).

Analysis of the seasonal variation in SST intensity revealed common patterns across all four regions (Fig. 6), as well as distinct regional features. All regions share a primary minimum in the intensity of fluctuations across all bands during winter and early spring, as well as a less pronounced local minimum in early autumn. The variability maximum occurs in summer and late autumn, with the autumn peak being more pronounced for interannual variability. Karkinit Bay is an exception, as it exhibits a relatively flat seasonal cycle of interannual fluctuations. Unlike the other areas, these fluctuations reach their maximum intensity in winter.

Temperature variations during the summer and autumn period are more intense in the Kerch–Feodosia region than in other areas, peaking in early summer along the SCC. The lowest values across all temporal variability bands are recorded in southwestern Crimea.

The seasonal pattern of interannual variability in the northeastern part of the sea, near the Kerch Strait, is in quantitative and qualitative agreement with the data from [11]. However, noticeable differences were found on the SCC: the present study recorded the maximum in autumn, whereas it was recorded in summer in [11]. Significant differences were also revealed in terms of synoptic variability. In [12], two distinct maxima were noted, in May and October. However, according to our data, the main maximum shifts to June, with October characterised as a local minimum.

**Conclusion**

The temporal variability characteristics of SST in the shelf areas along the Black Sea coast of Crimea were calculated using daily averages from the Black Sea High Resolution L4 Sea Surface Temperature Reprocessed dataset, with a spatial resolution of 0.05° × 0.05°, over the WMO 1991–2020 climate period.

Of four investigated regions, which are distinguished by their oceanographic characteristics, Karkinit Bay exhibits the most pronounced variability. This region is characterised by the largest seasonal range of SST and the highest intensity of variability (especially interannual) across all temporal bands during the winter period, which is particularly evident at the interannual scale. This type of interannual fluctuation regime is typical of shallow, ice-prone areas of the northwestern shelf, and is driven by sharp alternations between unusually warm and cold winters.

Conversely, the western region, which is adjacent to Karkinit Bay, exhibits the lowest level of temporal SST variability of all the areas of the Crimean shelf that were studied. In winter, the Rim Current warming influence reduces the seasonal temperature range significantly, while the Sevastopol anticyclone favours the accumulation and spread of warmer waters over the shelf. The low intensity of higher-frequency SST fluctuations is generally caused by weak water circulation in this area.

The Kerch–Feodosia region experiences the greatest SST variability across all bands in autumn, due to increased atmospheric synoptic activity in the northeastern part of the Black Sea and the exchange of water with the rapidly cooling Sea of Azov.

Conversely, this region exhibits the lowest seasonal range of SST due to the Rim Current warming effect in winter.

The characteristics of temporal SST variability along the SCC occupy an intermediate position between those of the Western region and the Kerch–Feodosia region. However, the seasonal range is larger here due to the absence of quasi-stationary anticyclonic eddies such as the Kerch and Sevastopol ones. These eddies promote the spread of Rim Current waters across the shelf area. Consequently, the Rim Current warming effect is largely confined to its core jet, rather than extending over the shelf. The summer peak in daily and 10-day variability is associated with frequent upwelling and downwelling events driven by variability in the wind field.

Overall, the Crimean shelf zone is characterised by increased spatial contrast in both overall intensity and seasonal variations of SST across different temporal scales. These parameters are therefore highly effective for categorising the region waters.

## REFERENCES


1. Blatov, A.S., Bulgakov, N.P., Ivanov, V.A., Kosarev, A.N. and Tuljulkin, V.S., 1984. *Variability of the Black Sea Hydrophysical Fields*. Leningrad: Gidrometeoizdat, 240 p. (in Russian).
2. Simonov, A.I. and Altman, E.N, eds., 1991. *Hydrometeorology and Hydrochemistry of Seas in the USSR. Vol. IV. Black Sea. Issue 1*. [*Hydrometeorological Conditions*]. Saint Petersburg: Gidrometoizdat, 432 p. (in Russian).
3. Ivanov, V.A. and Belokopytov, V.N., 2013. *Oceanography of the Black Sea*. Sevastopol: ECOSI-Gidrofizika, 210 p.
4. Ilyin, Yu.P., Repetin, L.N., Belokopytov, V.N., Goryachkin, Yu.N., Dyakov, N.N., Kubryakov, A.A. and Stanichny, S.V., 2012. *Hydrometeorological Conditions of the Ukrainian Seas. Vol. 2. The Black Sea*. Sevastopol: ECOSI-Gidrofizika, 421 p. (in Russian).
5. Ginzburg, A.I., Kostianoy, A.G. and Sheremet, N.A., 2001. On Use of Satellite Data for Studying Seasonal And Interannual Variability of the Black Sea Surface Temperature. *Issledovanie Zemli iz Kosmosa*, (1), pp. 51–61 (in Russian).
6. Ginzburg, A.I., Kostianoy, A.G. and Sheremet, N.A., 2004. Seasonal and Interannual Variability of the Black Sea Surface Temperature as Revealed from Satellite Data (1982–2000). *Journal of Marine Systems*, 52(1–4), pp. 33–50. http://doi.org/10.1016/j.jmarsys.2004.05.002
7. Ginzburg, A.I., Kostianoy, A.G. and Sheremet, N.A., 2008. Sea Surface Temperature Variability. In: A.G. Kostianoy, A.N. Kosarev, eds. *The Black Sea Environment. The Handbook of Environmental Chemistry*. Berlin, Heidelberg: Springer-Verlag. Vol. 5Q, pp. 255–275. https://doi.org/10.1007/698_5_067
8. Ginzburg, A.I., Kostianoy, A.G. and Sheremet, N.A., 2008. [Long-Term Variability of the Black Sea Surface Temperature and its Response to Global Atmospheric Effects]. *Sovremennye Problemy Distantsionnogo Zondirovaniya Zemli iz Kosmosa*, 5(2), pp. 76–83 (in Russian).
9. Artamonov, Yu.V., Babiy, M.V. and Skripaleva, E.A., 2005. [Regional Features of Interannual Variability of the Temperature Field on the Surface of the Black Sea]. In: MHI, 2005. *Monitoring Systems of Environment*. Sevastopol: ECOSI-Gidrofizika, Iss. 8, p. 240 (in Russian).

10. Artamonov, Yu.V., Belokopytov, V.N. and Skripaleva, E.A., 2012. [Features of Variability in Hydrological and Bio-Optical Characteristics on the Surface of the Black Sea Based on Satellite and *In Situ* Measurements]. In: V. N. Eremeev and S. K. Konovalov, eds., 2012. [*Stability and Evolution of Oceanographic Characteristics of the Black Sea Ecosystem*]. Sevastopol: ECOSI-Gidrofizika, pp. 88–115 (in Russian).
11. Artamonov, Y.V., Skripaleva, E.A. and Fedirko, A.V., 2017. Regional Features of Long-Term Variability of the Black Sea Surface Temperature. *Russian Meteorology and Hydrology*, 42(2), pp. 105–112. https://doi.org/10.3103/S1068373917020042
12. Artamonov, Yu.V., Skripaleva, E.A. and Fedirko, A.V., 2020. Regional Features of the Temperature Field Synoptic Variability on the Black Sea Surface from Satellite Data. *Physical Oceanography*, 27(2), pp. 186–196. https://doi.org/10.22449/1573-160X-2020-2-186-196
13. Rubakina, V.A., Kubryakov, A.A. and Stanichny, S.V., 2019. Seasonal Variability of the Diurnal Cycle of the Black Sea Surface Temperature from the SEVIRI Satellite Measurements. *Physical Oceanography*, 26(2), pp. 157–169. https://doi.org/10.22449/1573-160X-2019-2-157-169
14. Rubakina, V.A., Kubryakov, A.A. and Stanichny, S.V., 2019. Seasonal and Diurnal Cycle of the Black Sea Water Temperature from Temperature-Profiling Drifters Data. *Sovremennye Problemy Distantsionnogo Zondirovaniya Zemli iz Kosmosa*, 16(5), pp. 268–281 (in Russian).
15. Rubakina, V.A., Kubryakov, A.A. and Stanichny, S.V., 2021. Characteristics of Seasonal and Diurnal Variability of the Thermal Skin Layer Based on Comparison of Satellite Measurements of SEVIRI and Temperature-Profiling Drifters Data. *Issledovanie Zemli iz Kosmosa*, (3), pp. 30–44 (in Russian).
16. Merchant, C.J., Embury, O., Bulgin, C.E., Block, T., Corlett, G.K., Fiedler, E., Good, S.A., Mittaz, J., Rayner, N.A. [et al.], 2019. Satellite-Based Time-Series of Sea-Surface Temperature since 1981 for Climate Applications. *Scientific Data*, 6, 223. https://doi.org/10.1038/s41597-019-0236-x
17. Nardelli, B.B., Colella, S., Santoleri, R., Guarracino, M. and Kholod, A., 2010. A Re-Analysis of Black Sea Surface Temperature. *Journal of Marine Systems*, 79(1–2), pp.50–64. http://doi.org/10.1016/j.jmarsys.2009.07.001

Submitted 05.03.2025; accepted after review 26.05.2025;
revised 17.09.2025; published 30.12.2025

*About the authors:*

**Oksana A. Lukashova**, Senior Research Engineer, Marine Hydrophysical Institute of RAS (2 Kapitanskaya St., Sevastopol, 299011, Russian Federation), *luk_ok@mail.ru*

**Vladimir N. Belokopytov**, Leading Research Associate, Head of Oceanography Department, Marine Hydrophysical Institute of RAS (2 Kapitanskaya St., Sevastopol, 299011, Russian Federation), DSc (Geogr.), **ORCID ID: 0000-0003-4699-9588, ResearcherID: ABA-1230-2020, Scopus Author ID: 6602381894**, *belokopytov.vn@mhi-ras.ru*

*Contribution of the authors:*

**Oksana A. Lukashova** – literature review, calculations, preparation of graphical materials, analysis and interpretation of the results

**Vladimir N. Belokopytov** – study tasks statement, formation of the article structure, analysis and interpretation of the results

*All the authors have read and approved the final manuscript.*

ISSN 2413-5577, Ecological Safety of Coastal and Shelf Zones of Sea, 2025, No. 4, pp. 64–75.

Original paper

# Theoretical Calculations of Sea Surface Elevation Excess Kurtosis

**A. V. Garmashov, A. S. Zapevalov ***

*Marine Hydrophysical Institute of RAS, Sevastopol, Russia*
* *e-mail: sevzepter@mail.ru*

**Abstract**
The excess kurtosis of sea surface elevation is a predictor of rogue waves. This paper verifies the dependencies of excess kurtosis on wave steepness ε and inverse wave age ζ, obtained for the JONSWAP wave spectrum. For verification, the paper uses data from *in situ* wave measurements conducted from a stationary oceanographic platform located in the coastal zone of the Black Sea. It is shown that in a real sea wave field, the excess kurtosis changes within significantly wider limits than those described by both model dependencies. The correlation coefficient between $\lambda_4^E$ and ε is 0.06, and between $\lambda_4^E$ and ζ is 0.05. The model dependence of $\lambda_4^E$ on steepness ε is close to the linear regression constructed for wind waves, i. e., it allows describing only its average changes. The model dependence of excess kurtosis on inverse wave age overestimates its average values; the overestimation is approximately 0.1 and depends on ζ. Thus, the dependencies of the excess kurtosis of sea surface elevation on wave steepness and inverse wave age, constructed on the basis of the JONSWAP spectrum, do not allow describing the entire range of excess kurtosis changes in a real wave field. Rogue waves are observed in the sea when $\lambda_4^E$ exceeds the threshold level of 0.6–0.7, while the maximum model values of excess kurtosis at the limiting Stokes wave steepness do not exceed the level of 0.3.

**Keywords**: wind wave modelling, excess kurtosis, surface wave spectrum, wave steepness, inverse wave age, Black Sea, JONSWAP spectrum, rogue waves

**Acknowledgments**: The work was carried out under state assignment FNNN-2024-0001 “Fundamental research of the processes determining the flows of matter and energy in the marine environment and at its borders, the state and evolution of the physical and biogeochemical structure of marine systems in modern conditions” and FNNN-2024-0014 “Fundamental studies of interaction processes in the sea–air system that form the physical state variability of the marine environment at various spatial and temporal scales”.

**For citation**: Garmashov, A.V. and Zapevalov, A.S., 2025. Theoretical Calculations of Sea Surface Elevation Excess Kurtosis. *Ecological Safety of Coastal and Shelf Zones of Sea*, (4), pp. 64–75.

# Теоретические расчеты эксцесса возвышений морской поверхности

**А. В. Гармашов, А. С. Запевалов ***

*Морской гидрофизический институт РАН, Севастополь, Россия*
* *e-mail: sevzepter@mail.ru*

**Аннотация**
Эксцесс возвышений морской поверхности является предиктором возникновения аномально высоких волн. В работе верифицируются полученные для волнового спектра *JONSWAP* зависимости эксцесса от крутизны ε и от обратного возраста волн ζ. Для верификации используются данные прямых волновых измерений, проведенных со стационарной океанографической платформы, установленной в прибрежной зоне Черного моря. Показано, что в реальном поле морских волн эксцесс $\lambda_4^E$ изменяется в значительно более широких пределах, чем предсказывается обеими модельными зависимостями. Коэффициент корреляции между $\lambda_4^E$ и ε равен 0.06, между $\lambda_4^E$ и ζ – 0.05. Модельная зависимость обратного возраста волн $\lambda_4^E$ от крутизны ε близка к линейной регрессии, построенной для ветровых волн, то есть позволяет описать только его средние изменения. Модельная зависимость эксцесса от обратного возраста волн завышает его средние значения приблизительно на 0.1, причем завышение зависит от ζ. Таким образом, построенные на основе спектра *JONSWAP* зависимости эксцесса возвышений морской поверхности от крутизны волн и обратного возраста волн не позволяют описать весь диапазон изменчивости эксцесса в реальном волновом поле. Аномальные волны наблюдаются в море при превышении $\lambda_4^E$ порогового уровня 0.6–0.7, тогда как максимальные модельные значения эксцесса при предельной крутизне волны Стокса не превышают уровень 0.3.

**Ключевые слова**: моделирование ветровых волн, эксцесс, спектр поверхностных волн, крутизна волн, обратный возраст волн, Черное море, спектр *JONSWAP*, аномальные волны

**Благодарности**: работа выполнена в рамках государственного задания ФГБУН ФИЦ МГИ по теме FNNN-2024-0001 «Фундаментальные исследования процессов, определяющих потоки вещества и энергии в морской среде и на ее границах, состояние и эволюцию физической и биогеохимической структуры морских систем в современных условиях» и FNNN-2024-0014 «Фундаментальные исследования процессов взаимодействия в системе океан-атмосфера, формирующих изменчивость физического состояния морской среды на различных пространственно-временных масштабах».

**Для цитирования**: *Гармашов А. В., Запевалов А. С.* Теоретические расчеты эксцесса возвышений морской поверхности // Экологическая безопасность прибрежной и шельфовой зон моря. 2025. № 4. С. 64–75. EDN VCOCEY.

## Introduction

The number of global and regional spectral wave models of the sea surface has increased and the quality of forecasts produced by these models has improved [1]. Verification against *in situ* and remote sensing data demonstrates that these models represent significant wave height accurately [2–4].

A linear wave field obeys Gaussian statistics and, under the additional assumption of a narrow-band wave spectrum, the wave height distribution follows the Rayleigh distribution [5, 6]. Sea waves are a weakly nonlinear process whose cumulants deviate from zero values [7–10]. The deviation of the wave height distribution induced by nonlinearity is small for most of the distribution; however, it is significant for the tail of the distribution and is therefore of great importance for predicting the occurrence of rogue waves [11].

Rogue waves are typically characterized by the abnormality index (*AI*) which is the ratio of the maximum wave height recorded during the measurement period to the significant wave height. A wave is considered rogue if $AI > 2$ [12]. Studies conducted in various regions of the World Ocean have shown that *AI* statistically depends only on the excess kurtosis of sea surface elevation [13–15]. These studies suggest that excess kurtosis could be used to predict the probability of rogue waves occurring, which has led to the development of methods for calculating it based on spectral wave models [16–18]. The representation of excess kurtosis in the form of multidimensional integrals of wave spectra is used for these calculations [19, 20].

The study [1)] proposes simple parameterizations for the dependence of statistical moments of surface elevations on the wave field development stage. These parameterizations have various applications, including operational wave forecasting. They are derived under the same assumptions as those underpinning the kinetic equation in spectral wave models. However, the situations in which these parameterizations are applicable, as well as the feasibility of calculating excess kurtosis within spectral models, require further discussion.

This study aims to verify the relationship between excess kurtosis, wave steepness and inverse wave age, as obtained from the JONSWAP wave spectrum.

## Methods and materials

*Excess kurtosis.* The higher order cumulants of a random variable serve as a measure of how much its distribution deviates from a Gaussian distribution. The fourth order cumulant, or excess kurtosis, is related to the statistical moments by the following expression:

$$\lambda_4 = \frac{\mu_4}{\mu_2^2} - 3,$$

where $\mu_2$, $\mu_4$ are the central statistical moments of the second and fourth orders, respectively.

---

[1)] Janssen, P.A.E.M. and Bidlot, J.R., 2009. *On the Extension of the Freak Wave Warning System and its Verification*. ECMWF Technical Memoranda; 588. ECMWF, 42 p. https://doi.org/10.21957/uf1sybog

Studies [17, 19] developed an approach for calculating third and fourth order cumulants directly from known wave spectra. The wave spectrum derived from the Joint North Sea Wave Project (JONSWAP) remains the most widely used representation of the sea surface. The project was designed to investigate the generation and evolution of wind-driven waves in the North Sea [21, 22]. One of its key outcomes was the development of an empirical frequency-angular spectrum for the surface wave field. The two-dimensional JONSWAP frequency-angular spectrum takes the following form:

$$E(\omega,\theta) = 4\pi^2 \frac{\alpha g^2}{\omega^5}\left(\frac{\omega}{\omega_p}\right)\exp\left[-\frac{5}{4}\left(\frac{\omega}{\omega_p}\right)^2\right]\gamma^{\exp\left[-\left(\frac{\omega}{\omega_p}-1\right)^2 \Big/ \left(2\sigma^2\right)\right]}\Theta(\theta), \quad (1)$$

where ω is angular frequency; α is parameter that determines the wave energy; $g$ is gravitational acceleration; γ and σ are parameters that determine the shape of the spectrum; Θ(θ) is angular distribution function of wave energy; θ is azimuthal angle. Here and subsequently, index $p$ indicates that the given parameter corresponds to the peak frequency of the wave spectrum.

Parameter $\sigma$ has two fixed values: σ = 0.07 when the condition $\omega < \omega_p$ is satisfied and σ = 0.09 otherwise. Therefore, the one-dimensional spectrum depends on two parameters α and γ. The value of α, which determines the wave energy, is proportional to the square of the wave steepness ε:

$$\varepsilon = k_p\sqrt{\mu_2},$$

where $k$ is the wave number. Accordingly, the steepness can be estimated by knowing the spectrum parameters (formula (1)). Parameters $\omega_p$ and $k_p$ are related to each other by the dispersion relation for gravity waves in deep water, $\omega^2 = gk$. Parameter γ determines the excess in the spectral peak region relative to the Pierson – Moskowitz spectrum [23].

A two-parameter equation has been proposed for the JONSWAP spectrum based on the approach developed in [17, 19, 20], which relates the cumulants of sea surface elevations to the wave spectrum. This equation allows the excess kurtosis to be calculated [1)]:

$$\lambda_4^{SJ} = 12.6\,\gamma^{-0.328}\varepsilon^2. \quad (2)$$

Here and thereafter, the superscript *SJ* indicates that the given parameter has been calculated for the JONSWAP spectrum. Equation (2) was derived for cases where the angular distribution function Θ(θ) is specified in the following form:

$$\Theta(\theta) = \frac{1}{2}\beta\,\mathrm{sech}^2(\beta\theta), \quad (3)$$

where

$$\beta = \begin{cases} 261\left(\omega/\omega_p\right)^{1.3} & \text{at } 0.56 \le \omega/\omega_p < 0.95, \\ 228\left(\omega/\omega_p\right)^{-1.3} & \text{at } 0.95 \le \omega/\omega_p < 1.6, \\ 1.24 & \text{at } 1.6 < \omega/\omega_p. \end{cases} \quad (4)$$

The mean direction of wave propagation is defined as the angle θ = 0 in equation (3).

To calculate the dependence of excess kurtosis on the wave field development stage, a modified JONSWAP spectrum was employed in [1] [24]. The parameters of this spectrum (also known as the Donelan spectrum) are explicit functions of the inverse wave age:

$$\zeta = U_{10} / C_p,$$

where $U_{10}$ is wind speed at a height of 10 m; $C_p$ is phase speed. Higher values of $\zeta$ correspond to an earlier stage of wave development. A fully developed wind sea corresponds to $\zeta_0 = 0.83$; for $\zeta > \zeta_0$, the waves are considered wind-driven, whereas for $\zeta < \zeta_0$, they are classified as swell.

The Donelan spectrum has the form

$$E_D(\omega,\theta) = 4\pi^2 \frac{\alpha_D g^2}{\omega^5}\left(\frac{\omega}{\omega_p}\right)\exp\left[-\left(\frac{\omega}{\omega_p}\right)^2\right]\gamma_D^{\exp\left[-\left(\frac{\omega}{\omega_p}-1\right)^2 \Big/ \left(2\sigma^2\right)\right]}\Theta(\theta), \quad (5)$$

where

$$\alpha_D = 0.006\,\zeta^{0.55} \quad \text{at} \quad 0.83 < \zeta < 5,$$

$$\sigma_D = 0.08\,(1 + 4/\zeta^3) \quad \text{at} \quad 0.83 < \zeta < 5,$$

$$\gamma_D = \begin{cases} 1.7 & \text{at} \quad 0.83 < \zeta < 1, \\ 1.7 + 6.0\lg\zeta & \text{at} \quad 1 < \zeta < 5. \end{cases}$$

The following dependence [1] has been obtained for the Donelan spectrum and the angular distribution function in the form of equations (3) and (4):

$$\lambda_4^{SD} = 0.04 + 0.082\,\zeta^{0.87}, \quad (6)$$

where the superscript *SD* indicates that the excess kurtosis has been calculated using the Donelan spectrum. The accuracy of model (6) largely depends on how well wave spectrum (5) captures the dependence on inverse wave age. A previous analysis compared wind wave spectra with the Donelan spectrum based on measurements from an oceanographic platform under conditions of variable wind speed and strong swell [25]. This analysis showed that, on average, the dependencies of spectral parameters on wave age obtained under different conditions align with the formulas derived for a pure wind sea under stable wind conditions.

*Data and measurement conditions.* We use data from wave measurements conducted on the stationary oceanographic platform operated by Marine Hydrophysical Institute of RAS to verify the relationships describing the dependence of excess kurtosis on wave steepness and inverse wave age. The platform is located in the coastal zone of the Black Sea, off the southern coast of Crimea. The minimum distance from the platform to the shoreline is approximately 600 m, with the water depth at the site around 30 m. Wave measurements were performed using a resistive wave gauge consisting of a nichrome wire wound with constant pitch on a supporting cable. Wind speed was measured with a cup anemometer [26].

Wave measurements were conducted from May 2018 to January 2019. For the analysis, continuous records were divided into 20-minute segments and statistical characteristics of waves and wind speed were calculated for each segment. The conditions for conducting wave measurements on the stationary oceanographic platform are described in [9, 10]. The wind regime in the vicinity of the platform was analysed in [27].

During the measurement period, the significant wave height $H_s$ reached 2.3 m and the mean wind speed at 10 m height ($U_{10}$) reached 26 m/s. Wave steepness ε and inverse wave age ζ ranged from $0 < \varepsilon < 0.14$ and $0 < \zeta < 6.3$, respectively. Value $\zeta = 0$ corresponds to wind speeds below the anemometer startup threshold. High values of ζ were observed under short-fetch conditions, which corresponded to onshore winds.

**Results and discussion**

Two components of nonlinearity that cause deviations from the Gaussian distribution in a random wave field have been identified [17]. The first component, arising from nonlinear inter-wave interactions, is referred to as "dynamic" as it is associated with the evolution of the wave field. The second component is related to the presence of bound waves in the field. The term "bound components" includes Stokes wave harmonics, as well as all harmonics generated by nonlinear inter-wave interactions that do not satisfy the linear dispersion relation [1)].

In the general case of a broadband random wave field, the dynamic contribution to excess kurtosis is small in absolute value and negligible compared to the contribution of bound components [17]. We can compare relation (6) obtained within the spectral wave model framework, with the dependence of excess kurtosis on wave steepness, as obtained within the second order nonlinear model. In this model, the deviation from Gaussian distribution is determined by bound components [28].

The second order nonlinear model is built up from a combination of linear and nonlinear elements:

$$\eta(x,t) = \eta_L(x,t) + \eta_N(x,t),$$

where η is sea surface elevation; $x$ is spatial coordinate; $t$ is time;

$$\eta_L(x,t) = \sum_{n=1}^{\infty} a_n \cos\psi_n,$$

$$\eta_N(x,t) = \sum_{m=1}^{\infty}\sum_{n=1}^{\infty}\left\{ a_n a_n \left[ B_{mn}^{-}\cos(\psi_m - \psi_n) + B_{mn}^{+}\cos(\psi_m + \psi_n)\right]\right\},$$

$\psi_n = k_n x - \omega_n t + \varphi_n$, $\varphi_n$ is the phase; $B_{mn}^{-}$ and $B_{mn}^{+}$ are second order transfer functions. Functions $B_{mn}^{-}$ and $B_{mn}^{+}$ are derived from the Laplace equation for the velocity potential, subject to nonlinear boundary conditions. The model includes second order bound waves arising from interactions of free wave components.

According to the second order nonlinear model, excess kurtosis is related to wave steepness through the equation provided in [28].

$$\lambda_4^N = 12\,\varepsilon^2 + O(\varepsilon^4). \quad (7)$$

Unlike relation (7), dependence (2) does not assume a one-to-one correspondence between excess kurtosis and wave steepness. When the wave field approaches a fully developed state, the average value of $\gamma \approx 1.7$; higher values of $\gamma$ correspond to earlier stages of development. Within the observed range of $\gamma$, the inequality $\lambda_4^N > \lambda_4^{SJ}$ holds. This discrepancy increases with increasing $\gamma$.

Fig. 1 shows the dependence of excess kurtosis on wave steepness for wind waves, as determined from measurements in the coastal zone of the Black Sea, as well as theoretical dependencies (2) and (7). The dependencies $\lambda_4^N = \lambda_4^{SJ}(\varepsilon)$ were constructed for two values of the parameter $\gamma$: 1.7 and 3.3. As evident from the figure, the discrepancies between the theoretical dependencies are considerably smaller than the scatter in the measured excess kurtosis values. Fig. 1 also presents the linear regression:

$$\lambda_4^E = 0.94\,\varepsilon + 0.01 \pm 0.21 \quad (8)$$

and the regression in the form $\lambda_4^E = \alpha^E \varepsilon^2$. Coefficient $\alpha^E$ is 19.5.

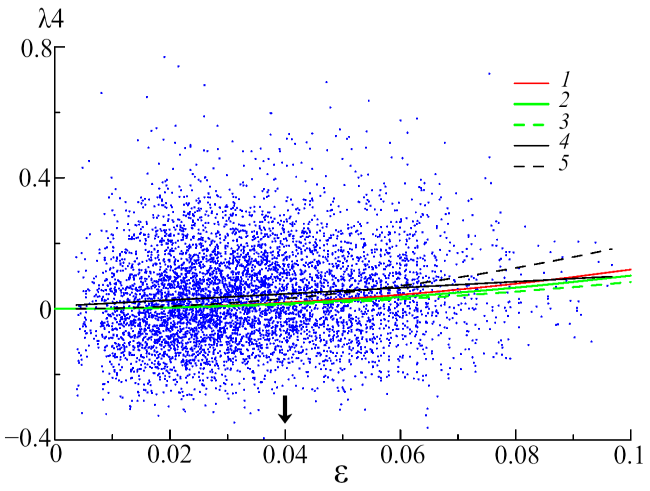


F i g . 1 . Dependency of excess kurtosis $\lambda_4$ on steepness $\varepsilon$. The dots are experimental data; curve 1 is dependency (7), curves 2 and 3 are dependencies (2) obtained at $\gamma = 1.7$ and $\gamma = 3.3$; curve 4 is linear regression (8); curve 5 is regression in the form of $\lambda_4^E = \alpha^E \varepsilon^2$. The arrow shows the steepness calculated for the Pierson–Moskowitz spectrum

The fully developed wind sea spectrum is typically represented by the Pierson – Moskowitz spectrum [23]. The characteristic steepness value for this spectrum $\varepsilon_{PM} = 0.04$ is shown by the arrow in Fig. 1.

The correlation coefficient between $\lambda_4^E$ and $\varepsilon$ is 0.06. The absence of significant correlation between excess kurtosis and wave steepness, as determined by *in situ* measurements, is consistent with the results of laboratory experiments conducted in a wind wave flume [29, 30]. These experiments led to the conclusion that cumulants up to the eighth order (inclusive) depend on steepness, with the notable exception of excess kurtosis, for which no clear dependence on $\varepsilon$ was identified.

As Fig. 1 shows, the changes in excess kurtosis calculated using models (2) and (7) when steepness varies from 0 to 0.1 are much smaller than the observed changes in excess kurtosis in a real wave field. At the same time, the model dependencies closely resemble the linear and quadratic regression dependencies and adequately describe the average state of the sea surface.

Fig. 2 shows the experimental and model dependencies of excess kurtosis $\lambda_4$ on inverse wave age $\zeta$. Similar to the $\lambda_4^E = \lambda_4^E(\varepsilon)$ dependence, the $\lambda_4^E = \lambda_4^E(\zeta)$ dependence is characterized by a large scatter in the values of $\lambda_4^E$. The correlation coefficient between $\lambda_4^E$ and $\zeta$ is 0.05. A comparison of dependence (6) with the linear regression described by the equation

$$\lambda_4^{ER} = 0.001 + 0.0288\,\zeta \pm 0.20, \qquad (9)$$

shows that the model estimates of excess kurtosis exceed consistently the average values obtained through experimentation. Overestimation $\lambda_4^{SD}(\zeta) - \lambda_4^{ER}(\zeta)$ increases from 0.085 at $\zeta = 0.83$ to 0.18 at $\zeta = 3.3$.

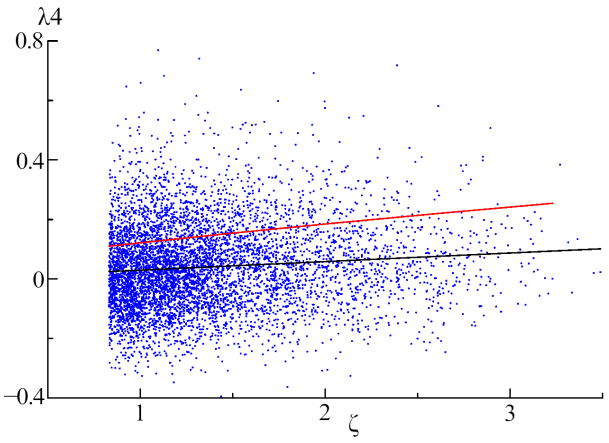


Fig. 2. Dependency of excess kurtosis $\lambda_4$ on inverse wave age $\zeta$. The dots are experimental data; the red line is dependency (6); the black line is linear regression (9)

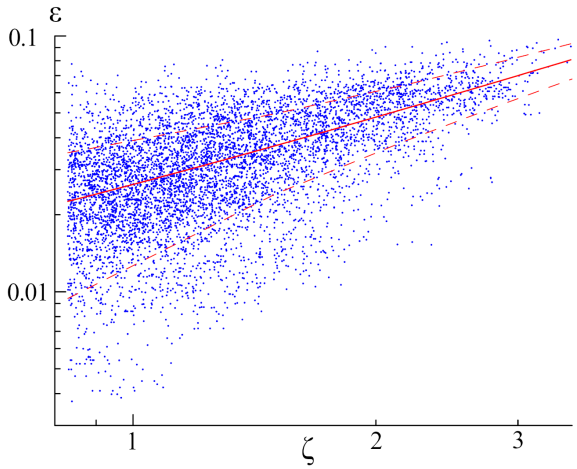


Fig. 3. Dependency of steepness ε on inverse wave age ζ. The dots are experimental data; the solid line is linear regression (10); the dashed lines show deviations ±0.013

Rogue waves occur when excess kurtosis values exceed a critical level estimated to lie within the range of 0.6–0.7. However, as can be seen from Figs. 1 and 2, the model values of excess kurtosis never exceed 0.3, meaning they cannot be used to forecast the occurrence of rogue waves.

Another drawback of dependencies (2) and (7) should be noted. The excess kurtosis values obtained using these are always positive, which does not correspond with *in situ* measurement results.

Dependence (6), as proposed in [1)] relies on the assumption that specifying the inverse wave age alone provides a sufficiently accurate description of the spectrum and integral parameters of the wave field, including variations in steepness across different stages of wave development. However, the validity of this assumption depends on the accuracy and clarity of the parameterization used for the Donelan spectrum.

Fig. 3 shows the dependence of wave steepness on inverse wave age, as determined from wave measurements. As evident from the figure, the relationship between ε and ζ for wind waves is stochastic. Cases, where $\zeta > 3.5$, are rare and have therefore been excluded from the present study. At the same value of ζ, the values of ε can differ by an order of magnitude. For the dataset analyzed in this study, the correlation coefficient between ε and ζ is 0.63. The linear regression equation takes the form

$$\varepsilon = 0.022\,\zeta + 0.004 \pm 0.013. \qquad (10)$$

## Conclusion

The rogue wave index depends statistically only on the excess kurtosis of sea surface elevations. This relationship suggests the potential for using excess kurtosis to predict the probability of rogue waves occurrence and has stimulated the development of computational methods based on various models. However, verification of the predicted dependence of excess kurtosis on wave steepness ε and inverse wave age ζ, as derived from the JONSWAP spectrum, demonstrates that these dependencies cannot describe the full range of excess kurtosis variations in a real wave field. Negligible correlation is observed between excess kurtosis and parameters ε and ζ, which makes it impossible to use these dependencies to forecast rogue wave occurrence. Additionally, a significant discrepancy exists between dependencies (2) and (7) and the observational data: the excess kurtosis values calculated using these dependencies are invariably positive, whereas negative values are frequently observed in field measurements.

## References


1. Grigorieva, V.G., Gulev, S.K. and Sharmar, V.D., 2020. Validating Ocean Wind Wave Global Hindcast with Visual Observations from VOS. *Oceanology*, 60(1), pp. 9–19. https://doi.org/10.1134/S0001437020010130
2. Mikhailichenko, S.Yu., Garmashov, A.V. and Fomin, V.V., 2016. Verification of the Swan Wind Waves Model by Observations on the Stationary Oceanographic Platform of the Black Sea Hydrophysical Polygon of RAS. *Ecological Safety of Coastal and Shelf Zones of Sea*, (2), pp. 52–57 (in Russian).
3. Stopa, J.E. and Cheung, K.F., 2014. Intercomparison of Wind and Wave Data from the ECMWF Reanalysis Interim and the NCEP Climate Forecast System Reanalysis. *Ocean Model*, 75, pp. 65–83. https://doi.org/10.1016/j.ocemod.2013.12.006
4. Stopa, J.E., Ardhuin, F., Bababin, A.V. and Zieger, S., 2016. Comparison and Validation of Physical Wave Parameterizations in Spectral Wave Models. *Ocean Model*, 103, pp. 2–17. https://doi.org/10.1016/j.ocemod.2015.09.003
5. Longuet-Higgins, M.S., 1957. The Statistical Analysis of a Random, Moving Surface. *Philosophical Transactions of the Royal Society of London. Series A, Mathematical and Physical Sciences*, 249(966), pp. 321–387. https://doi.org/10.1098/rsta.1957.0002
6. Goda, Y., 2000. *Random Seas and Design of Maritime Structures*. Singapore: World Scientific Publishing Co., 443 p.
7. Babanin, A.V. and Polnikov, V.G., 1995. On Non-Gaussian Wind Waves. *Physical Oceanography*, 6(3), pp. 241–245. https://doi.org/10.1007/BF02197522
8. Guedes Soares, C., Cherneva, Z. and Antão E.M., 2004. Steepness and Asymmetry of the Largest Waves in Storm Sea states. *Ocean Engineering*, 31(8-9), pp. 1147–1167. https://doi.org/10.1016/J.OCEANENG.2003.10.014
9. Zapevalov, A.S. and Garmashov, A.V., 2021. Skewness and Kurtosis of the Surface Wave in the Coastal Zone of the Black Sea. *Physical Oceanography*, 28(4), pp. 414–425. https://doi.org/10.22449/1573-160X-2021-4-414-425
10. Zapevalov, A.S. and Garmashov, A.V., 2022. The Appearance of Negative Values of the Skewness of Sea-Surface Waves. *Izvestiya, Atmospheric and Oceanic Physics*, 58(3), pp. 263–269. https://doi.org/10.1134/s0001433822030136
11. Stansell, P., 2004. Distributions of Freak Wave Heights Measured in the North Sea. *Applied Ocean Research*, 26(1-2), pp. 35–48. https://doi.org/10.1016/j.apor.2004.01.004

12. Annenkov, S.Y. and Shrira, V.I., 2013. Large-Time Evolution of Statistical Moments of Wind-Wave Fields. *Journal of Fluid Mechanics*, 726, pp. 517–546. https://doi.org/10.1017/jfm.2013.243
13. Kharif, C., Pelinovsky, E. and Slunyaev, A., 2009. *Rogue Waves in the Ocean*. Advances in Geophysical and Environmental Mechanics and Mathematics. Berlin; Heidelberg: Springer, 216 p. https://doi.org/10.1007/978-3-540-88419-4
14. Tomita, H. and Kawamura, T., 2000. Statistical Analysis and Inference from the In Situ Data of the Sea of Japan with Reference to Abnormal and/or Freak Waves. In: ISOPE, 2000. *Proceedings of 10th ISOPE Conference. May 28 – June 2, 2000. Seattle, USA*. The International Society of Offshore and Polar Engineers, ISOPE-I-00-232.
15. Ivanov, V.A., Dulov, V.A., Kuznetsov, S.Yu., Dotsenko, S.F., Shokurov, M.V., Saprykina, Y.V., Malinovsky, V.V. and Polnikov, V.G., 2012. Risk Assessment of Encountering Killer Waves in the Black Sea. *Geography, Environment, Sustainability*, 5(1), pp. 84–111. https://doi.org/10.24057/2071-9388-2012-5-1-84-111
16. Zapevalov, A.S. and Garmashov, A.V., 2022. Probability of the Appearance of Abnormal Waves in the Coastal Zone of the Black Sea at the Southern Coast of Crimea. *Ecological Safety of the Coastal and Shelf Zones of the Sea*, (3), pp. 6–15.
17. Annenkov, S.Y. and Shrira, V.I., 2009. Evolution of Kurtosis for Wind Waves. *Geophysical Research Letters*, 36(13), L13603. https://doi.org/10.1029/2009GL038613
18. Annenkov, S.Y. and Shrira, V.I., 2013. Large-Time Evolution of Statistical Moments of Wind-Wave Fields. *Journal of Fluid Mechanics*, Vol. 726, pp. 517–546. https://doi.org/10.1017/jfm.2013.243
19. Mori, N., Onorato, M. and Janssen, P.A.E.M., 2011. On the Estimation of the Kurtosis in Directional Sea States for Freak Wave Forecasting. *Journal of Physical Oceanography*, 41(8), pp. 1484–1497. https://doi.org/10.1175/2011JPO4542.1
20. Janssen, P.A.E.M., 2003. Nonlinear Four-Wave Interactions and Freak Waves. *Journal of Physical Oceanography*, 33(4), pp. 863–884. https://doi.org/10.1175/1520-0485(2003)33<863:NFIAFW>2.0.CO;2
21. Annenkov, S.Y. and Shrira, V.I., 2014. Evaluation of Skewness and Kurtosis of Wind Waves Parameterized by JONSWAP Spectra. *Journal of Physical Oceanography*, 44(6), pp. 1582–1594. https://doi.org/10.1175/JPO-D-13-0218.1
22. Hasselmann, K., Barnett, T.P., Bouws, E., Carlson, H., Cartwright, D.E., Enke, K., Ewing, J.A., Gienapp, H., Hasselmann, D.E. [et al.], 1973. Measurements of Wind-Wave Growth and Swell Decay During the Joint North Sea Wave Project (JONSWAP). *Ergänzungsheft zur Deutschen Hydrographischen Zeitschrift Reihe A(8)*, (12), 95 p.
23. Young, I.R., 1999. *Wind Generated Ocean Waves*. Amsterdam: Elsevier, 287 p.
24. Pierson, W.I. and Moskovitz, L., 1964. A Proposed Spectral Form for Fully Developed Wind Seas Based on the Similarity Theory of S. A. Kitaigorodskii. *Journal of Geophysical Research*, 69(24), pp. 5181–5190. https://doi.org/10.1029/JZ069i024p05181
25. Donelan, M.A., Hamilton, J. and Hui, W.H., 1985. Directional Spectra of Wind-Generated Waves. *Philosophical Transactions of the Royal Society of London. Series A, Mathematical and Physical Sciences*, 315(1534), pp. 509–562. https://doi.org/10.1098/rsta.1985.0054
26. Zapevalov, A.S., Dulov, V.A., Bolshakov, A.N., Smolov, V.E., Mostsipan, T.N. and Pokazeev, K.V., 2003. [On Spectral Characteristics of Wind Waves in the Coastal Area of the Black Sea]. In: Yu. D. Chashechkin and V. G. Baydulov, eds., 2003. *Fluxes and Structures in Fluids: Proceedings of the International Conference, 23–26 June 2003, Saint Petersburg*. Moscow, pp. 169–172 (in Russian).

27. Toloknov, Yu.N. and Korovushkin, A.I., 2010. The System of Collecting Hydrometeorological Information. In: MHI, 2010. *Monitoring Systems of Environment*. Sevastopol: ECOSI-Gidrofizika. Iss. 13, pp. 50–53 (in Russian).
28. Solov'ev, Y.P. and Ivanov, V.A., 2007. Preliminary Results of Measurements of Atmospheric Turbulence over the Sea. *Physical Oceanography*, 17(3), pp. 154–172. https://doi.org/10.1007/s11110-007-0013-9
29. Tayfun, M.A. and Alkhalidi, M.A., 2016. Distribution of Surface Elevations in Nonlinear Seas. In: OTC, 2016. *Proceedings of Offshore Technology Conference. Kuala Lumpur, Malaysia, 22–25 March 2016*. pp. 1274–1287. https://doi.org/10.4043/26436-MS
30. Huang, N. and Long, S., 1980. An Experimental Study of the Surface Elevation Probability Distribution and Statistics of Wind-Generated Waves. *Journal of Fluid Mechanics*, 101(1), pp. 179–200. https://doi.org/10.1017/S0022112080001590

Submitted 15.02.2025; accepted after review 23.06.2025;
revised 17.09.2025; published 30.12.2025

*About the authors:*

**Anton V. Garmashov**, Senior Research Associate, Marine Hydrophysical Institute of RAS (2 Kapitanskaya St., Sevastopol, 299011, Russian Federation), PhD (Geogr.), **Scopus Author ID: 54924806400, ResearcherID: P4155-2017**, *ant.gar@mail.ru*

**Aleksandr S. Zapevalov**, Chief Research Associate, Marine Hydrophysical Institute of RAS (2 Kapitanskaya St., Sevastopol, 299011, Russian Federation), DSc (Phys.-Math.), **ResearcherID: V-7880-2017, Scopus Author ID: 7004433476, ORCID ID: 0000-0001-9942-2796**, *sevzepter@mail.ru*

*Contribution of the authors:*

**Anton V. Garmashov** – collection of in situ measurement data, its systematisation, processing and analysis, analysis of literature sources

**Aleksandr S. Zapevalov** – problem statement, processing, analysis and description of the study results, preparation of the article text and graphic materials

*All the authors have read and approved the final manuscript.*

ISSN 2413-5577, Ecological Safety of Coastal and Shelf Zones of Sea, 2025, No. 4, pp. 76–96.

Original paper

# Climatic Variability of the Water Thermohaline Structure in the Weddell-Scotia Confluence

**Yu. V. Artamonov, E. A. Skripaleva *, N. V. Nikolskii**

*Marine Hydrophysical Institute of RAS, Sevastopol, Russia*
* *e-mail: sea-ant@yandex.ru*

**Abstract**
Based on the ECMWF ORA-S5 reanalysis data for 1958–2023, the paper analyses the average long-term structure of waters in the Weddell–Scotia Confluence and the climatic variability of its boundary characteristics. It is shown that this zone was most clearly manifested between Shishkov Island and the South Orkney Shelf. The northern boundary of this zone (Scotia Sea Front) was located above the southern slope of the South Scotia Ridge, and the southern boundary (Weddell Sea Front) was south of the Phillip Ridge. Both fronts were most intense in the 150–500 m layer. Near the South Orkney Shelf, the width of the Weddell–Scotia Confluence zone decreased by more than five times. The intensity of the fronts also weakened in the easterly direction, and they were mostly not traced east of the South Orkney Islands. On an interannual scale, the displacements of the Scotia Sea Front and the Weddell Sea Front in latitude did not exceed 0.5 degrees, while their intensity changed synchronously. From 1983 to 2010, a decrease in their intensity was observed, whereas from 1958 to 1982 and after 2010 there was an increase. In the time series of annual mean anomalies of temperature gradient values characterizing interannual changes in the intensity of the Scotia Sea Front and the Weddell Sea Front, a periodicity of 4 and 6 years was revealed. A significant positive correlation was found between the Antarctic Oscillation index and the interannual intensity anomalies of the fronts, with a phase lag of 0–3 years for the Weddell Sea Front and 3–5 years for the Scotia Sea Front. The tendency to increase the intensity of the Weddell–Scotia Confluence boundaries with an increase of the Antarctic Oscillation index values was especially clear over the past 10 years. During this period the high positive values of this index and maximum positive values of the Weddell Sea Front intensity anomalies were observed. Over the past 10 years, the Weddell–Scotia Confluence boundaries have strengthened markedly as the Antarctic Oscillation index increased. This period featured persistently high positive index values alongside maximum positive intensity anomalies in the Weddell Sea Front.

**Keywords**: Weddell Sea, Scotia Sea, potential sea water temperature, salinity, vertical water structure, water masses, thermohaline fronts, spatio-temporal variability, Antarctic Oscillation, South Oscillation

**Acknowledgements**: The work was carried out under FSBSI FRC MHI state assignment FNNN-2024-0014 “Fundamental studies of interaction processes in the ocean-atmosphere system forming the variability of the marine environment physical state on different spatio-temporal scales”.

**For citation**: Artamonov, Yu.V., Skripaleva, E.A. and Nikolskii, N.V., 2025. Climatic Variability of the Water Thermohaline Structure in the Weddell-Scotia Confluence. *Ecological Safety of Coastal and Shelf Zones of Se*a, (4), pp. 76–96.

# Климатическая изменчивость термохалинной структуры вод в зоне слияния морей Уэдделла и Скоша

**Ю. В. Артамонов, Е. А. Скрипалева *, Н. В. Никольский**

*Морской гидрофизический институт РАН, Севастополь, Россия*
***** *e-mail: sea-ant@yandex.ru*

**Аннотация**
По данным реанализа *ECMWF ORA-S*5 за 1958–2023 гг. проанализирована среднемноголетняя структура вод в зоне слияния морей Уэдделла и Скоша и климатическая изменчивость характеристик ее границ. Показано, что эта зона наиболее четко выражена между о-вом Шишкова и Южно-Оркнейским шельфом. Ее северная граница (фронт моря Скоша) располагается над южным склоном хребта Южный Скоша, а южная (фронт моря Уэдделла) – южнее хребта Филипп. Оба фронта наиболее интенсивны в слое 150–500 м. В районе Южно-Оркнейского шельфа ширина зоны слияния уменьшается более чем в пять раз. Интенсивность фронтов также ослабевает в восточном направлении, восточнее Южно-Оркнейских о-вов они почти не прослеживаются. На межгодовом масштабе смещения фронта моря Скоша и фронта моря Уэдделла по широте не превышают 0.5°, при этом их интенсивность изменяется синхронно. С 1983 по 2010 г. наблюдалось понижение их интенсивности, с 1958 г. по 1982 г. и после 2010 г. – повышение. Во временны́х рядах среднегодовых аномалий значений градиентов температуры, характеризующих межгодовые изменения интенсивности фронта моря Скоша и фронта моря Уэдделла, выявлена периодичность в 4 и 6 лет. Между индексом Антарктического колебания и межгодовыми аномалиями интенсивности фронтов выявлена значимая положительная корреляция: для фронта моря Уэдделла – при фазовом сдвиге 0–3 года, для фронта моря Скоша – при фазовом сдвиге от 3 до 5 лет. Особенно четко тенденция к повышению интенсивности границ зоны слияния морей Уэдделла и Скоша при росте значений индекса Антарктического колебания проявилась в течение последних 10 лет. В этот период наблюдались высокие положительные значения этого индекса и максимальные положительные значения аномалий интенсивности фронта моря Уэдделла.

**Ключевые слова**: море Уэдделла, море Скоша, температура воды, соленость, вертикальная структура вод, водные массы, термохалинный фронт, пространственно-временная изменчивость, Антарктическое колебание, Южное колебание

**Благодарности**: работа выполнена в рамках темы государственного задания ФГБУН ФИЦ МГИ FNNN-2024-0014 «Фундаментальные исследования процессов взаимодействия в системе океан-атмосфера, формирующих изменчивость физического состояния морской среды на различных пространственно-временных масштабах».

**Для цитирования**: *Артамонов Ю. В., Скрипалева Е. А., Никольский Н. В.* Климатическая изменчивость термохалинной структуры вод в зоне слияния морей Уэдделла и Скоша // Экологическая безопасность прибрежной и шельфовой зон моря. 2025. № 4. С. 76–96. EDN XKZNOE.

## Introduction

The Weddell-Scotia Confluence (WSC) is located in the southwestern part of the Atlantic Ocean Antarctic sector. It extends eastward from the South Shetland Islands along the South Scotia Ridge [1)]. This zone is one of the most biologically productive regions of the Southern Ocean, with high concentrations of phytoplankton and chlorophyll a in its waters. It is a key migration route for Antarctic krill, which travel eastward from their spawning grounds on the shelves of the Antarctic Peninsula [2)] [1–9]. The area's commercial importance has led to numerous publications analysing the features of the WSC thermohaline structure, which is a key abiotic factor influencing the spatial and temporal variability of water bioproductivity [3), 4), 5)] [10–21]. The vertical thermohaline structure of WSC waters differs qualitatively from that of the surrounding Antarctic-type waters. The Circumpolar Deep Water (CDW) layer, which is characterised by elevated temperature and salinity and is typical of Antarctic waters, undergoes noticeable transformation in the WSC. WSC waters are characterised by their own vertical structure with relatively weak stratification, and the subsurface layer down to a depth of 1000 m is almost homogeneous [1), 3), 5)] [10–18, 20]. According to [3)] [10, 12, 13], the causes of CDW transformation and the formation of a quasi-homogeneous layer with weak stratification can include winter vertical convection and subsidence of cold water observed during the warm season due to the melting of icebergs that accumulate on the South Scotia Ridge shelves. According to [17, 21], the WSC is characterized by subsidence of surface and subsurface waters, which leads to the formation of a water column with relatively low temperature and salinity. Moreover, according to [21], cold fresh shelf waters formed near the tip of the Antarctic Peninsula penetrate the WSC. These waters spread eastward along the northwestern periphery of the Weddell Sea Gyre, subsiding to intermediate depths due to their increased density resulting from the low temperature close to the ice melting point. This process results in cooling and freshening of the WSC waters. According to [19], the formation of the WSC water structure is influenced by convective mixing due to ice melting and by vertical currents within a system of numerous quasi-stationary topographic vortex formations characteristic of this area.

---

[1)] Gordon, A.L., 1967. Structure of Antarctic Water Between 20W and 170W. In: V. Bushnell, ed., 1967. *Antarctic Map Folio series. Folio 6*. American Geographical Society, 10 p.

[2)] Shulgovsky, K.E., 2005. [*Large-Scale Variability of Oceanological Conditions in the Western Part of the Atlantic Sector of the Antarctic and its Influence on the Distribution of Krill*]. Kaliningrad: AtlantNIRO, 148 p. (in Russian).

[3)] Chernyavsky, E.B., 1977. [*Frontal and Gradient Zones of the South Ocean*]. Moscow: Promyslovaya Okeanologiya. Iss. 6, 50 p. (in Russian).

[4)] Burkov, V.A., 1995. [Weddell-Scotia Confluence Zone]. In: IO RAS, 1995. [*Pelagic Ecosystems of the Atlantic Sector of Antarctica*]. Moscow: IO RAN, pp. 7–14 (in Russian).

[5)] Smith, S.G., 1989. *On the Weddell-Scotia Confluence and the Scotia Front:* Master's Thesis in Oceanography. Texas A&M University, 85 p. Available at: https:hdl.handle.net/1969.1/ETD-TAMU-1989-THESIS-S661 [Accessed: 24 November 2025].

According to existing concepts [3), 6)] [15, 18–20], the northern boundary of the WSC, which separates it from the waters of the southern Scotia Sea, is the Scotia Sea Front (SSF). The southern boundary, which separates the WSC from the waters of the northern Weddell Sea, is the Weddell Sea Front (WSF). In accordance with [15, 22–24], the SSF and WSF can be observed on the surface. Note that on the surface, they divide the modifications of the same body of water, the Antarctic Surface Water. At the same time, in the subsurface layer, they delineate the northern and southern limits of the transformed CDW layer [19, 20]. The SSF extends the continental water boundary east of Mordvinov (Elephant) Island and coincides with a relatively weak deep stream identified in the southern Scotia Sea, south of the Antarctic Circumpolar Current system [15, 22]. The branches of the WSF correspond to deep streams that form the north-western periphery of the Weddell Sea Gyre [15, 22, 24].

Most studies analysing the water structure of the WSC and the variability of its boundaries are based on data from contact measurements performed in different years and seasons on individual synoptic sections located relatively far from each other [5)] [10–13, 16, 18] or on outdated hydrological databases with low spatial and temporal coverage [17, 19, 20]. Due to high heterogeneity of contact measurement data and almost complete absence of information during the cold season, contradictions in the description of the WSC water structure persist to this day. Thus, according to [3)] [10], the temperature of the WSC waters is low from the surface to the bottom, whereas study [12] shows that a temperature maximum is observed at the surface of the WSC. It is claimed in [3)] [10–13] that the WSC surface salinity is elevated, while data from [3)] [10] show that high salinity is present at the bottom. Furthermore, the results of studies [13, 17] suggest that the salinity of the WSC waters is lower at depths of 200 m and below.

Based on archival climatic data from works [19, 20], the manifestations of the WSC boundaries (SSF and WSF) in the long-term average thermohaline fields were evaluated. The SSF is most clearly manifested in the temperature field at depths greater than 200 m and in the salinity field in the upper 250 m layer. The WSF is manifested deeper than 100 m in the temperature field and deeper than 300 m in the salinity field. These works also analysed the seasonal variability of the SSF. It was demonstrated that the front is located between 58° and 60° S at the surface throughout the year and reaches maximum intensity in March. However, due to the limited availability of hydrological data in the Weddell Sea and their complete absence in winter, the seasonal variations of the WSF could not be evaluated [19, 20].

Some studies have analysed the features of the water structure in the WSC area based on relatively short series of drifter and satellite measurements [4, 14, 15, 21, 23]. Higher spatio-temporal resolution satellite temperature measurements allowed the SSF to be detected in the sea surface temperature (SST) field and the features

---

[6)] Bogdanov, M.A., Oradovsky, S.G., Solyankin, E.V. and Khvatsky, N.V., 1969. [On the Frontal Zone of the Scotia Sea]. *Okeanologiya*, 9(6), pp. 966–974 (in Russian).

of the average long-term seasonal and interannual variability of this front's characteristics to be refined [23]. Using AVHRR Ocean Pathfinder data from JPL NOAA/NASA for the period 1985–2001, it was demonstrated that during the climatic seasonal cycle, an increase in SSF intensity at the surface was observed during the warm season. Meanwhile, interannual variations in the characteristics of the front manifest as changes in its intensity and latitudinal displacement. A significant relationship was identified between interannual anomalies in the characteristics of the front and anomalies in the areas of warm tropical waters in the Pacific Ocean caused by El Niño events. At the same time, the characteristics of the front responded weakly to changes in the Southern Oscillation index [23].

In recent years, high-resolution hydrological datasets have emerged that assimilate continuously updated SST data from contact and satellite measurements, optimally interpolated onto regular grids (e.g. NOAA OISST). This has enabled features in the climatic structure and seasonal variability of the WSF at the ocean surface to be refined [24]. It has been demonstrated that, to the west of the South Orkney Islands, the WSF is characterised by two branches in the average long-term SST field, intensifying during the summer period of the Southern Hemisphere (February–April) [24]. However, the structure and climatic variability of the SSF and WSF in the ocean subsurface layers, which form the boundaries of the WSC, remain largely unexplored.

The study aims to refine the characteristics of WSC manifestations in average long-term thermohaline fields, based on modern oceanic reanalysis data (ECMWF ORA-S5 курсив наверное не нужен), to analyse the climatic variability of SSF and WSF boundaries as well as to evaluate the influence of large-scale atmospheric circulation modes (Southern Annular Mode and Southern Oscillation) on interannual front characteristics.

**Materials and methods**

The study considers the region of the Southern Ocean located east of Mordvinov (Elephant) Island, between 55° and 40°W, and 59° and 62.5°S (Fig. 1, *a*, *b*). To construct the bottom relief scheme, data from General Bathymetric Chart of the Oceans (GEBCO) [7)] with a spatial resolution of 15″ were used. Monthly mean values of potential temperature (θ, °C) and salinity *S* (PSU), as well as zonal *U* and meridional *V* components of current velocities $\vec{V}$ (m/s), were utilised for each year from 1958 to 2023. These data were obtained from the reanalysis of the European Centre for Medium-Range Weather Forecasts OCEAN5 system (ECMWF ORAS5) [27]. They were interpolated onto grid nodes with a resolution of approximately 1/4° in longitude and 1/8° in latitude, distributed across 75 vertical levels in σ coordinates ranging from 0.5 to 5500 m [8)]. The reanalysis used the ocean model Nucleus for European Modelling of the Ocean (NEMO) and the ocean assimilation system NEMOVAR, which incorporates surface and subsurface temperature, salinity, sea ice concentration and sea level anomalies [25].

---

[7)] GEBCO. *Gridded Bathymetry Data*. [online] Available at: http://www.gebco.net/data_and_products/gridded_bathymetry_data/ [Accessed: 24 November 2025].

[8)] Copernicus Climate Change Service, Climate Data Store. 2021. *ORAS5 Global Ocean Reanalysis Monthly Data from 1958 to Present*. https://doi.org/10.24381/cds.67e8eeb7

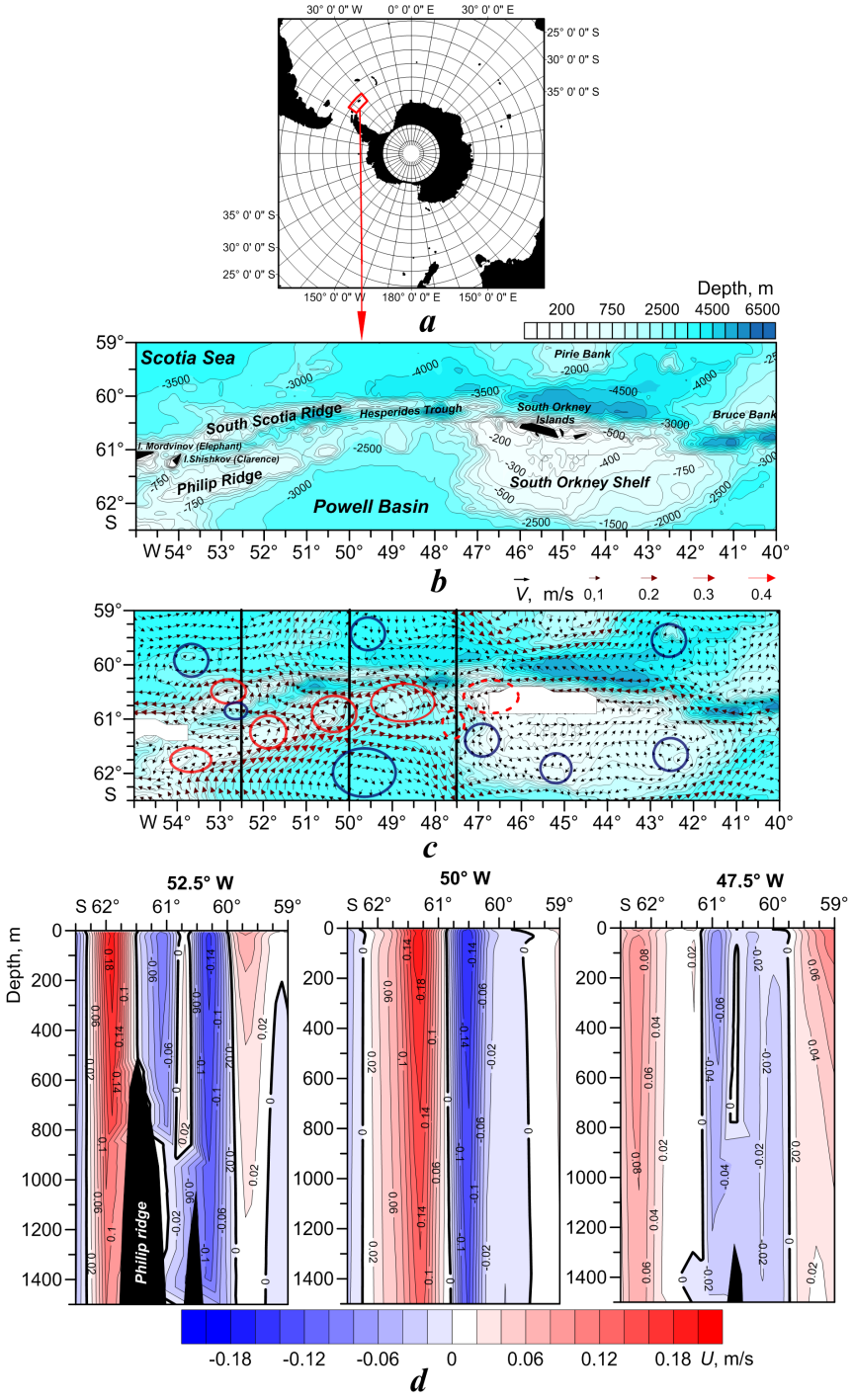


Fig. 1. Study area on the map of the South Ocean (*a*); bottom relief map of the area (*b*); distribution of current vectors at a depth of 200 m: the red ellipses denote anticyclonic gyres, the blue ellipses are cyclonic ones (*c*); vertical distributions of *U* values along 52.5°, 50° and 47.5°W (*d*)

Based on the source data, the average long-term and monthly climatic mean values of θ, S, the velocity modulus $\bar{V}$ and the direction of current vectors were calculated (Fig. 1, *c*). According to [9], the time series of the data used is sufficient for determining statistically reliable climatic norms.

The boundaries of the WSC (SSF and WSF) were determined by locating the extremes of the meridional temperature gradients (MTG) and meridional salinity gradients (MSG) on sections spaced 0.25° apart along meridians. Positive (negative) MTG and MSG values indicate an increase (decrease) in temperature and salinity values in the southern direction.

The interannual variability of the WSC boundaries was analysed in the temperature field, because this parameter largely determines the course of large-scale processes in the ocean–atmosphere system, serving as an indicator of the heat content of the active ocean layer [26, 27]. For this purpose, anomalies of the annual mean values of MTG extremes (AnMTG), which characterise the SSF and WSF, were calculated for each year relative to their average long-term values over the entire analysed period of 66 years. When calculating the anomalies, the absolute values of the MTG extremes were used. To assess the connections between the variability of atmospheric circulation and interannual variations in the intensity of the SSF and WSF, cross-correlation functions with a 95% statistical significance level ($\alpha = 0.05$) were analysed between the time series of annual mean AnMTG values and the indices of the Southern Oscillation (SO) and Antarctic Oscillation (AAO), which characterise the Southern Annular Mode [1, 28, 29]. When calculating the cross-correlation functions between the AnMTG values and the AAO index, the AnMTG time series from 1979 to 2023 were used, corresponding to the period for which AAO index data is available. SO and AAO index values were obtained from the National Oceanic and Atmospheric Administration (NOAA) website [10), 11)].

**Results and discussion**

Figs. 2–4 show examples of the vertical distribution of the long-term mean temperature and salinity values and their meridional gradients. Analysis of these distributions revealed no clear signs of the WSC (the absence of sharp thermohaline extremes in the vertical structure due to the subsidence of colder, fresher waters) in the climatic fields of the upper 100–150 m layer, which is consistent with earlier studies [1), 3), 5)] [10–21]. The upper 100–150 m layer has the typical vertical structure of the Antarctic zone characterised by a well-defined subsurface layer of Antarctic Winter Water (AWW) with a minimum temperature and relatively low salinity.

---

9) Monin, A.S., 1999. [*Hydrodynamics of the Ocean Atmosphere and Earth's Interior*]. Saint Petersburg: Gidrometeoizdat, 523 p. (in Russian).

10) Climate Prediction Center. *The Southern Oscillation Index (SOI).* 2025. [online] Available at: https://www.cpc.ncep.noaa.gov/products/analysis_monitoring/ensocycle/soi.shtml [Accessed: 24 November 2025].

11) Climate Prediction Center. *Antarctic Oscillation (AAO).* 2025. [online] Available at: https://www.cpc.ncep.noaa.gov/products/precip/CWlink/daily_ao_index/aao/aao.shtml [Accessed: 24 November 2025].

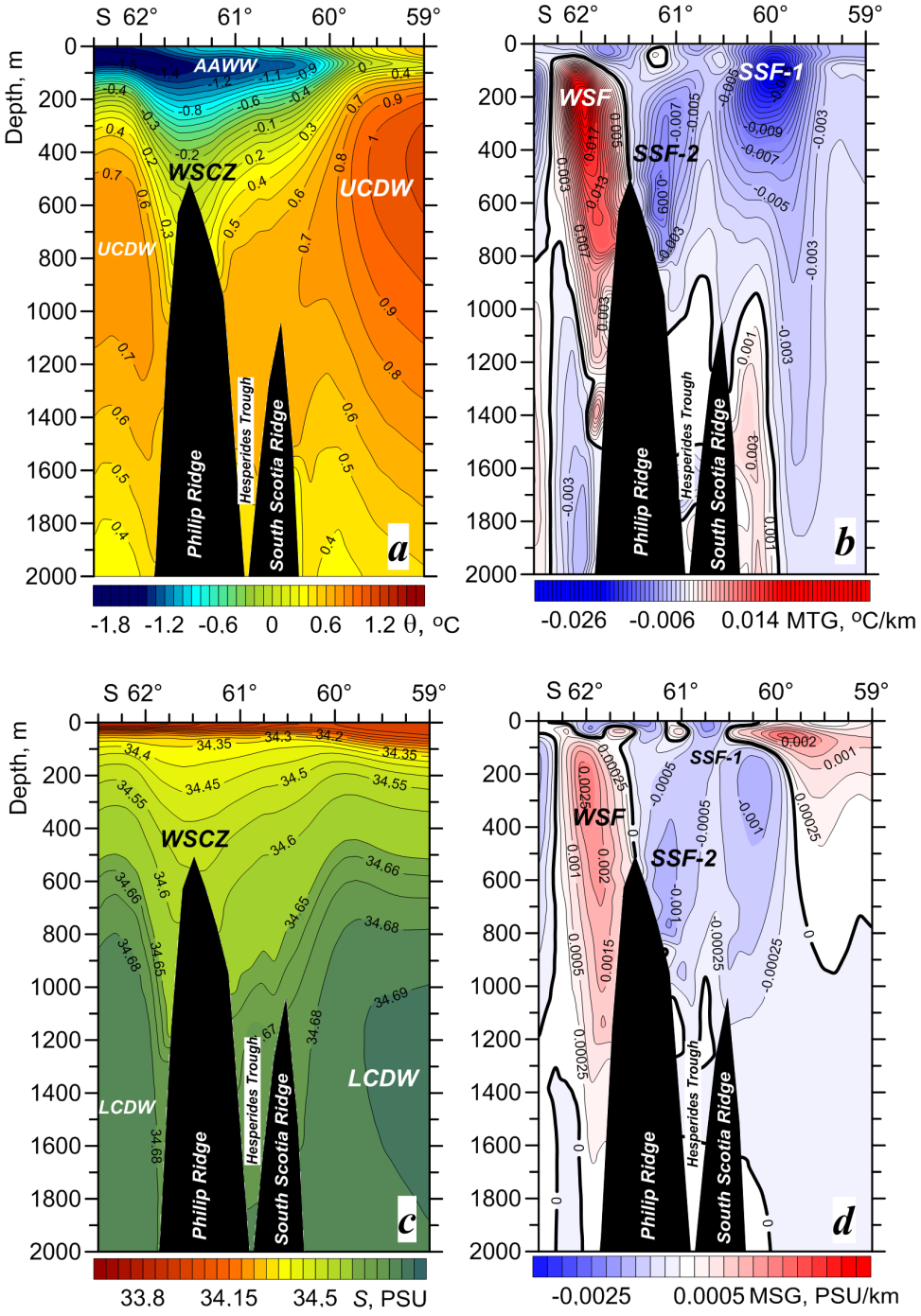


Fig. 2. Vertical distributions of annual mean values of temperature (*a*), meridional temperature gradients (MTG) (*b*), salinity (*c*), meridional salinity gradients (MSG) (*d*) along 52.5°W

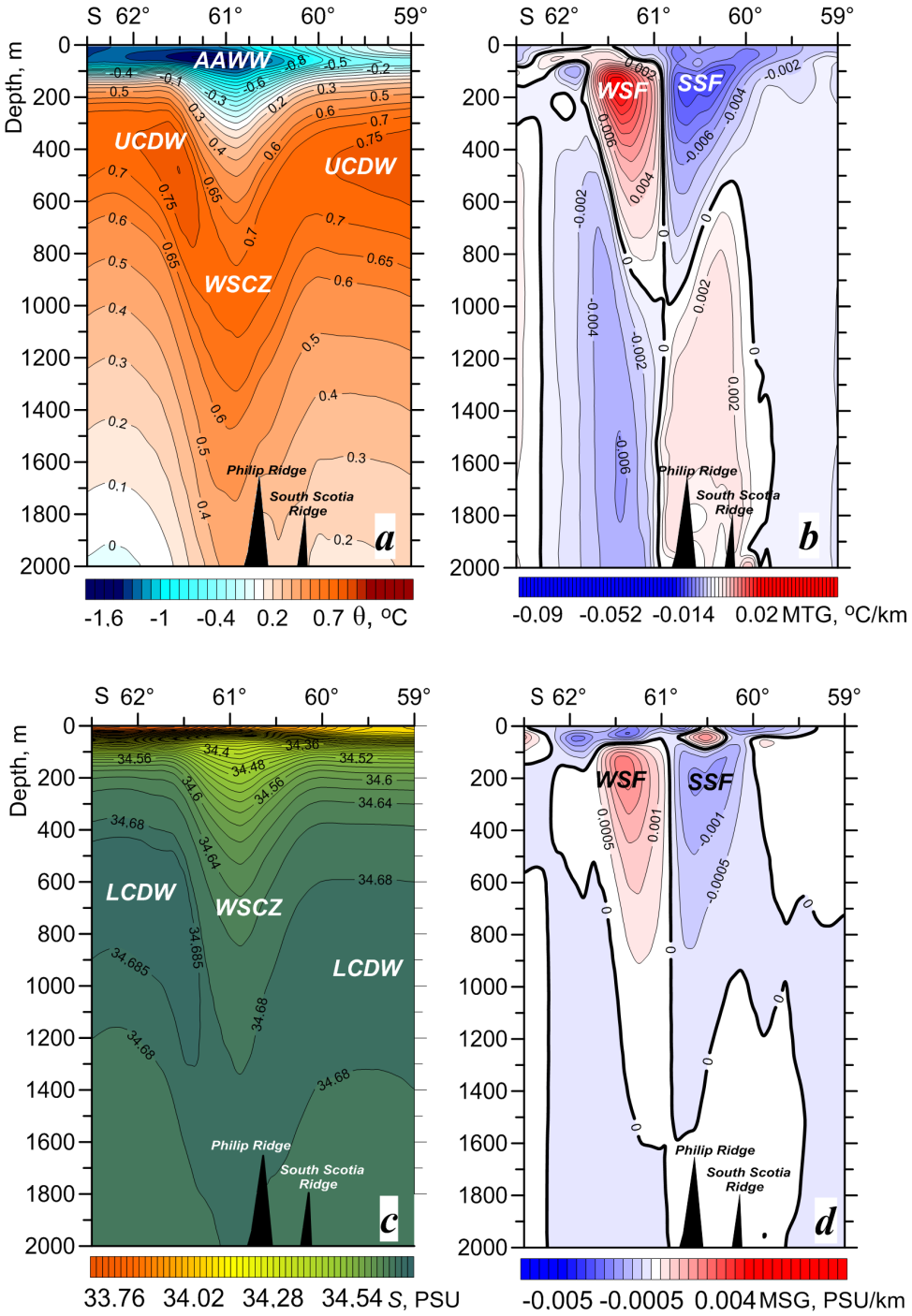


Fig. 3. Vertical distributions of annual mean values of temperature (*a*), MTG (*b*), salinity (*c*), MSG (*d*) along 50°W

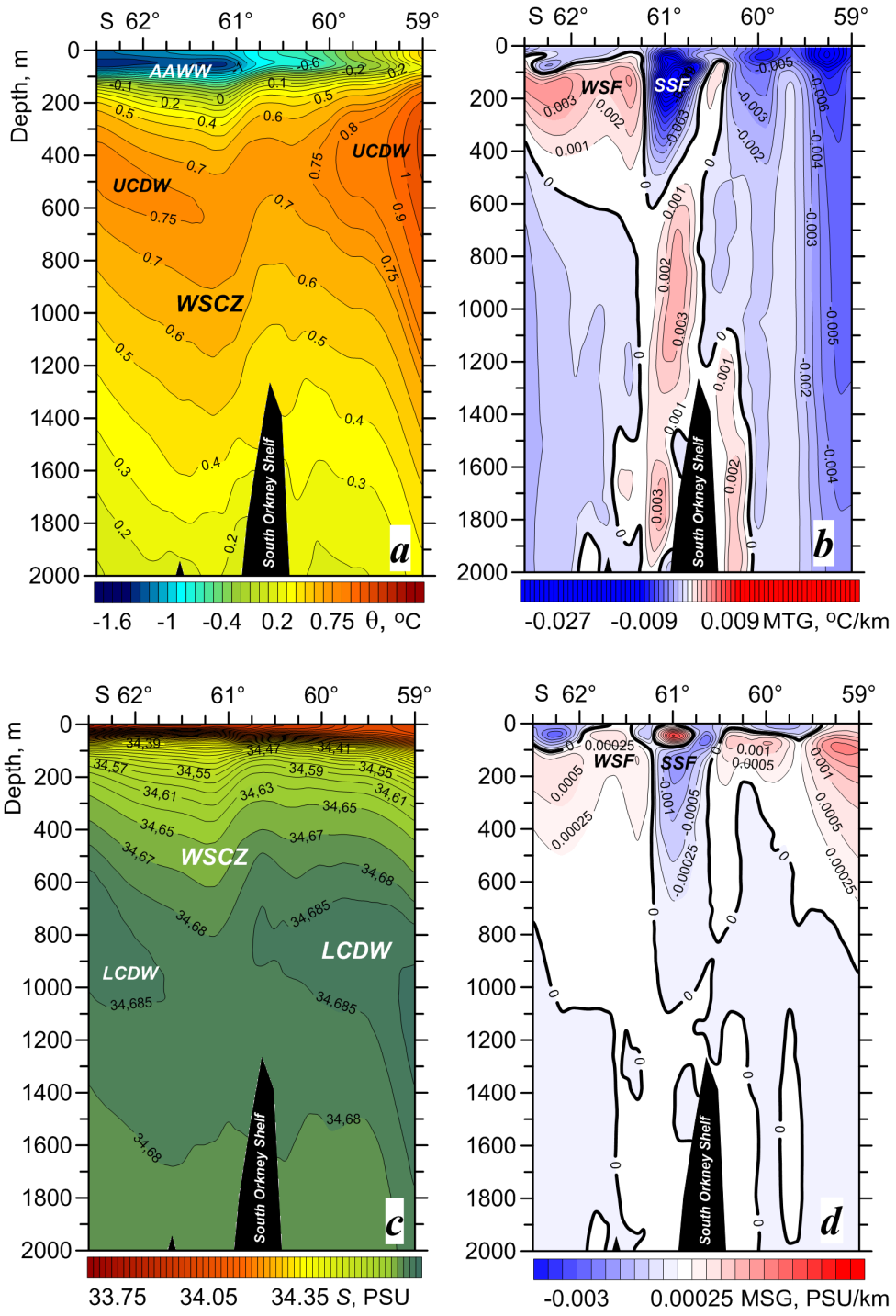


Fig. 4. Vertical distributions of annual mean values of temperature (*a*), MTG (*b*), salinity (*c*), MSG (*d*) along 47.5°W

The subsidence of colder, less saline water, which is characteristic of the WSC, is clearly evident in the long-term average thermohaline fields below the AWW layer. This disrupts the CDW layer (Figs. 2, *a*, *c*; 3, *a*, *c*; 4, *a*, *c*).

The transformation of the vertical water structure in the WSC is reflected in the θ and S curves (Fig. 5). The waters of the Scotia Sea to the north and the Weddell Sea (Powell Basin) to the south of the WSC are characterised by well-defined extremes corresponding to the AWW and CDW cores. In the WSC area, however, only the AWW core manifests as an extremum, below which a quasi-homogeneous layer is evident, with no clearly expressed extremum corresponding to the CDW (Fig. 5).

The waters of the WSC are characterised by weak temperature and salinity gradients. The northern boundary (SSF) has maximum negative MTG and MSG values, while the southern boundary (WSF) has maximum positive MTG and MSG values (Figs. 2, *b*, *d*; 3, *b*, *d*; 4, *b*, *d*).

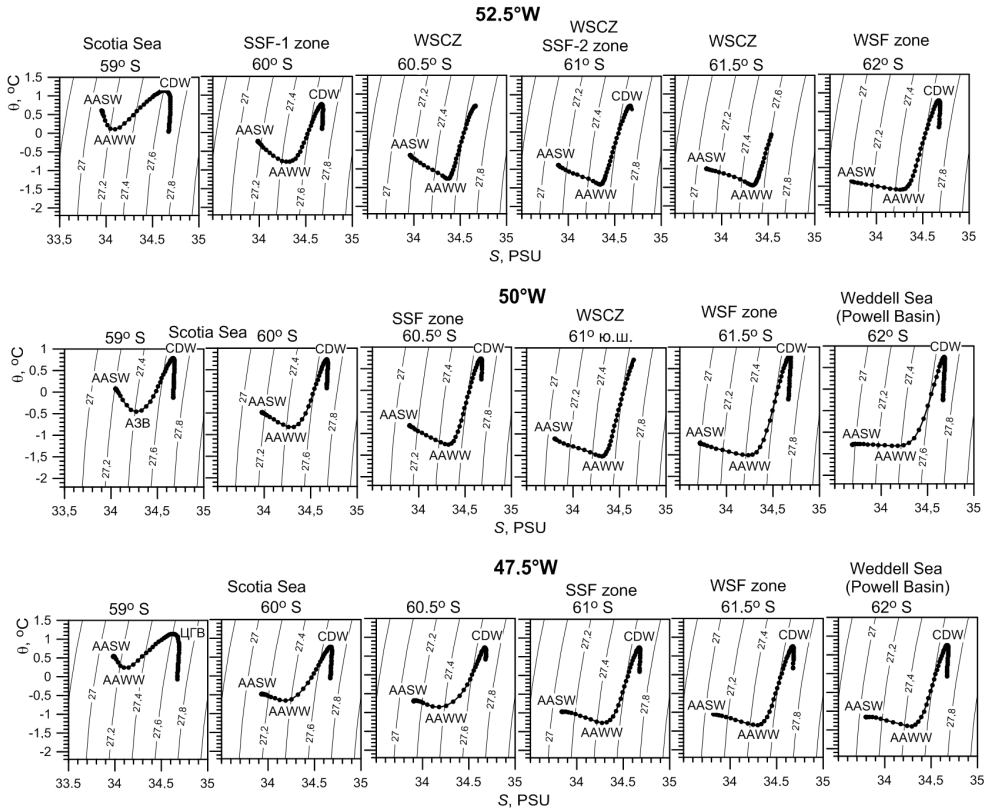


Fig. 5. Annual averaged θ,*S*-curves at different grid nodes on the meridians 52.5°W, 50°W and 47.5°W

While the general features of the WSC are preserved (subsidence of cold, low-salinity waters, and high MTG and MSG values at its boundaries), the position of its boundaries and the depth of water subsidence in different areas of the body of water differ. This is related to the features of water circulation caused by the bottom relief. Current vector distribution at a depth of 200 m revealed a significant presence of anticyclonic vortices and meanders over the South Scotia and Phillip Ridges, and cyclonic vortices in the Scotia Sea, the Hesperides Trough, the Powell Basin and the southern part of the South Orkney Shelf (Fig. 1, *b*, *c*). The vertical distribution of the zonal velocity component $U$ clearly shows oppositely directed flows, which correspond to the northern and southern peripheries of these vortex formations and extend to depths of 900–1500 m (Fig. 1, *d*).

Analysis of the vertical distribution of temperature, salinity, MTG and MSG revealed that the WSC was most pronounced to the east of Mordvinov (Elephant) Island. Here, subsidence of the waters occurs over the South Scotia and Phillip Ridges. At 52.5°W, the WSC extends almost to the bottom over the Phillip Ridge, completely disrupting the CDW layer and the cores of its upper (UCDW) and lower (LCDW) modifications (Fig. 2, *a*, *c*). Within the latitudinal limits of the WSC over the deep-water Hesperides Trough, a slight rise in isotherms and isohalines is evident, which is associated with the topographic cyclonic meander observed in this area (Fig. 1, *c*, *d*). Consequently, the northern boundary of the WSC in the thermohaline fields exhibits a bimodal structure. One branch of the SSF is located approximately at 60°S (over the South Scotia Ridge) and is most developed in the 100–400 m layer. The second branch of the SSF is located north of the Phillip Ridge, approximately at 61°S, and is most developed in the 200–800 m layer (Fig. 2, *b*, *d*). The distributions of the annual mean MTG and MSG at the 200 m horizon along 52.5°W show two branches of the SSF (SSF-1 and SSF-2) in the temperature and salinity fields (Fig. 6). The southern boundary of the WSC (WSF) is located south of Phillip Ridge at 62°S, where it is most intense in the 100–700 m layer (Figs. 2, *b*, *d*; 6).

In the central part of the water area (50° W), colder, less saline waters descend over the Phillip Ridge spur in an anticyclonic meander area (Fig. 1, *c*) to depths of approximately 1000 m in the temperature field and 1500 m in the salinity field. This results in a significant transformation and deepening of the CDW layer as well as the disruption of the UCDW and LCDW cores (Fig. 3, *a*, *c*). The SSF is clearly visible in the temperature and salinity fields at approximately 60.5–60.75°S over the southern slope of the South Scotia Ridge, while the WSF is visible at the northern boundary of the Powell Basin at 61.375°S (Fig. 6). Both fronts are most intense in the 100–600 m layer (Fig. 3, *b*, *d*).

Further east, at the western boundary of the South Orkney Shelf (47.5°W), the main subsidence of waters also occurs in the area characterised by an anticyclonic meander (Fig. 4, *a*, *c*). The intensity and vertical extent of the SSF and WSF decrease; both fronts are most developed in the 100–400 m layer. The SSF is located at approximately 60.85–61°S and the WSF at approximately 61.375°S (Fig. 4, *b*, *d*; 6).

Overall, closer to the South Orkney Shelf, the width of the WSC and the intensity of its boundaries decrease noticeably (Fig. 6). At a depth of 200 m, the intensity of the SSF decreases from 0.02 °C/km in the western part of the WSC to 0.01 °C/km at the western boundary of the South Orkney Shelf while the intensity of the WSF decreases from 0.025 to 0.005 °C/km (Fig. 6, *a*).

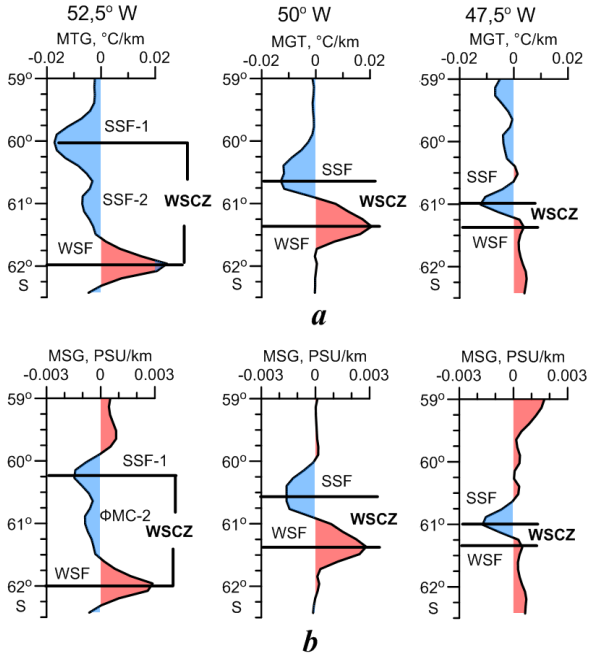


Fig. 6. Distributions of annual averaged MTG (*a*) and MSG (*b*) and the position of the Weddell–Scotia Confluence boundaries (Scotia Sea Front (SSF) and Weddell Sea Front (WSF)) at a depth of 200 m along the 52.5°W, 50°W and 47.5°W

In the salinity field, the intensity of the SSF remains relatively consistent across the landscape, whereas the intensity of the WSF decreases from west to east, dropping from 0.003 to 0.001 PSU/km (Fig. 6, *b*). In the thermohaline fields, the width of the WSC (the distance between the SSF and WSF axes) decreases from west to east, dropping from approximately 223 km (2° latitude) at 52.5°W to 42 km (0.375° latitude) at 47.5°W (Fig. 6). East of the South Orkney Islands, the WSC does not manifest in the annual mean climatic thermohaline fields, and the Scotia Sea and Weddell Sea fronts are almost indistinguishable.

Thus, examining distributions of thermohaline characteristics on vertical sections showed that the WSC was not clearly expressed in the climatic fields in the upper layer occupied by the Antarctic surface and Antarctic winter water masses. The horizontal distributions of temperature and salinity in the WSC area at the surface (Fig. 7, *a*, *b*) and below the AWW layer (Fig. 7, *c*, *d*) differ considerably. Within the latitudinal limits of the WSC at the surface, a decrease in temperature and salinity is observed in the southern direction, with a fall of 0 to −1 °C and 33.95 to 33.8 PSU, respectively (Fig. 7, *a*, *b*). Between approximately 49.5° and 47.5°W, the quasi-zonality of isohalines in the WSC area is noticeably disrupted.

Here, an elongated tongue of lower-salinity waters is present in the northwestern direction (Fig. 7, *b*). In this area temperature field, a slight shift of isotherms to the north is also observed (Fig. 7, *a*). Analysis of the distribution of current vectors in the upper 100 m layer revealed a large-scale anticyclonic meander, along the eastern edge of which waters with reduced temperature and salinity from the Powell Basin enter the WSC via the deep-water passage to the west of the South Orkney Shelf (Fig. 1, *b*). The surface distributions of temperature and salinity (the absence of temperature extremes and a salinity decrease in the central part of the WSC) refine the results of previous studies which claim an increase in salinity in the surface layer of waters in the WSC [10, 13], as well as extreme temperature values (maximum [12] or minimum [3)] [10]).

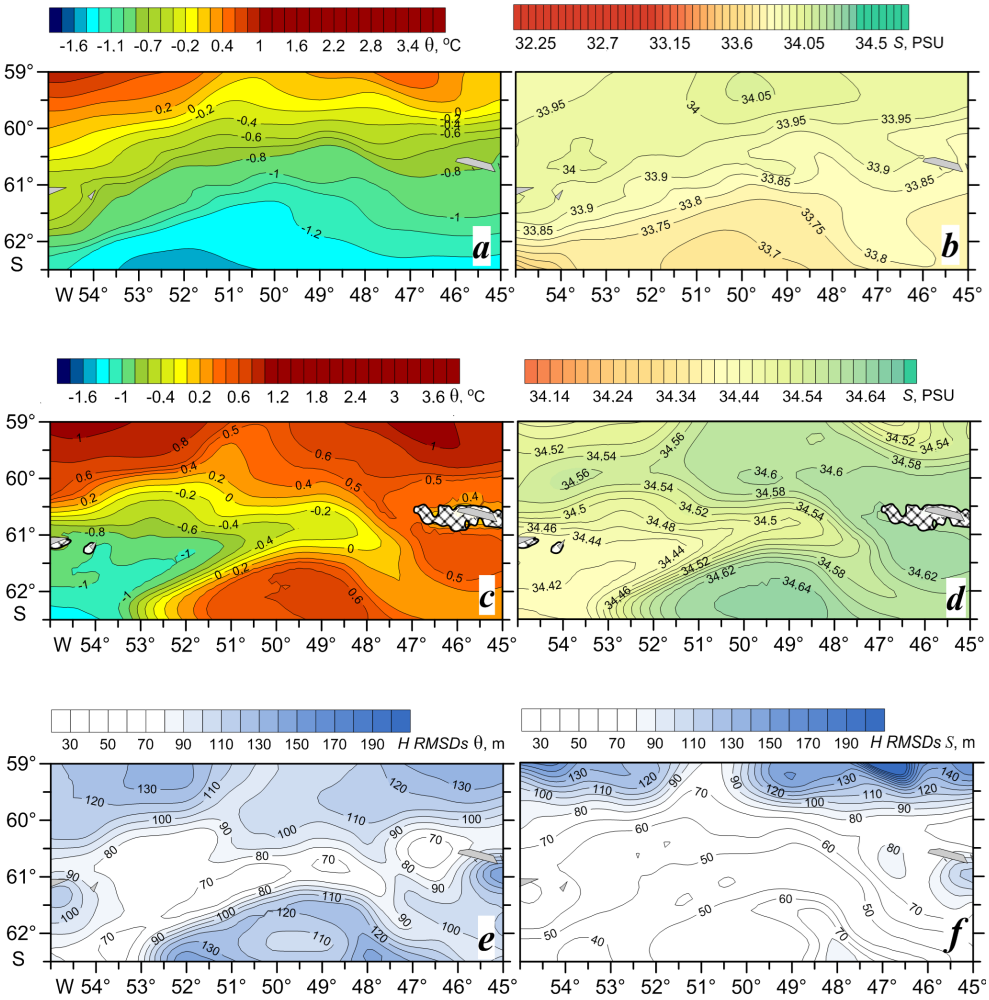


F i g . 7. Distributions of annual mean values of temperature (*a*, *c*) and salinity (*b*, *d*) at the surface (*a*, *b*) and at a depth of 200 m (*c*, *d*), depth of the seasonal signal penetration in the temperature (*e*) and salinity (*f*) fields

In contrast to the surface, the temperature and salinity distribution maps below the AWW layer at a depth of 200 m (рис. 7, *c*, *d*) reveal a distinct tongue of cooler, less salty water. This tongue extends along Phillip Ridge toward the South Orkney Shelf to the east. Clustering of isotherms and isohalines is observed at the boundaries of this tongue, which characterises the manifestation of the WSC boundaries. The configuration of the tongue of waters with reduced temperature and salinity, as well as the current vectors at the 200 m horizon (Fig. 1, *c*), indicate the penetration of colder and less saline shelf waters into the WSC area from the Powell Basin. These waters are formed over the shallow shelf of the Antarctic Peninsula. This finding is consistent with the results of the study [21].

When assessing the climatic variability of the WSC boundary characteristics (SSF and WSF), the depth of penetration of the seasonal signal (H SDseason) in the thermohaline fields was analysed. This depth was conventionally defined as the point at which the intra-annual standard deviation of temperature and salinity decreased by an order of magnitude (see Fig. 7, *e*, *f*). Within the WSC, the H SDseason values did not exceed 70–90 m in the temperature field and 50–80 m in the salinity field (Fig. 7, *e*, *f*). In other words, the layer of transformed CDW in the WSC area is almost unaffected by seasonal changes. Since seasonal fluctuations in the thermohaline fields do not penetrate to the upper depth at which the SSF and WSF manifest (100–150 m), the climatic variability of the WSC boundaries was analysed on the interannual scale using the annual mean values of the front characteristics.

Despite significant progress in creating and improving modern reanalyses, their quality for Antarctica remains low due to a key limitation: the extremely small amount of source data available for model assimilation. In the subsurface layers, where there is significantly less source data than at the surface, any interannual trends obtained should be considered estimates.

Some features of the interannual variability of the characteristics of the SSF and WSF in the subsurface layer, which is deeper than the AWW, can be explained by physical and geographical factors, as identified through the reanalysis data used. Thus, analysing the time series of the latitudinal positions of the MTG extremes that characterise the SSF and WSF in the temperature field revealed that, on the interannual scale from 1958 to 2023, the latitudinal displacement of the fronts does not exceed 0.5°. At the same time, the stable position of the WSC boundaries is determined by the features of the bottom relief. For instance, at the 50° W meridian, which passes through the centre of the WSC, the SSF is located over the southern slope of the South Scotia Ridge within the latitudinal band 60.25–60.75° S (Fig. 8, *a*) throughout all 66 years, while the WSF is situated south of Phillip Ridge at the northern boundary of the Powell Basin within the latitudinal band 61.25–61.75° S (Fig. 8, *c*).

The distribution of annual mean MTG extremes (AnMTG) anomalies corresponding to the SSF and WSF showed that these fronts intensified and weakened in synchrony on the interannual scale (Fig. 8, *a*, *c*). From 1983 to 2010, a general decrease in the intensity of the SSF and WSF was observed, with both fronts being significantly weakened from 1987 to 1990. During this period, the width of the WSC increased by almost one degree due to maximum displacement of the SSF

northward to 60.25°S and the WSF southward to 61.75°S. From 1958 to 1982 and after 2010, the intensity of the SSF and WSF increased. During periods of significant change in the intensity of the WSC boundaries, the southern boundary exhibited the greatest change, with extreme interannual variations in WSF intensity noticeably exceeding those in SSF intensity. The maximum positive values of AnMTG are 0.008 °C/km for the SSF and 0.012 °C/km for the WSF. The maximum negative values of AnMTG for the SSF are −0.01 °C/km and for the WSF they are −0.25 °C/km (Fig. 8, *a*, *c*).

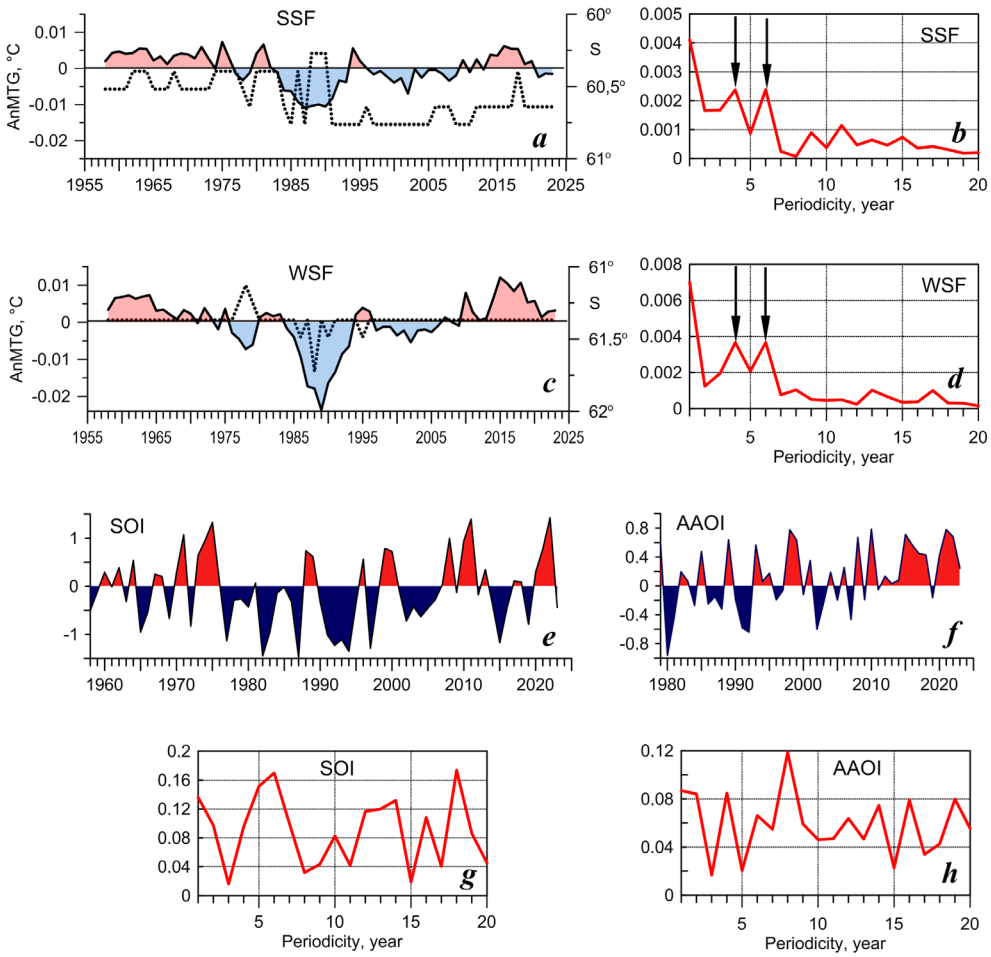


Fig. 8. Interannual variability of MTG annual mean anomalies and latitudinal position (black dotted line) of the SSF (*a*) and WSF (*c*), spectra of AnMTG time series of the SSF (*b*) and WSF (*d*) at a depth of 200 m at 50°W, distributions of annual mean values of the South Oscillation (SO) (*e*) and Antarctic Oscillation (AAO) (*f*) indices and their spectra (*g*, *h*)

No significant trends characterising the general tendencies of long-period variability in the intensity of the SSF and WSF were identified in the time series of annual mean AnMTG. The spectra of the AnMTG time series revealed periodicities of four and six years in the interannual changes in the intensity of the SSF and WSF (Fig. 8, *b, d*), similar to the variability periods of the Southern Oscillation (SO) and Antarctic Oscillation (AAO) indices (Fig. 8, *e–h*). Features similar to those observed in the interannual variability of the WSC boundaries (absence of a significant trend in the interannual anomaly time series and periodic alternation of positive and negative anomalies every 2–5 years) were also observed in the sea surface temperature field in the Atlantic sector of Antarctica [30].

Analysis of the cross-correlation functions revealed no significant relationship between the interannual changes in the SSF and WSF intensity anomalies and the changes in the SOI. A significant positive correlation was noted between the intensity of the WSF and the AAO index, with a maximum value of $R \sim 0.4$ at zero phase shift at a depth of 100 m (Fig. 9, *a*) and at a shift of 3 years at a depth of 200 m (Fig. 9, *b*).

A significant positive relationship is also observed between the SSF intensity and the AAO index, with a maximum value of $R \sim 0.35$ at a phase shift of 5 years at a depth of 100 m (Fig. 9, *a*) and at a phase shift of 3–5 years at a depth of 200 m (Fig. 9, *b*). Thus, an increase (decrease) in AAO index values tends to be accompanied by an increase (decrease) in WSC boundary intensity. This tendency has been particularly evident over the last 10 years, when high positive values of the AAO index (except in 2019) and maximum positive values of the WSC intensity anomalies have been observed. As oceanic fronts act as “mixing barriers” [1, 4, 31], strengthening the frontal boundaries of the WSC hinders the exchange of water between the WSC and the Scotia and Weddell Seas. This contributes to the concentration of biogenic elements and krill juveniles within the WSC, increasing the bioproductivity of its waters. One possible cause of the strengthening of the fronts that limit the WSC, as the AAO index values increase, may be the intensification of eastward transport in the atmospheric boundary layer and the zonal component of wind stress. At the same time, the band of intense westerly winds shifts southwards towards the WSC, reaching approximately 60°S [29, 32–34].

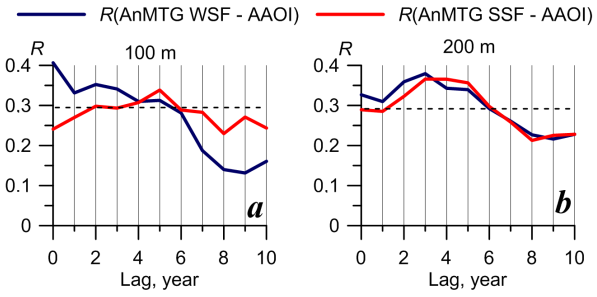


Fig. 9. Cross-correlation functions between the annual averaged values of the MTG anomalies of the SSF and WSF and the Arctic Oscillation index values at depths of 100 m (*a*) and 200 m (*b*). Dashed lines are the boundaries of the confidence interval of the 95% level of statistical significance ($\alpha = 0.05$)

**Conclusion**

Based on ECMWF ORA-S5 reanalysis data from 1958 to 2023, the characteristics of WSC manifestation in average long-term thermohaline fields have been refined. The WSC is most clearly manifested between Shishkov (Clarence) Island and the western boundary of the South Orkney Shelf. Below the AWW layer here, subsidence of colder, less saline water is observed, accompanied by transformation of the CDW layer and disruption to the cores of its upper and lower modifications. The northern boundary of the WSC (the Scotia Sea Front) is found to be situated over the southern slope of the South Scotia Ridge, while the southern boundary (the Weddell Sea Front) is found to pass south of the Phillip Ridge at the northern boundary of the Powell Basin. Both fronts are most intense in the 150–500 m layer. Closer to the South Orkney Shelf, the width of the WSC decreases by more than fivefold (from 2° to 0.375° of latitude). The intensity of the SSF and WSF decreases towards the east, and east of the South Orkney Islands, these fronts become indistinct.

On the interannual scale it is shown that the latitudinal displacements of the WSC boundaries do not exceed 0.5°, while their stable latitudinal position is determined by the bottom relief features. Throughout the entire analysed period, the SSF is located over the southern slope of the South Scotia Ridge in the central part of the WSC, between 60.25° and 60.75°S, while the WSF is located south of the Phillip Ridge, between 61.25° and 61.75°S.

It is established that the boundaries of the WSC both intensify and weaken in synchrony on the interannual scale. From 1983 to 2010, a decrease in the intensity of the SSF and WSF was observed, and both fronts were at their weakest from 1987 to 1990. The intensity of the SSF and WSF increased from 1958 to 1982 and after 2010. During periods of significant intensification or weakening of the WSC boundaries, the intensity anomalies of the WSF exceed those of the SSF by 1.5–2.5 times.

No significant trends characterising the general tendencies of long-period variability in the intensity of the SSF and WSF temperature gradient values were identified in the time series of annual mean anomalies. However, periodicities of four and six years were detected, which are close to the periodicities of the Southern Oscillation and the Southern Annular Mode. A significant positive correlation ($R \sim 0.4$) was identified between the intensity anomalies of the WSF and the AAO index at zero phase shift at a depth of 100 m, and at a shift of three years at a depth of 200 m. A significant positive relationship ($R \sim 0.35$) is also observed between the intensity anomalies of the SSF and the AAO index at a phase shift of 5 years at a depth of 100 m, and at a phase shift of 3–5 years at a depth of 200 m. This tendency for the WSF boundaries to increase in intensity with rising AAO index values has been particularly evident over the last 10 years, when high positive AAO index values and maximum positive WSF intensity anomaly values were observed. However, no significant relationship was identified between interannual changes in SSF and WSF intensity anomalies and changes in the SOI.

REFERENCES

1. Maslennikov, V.V., 2003. *Climatic Variability and Marine Ecosystem of the Antarctica*. Moscow: VNIRO Publishing, 295 p. (in Russian).
2. Zimin, A.V., 2005. The Monitoring of Dynamic Processes in the Scotia Sea and Forecast Opportunity of Commercial Fishery Conditions Using Satellite Altimetry Data. *Issledovanie Zemli iz Kosmosa*, 3, pp. 66–72 (in Russian).
3. Kahru, M., Mitchell, B.G., Gille, S.T., Hewes, C.D. and Holm-Hansen, O., 2007. Eddies Enhance Biological Production in the Weddell-Scotia Confluence of the Southern Ocean. *Geophysical Research Letters*, 34(14), L14603. https://doi.org/10.1029/2007GL030430
4. Venables, H., Meredith, M.P., Atkinson, A. and Ward, P., 2012. Fronts and Habitat Zones in the Scotia Sea. *Deep-Sea Research Part II: Topical Studies in Oceanography*, 59–60, pp. 14–24. https://doi.org/10.1016/j.dsr2.2011.08.012
5. Thompson, A.F. and Youngs, M.K., 2013. Surface Exchange Between the Weddell and Scotia Seas. *Geophysical Research Letters*, 40(22), pp. 5920–5925. https://doi.org/10.1002/2013GL058114
6. Arzhanova, N.V. and Artamonova, K.V., 2014. Hydrochemical Structure of Water Masses in Areas of the Antarctic Krill (*Euphausia superba Dana*) Fisheries. *Trudy VNIRO*, 152, pp. 118–132 (in Russian).
7. Siegel, V. and Watkins, J.L., 2016. Distribution, Biomass and Demography of Antarctic Krill, Euphausia superba. In: V. Siegel, ed., 2016. *Biology and Ecology of Antarctic Krill*. Advances in Polar Ecology, vol. 1. Cham: Springer, pp. 21–100. https://doi.org/10.1007/978-3-319-29279-3_2
8. Spiridonov, V.A., Zalota, A.K., Yakovenko, V.A. and Gorbatenko, K.M., 2020. Composition of Population and Transport of Juveniles of Antarctic Krill in Powell Basin Region (Northwestern Weddell Sea) in January 2020. *Trudy VNIRO*, 181, pp. 33–51. https://doi.org/10.36038/2307-3497-2020-181-33-51 (in Russian).
9. Morozov, E.G., Spiridonov, V.A., Molodtsova, T.N., Frey, D.I., Demidova, T.A. and Flint, M.V., 2020. Investigations of the Ecosystem in the Atlantic Sector of Antarctica (Cruise 79 of the R/V Akademik Mstislav Keldysh). *Oceanology*, 60(5), pp. 721–723. https://doi.org/10.1134/S0001437020050161
10. Deacon, G.E.R. and Moorey, J.A., 1975. The Boundary Regions Between Currents from the Weddell Sea and Drake Passage. *Deep Sea Research*, 22(4), pp. 265–268. https://doi.org/10.1016/0011-7471(75)90031-5
11. Deacon, G.E.R. and Foster, T.D., 1977. The Boundary Region Between the Weddell Sea and Drake Passage Currents. *Deep Sea Research*, 24(6), pp. 505–510. https://doi.org/10.1016/0146-6291(77)90525-2
12. Gordon, A.L., Georgi, D.T. and Taylor, H.M., 1977. Antarctic Polar Frontal Zone in Western Scotia Sea Summer 1975. *Journal of Physical Oceanography*, 7(3), pp. 309–328. https://doi.org/10.1175/1520-0485(1977)007<0309:APFZIT>2.0.CO;2
13. Patterson, S.L. and Sievers, H.A., 1980. The Weddell-Scotia Confluence. *Journal of Physical Oceanography*, 10(10), pp. 1584–1610. https://doi.org/10.1175/1520-0485(1980)010<1584:TWSC>2.0.CO;2
14. Muench, R.D., Gunn, J.T. and Husby, D.M., 1990. The Weddell-Scotia Confluence in Midwinter. *Journal of Geophysical Research: Oceans*, 95(C10), pp. 18177–18190. https://doi.org/10.1029/JC095iC10p18177
15. Peterson, R.G. and Stramma, L., 1991. Upper-Level Circulation in the South Atlantic Ocean. *Progress in Oceanography*, 26(1), pp. 1–73. https://doi.org/10.1016/0079-6611(91)90006-8

16. Whitworth, T., Nowlin, W.D., Orsi, A.H., Locarnini, R.A. and Smith, S.G., 1994. Weddell Sea Shelf Water in the Bransfield Strait and Weddell-Scotia Confluence. *Deep Sea Research*. *Part I: Oceanographic Research Papers*, 41(4), pp. 629–641. https://doi.org/10.1016/0967-0637(94)90046-9
17. Artamonov, Yu.V., 2002. Features of the Hydrological Structure of the Confluence Zone of the Weddell and Scotia Seas in the Summer of the Southern Hemisphere. In: MHI, 2002. *Monitoring Systems of Environment*. Sevastopol: MHI. Iss. 4, pp. 371–380. (in Russian).
18. Heywood, K.J., Naveira Garabato, A.C., Stevens, D.P. and Muench, R.D., 2004. On the Fate of the Antarctic Slope Front and the Origin of the Weddell Front. *Journal of Geophysical Research*, 109(C6), C06021. https://doi.org/10.1029/2003JC002053
19. Artamonov, Yu.V., Bulgakov, N.P., Lomakin, P.D. and Skripaleva, E.A., 2004. Vertical Thermohaline Structure, Water Masses, and Large-Scale Fronts in the Southwest Atlantic and Neighboring Antarctic Water Areas. *Physical Oceanography*, 14(3), pp. 161–172. https://doi.org/10.1023/B:POCE.0000048898.31072.cc
20. Lomakin, P.D. and Skripaleva, E.A., 2008. *Circulation and Waters Structure in Southwestern Part of Atlantic Ocean and Adjacent Areas of Antarctica.* Sevastopol: ECOSI-Gidrofizika, 116 p. (in Russian).
21. Meredith, M.P., Meijers, A.S., Naveira Garabato, A.C., Brown, P.J., Venables, H.J., Abrahamsen, E.P., Jullion, L. and Messias, M.-J., 2015. Circulation, Retention, and Mixing of Waters Within the Weddell-Scotia Confluence, Southern Ocean: The Role of Stratified Taylor Columns. *Journal of Geophysical Research: Oceans*, 120(1), pp. 547–562. https://doi.org/10.1002/2014JC010462
22. Artamonov, Yu.V., Skripaleva, E.A. and Nikolsky, N.V., 2022. Climatic Structure of the Dynamic and Temperature Fronts in the Scotia Sea and the Adjacent Water Areas. *Physical Oceanography*, 29(1), pp. 117–138. https://doi.org/10.22449/1573-160X-2022-2-117-138
23. Artamonov, Y.V., Lomakin, P.D. and Skripaleva, E.A., 2008. Seasonal and Interannual Variability of the characteristics of Scotia-Sea front based on the Satellite Measurements of Sea-Surface Temperature. *Physical Oceanography*, 18(1), pp. 52–62. https://doi.org/10.1007/s11110-008-9009-3
24. Artamonov, Yu.V., Skripaleva, E.A. and Nikolsky, N.V., 2020. Spatial Structure and Intra-Annual Variability of Weddell Sea Front Based on the Data of NOAA OI SST Reanalysis. *Ecological Safety of Coastal and Shelf Zones of Sea*, (4), pp. 89–102. https://doi.org/10.22449/2413-5577-2020-4-89-102 (in Russian).
25. Zuo, H., Balmaseda, M.A., Tietsche, S., Mogensen, K. and Mayer, M., 2019. The ECMWF Operational Ensemble Reanalysis-Analysis System for Ocean and Sea Ice: A Description of the System and Assessment. *Ocean Science*, 15(3), pp. 779–808. https://doi.org/10.5194/os-15-779-2019
26. Turner, J., 2004. The El Niño – Southern Oscillation and Antarctica. *International Journal of Climatology*, 24(1), pp. 1–31. https://doi.org/10.1002/joc.965
27. Turner, J., Colwell, S.R., Marshall, G.J., Lachlan-Cope, T.A., Carleton, A.M., Jones, P.D., Lagun, V., Reid, P.A. and Iagovkina, S., 2005. Antarctic Climate Change during the Last 50 Years. *International Journal of Climatology*, 25(3), pp. 279–294. https://doi.org/10.1002/joc.1130
28. Gong, D. and Wang, S., 1999. Definition of Antarctic Oscillation Index. *Geophysical Research Letters*, 26(4), pp. 459–462. https://doi.org/10.1029/1999GL900003

29. Wang, G. and Cai, W., 2013. Climate-Change Impact on the 20th-Century Relationship Between the Southern Annular Mode and Global Mean Temperature. *Scientific Reports*, 3, 2039. https://doi.org/10.1038/srep02039

30. Nikolskii, N.V., Artamonov, Y.V. and Skripaleva, E.A., 2023. Interannual Variability of Sea Surface Temperature at the Polar Latitudes of the Atlantic Ocean. *Gidrometeorologiya i Ekologiya*, 71, pp. 293–310. https://doi.org/1033933/2713-3001-2023-71-293-310 (in Russian).

31. Chapman, C.C., Lea, M.-A., Meyer, A., Sallee, J.-B. and Hindell, M., 2020. Defining Southern Ocean Fronts and their Influence on Biological and Physical Processes in a Changing Climate. *Nature Climate Change*, 10, pp. 209–219. https://doi.org/10.1038/s41558-020-0705-4

32. Lee, D.Y., Petersen, M.R. and Lin, W., 2019. The Southern Annular Mode and Southern Ocean Surface Westerly Winds in E3SM. *Earth and Space Science*, 6(12), pp. 2624–2643. https://doi.org/10.1029/2019EA000663

33. Thompson, D.W.J., Solomon, S., Kushner, P.J., England, M.H., Grise, K.M. and Karoly, D.J., 2011. Signatures of the Antarctic Ozone Hole in Southern Hemisphere Surface Climate Change. *Nature Geoscience*, 4, pp. 741–749. https://doi.org/10.1038/NGEO1296

34. Serykh, I.V. and Sonechkin, D.M., 2022. Link of El Niño – Southern Oscillation and Southern Annular Mode as Elements of Global Atmospheric Oscillation. *Vestnik of Saint-Petersburg University. Earth Sciences*, 67(4), pp. 614–630. https://doi.org/10.21638/spbu07.2022.404 (in Russian).

Submitted 17.12.2024; accepted after review 20.01.2025;
revised 17.09.2025; published 30.12.2025

*About the authors*:

**Yuri V. Artamonov**, Leading Research Associate, Marine Hydrophysical Institute of RAS (2 Kapitanskaya St., Sevastopol, 299011, Russian Federation), DSc (Geogr.), **ResearcherID: AAC-6651-2020**, **ORCID ID: 0000-0003-2669-7304**, *artam-ant@yandex.ru*

**Elena A. Skripaleva**, Senior Research Associate, Marine Hydrophysical Institute of RAS (2 Kapitanskaya St., Sevastopol, 299011, Russian Federation), PhD (Geogr.), **ResearcherID: AAC-6648-2020**, **ORCID ID: 0000-0003-1012-515X**, *sea-ant@yandex.ru*

**Nikolay V. Nikolskii**, Junior Research Associate, Marine Hydrophysical Institute of RAS (2 Kapitanskaya St., Sevastopol, 299011, Russian Federation), **ResearcherID: AAT-7723-2020**, **ORCID ID: 0000-0002-3368-6745**, *nikolsky.geo@gmail.com*

*Contribution of the authors:*

**Yuri V. Artamonov** – general scientific supervision of the study, statement of the study aims and objectives, method development, qualitative analysis of the results and their interpretation, discussion of the work results, conclusion drawing

**Elena A. Skripaleva** – review of literature on the study problem, qualitative analysis of the results and their interpretation, processing and description of the study results, discussion of the work results, conclusion drawing, preparation of the manuscript, text refinement

**Nikolay V. Nikolskii** – development and debugging of computer programmes for data processing, algorithm programming, graph plotting, participation in discussion of the article materials

*All the authors have read and approved the final manuscript.*

ISSN 2413-5577, Ecological Safety of Coastal and Shelf Zones of Sea, 2025, No. 4, pp. 97–116.

Original paper

# Ichthyoplankton off the Coast of Crimea and its Trophic Relationships in Plankton Community During the Changing Hydrological Seasons (October 2022)

**T. N. Klimova [1] *, A. A. Subbotin [1], B. E. Anninsky [1], I. V. Vdodovich [1], D. A. Zabrodin [1], T. N. Petrova [2], N. A. Datsyk [1]**

[1] *A. O. Kovalevsky Institute of Biology of the Southern Seas of RAS, Sevastopol, Russia*

[2] *T. I. Vyazemsky Karadag Scientific Station – Nature Reserve of RAS, Branch of A. O. Kovalevsky Institute of Biology of the Southern Seas RAS, Feodosiya, Russia*

* *e-mail: tnklim@ibss-ras.ru*

**Abstract**

As a continuation of research on the adaptation of reproduction of natural fish populations to regional changes of hydrological regime, ichthyoplankton studies were performed in the Black Sea in the autumn of 2022. The paper provides data on species composition and spatial distribution of ichthyo-, meso- and gelatinous macroplankton in coastal, shelf, and deep-sea areas near the Crimean Peninsula, obtained within 2–19 October during cruise 124 of R/V *Professor Vodyanitsky.* We identified eggs and larvae of 12 warm-water fish species and 4 temperate-water fish species. The average abundance of eggs was 2.34 ind·m$^{-2}$, whereas the average abundance of larvae was 2.55 ind·m$^{-2}$, with the maximum abundance of 16 and 18 ind·m$^{-2}$ for eggs and larvae. A high number of species and low dominance (dominance index was 0.17) favoured the development of ichthyoplankton complexes with a high species diversity index (3.03), high richness index (20.31) and high evenness index (0.77). Optimal temperature conditions induced the formation of zooplankton communities dominated by small warm-water copepods, which are the primary food source for both the fish larvae and the gelatinous macroplankton. In spite of their trophic competition, gelatinous macroplankton apparently did not influence the survival of fish larvae. The spatial distribution of gelatinous macroplankton was mosaic and it was presumably caused by interpopulational trophic relationships, such as predation and competition, inside the macroplankton community. The most probable cause of the regional differences in species composition and abundance of ichthyo-, meso- and macroplankton were the conditions for the formation of the thermodynamic water structure, coinciding with the gradual seasonal cooling of the upper layer of the sea and the transition of surface circulation from summer-type to winter-type. Within the study region, the shallow waters of the southeastern coastal area experienced earlier cooling than the deeper areas near the South Coast of Crimea, which were well-protected from the cold northerly wind.

**Keywords**: ichthyoplankton, mesoplankton, macroplankton, fish larva feeding, species diversity, spatial distribution, hydrological regime, Black Sea

**Acknowledgements**: This work was carried out under the state research assignments of IBSS “Biodiversity as the basis for the sustainable functioning of marine ecosystems, criteria and scientific principles for its conservation” (no. 124022400148-4); “Functional, metabolic, and molecular-genetic mechanisms of adaptation of marine organisms to the conditions of extreme ecotopes of the Black Sea and the Sea of Azov, and other regions of the World Ocean” (no. 124030100137-6) and “Investigation of the fundamental characteristics of marine hydrobi onts that ensure their functioning in ecosystems and provide the foundation for their rational use and conservation” (no. 124030100100-0).

**For citation**: Klimova, T.N., Subbotin, A.A., Anninsky, B.E., Vdodovich, I.V., Zabrodin, D.A., Petrova, T.N., and Datsyk, N.A., 2025. Ichthyoplankton off the Coast of Crimea and its Trophic Relationships in Plankton Community During the Changing Hydrological Seasons (October 2022). *Ecological Safety of Coastal and Shelf Zones of Sea*, (4), pp. 97–116.

# Ихтиопланктон у берегов Крыма и его трофические связи в планктонном сообществе в период смены гидрологических сезонов (октябрь 2022 года)

**Т. Н. Климова [1]*, А. А. Субботин [1], Б. Е. Аннинский [1], И. В. Вдодович [1], Д. А. Забродин [1], Т. Н. Петрова [2], Н. А. Дацык [1]**

[1] *ФГБУН ФИЦ «Институт биологии южных морей имени А. О. Ковалевского РАН», Севастополь, Россия*

[2] *Карадагская научная станция им. Т. И. Вяземского – природный заповедник РАН – филиал ФГБУН ФИЦ «Институт биологии южных морей имени А.О. Ковалевского РАН», Феодосия, Россия*

* *e-mail: tnklim@ibss-ras.ru*

**Аннотация**

Исследования ихтиопланктона в Черном море осенью 2022 г. были проведены в продолжение ранее выполненных работ в целях изучения адаптации воспроизводства природных популяций рыб в условиях региональных изменений гидрологического режима, обусловленных потеплением климата. В статье представлены данные о видовом составе и пространственном распределении ихтио-, мезо- и желетелого макропланктона в прибрежных, шельфовых и глубоководных районах у Крымского полуострова, собранные в 124-м рейсе НИС «Профессор Водяницкий» с 2 по 19 октября 2022 г. Идентифицированы икра и личинки 12 видов тепловодных и 4 видов умеренноводных рыб. Средняя численность икры составляла 2.34 экз.·м$^{-2}$, личинок – 2.55 экз.·м$^{-2}$, а максимальная – 16 и 18 экз.·м$^{-2}$ соответственно. Большое количество видов в ихтиопланктоне в осеннее межсезонье и слабо выраженное доминирование (индекс доминирования 0.17) способствовали развитию ихтиопланктонных комплексов с высоким индексом видового разнообразия (3.03), богатства (20.31) и выравненности (0.77). Благоприятные температурные условия сформировали зоопланктонные сообщества с преобладанием мелких тепловодных Copepoda – основных объектов питания, как личинок рыб, так и желетелого макропланктона. Желетелый макропланктон, будучи пищевым конкурентом личинок рыб, не оказывал существенного влияния на их выживание. Пространственное распределение желетелого макропланктона

было мозаичным и зависело от межпопуляционных трофических отношений – хищничества и конкуренции в самом макропланктонном сообществе. Наиболее вероятной причиной региональных различий в видовом составе и численности ихтио-, мезо- и макропланктона являлись условия формирования термодинамической структуры вод на фоне плавного сезонного выхолаживания верхнего слоя моря и перестройки летнего типа поверхностной циркуляции на зимнюю. В районе исследований наблюдалось опережающее выхолаживание вод мелководного Юго-Восточного Крыма по сравнению с глубоководным, защищенным от холодных северных ветров районом Южного берега Крыма.

**Ключевые слова**: ихтиопланктон, мезопланктон, макропланктон, питание личинок рыб, видовое разнообразие, пространственное распределение, гидрологический режим, Черное море

**Благодарности**: работа выполнена в рамках госзадания ФИЦ ИнБЮМ по темам госзадания № 124022400148-4 «Биоразнообразие как основа устойчивого функционирования морских экосистем, критерии и научные принципы его сохранения»; № 124030100137-6 «Функциональные, метаболические и молекулярно-генетические механизмы адаптации морских организмов к условиям экстремальных экотопов Черного и Азовского морей и других акваторий Мирового океана»; № 124030100100-0 «Изучение фундаментальных характеристик морских гидробионтов, обеспечивающих их функционирование в экосистемах и служащих основой их рационального использования и сохранения».

**Для цитирования**: Ихтиопланктон у берегов Крыма и его трофические связи в планктонном сообществе в период смены гидрологических сезонов (октябрь 2022 года) / Т. Н. Климова [и др.] // Экологическая безопасность прибрежной и шельфовой зон моря. 2025. № 4. С. 97–116. EDN ZFXLJK.

## Introduction

The relatively high biological productivity of the Black Sea shelf waters promotes the formation of a diverse ichthyofauna, comprising around 200 species and playing a key role in trophic relationships. In 2000–2016, eggs and larvae of 69 fish species were identified in the ichthyoplankton [1)] [1].

By the end of the 1980s, the Black Sea shelf ecosystem had degraded at all trophic levels due to increased anthropogenic load. The invasion and mass proliferation of the ctenophore *Mnemiopsis leidyi* A. Agassiz, 1865 altered the composition of the plankton community and depleted the food source for larval and adult planktivorous fish. In the early 1990s, a catastrophic decline occurred in the species diversity and abundance of ichthyoplankton, which is highly sensitive to changes in biotic and abiotic environmental factors. Concurrently, catches of commercially important fish species decreased. Recovery of the food base for planktivorous fish did not begin until the end of the 1990s, due to the invasion of the ctenophore *Beroe ovata* Bruguière, 1789 which feeds exclusively on planktivorous ctenophores, including *M. leidyi* [2, 3].

---

[1)] Rass, T.S., 2001. [The Black Sea Region and its Productivity]. *Voprosy Ikhtiologii*, 41(6), pp. 742–749 (in Russian).

The increase in commercial fish catches, as well as the recovery of warm-water ichthyoplankton complexes, began only in the 2000s. This occurred against the backdrop of climate-related changes to the Black Sea's hydrological regime [2)], which have been observed since the mid-1990s [1, 3–6]. The most significant consequences of climate changes in the hydrological regime of the Black Sea are the steady increase in the mean annual temperature of its active layer, the transformation of its cold intermediate layer (CIL) and changes in the parameters of hydrological seasons, particularly the winter (WHS) and summer (SHS) ones [2)] [7, 8]. The biological cycles of hydrobionts, including the phenology of spawning in temperate-water and warm-water fish species, the periods of mass development of food zooplankton, and ultimately the trophic relationships in the plankton community, are determined by the timing of the onset and end of hydrological seasons [3), 4), 5)].

The autumn hydrological season (AHS) is characterized by maximum temperature gradients in the upper sea layer and the transition from summer to winter circulation patterns in the surface current system [7, 9, 10]. The survival success of the spring generation of the scyphomedusa *Aurelia aurita* (Linnaeus, 1758) and the degree to which individuals of the ctenophore *M. leidyi* are eliminated by predation from the ctenophore *B. ovata* are determined during the AHS. For several mesoplankton species (*Oithona davisae* Ferrari F. D & Orsi, 1984; *Paracalanus parvus* Claus, 1863, etc.), the AHS is a period of active growth and reproduction. Interactions between different links in the trophic chain within epipelagic complexes influence the efficiency of spawning and the survival of fish at early developmental stages. These factors determine the success of recruitment to future fish generations [6, 11–14].

The purpose of the conducted research is to study the adaptation of ichthyoplankton to structural changes in the plankton community in relation to the hydrological features of the Black Sea in the context of climate warming.

**Materials and methods**

Ichthyoplankton, mesoplankton and gelatinous macroplankton were collected during cruise 124 of R/V *Professor Vodyanitsky* on 2–19 October 2022 at 56 stations off the Crimean Peninsula (the Black Sea), at depths ranging from 21 to 2000 m. The survey was conducted in a reverse mode, starting from the Century Transect in the western part of the study area to Feodosiya Bay and back. The majority of the stations (except those of the Century Transect) were located in two physiographic

---

[2)] Belokopytov, V.N., 2017. [*Climate Changes of the Black Sea Hydrological Regime. Extended Abstract of Doctoral Dissertation*]. Sevastopol, 42 p. (in Russian).

[3)] Dekhnik, T.V., 1973. [*Ichtyoplankton of the Black Sea*]. Kiev: Naukova Dumka, 235 p. (in Russian).

[4)] Dekhnik, T.V. and Pavlovskaya, P.M., 1979. [Seasonal Variations of the Species Composition, Distribution and Abundance of Ichthyoplankton]. In: V. N. Greze, 1979. *Productivity of the Black Sea*. Kiev: Naukova Dumka, pp. 268–272 (in Russian).

[5)] Odum, E., 1983. *Basic Ecology*. Philadelphia: Saunders College Pub., 613 p.

regions with distinct hydrological regimes characteristic of the coastal and shelf zone of Crimea: the South Coast of Crimea (SCC) (from Laspi Bay to the Alushta area) and Southeastern Crimea (from the Sudak area to Feodosiya Bay), both characterized by a narrow shelf (shelf edge depth close to 100 m) [7, 15, 16, 19]. Additionally, on 1 and 13 October, 14 ichthyoplankton samples were collected from the coastal waters of the Karadag Nature Reserve over depths from 3 to 20 m using vertical and five-minute horizontal surface tows with an ichthyoplankton conical net (ICN-80). When analyzing the state of ichthyoplankton complexes and associated data, both regions were distinguished as western and eastern sectors. Considering the sequence of the survey stages, the data array for the western sector included stations performed from 2 to 7 October and from 14 to 19 October while the eastern sector included stations from 9 to 13 October.

Ichthyoplankton and macroplankton were collected using a reverse-conical BR-80/113 net and a conical IGN-80 net, both with an inlet area of 0.5 m² and a mesh size of 400 μm. Mesoplankton were collected using a standard Juday net (inlet area 0.1 m², mesh size 112 μm) in the vertical towing mode. At deep-water stations, sampling was conducted from the lower boundary of the oxygen layer ($\sigma_t$ = 16.2 according to Sea-Bird 911plus probe data) to the surface. At shelf stations, sampling was conducted from the bottom to the surface. Ichthyoplankton were identified to the species level using monographs [3), 6)]. Diversity indices were calculated according to the monograph [5)]. Primary processing of gelatinous macroplankton samples (determination of taxonomic composition, abundance, and sizes of individuals larger than 5 mm) was carried out on board the vessel. Body mass of individuals was calculated using previously established length-weight relationships. Data on early developmental stages of ctenophores (less than 5 mm), ephyrae of *A. aurita* and hydromedusae were adjusted after microscopy of fixed net samples in stationary laboratories. All net samples were fixed in 4% neutralized formalin and processed using an MBS-9 stereomicroscope within two months after collection. The species and size-age composition of each sample were identified, and the abundance of captured organisms was counted. The body mass of mesoplankton and macroplankton was determined using length-weight relationships, and the total biomass was calculated based on organism abundance. With the exception of gelatinous forms and the heterotrophic dinoflagellate *Noctiluca scintillans* (Macartney) Kofoid & Swezy, 1921, all planktonic organisms were classified as food zooplankton. Species names of hydrobionts are given according to WoRMS [7)]. Fish larvae feeding was studied using the method [8)]. The total length (TL) of fish larvae was measured using an ocular micrometer. The body weight (W) of fish larvae was measured using a torsion balance, while that of juveniles was measured using an electronic balance (AXIS ADG500C).

---

6) Russell, F.R.S., 1976. *The Eggs and Planktonic Stages of British Marine Fishes. Family Gadidae*. London; New York; San Francisco: ACADEMIC PRESS, pp. 94–178.

7) Available: http://www.marinespecies.org [Accessed: 01 December 2023].

8) Duka, L.A. and Sinyukova, V.I., 1976. [*Guide to Studying the Nutrition of Marine Fish Larvae and Juveniles in Natural and Experimental Conditions*]. Kiev: Naukova Dumka, 134 p. (in Russian).

We analyzed the hydrological regime using expeditionary data from vertical profiling with a Sea-Bird 911plus CTD probe. Additional information came from satellite observations of sea surface temperature (SST) [9].

**Results and discussion**

*Hydrological regime.* In 2022, the AHS began in the third decade of September in the study area, following a sharp decrease in SST from 24.5–25.0°C to 22.5–23.0°C during the second decade of the month, in the final phase of the SHS. Progress on the study was complicated by brief periods of active cyclonic activity across the entire Black Sea region. Most of the time, the sea state was 2, briefly increasing to 3–4.

At the beginning of the survey, the SST spatial distribution was characterized by higher values (22.0–22.5°C) in the coastal and shelf zone of the SCC and lower values (21.0–21.5°C) in the Sudak and Feodosiya area (Fig. 1, *a*). By the end of the survey, seasonal radiative cooling and wind-wave mixing had decreased the SST to 19.5–20.0°C in the SCC area and 18.0–18.5°C in the southeastern coastal and shelf zone (Fig. 1, *b*). The subsequent slow decrease in SST continued until the end of October, reaching 17.5–17.0°C [9]. Thus, the survey period corresponded to the initial phase of the AHS.

The circulation of surface waters in the northern part of the Black Sea, adjacent to the Crimean Peninsula, was characterized by the instability of the Rim Current (RC). This instability is typical of the transition from summer to winter circulation, which occurs when the RC intensifies and penetrates the coastal and shelf zone. Throughout September, strengthening winds from the north (shifting from northwesterly to northeasterly directions) led to the blocking of the RC jet in the northeastern part

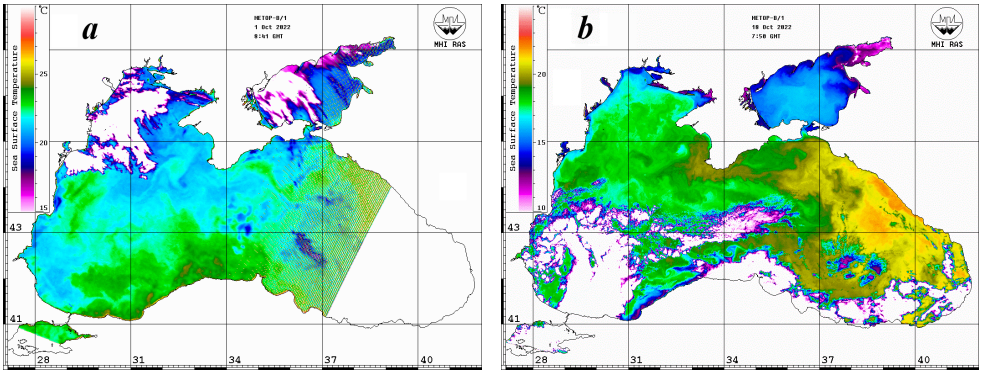


Fig. 1. Satellite maps of sea surface temperature distribution during the ichthyoplankton sampling: 01.10.2022 (*a*); 18.10.2022 (*b*)

[9] Available: http://dvs.net.ru/mp/index_ru.shtml [Accessed: 01 December 2023].

of the Black Sea. This resulted in active meandering of the RC along the shelf edge to the southwestern tip of the Crimean Peninsula. The distinctive features of the current surface circulation structure were two RC cyclonic meanders: one in the coastal and shelf zone southeast of the Kerch Strait and the second one in the coastal and shelf zone from the Alushta area to the Heraclean Peninsula. In the deep trough between these meanders, from the Kerch pre-strait zone to Sudak, an anticyclonic eddy was observed, which existed in this area from mid-September to the end of October [9]. It should be noted that this dynamic feature likely forms during the transition from one hydrological season to another (from spring to summer and from summer to autumn) under conditions of strengthening northerly and northeasterly winds over eastern Crimea and the northeastern part of the Black Sea [17]. Analysis of satellite images from the previous period revealed that this eddy originated from a vortex dipole forming in the coastal area between Anapa and Gelendzhik, which then transformed onto the Kerch shelf [9] [18]. Elevated SST values were observed within the RC cyclonic meanders, whereas lowered values were observed within the anticyclonic eddy, which was largely maintained by the inflow of cold Azov Sea waters along the coast of Southeastern Crimea (Fig. 1, *a*, *b*).

The thickness of the upper quasi-homogeneous layer (UQHL) generally corresponded to values typical for this season [19] and varied depending on the degree of wind-induced wave agitation and the position of stations relative to the corresponding thermodynamic structures during the survey [9]. In the first decade of October, under sea state 2 conditions, the UQHL thickness on the shelf and over the continental slope ranged from 13–22 m in the warmest waters of the RC to 23–27 m in the narrow coastal zone from Cape Sarych to Alushta. Following the storm on 7 October, the UQHL thickness in the RC waters increased to 26–31 m. In the eastern sector, within the anticyclonic eddy, the UQHL thickness varied from 27–35 m at the periphery to 35–43 m in the central part. By the end of the survey, after strengthening of wind-wave activity (15–16 October) to 3–4 points, the UQHL thickness in the coastal and shelf zone of the SCC increased to 37–57 m. During the survey period, the CIL in its classical form, bounded by the 8°C isotherm, was not observed. Throughout the entire area, minimum water temperature values in the water column varied within a narrow range of 8.16–8.30°C, with regional variability in the depth of the CIL core ranging from 53 to 92 m.

The spatial distribution of surface water salinity was characterized by elevated values (18.74–18.84‰) in the open waters at the stations along the Century Transect and in the RC waters in the western sector as well as by lowered values (18.56–18.66‰) in the narrow coastal zone off the SCC and in the Feodosiya Bay waters.

*Ichthyoplankton studies*. In recent years, the steady trend of extending the SHS until the end of September has resulted in the effective spawning of warm-water fish, continuing into the first and second decades of October [13, 20]. The species composition and abundance of ichthyoplankton depended on the cooling rate of the upper mixed layer during the transition from the final phase of the SHS to the developed AHS temperature regime.

A total of 16 fish species from 12 families were identified in the coastal, shelf, and deep-sea areas off the Crimean Peninsula in October 2022 (12 species from 9 families of warm-water fish and 4 species from 3 families of temperate-water fish).

The coastal waters of Karadag were located in the zone of anticyclonic eddy, characterized by lowered SST values due to advanced radiative cooling and the inflow of cold Azov Sea waters along the southeastern coast of Crimea. In October 2022, SST did not exceed 18°C. Spawning was unsuccessful, and larvae were absent from the samples. In the ichthyoplankton, only eggs of one temperate-water fish species, *Gaidropsarus mediterraneus* (Linnaeus, 1758), and of six warm-water fish species, *Engraulis encrasicolus* Linnaeus, 1758; *Chelon saliens* (Risso, 1810); Callionymus sp.; *Trachinus draco* Linnaeus, 1758; *Uranoscopus scaber* Linnaeus, 1758; *Pegusa nasuta* (Pallas, 1814), were encountered. All species except *P. nasuta* were also recorded in the open waters off the Crimean Peninsula. In the first decade of October, eggs of all seven species were identified in horizontal surface tows. However, in vertical tows, only the eggs of the warm-water *E. encrasicolus* and the temperate-water *G. mediterraneus* were recorded. Eggs of these two species were also encountered in the second decade of October, when spawning of the remaining species had already ceased in this area. The average abundance of eggs in the first decade of October was 0.9 ind·m$^{-2}$, decreasing to 0.5 ind·m$^{-2}$ in the second decade.

In contrast to the coastal waters of Karadag, elevated SST values were observed in the open waters in October 2022, ranging from 21.0–22.5°C at the beginning of the survey to 18.5–20.5°C at the end. Eggs and larvae of 11 warm-water fish species from 8 families were identified in the ichthyoplankton, as well as 4 temperate-water fish species from 3 families below the thermocline layer. Due to the relatively large number of ichthyoplankton species for the autumn season and the weak dominance of individual species (dominance index was 0.17), the ichthyoplankton community exhibited high diversity indices. The species diversity index was 3.03, the richness index was 20.31, the evenness index was 0.77 [5)].

In the deep-sea zone, eggs and larvae of nine species were identified, with their average abundances being 1.43 and 4.56 ind.·m$^{-2}$, respectively. In the shelf waters, eggs and larvae were represented by 14 species, with their average abundances being 2.64 and 2.01 ind.·m$^{-2}$, respectively. On the shelf, over depths from 78 to 92 m, the maximum abundance (from 10 to 16 ind.·m$^{-2}$) of eggs was recorded only for temperate-water species (*Sprattus sprattus* (Linnaeus, 1758), *Merlangius merlangus* Linnaeus, 1758 and *G. mediterraneus*). The maximum abundance of larvae (16 to 18 ind.·m$^{-2}$) was recorded over depths exceeding 200 m, where the larvae were represented exclusively by warm-water species *E. encrasicolus* and *Syngnathus schmidti* Popov, 1927 (Fig. 2).

The average abundances of eggs and larvae were 2.34 and 2.55 ind.·m$^{-2}$, respectively. Eggs of 3 temperate-water species (*S. sprattus, M. merlangus, G. mediterraneus*) dominated the samples, accounting for 81.2% of the total egg abundance, with *S. sprattus* being predominant (51.7%). The proportion of larvae of temperate-water species was 18.5%, with the Mediterranean invader *Trisopterus luscus* (Linnaeus 1758) prevailing (13.3 %). Usually, spawning of warm-water fish ended

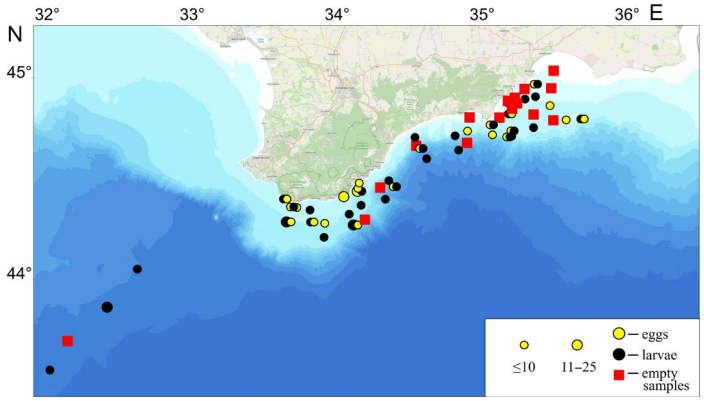


Fig. 2. Spatial distribution of ichthyoplankton (ind.·m$^{-2}$) in October 2022

in September, and in October, only larvae of the older age group were encountered [3]. In October 2022, SST was still favorable for spawning of 3 warm-water fish species, with successful spawning of *E. encrasicolus* and *C. saliens*. Larvae of 10 warm-water fish species dominated the samples, accounting for 81.6% of the total abundance, with larvae of *E. encrasicolus* prevailing (38%) (Table 1).

The ichthyoplankton species composition was quite similar between the western and eastern sectors, with 13 species of fish eggs and larvae in each (Table 1). However, larvae of *Pomatoschistus marmoratus* (Risso, 1810) and *T. draco* were absent from the western sector, and larvae of *Ophidion rochei* Müller, 1845 and *Gobius bucchichi* Steindachner, 1870 were absent from the eastern sector. Temperate-water species *S. sprattus*, *M. merlangus* and *G. mediterraneus* dominated among the eggs. They accounted for 78.2% and 82.2% of the total abundance of eggs of all identified species in the western and eastern sectors, respectively. Warm-water species dominated among the larvae, accounting for 81.4% in the western sector and 81.8% in the eastern sector. In the western sector, where the SST was higher, the average abundances of eggs and larvae were 4.53 and 4.75 ind.·m$^{-2}$, respectively, whereas in the eastern sector, they were only 1.35 and 1.65 ind.·m$^{-2}$, respectively (Table 1).

Due to the limited number of observations on the state of ichthyoplankton during the transition from the SHS to the AHS, it is interesting to compare these data with those obtained in cruise 89 of R/V *Professor Vodyanitsky*, which was conducted during the first and second decades of October 2016. During the first decade of October 2022, high sea surface temperature (SST) values (22.0–22.5°C) were observed in open waters in the western sector. Fifteen species of fish eggs and larvae were recorded in the ichthyoplankton (11 warm-water and 4 temperate-water species). The average abundances of eggs and larvae were 4.46 and 4.62 ind.·m$^{-2}$, respectively. Temperate-water species dominated with 69.5% of the eggs, while warm-water species accounted for 84.4% of the larvae. In October 2016, the SST in the open waters of the western sector off the Crimean Peninsula, from Cape Tarkhankut to Alupka, was lower than in 2022 (19.0–21.5°C).

Table 1. Species composition of ichthyoplankton off the coast of Crimea in the western and eastern research areas, number of species and the average abundances of eggs and larvae of fish in October 2022

| Taxonomic groups | Total | Study area | |
|---|---|---|---|
| | | western | eastern |
| *Share in species composition, %* | | | |
| *Temperate water fish species* | | | |
| **Family: Clupeidae**<br>*Sprattus sprattus* (Linnaeus, 1758) | 51.7*<br>1.2 | 58.7<br>2.3 | 40.8<br>0 |
| **Family: Gadidae**<br>*Merlangius merlangus* Linnaeus, 1758 | 17.5<br>2.8 | 12.2<br>4.6 | 25.9<br>0 |
| *Trisopterus luscus* (Linnaeus, 1758) | 0<br>13.3 | 0<br>11.7 | 0<br>152 |
| **Family: Lotidae**<br>*Gaidropsarus mediterraneus* (Linnaeus, 1758) | 12.0<br>1.2 | 7.3<br>0 | 18.5<br>3.0 |
| *Warm water fish species* | | | |
| **Family: Engraulididae**<br>*Engraulis encrasicolus* Linnaeus, 1758 | 14.5<br>38.0 | 17.0<br>46.8 | 11.1<br>27.3 |
| **Family**: **Ophidiidae**<br>*Ophidion rochei* Muller, 1845 | 0<br>1.2 | 0<br>2.3 | – |
| **Family**: **Syngnathidae**<br>*Syngnathus schmidti* Popov, 1927 | 0<br>20.4 | 0<br>16.2 | 0<br>24.2 |
| **Family: Callionymidae**<br>*Callionymus sp.* | 0<br>3.9 | 0<br>2.3 | 0<br>6.1 |
| **Family: Gobiidae**<br>*Gobius bucchichi* Steindachner 1870 | 0<br>1.2 | 0<br>2.3 | – |
| *Pomatoschistus marmoratus* (Risso, 1810) | 0<br>3.9 | – | 0<br>9.1 |
| *P. minutus* (Pallas, 1770) | 0<br>3.9 | 0<br>2.3 | 0<br>6.1 |
| *Knipowitschia longecaudata* (Berg, 1916) | 0<br>3.9 | 0<br>4.6 | 0<br>3.0 |
| **Family: Mugilidae**<br>*Chelon saliens* (Risso, 1810) | 1.3<br>3.9 | 2.4<br>4.6 | 0<br>3.0 |
| **Family**: **Trachinidae**<br>*Trachinus draco* Linnaeus, 1758 | 0<br>1.2 | – | 0<br>3.0 |
| **Family**: **Uranoscopidae**<br>*Uranoscopus scaber* Linnaeus, 1758 | 3.0<br>0 | 2.4<br>0 | 3.7<br>0 |

*Continued*

| Taxonomic groups | Total | Study area | |
|---|---|---|---|
| | | western | eastern |
| *Community parameters* | | | |
| Number of species | 15 | 13 | 13 |
| Average abundance, ind.·m$^{-2}$ | 2.34<br>2.55 | 4.53<br>4.75 | 1.35<br>1.65 |
| Standard deviation | 3.71<br>3.82 | 5.26<br>5.70 | 2.19<br>2.11 |

* The numerator – values for eggs, the denominator – those for larvae.

However, the surface water circulation system corresponded to the summer type. Eggs and larvae of 10 fish species were identified. The average abundances (eggs 3.4 ind.·m$^{-2}$, larvae 4.7 ind.·m$^{-2}$) and the species composition (eggs of temperate-water fish species dominated, accounting for 61.8%, and larvae of warm-water species, dominated accounting for 85.1%) were quite comparable with the data from the first decade of October 2022 [13].

In the second decade of October 2022, the early seasonal cooling and wind-wave mixing caused a decrease in SST values in the coastal and shelf zone of Southeastern Crimea to 18.0–18.5°C, which corresponded to the initial phase of the AHS. Ichthyoplankton in the open waters of the eastern sector off the Crimean Peninsula was represented by 10 species (4 temperate-water and 6 warm-water fish species). The average abundance of eggs was 1.06 ind.·m$^{-2}$, and that of larvae was 1.4 ind.·m$^{-2}$. Eggs of temperate-water species (94.3%) and larvae of warm-water species (75.7%) dominated. In the second decade of October 2016, in the eastern sector off the Crimean Peninsula from Alupka to the Kerch Peninsula, after a strong storm, SST was on average 2°C lower than in 2022 and amounted to 16.0–16.5°C only, which corresponded to the developed AHS. Eggs and larvae of 5 temperate-water fish species and larvae of older age groups of 7 warm-water fish species were identified. The average abundances of eggs (2.76 ind.·m$^{-2}$) and larvae (2.55 ind.·m$^{-2}$) were twice as high as in October 2022, due to the dominance of temperate-water species in the samples: their eggs accounted for 100% and larvae accounted for 54.5% [13].

*Fish larvae and juvenile feeding*. In the first decade of October 2022, in the western sector, larvae of *E. encrasicolus* predominated. Their proportions were 50% yolk-sac feeding, 19% mixed feeding and 31% on exogenous feeding. The high proportion of larvae on the yolk-sac feeding type indicated successful spawning of

*E. encrasicolus*. According to studies [3), 10)], in the Black Sea, eggs and early-stage larvae of *E. encrasicolus* were extremely rare during this period. Spawning of other warm-water fish species continued. The TL of a *P. minutus* goby larva caught over a depth of 1336 m did not exceed 2.4 mm, which corresponded to an age of one day. The remaining representatives of the family Gobiidae were large specimens with TL 17–40 mm and W 1–240 mg. At deep-water stations, juvenile individuals and juveniles of *S. schmidti* with TL 26–33 mm and W 2.5–58 mg, as well as *Callionymus* sp. with TL 6 mm, were caught. Over a depth of 123 m, a single larva of the mullet *C. saliens* with TL 4.2 mm was caught. Among temperate-water species, prelarvae of the family Gadidae were recorded at the beginning of October. A single juvenile specimen of *S. sprattus* with TL 26 mm and W 348 mg was caught over a depth of 1773 m. In the eastern sector, collections were carried out only over depths from 40 to 98 m. According to study [10)], spawning of the warm-water *E. encrasicolus* ended in the eastern sector earlier than in the western sector. We also recorded mainly large specimens of larvae of thermophilic fish species. The TL of *E. encrasicolus* larvae varied from 6.7 to 9.9 mm, and that of larvae of the family Gobiidae from 6.3 to 39.0 mm. A larva of *T. draco* with TL 6.1 mm was also found.

Analysis of data on the size-mass structure of ichthyoplankton in the second decade of October revealed a steady decline in the spawning of warm-water species and an increase in the proportion of temperate-water species. Only large specimens of fish larvae and juveniles were caught: *E. encrasicolus* with TL 14.2 mm in the eastern sector and TL 34 mm in the western sector. In both areas, juvenile and maturing individuals of *S. schmidti* with TL 26–34 mm were recorded. In the eastern sector, at shallow-water stations, size-varied representatives of the family Gobiidae with TL 3.8–6.3 mm and *C. saliens* with TL 4.8 mm were identified in the samples. Temperate-water species in the ichthyoplankton were represented by the family Gadidae, among which larvae of the Mediterranean invader *T. luscus* with TL 6.5–7.6 mm dominated. In the food boluses of fish larvae and juveniles, calanoid copepods (adults and juveniles) were identified. The number of food items in their intestines varied from 1 to 56 specimens, indicating a good food base and favorable conditions for their survival.

*Mesoplankton.* In the mesoplankton of the Black Sea in October 2022, adult individuals and copepodites of copepod species typical for this period dominated: *Acartia clausi* Giesbrecht, 1889; *A. tonsa* Dana, 1849; *Calanus euxinus* Hulsemann, 1991; *Pseudocalanus elongatus* Boeck, 1865; *Paracalanus parvus* Claus, 1863; *Centropages ponticus* Karavaev, 1895; *Oithona davisae* Ferrari F.D. & Orsi, 1984; and *Oithona similis* Claus, 1866. In addition to them, chaetognaths *Parasagitta setosa* J. Müller, 1847 and appendicularians *Oikopleura (Vexillaria) dioica* Fol, 1872 were also encountered in significant quantities (Table 2).

The average abundances of mesoplankton were 626.3 ± 79.2 thousand ind.·m$^{-2}$ in the deep-sea part of the sea and 739.2 ± 128.1 thousand ind.·m$^{-2}$ on the outer shelf; the biomasses was 11.8 ± 0.5 g·m$^{-2}$ and 11.3 ± 0.4 g·m$^{-2}$, respectively.

---

[10)] Dekhnik, T.V., 1954. [Reproduction of Anchovies and Mullet in the Black Sea]. *Trudy VNIRO*, 27, pp. 34–48 (in Russian).

Table 2. Abundance (thous. ind.·m$^{-2}$) and biomass (g·m$^{-2}$) of mass mesoplankton species in the Black Sea in October 2022

| Species composition of mesoplankton | Outer shelf | | Deep water part | |
|---|---|---|---|---|
| | Abundance | Biomass | Abundance | Biomass |
| *Acartia sp.* | 49.5 | 0.54 | 39.4 | 0.5 |
| *Calanus euxinus* | 3.2 | 0.8 | 5.1 | 3.8 |
| *Pseudocalanus elongates* | 10.7 | 0.2 | 30.8 | 0.7 |
| *Paracalanus parvus* | 274.5 | 1.8 | 129.6 | 0.9 |
| *Centropages ponticus* | 23.2 | 0.5 | 51.0 | 0.7 |
| *Oithona similis* | 14.8 | 0.06 | 29.9 | 0.1 |
| *Oithona davisae* | 157.0 | 0.7 | 77.7 | 0.3 |
| *Noctiluca scintillans* | 3.5 | 0.4 | 5.4 | 0.6 |
| *Parasagitta setosa* | 21.9 | 3.5 | 14.5 | 2.0 |
| *Oikopleura dioica* | 39.5 | 1.2 | 38.8 | 1.0 |
| Cladocera | 40.0 | 1.3 | 28.0 | 0.8 |
| Total zooplankton | 739.2 | 11.3 | 626.3 | 11.8 |
| Forage zooplankton | 735.2 | 10.9 | 620.9 | 11.2 |

In terms of abundance, both on the shelf and in the deep-sea areas, the copepods *P. parvus* and *O. davisae* dominated; these are the primary food objects for fish larvae and juveniles. In terms of biomass, *C. euxinus* and *P. setosa* prevailed, especially in the deep sea. The chaetognaths biomass increased from the western sector to the eastern sector (Fig. 3).

Compared to the mesozooplankton biomass in the open sea during the corresponding period of 2019 (cruise 110 of R/V *Professor Vodyanitsky*), the biomass of most species increased 1.5-fold or more. In particular, the biomass of *C. euxinus* increased from 2.8 to 3.8 g·m$^{-2}$, *P. elongatus* from 0.4 to 0.7 g·m$^{-2}$, *O. davisae* from 0.1 to 0.3 g·m$^{-2}$, and the chaetognath *P. setosa* from 0.2 to 2.0 g·m$^{-2}$. Among Copepoda, the biomass of small warm-water species increased particularly strongly, whereas that of cold-water species (*C. euxinus*, *P. elongatus* and *O. similis*) still did not reach the long-term average level. Such interannual population dynamics of mesoplankton species may be associated with the ongoing warming of the upper sea layer and the CIL [2] [14]. Thus, zooplankton communities underwent radical changes.

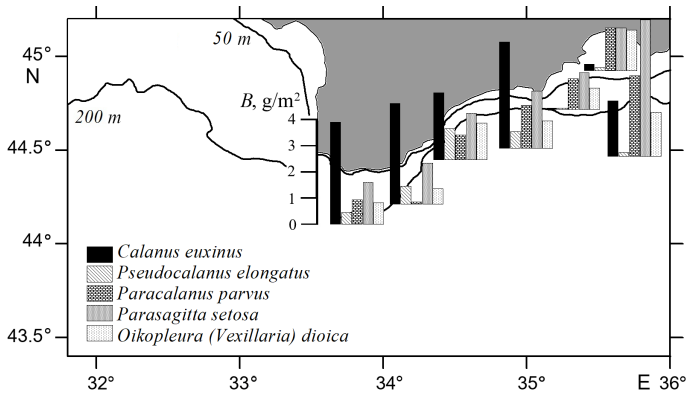


Fig. 3. Biomass *B* distribution of some mesozooplankton species on the outer shelf and in deepwater areas of the Black Sea near Southern Coast of Crimea in October 2022

The biomass of mesozooplankton and all gelatinous forms decreased sharply, while the total abundance of mesoplanktonic organisms increased due to a greater number of copepod nauplii, small cyclopoid crustaceans (*O. davisae* and *O. similis*), and the appendicularian *Oikopleura (Vexillaria) dioica* in the plankton [14]. This increase in the abundance of small-sized food organisms contributed apparently to the prolongation of the periods of mass successful spawning of both warm-water and temperate-water species into the initial phase of the AHS [13, 20].

During the study period, gelatinous macroplankton was mainly represented by size- and age-varied individuals of the scyphomedusa *A. aurita* and three ctenophore species: *B. ovata*, *M. leidyi*, and *Pleurobrachia pileus* (O. F. Müller, 1776). At the same time, *A. aurita* and *P. pileus* were encountered at 55 plankton stations, *B. ovata* at 53 stations and *M. leidyi* at 35 stations (Table 3).

The quantitative distribution of all these species was, to a greater or lesser extent, mosaic ($\sigma^2 > M$) and evidently depended on their own temperature tolerance, regional thermodynamic structures and interpopulational trophic relationships (predation and competition) within the macroplankton community itself and in the epipelagic biota as a whole (Fig. 4). No significant relationship was found between the distribution of the jellyfish *A. aurita* and the specific features of the hydrological regime of the sea. Abundance was noticeably higher in the area of the Western Cyclonic Gyre northern periphery, while biomass was higher in the convergence zone at the outer boundary of the cyclonic meander of the RC, where mesoplankton aggregations are common. It is possible that food zooplankton was the determining factor in the distribution of *A. aurita*, which was observed more frequently on the outer shelf and in the deep-water epipelagic zone. The early planktonic stages of the jellyfish, ephyrae (up to 9 mm in diameter), were observed singly at 9 shelf stations (Table 3, Fig. 4, *a*).

Table 3. Abundance (numerator), ind.·m$^{-2}$, and biomass (denominator), g·m$^{-2}$, of gelatinous macroplankton near Southern coast of Crimea in October 2022

| Species | Shelf | | Deep water areas (> 200 m) $n$ = 18 |
|---|---|---|---|
| | inner (< 50 m) $n$ = 8 | outer (> 50 m) $n$ = 30 | |
| *A. aurita* | 3.2 ± 1.1<br>29.3 ± 16.8 | 10.0 ± 1.2<br>178.3 ± 28.2 | 7.5 ± 1.2<br>177.1 ± 38.1 |
| *P. pileus* | 8.7 ± 3.3<br>0.4 ± 0.2 | 54.5 ± 9.0<br>4.4±1.4 | 119.4 ± 14.0<br>20.9 ± 3.1 |
| *M. leidyi* | < 0.1<br>< 0.1 | 4.4 ± 1.1<br>12.2 ± 4.9 | 8.8 ± 1.5<br>18.2 ± 5.9 |
| *B. ovata* | 20.1 ± 4.3<br>20.2 ± 7.9 | 17.7 ± 2.7<br>15.3 ± 3.4 | 10.6 ± 2.5<br>16.1 ± 4.8 |

Note: $n$ – number of determinations; the average ± errors of the averages are given.

The ctenophore *P. pileus* was more confined to deep-water areas in its distribution (Fig. 4, *b*). As the thermocline deepened, this species was encountered in significantly lower quantities. Its abundance and biomass increased from the inner shelf to the outer shelf and then to the deep sea. Individuals were distributed in a mosaic pattern, approaching homogeneity only in deep-water areas.

The distribution of *M. leidyi* in the sea corresponded primarily to the features of the spatial distribution of the upper layer sea temperature. This species was recorded primarily within the warmest waters of the RC and to a lesser extent in the zone of the anticyclonic eddy (Fig. 4, *c*). The abundance of the ctenophore was positively correlated with sea surface temperature ($r = 0.62$; $p < 0.001$), whereas the correlation for biomass was significantly weaker ($r = 0.22$; $p > 0.05$). Such a pattern in the distribution of *M. leidyi* is likely associated with predation by *B. ovata*, which, when selecting prey, is guided by stronger chemical signals from larger individuals, while juveniles more often manage to avoid the predator's attention. Predation can also explain the minimal presence of *M. leidyi* on the inner shelf, where *B. ovata* expands seasonally each year. The abundance and biomass of *M. leidyi* increased from the inner shelf to the deep-water areas, where the average abundance reached 8.8 ± 1.5 ind.·m$^{-2}$ and biomass reached 18.2 ± 5.9 g·m$^{-2}$.

Like *M. leidyi*, *B. ovata* was predominantly distributed in the warmer water column. Additionally, the abundance of *B. ovata* depended on the depth of the thermocline ($r = 0.27$; $p < 0.05$) and decreased from the inner shelf (20.1 ± 4.3 ind.·m$^{-2}$) to the deep sea (10.6 ± 2.5 ind.·m$^{-2}$) (Fig. 4, *d*). Nevertheless, the abundance and

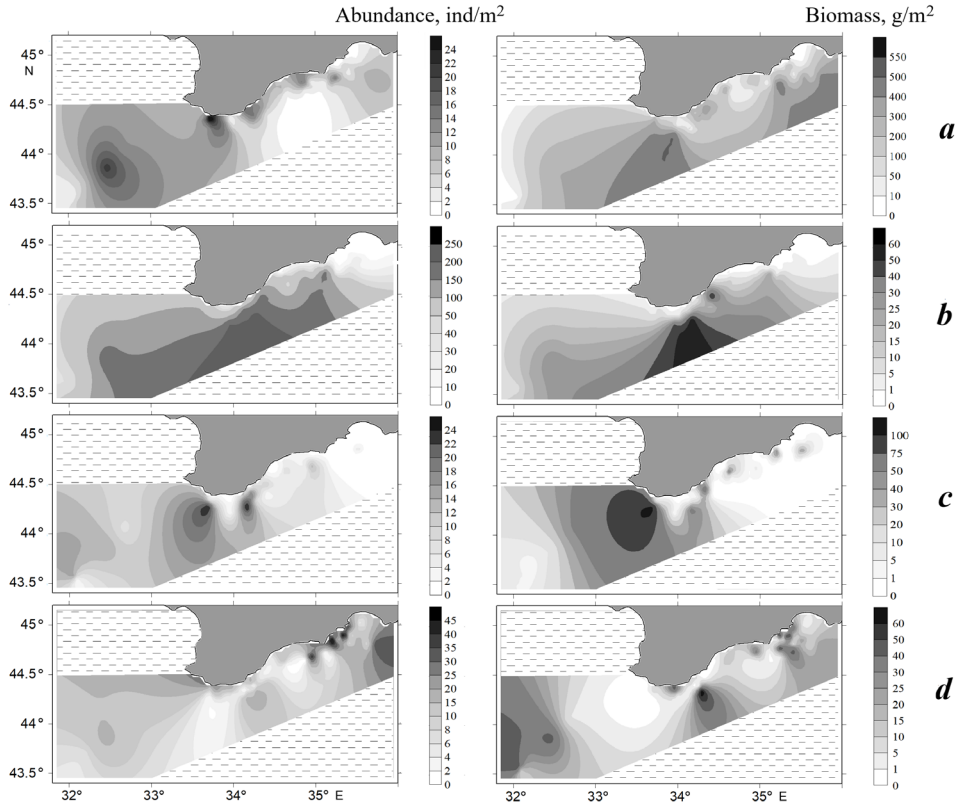


F i g . 4 . Distribution of abundance and biomass of gelatinous macroplankton in October 2022: *a – Aurelia aurita*; *b – Pleurobrachia pileus*; *c – Mnemiopsis leidyi*; *d – Beroe ovata*

biomass of *B. ovata*, which primarily feeds on planktivorous ctenophores, depend on their spatial distribution. Compared to the 2019 data, the biomass of *B. ovata* increased significantly ($p < 0.001$) in the deep-water areas of the sea, while the biomass of its prey, planktivorous ctenophores, decreased significantly ($p < 0.01$) [14].

In October 2022, plankton studies showed that the gelatinous macroplankton of the Black Sea had maintained a constant species composition and a dynamically equilibrium structure in recent years. This structure is determined by the responses of its individual populations to climatic factors, changes in the hydrological regime of the sea and trophic habitat conditions that develop as a result of interpopulational relationships. Quantitatively, gelatinous macroplankton in 2022 was moderately developed, with no clear dominance of any mass species. This is likely to be its average or typical state, corresponding to the potential of the current development of the *A. aurita* population and the degree of modern control exerted by the ctenophore *B. ovata* over planktivorous ctenophores. Due to the ongoing warming

in the Black Sea basin and weakening of seawater convective mixing in winter, the gelatinous community can further transform along the path of weakening of the positions of cold-water species (*A. aurita* and *P. pileus*) and increasing of the ecological valence of warm-water ctenophores (*M. leidyi* and *B. ovata*).

Extending the SHS to the end of September or the beginning of October shifts the developmental phases of both warm- and cold-water species of gelatinous macroplankton. This forms new relationships in the predator–prey chain that are characteristic of the autumn interseason.

**Conclusion**

As SHS duration in the study area steadily increases into the second to third decades of September, successful spawning of thermophilic fish species is prolonged into the first to second decades of October. This depends on the intensity with which the upper sea layer cools during the transition of the temperature regime from the final phase of the SHS to the developed AHS.

In October 2022, during the initial phase of the AHS, the gradual cooling of the upper sea layer was the most probable cause of regional differences in the abundance of ichthyoplankton, mesoplankton, and gelatinous macroplankton. This was due to the conditions of thermal structure formation in both study areas. Specifically, the waters in shallow Southeastern Crimea cooled more quickly than the deep-water area of the SCC, which is protected from cold northerly winds. Other factors included the inflow of cold waters from the Azov Sea into the coastal zone of the eastern sector and the determining influence of the warm waters of the RC on the thermohaline structure of the coastal waters of the SCC.

In October 2022, off the Crimean Peninsula, 16 species of fish from 12 families were recorded (12 species from 9 families of warm-water fish and 4 species from 3 families of temperate-water fish). The average abundances of fish eggs and larvae were 2.34 ind.·$m^{-2}$ and 2.55 ind.·$m^{-2}$, respectively. Eggs of temperate-water species and larvae of warm-water fish species dominated. Due to the relatively large number of species in October and low dominance index of 0.17, the ichthyoplankton complex off the Crimean Peninsula exhibited high diversity indices. The species diversity index was 3.03, the richness index was 20.31 and the evenness index was 0.77.

In recent years, gelatinous macroplankton has grown moderately. Despite an unchanged species composition and dynamically balanced structure determined by the hydrological regime of the sea and trophic interpopulational relationships, gelatinous macroplankton did not significantly impact the state of food mesoplankton in October 2022. The predominance of small-sized fractions of warm-water Copepoda, which are the main food source for the larvae of warm-water and temperate-water fish, in the mesoplankton provided favorable feeding conditions for their survival and growth. A high diversity of species with larvae of various sizes and feeding types (from yolk to exogenous) was recorded in the ichthyoplankton.

REFERENCES

1. Klimova, T.N. and Podrezova, P.S., 2018. Seasonal distribution of the Black Sea ichthyoplankton near the Crimean Peninsula. *Regional studies in Marine Science*, 24, pp. 260–269. http://doi.org/10.1016/j.rsma.2018.08.013
2. Gordina, A.D. and Klimova, T.N., 1996. Dynamics of Species Structure and Ichthyoplankton Abundance in the Coastal and Open Waters of the Black Sea. In: S.M. Konovalov, ed., 1996. *The Modern State of Black Sea Ichthyofauna*. Sevastopol: IBSS, pp. 74–95 (in Russian).
3. Klimova, T.N. and Vdodovich, I.V., 2011. [Abundance, Species Diversity of Ichthyoplankton and Feeding Peculiarities of Fish Larvae in the Coastal Waters of South-Western Crimea in 2000–2009]. In: V. N. Eremeev, A. V. Gaevskaya, G. E. Shulman, Ju. A. Zagorodnyaya, eds., 2011. *Biological resources of the Black Sea and Sea of Azov*. Sevastopol: EKOSI-Gidrofizika, pp. 101–116 (in Russian).
4. Turan, C. and Gürlek, M., 2016. Climate Change and Biodiversity Effects in Turkish Seas. *Natural and Engineering Sciences*, 1(2), pp. 15–24. https://doi.org/10.28978/nesciences.286240
5. Markova, N.V., Belokopytov, V.N., Dymova, O.A. and Miklashevskaya, N.A., 2021. Assessment of the Black Sea Temperature and Salinity Climatic Fields for the Recent Climatological Period (1991–2020). *Physical Oceanography*, 28(4), pp. 392–403. http://doi.org/10.22449/1573-160X-2021-4-392-403
6. Shlyakhov, V.A. and Piatinskii, M.M., 2023. Stock Assessment of the Marine Fish Species in the Black Sea (Russian Waters) in 2021. *Aquatic Bioresources and Environment*, 6(3), pp. 96–113. (in Russian).
7. Ilyin, Yu.P., Repetin, L.N., Belokopytov, V.N., Goryachkin, Yu.N., Dyakov, N.N., Kubryakov, A.A. and Stanichny, S.V., 2012. *Hydrometeorological Conditions of the Ukrainian Seas. Vol. 2. The Black Sea*. Sevastopol: ECOSI-Gidrofizika, 421 p. (in Russian).
8. Polonskii, A.B. and Novikova, A.M., 2020. Interdecadal Variability of the Black Sea Cold Intermediate Layer and Its Causes. *Russian Meteorology and Hydrology*, 45(10), pp. 694–700. http://doi.org/10.3103/S1068373920100039
9. Artamonov, Yu.V., Alekseev, D.V., Skripaleva, E.A., Shutov, S.A., Deriushkin, D.V., Zavyalov, D.D., Kolmak, R.V., Shapovalov, R.O., Shapovalov, Yu.I., Fedirko, A.V. and Shcherbachenko, S.V., 2018. Peculiarities of Seasonal and Synoptic Variability of Water Structure in the Zone of the Rim Current at Autumn and Winter 2016. *Ecological Safety of Coastal and Shelf Zones of Sea*, (1), pp. 32–43. https://doi.org/10.22449/2413-5577-2018-1-32-43 (in Russian).
10. Artamonov, Yu.V., Skripaleva, E.A., Fedirko, A.V., Shutov, S.A., Derjushkin, D.V., Shapovalov, R.O., Shapovalov, Yu. I. and Shcherbachenko, S.V., 2020. Waters Circulation in the Northern Part of the Black Sea in Summer – Winter of 2018. *Ecological Safety of Coastal and Shelf Zones of Sea*, (1), pp. 69–90. https://doi.org/10.22449/2413-5577-2020-1-69-90 (in Russian).
11. Klimova, T.N., Vdodovich, I.V. and Anninskyi, B.E., 2010. Ichthyoplankton in the Plankton Community of the Western Sector of the Black Sea in October 2005. *Journal of Ichthyology*, 50(4), pp. 314–320. http://doi.org/10.1134/S0032945210040041
12. Klimova, T.N., Vdodovich, I.V., Anninsky, B.E., Subbotin, A.A., Podrezova, P.S. and Melnikov, V.V., 2021. Effect of Certain Abiotic and Biotic Factors on Spawning of the European Sprat *Sprattus sprattus* (Linnaeus, 1758) in the Black Sea in November 2016–2017. *Oceanology*, 61(1), pp. 58–68. http://doi.org/10.1134/S0001437021010082

13. Klimova, T.N., Anninsky, B.E., Subbotin, A.A., Vdodovich, I.V. and Podrezova, P.S., 2023. State of the Ichthyo-, Meso-, and Macroplankton Complexes off the Crimean Peninsula (the Black Sea) in Connection with the Hydrobiological Regime Features in October 2016. *Marine Biological Journal*, 8(2), pp. 55–73.
14. Anninsky, B.E., Finenko, G.A. and Datsyk, N.A., 2023. Interannual Population Dynamics of the Ctenophore *Beroe ovata* Bruguière, 1789 at the Outer Shelf of Sevastopol Bay of the Black Sea. *Russian Journal of Biological Invasions*, 14(2), pp. 131–143. http://doi.org/10.1134/S2075111723020030
15. Troshchenko, O.A. and Subbotin, A.A., 2018. [Hydrological Features]. In: N. S. Kostenko, ed., 2018. *The Biology of the Black Sea Offshore Area at the South-Eastern Crimea*. Simferopol: PP "ARIAL", pp. 46–59 (in Russian).
16. Belokopytov, V.N., 2019. Seasonal Variability of Vertical Thermohaline Stratification on the Black Sea Shelf of Crimea. *Ecological Safety of Coastal and Shelf Zones of Sea*, (3), pp. 19–24. https://doi.org/10.22449/2413-5577-2019-3-19-24 (in Russian).
17. Belokopytov, V.N. and Nikol'sky, N.V., 2015. Stationary Anticyclonic Eddies near the South and West Coasts of Crimea. *Ecological Safety of Coastal and Shelf Zones of Sea*, (1), pp. 47–53 (in Russian).
18. Zatsepin, A.G., Kremenetskiy, V.V., Piotukh, V.B., Poyarkov, S.G., Yakubenko, V.G., Ratner, Yu.B., Soloviev, D.M., Stanichnaya, R.R. and Stanichny, S.V., 2008. Formation of the Coastal Current in the Black Sea Caused by Spatially Inhomogeneous Wind Forcing upon the Upper Quasi-Homogeneous Layer. *Oceanology*, 48(2), pp. 159–174. https://doi.org/10.1134/S0001437008020021
19. Ivanov, V.A. and Belokopytov, V.N., 2013. *Oceanography of Black Sea*. Sevastopol: ECOSI- Gidrofizika, 210 p.
20. Klimova, T.N., Subbotin, A.A., Vdodovich, I.V., Zagorodnyaya, Yu.A. and Zabrodin, D.A., 2024. Ichthyoplankton in the Northern Part of the Black Sea under the Prolongation of Summer Hydrological Season in 2020. *Inland Water Biology*, 17(1), pp. 197–207. https://doi.org/10.1134/S1995082924010085

Submitted 12.02.2025; accepted after review 05.06.2025;
revised 17.09.2025; published 30.12.2025

*About the authors:*

**Tatiana N. Klimova**, Senior Researcher Associate, A.O. Kovalevsky Institute of Biology of the Southern Seas of RAS (2 Nakhimov Av., Sevastopol, 299011, Russian Federation), PhD (Biol.), **ORCID ID: 0000-0002-4446-4646**, **Scopus Author ID: 7006082947**, *tnklim@ibss-ras.ru*

**Aleksandr A. Subbotin**, Senior Researcher Associate, A.O. Kovalevsky Institute of Biology of the Southern Seas of RAS (2 Nakhimov Av., Sevastopol, 299011, Russian Federation), PhD (Geogr.), **ORCID ID: 0000-0002-4241-7459**, **Scopus Author ID: 7005348588**, **ResearcherID: AAC-8689-2022**, *subbotin@ibss-ras.ru*

**Boris E. Anninsky**, Leading Researcher Associate, A.O. Kovalevsky Institute of Biology of the Southern Seas of RAS (2 Nakhimov Av., Sevastopol, 299011, Russian Federation), PhD (Biol.), **ORCID ID: 0000-0001-9614-9392**, **Scopus Author ID: 6507371085**, *anninsky_be@ibss-ras.ru*

**Irina V. Vdodovich**, Senior Researcher Associate, A.O. Kovalevsky Institute of Biology of the Southern Seas of RAS (2 Nakhimov Av., Sevastopol, 299011, Russian Federation), PhD (Biol.), **ORCID ID: 0000-0001-9514-8195**, **Scopus Author ID: 17347145500**, *irinavdodovich@ibss-ras.ru*

**Dmitry A. Zabrodin**, Leading Engineer, A.O. Kovalevsky Institute of Biology of the Southern Seas of RAS (2 Nakhimov Av., Sevastopol, 299011, Russian Federation), **ORCID ID: 0000-0001-8986-2237, Scopus Author ID: 58945582600**, *zabrodin@ibss-ras.ru*

**Tatiana N. Petrova**, Junior Researcher Associate, T. I. Vyazemsky Karadag Scientific Station – Nature Reserve of RAS, Branch of A. O. Kovalevsky Institute of Biology of the Southern Seas RAS (24 e Nauki Str. Feodosiya, vil. of Kurortnoe, 298188, Russian Federation), **ORCID ID: 0009-0002-4750-1171**, *tanysha_07011977@mail.ru*

**Natalia A. Datsyk**, Junior Researcher Associate, A.O. Kovalevsky Institute of Biology of the Southern Seas of RAS (2 Nakhimov Av., Sevastopol, 299011, Russian Federation), **ORCID ID: 0000-0002-8113-8786**, **Scopus AuthorID: 55612375600**, **ResearcherID: JPL-4910-2023**, *dacikn@ibss-ras.ru*

*Contribution of the authors:*

**Tatiana N. Klimova** – study problem statement, analysis of ichthyoplankton data, preparation of graphic materials, manuscript editing, analysis and discussion of the results, conclusion drawing

**Aleksandr A. Subbotin** – study objective statement, analysis and interpretation of hydrological data, preparation of graphic materials, manuscript editing, analysis and discussion of the results, conclusion drawing

**Boris E. Anninsky** – study objective statement, analysis of data on mesoplankton and gelatinous macroplankton, preparation of the article text and graphic materials, manuscript editing, analysis and discussion of the results, conclusion drawing

**Irina V. Vdodovich** – analysis of data on the nutrition of fish larvae and juveniles, preparation of article text, manuscript editing, analysis and discussion of the results

**Dmitry A. Zabrodin** – analysis of data on ichthyoplankton, preparation of graphic materials, manuscript editing

**Tatiana N. Petrova** – analysis of data on ichthyoplankton, manuscript editing

**Natalia A. Datsyk** – analysis of data on mesoplankton and gelatinous macroplankton, manuscript editing

*All the authors have read and approved the final manuscript.*

ISSN 2413-5577, Ecological Safety of Coastal and Shelf Zones of Sea, 2025, No. 4, pp. 117–132.

Original paper

# Quantitative Distribution of the Potentially Toxic Diatom *Halamphora coffeiformis* (C. Agardh) Levkov 2009 in the Microphytobenthos of the Crimean Coastal Waters

**D. S. Balycheva**

*A.O. Kovalevsky Institute of Biology of the Southern Seas of RAS, Sevastopol, Russia*
*e-mail: dashik8@gmail.com*

**Abstract**

*Halamphora coffeiformis* is a widespread benthic diatom. Despite being mentioned in the literature as a potential producer of the toxic domoic acid, it is of biotechnological interest, since it contains triacylglycerides, polyunsaturated fatty acids, pigments, vitamins and others. This work aims to summarize original data on the occurrence, quantitative distribution and habitat conditions of *H. coffeiformis* in the coastal waters of Crimea to assess the prospects for its isolation into a pure culture and evaluate its biotechnological potential. According to long-term monitoring (2011–2023) of the microphytobenthos in the Crimean coastal zone, the diatom was found in 16 areas of the Black Sea and the Sea of Azov. It was recorded at depths from 0 to 38 m, within a temperature range of 3–36°C, salinity of 14–126 $g \cdot L^{-1}$, and occurred year-round. On hard substrates and macrophytes, the species abundance (N) ranged from 100 to $24 \cdot 10^3$ cells$\cdot cm^{-2}$, and the biomass (B) varied from 0.00001 to 0.02292 $mg \cdot cm^{-2}$. In sediments, N varied from 100 to $253.6 \cdot 10^3$ cells$\cdot cm^{-3}$, and B was from 0.0004 to 0.6612 $mg \cdot cm^{-3}$. The maximum abundance and biomass on hard substrates and macrophytes ($N = 5.5 \cdot 10^3$ cells$\cdot cm^{-2}$, $B = 0.0196$ $mg \cdot cm^{-2}$) were recorded in 2011 on the shells of the mussel *Mytilus galloprovincialis* near the village of Katsiveli at a depth of 4 m and a temperature of 24°C. In sediments, the maximum values ($N = 253.6 \cdot 10^3$ cells$\cdot cm^{-3}$, $B = 0.66116$ $mg \cdot cm^{-3}$) were observed in November 2018 in Sivash Bay of the Sea of Azov at a depth of 0.2–0.6 m, temperature of 10–14°C and water salinity of 100 $g \cdot L^{-1}$. The integration and analysis of long-term data on the occurrence of *H. coffeiformis* in the Crimean coastal zone showed its wide distribution and tolerance to a broad range of temperatures and salinity. This confirms the species potential for biotechnological application and the need for further toxicological and genetic studies. The species can be recommended for isolation into a pure culture for subsequent genetic analysis and study of its biochemical, toxicological and ecological properties.

**Key words**: diatoms, *Halamphora coffeiformis*, Sea of Azov, Black Sea, Crimean coastal waters, algae bloom, microphytobenthos, biotechnological potential

**Acknowledgments**: I express my gratitude to Dr. L. I. Ryabushko for her valuable comments and editing of the manuscript. This work was carried out within the framework of IBSS state research assignment no. 124022400152-1. Data on hypersaline water bodies of Lake Chersonesskoye and Sivash Bay were obtained with the support of the Russian Science Foundation (grant no. 18-16-00001).

**For citation**: Balycheva, D.S., 2025. Quantitative Distribution of the Potentially Toxic Diatom *Halamphora coffeiformis* (C. Agardh) Levkov 2009 in the Microphytobenthos of the Crimean Coastal Waters. *Ecological Safety of Coastal and Shelf Zones of Sea*, (4), pp. 117–132.

# Количественное распределение потенциально токсичной диатомовой водоросли *Halamphora coffeiformis* (C. Agardh) Levkov, 2009 в микрофитобентосе акваторий крымского прибрежья

**Д. С. Балычева**

*ФГБУН ФИЦ «Институт биологии южных морей имени А. О. Ковалевского РАН», Севастополь, Россия*
*e-mail: dashik8@gmail.com*

**Аннотация**
*Halamphora coffeiformis* – широко распространенная бентосная диатомовая водоросль, хотя и упоминается в литературе как возможный продуцент токсичной домоевой кислоты, представляет биотехнологический интерес, поскольку содержит триацилглицериды, полиненасыщенные жирные кислоты, пигменты, витамины и др. Целью работы является обобщение собственных данных о встречаемости и количественном распределении вида *H. coffeiformis*, условиях его обитания в прибрежных акваториях Крыма для выявления перспектив его выделения в чистую культуру и оценки его биотехнологического потенциала. По данным мониторинга микрофитобентоса крымского прибрежья, с 2011 по 2023 г. диатомовая водоросль встречалась круглогодично в 16 районах Черного и Азовского морей на глубинах от 0 до 38 м в диапазоне температур 3–36 °С, солености 14–126 г·л$^{-1}$. На твердых субстратах и макрофитах численность $N$ вида колебалась от 100 до 24·10$^3$ кл.·см$^{-2}$, биомасса $B$ – от 0.00001 до 0.02292 мг·см$^{-2}$; в рыхлых грунтах $N$ варьировала от 100 до 253.6·10$^3$ кл.·см$^{-3}$, $B$ – от 0.0004 до 0.6612 мг·см$^{-3}$. Максимальные количественные показатели на твердых субстратах и макрофитах ($N$ = 5.5·10$^3$ кл.·см$^{-2}$, $B$ = 0.0196 мг·см$^{-2}$) зарегистрированы в 2011 г. на поверхности раковин мидии *Mytilus galloprovincialis*, отобранных в районе пос. Кацивели на глубине 4 м при температуре 24 °С. В рыхлых грунтах максимальные значения ($N$ = 253.6·10$^3$ кл.·см$^{-3}$ и $B$ = 0.66116 мг·см$^{-3}$) отмечены в ноябре 2018 г. в зал. Сиваш Азовского моря на глубине 0.2–0.6 м при температуре 10–14 °С и солености воды 100 г·л$^{-1}$. Обобщение и анализ многолетних данных о встречаемости *H. coffeiformis* в крымском прибрежье показали широкое распространение вида и толерантность к большому диапазону температуры и солености воды, что подтверждает его перспективность для биотехнологического применения и необходимость дальнейших токсикологических и генетических исследований. Вид можно рекомендовать для выделения в альгологически чистую культуру для дальнейшего генетического анализа и изучения биохимических, токсикологических и экологических свойств.

**Ключевые слова**: диатомовые водоросли, *Halamphora coffeiformis,* Азовское море, Черное море, крымское прибрежье, «цветение» воды, микрофитобентос, биотехнологический потенциал

**Благодарности**: выражаю благодарность д. б. н. Л. И. Рябушко за ценные замечания и редактирование рукописи. Работа выполнена в рамках государственного задания ФИЦ ИнБЮМ по теме «Комплексное исследование механизмов функционирования морских биотехнологических комплексов с целью получения биологически активных веществ из гидробионтов» (№ 124022400152-1). Данные о гиперсоленых водоемах озеро Херсонесское и залив Сиваш получены при поддержке Российского научного фонда (грант № 18-16-00001).

**Для цитирования**: *Балычева Д. С.* Количественное распределение потенциально токсичной диатомовой водоросли *Halamphora coffeiformis* (C. Agardh) Levkov, 2009 в микрофитобентосе акваторий крымского прибрежья // Экологическая безопасность прибрежной и шельфовой зон моря. 2025. № 4. С. 117–132. EDN AIMHIF.

## Introduction

Since the end of the 20th century, algologists have devoted considerable attention to studying harmful algal blooms, 'red tides', and potentially toxic algae [1), 2)] [1–4]. Diatoms include both toxic species containing domoic acid (many planktonic species of the genus *Pseudo-nitzschia*) and potentially dangerous species that cause water blooms (abundance outbreaks). Several studies also mention the benthic small-celled diatom *Halamphora coffeiformis* (C. Agardh) Levkov 2009 as a producer of domoic acid [2), 3)] [2, 5–7]. However, all of these sources refer to a single reported case of mass poisoning from mussels cultivated in Cardigan Bay, Prince Edward Island, Canada, in 1987 [8]. In the cited study, two people died. In [8], the authors detected domoic acid in extracts of these mussels and, using NMR spectroscopy, found the toxin in the culture of *H. coffeiformis* among the microorganisms isolated from the epizoon of these mussels [5].

In 2021, the results of a toxicological analysis of an Argentine strain of *H. coffeiformis*, which was isolated from the Blanca Bay waters at a salinity of 33 $g \cdot L^{-1}$, were published. Domoic acid was absent at all growth stages of the culture [9]. Previously, in [10], the authors suggested that strains of *H. coffeiformis* in which domoic acid had been detected could have been misidentified based solely on morphological features. It is also known that toxin production by microalgae can be influenced by symbiosis with bacteria. Thus, the dinoflagellate *Alexandrium tamarense* (Lebour) Balech 1995 is capable of producing saxitoxin and its analogues,

---

1) Garcés, E., Zingone, A., Montresor, M., Reguera, B. and Dale, B., eds., 2002. *LIFEHAB: Life Histories of Microalgal Species Causing Harmful Blooms. Report of a European Workshop*. Calvia, Majorca, Spain: Calvia Town Council, 208 p.

2) Lassus, P., Chomerat, N., Philipp, H. and Nézan, E., 2016. Toxic and Harmful Microalgae of the World Ocean. Denmark: International Society for the Study of Harmful Algae, Intergovernmental Oceanographic Commission of UNESCO, 523 p.

3) Hallegraeff, G.M., Anderson, D.M., Cembella, A.D. and Enevoldsen, H.O., eds., 2004. *Manual on Harmful Marine Microalgae. 2nd Revised Edition*. Paris, France, UNESCO, 793 p. (Monographs on Oceanographic Methodology, 11). https://doi.org/10.25607/OBP-1370

and can form both toxic and non-toxic strains [11]. Therefore, clarifying the species affiliation and toxicity of *H. coffeiformis* requires additional studies incorporating scanning electron microscopy data, as well as taxonomic, ecological, genetic and toxicological analyses.

At the same time, substantial evidence of the biotechnological potential of *H. coffeiformis* can be found in the literature [9, 12–17]. Biochemical analysis of its biomass revealed high levels of triacylglycerols (up to 18 $mg \cdot L^{-1}$), as well as free and esterified sterols, proteins and carbohydrates [15]. Essential polyunsaturated fatty acids accounted for 17.5% of total fatty acids, including 9% omega-3, 5% omega-6 and 3% omega-9, giving an omega-3/omega-6 ratio of 1.64. Among the sterols, sitosterol predominated, and 50% of the amino acids are essential for fish and other aquatic animals. Lipid analysis of *H. coffeiformis* showed promising results for biofuel production [18]. Furthermore, *H. coffeiformis* has been found to be a source of numerous pharmacologically active secondary metabolites, including vitamins C and E, alpha-tocopherol and flavonoids [13]. It also contains a variety of pigments, such as carotenoids (fucoxanthin and β-carotene) and chlorophyll, which exhibit antibacterial, antiviral, anti-inflammatory, anticancer and antioxidant properties, making them widely used in medicine. Study [19] also demonstrates the pronounced antioxidant activity of *H. coffeiformis*.

Thus, it remains unclear at present whether this species is capable of producing toxins under certain conditions or if it is completely safe. Nevertheless, there is substantial evidence in the literature of the biotechnological potential of *H. coffeiformis*. As identification of the species based solely on morphological features is difficult, research must include taxonomic, ecological, genetic and toxicological studies. In order to study this issue and assess the potential for using this species in biotechnology, work with pure cultures is required. Therefore, an important initial step is to isolate strains of the species from the natural environment.

The aim of the study is to summarise our data on the occurrence, quantitative distribution and ecological conditions of the benthic diatom *Halamphora coffeiformis* in the coastal waters of Crimea. This will help us to determine the prospects of isolating it as a pure culture and assess its bioresource potential and the possibility of subsequent biotechnological use.

**Materials and methods**

The study material consisted of microphytobenthos samples collected from various substrates at different depths and in different seasons between 2011 and 2023 in the coastal waters of the Crimean peninsula in the Black Sea and the Sea of Azov, as well as in coastal hypersaline water bodies: Sivash Bay, Lake Dzharylgach and Lake Chersonesskoye (Fig. 1, *b*). Samples were collected from the coastal waters of Sevastopol and the southern and western shores of Crimea in the Black Sea, and from the Gulf of Arabat and near capes Kazantip and Fonar in the Sea of Azov.

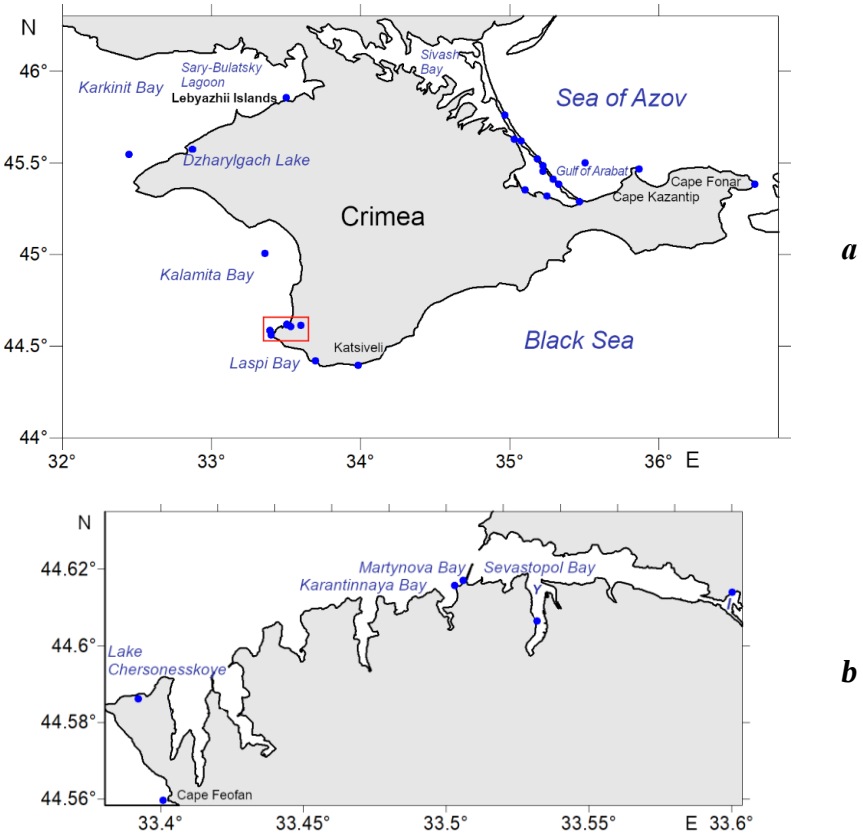


Fig. 1. Sampling points (blue dots) in the study area, the red rectangular highlights the Sevastopol coastal area (*a*); the enlarged image of the highlighted area (letter Y stands for Yuzhnaya Bay, letter I stands for Inkerman Bay) (*b*)

Macrophytes were used for the study of epiphytic microalgae: the red alga *Laurencia obtusa* and the green algae *Cladophora siwaschensis* and *Cladophora* sp. (see Appendix A).

Additionally, data on the seasonal abundance and biomass dynamics of *Halamphora coffeiformis* in periphyton on experimental glass plates (December 2010–January 2012), in epizoon of cultivated *Mytilus galloprovincialis* Lam. mussels and in sediments under mussel collectors (February 2015–February 2016) are presented. Data on the occurrence of *H. coffeiformis* were obtained from studies of cultivated mussel shells, faeces and pseudofaeces [20], as well as the intestines of the ostracod *Eucypris mareotica* Fischer, which were collected from Lake Chersonesskoye [21].

Samples were collected and processed according to previously described methodologies [22–26]. When processing microphytobenthos from solid substrates (experimental glass plates, mussel shells, stones) and from epiphyton of macrophytes, microalgae were scraped from the substrate surfaces with a synthetic brush. Microalgae were separated from loose sediments by repeated washing with filtered sea water followed by sedimentation. Processing of microalgae from mussel guts, faeces and pseudofaeces is described in [20] and the oyster's intestinal contents in [21]. The cells of *H. coffeiformis* were counted and their linear dimensions measured in Goryaev's chamber (volume 0.9 $mm^3$) using a Carl Zeiss Axioskop 40 light microscope. The method of geometric similarity was used for biomass calculations. Species identification was refined using a Hitachi SU3500 scanning electron microscope (Japan). When determining *H. coffeiformis*, the distinguishing features of the species [27] and photographs from the study [28] were considered, the latter of which also included a molecular phylogenetic analysis of the species.

**Results**

During the monitoring of the microphytobenthos in the Crimean coastal waters between 2011 and 2023, the diatom *Halamphora coffeiformis* (Fig. 2) was found in 16 study areas at depths ranging from 0 to 38 m year-round (see Appendix A). The temperature range at which the species was observed was between 3 and 36°C, with a salinity *S* range of 14 to 126 $g \cdot L^{-1}$. The alga *H. coffeiformis* was most frequently observed in August, when the water temperature was within the range of 22–32°C, and in October, when the temperature was 19.3°C. Cell length varied from 9.3 to 52.8 μm and width from 3 to 20 μm (in the girdle view). The abundance (*N*) of the species in the microphytobenthos of solid substrates and the epiphyton of macrophytes ranged from 100 to $24 \cdot 10^3$ cells$\cdot cm^{-2}$, and the biomass (*B*) ranged from 0.00001 to 0.02292 $mg \cdot cm^{-2}$; in sediments, *N* ranged from 100 to $253.6 \cdot 10^3$ cells$\cdot cm^{-3}$, *B* ranged from 0.0004 to 0.6612 $mg \cdot cm^{-3}$. The maximum quantitative values ($N = 5.5 \cdot 10^3$ cells$\cdot cm^{-2}$, $B = 0.0196$ $mg \cdot cm^{-2}$) were recorded in 2011 on the surface of *M. galloprovincialis* mussel shells collected from a mussel farm near Katsiveli at a depth of 4 m in water with a temperature of 24°C. The maximum abundance for sediments ($N = 253.6 \cdot 10^3$ cells$\cdot cm^{-3}$, $B = 0.66116$ $mg \cdot cm^{-3}$) was observed in November 2018 in Sivash Bay at a depth of 0.2–0.6 m, with a temperature of 10–14°C and a water salinity of 100 $g \cdot L^{-1}$.

During the annual experimental study of microphytobenthos in the periphyton on glass plates, which were exposed to the sea for one month at a depth of 2 m, the alga *H. coffeiformis* was found only in August at 24°C and only singly. However, the species was observed year-round throughout the annual study of the epizoon on mussel shells collected from a mussel farm. Conversely, it was not found in sediments under the farm between April 2015 and February 2016. It should be noted that the year-round study of the seasonal dynamics of the composition and quantitative characteristics of microalgae in the periphyton and epizoon was conducted in two water areas located near each other (about 500 m apart) at the exit from Karantinnaya Bay (Fig. 1, *b*).

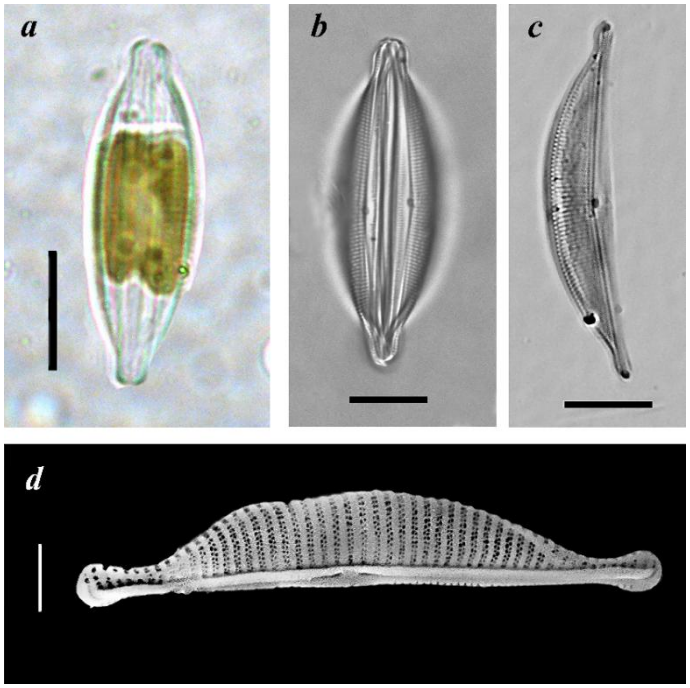


Fig. 2. *Halamphora coffeiformis*: images taken with a light (*a–c*) and scanning electron microscopes (*d*): alive cell (*a*); a frustule from the ventral side (*b*); a frustule from the valve side (*c*, *d*). Scale bar: 10 μm (*a–c*), 2 μm (*d*)

When analysing the seasonal dynamics of the abundance and biomass of *H. coffeiformis* in the epizoon of mussels, higher values were found in the first half of 2015. *N* increased from February to July, peaking in February and July, while *B* increased from February to June, peaking in April (Fig. 3).

The maximum abundance was $4.9 \cdot 10^3$ cells·cm$^{-2}$, accounting for 26% of the total abundance of epiphytic diatoms, in February 2015, which is close to the maximum value recorded over the entire monitoring period, also noted for the epizoon of mussels grown on a farm near Katsiveli. The maximum biomass was 0.0011 mg·cm$^{-2}$, accounting for 5% of the total biomass of epiphytic diatoms on the mussel epizoon, in April 2015. Additionally, *H. coffeiformis* was found in the faeces of mussels cultivated on the mussel farm.

The maximal quantitative indicators of *H. coffeiformis* in hypersaline water bodies were recorded in Sivash Bay: $N = 3.2 \cdot 10^3$ cells·cm$^{-2}$, $B = 0.02292$ mg·cm$^{-2}$ at $t = 19.5 \div 26.0$°C, $S = 30 \div 82$ g·L$^{-1}$ in the the epiphyton of Cladophora; $N = 253.6 \cdot 10^3$ cells·cm$^{-3}$, $B = 0.66116$ g·cm$^{-3}$ at $t = 10 \div 14$°C, $S = 100$ g·L$^{-1}$ for sediments.

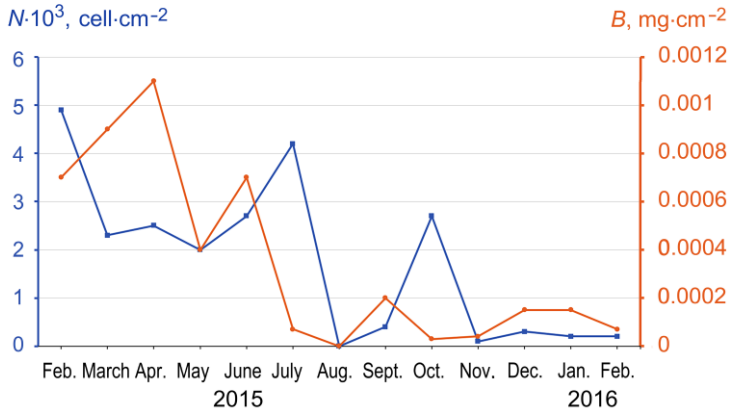


Fig. 3. Seasonal dynamics of abundance *N* and biomass *B* of *Halamphora coffeiformis* in the mussel epizoon in 2015–2016

This species was frequently found in the bay, and mass settlements on the thalli of *Cladophora* were sometimes observed. In Lake Chersonesskoye, *H. coffeiformis* was found in the intestines of ostracods.

In the coastal area of the Black Sea in Crimea, *H. coffeiformis* was found quite often in samples; however, only empty shells were noted in the Sea of Azov.

**Discussion**

Analysis of the accumulated data on the occurrence of the diatom *Halamphora coffeiformis* along the Crimean coast confirmed its widespread distribution and identified the temperature and salinity ranges within which it inhabits these areas. According to phytogeographical characterisation, the species belongs to the arctic-boreal-tropical climatic belts and has not yet been found only in the Antarctic [4), 5)]. In the Black Sea, *H. coffeiformis* is a dominant component of the microphytobenthos. Thus, the maximum abundance of the species (*N*) reached $14.8 \cdot 10^3$ cells·cm$^{-2}$ in the Romanian coastal waters and ranged from 1.4 to $8.7 \cdot 10^3$ cells·cm$^{-2}$ in the epizoon of mussels from Kazachya Bay on the Crimean coast in March 1996, when the species dominated [22]. Notable, that according to our own data and the literature [5, 20, 22], *H. coffeiformis* occurred frequently in the epizoon of mussels, where this alga reached relatively high abundances (see Appendix A).

---

4) Ryabushko, L.I. and Begun, A.A., 2016. [*Diatoms of Microphytobenthos of the Sea of Japan (Synopsis and Atlas)*]. In two volumes. Sevastopol: PK "KIA".Vol. 2, 324 p. (in Russian).

5) Available at: https://www.algaebase.org [Accessed: 11 November 2025].

In our study, live *H. coffeiformis* cells were not detected in the bottom sediments of the Sea of Azov, possibly due to lower water transparency compared to the Black Sea. However, this species is mentioned by numerous authors in the checklist of the benthos and plankton microalgae of the Sea of Azov [29]. For the Crimean coast of the Sea of Azov, *H. coffeiformis* is listed in the epiphyton of macroalgae near Kazantip in July–August 2023 at a water salinity of 13.6 $g \cdot L^{-1}$ at a depth of 0.1–1.0 m, though it was found to be of low abundance ($N = 20$ cells$\cdot cm^{-2}$) [30].

In the literature, *H. coffeiformis* is characterised as a marine and brackish water species [4), 5)]. However, its presence is noted also in freshwater bodies [31–33]. Thus, A. I. Proshkina-Lavrenko [6)] described it as "a brackish water and marine species that is widely distributed along the shores of depurated regions of the sea and in continental brackish waters" as well as "along the shores of the northwestern part of the Black Sea, especially near the Dnieper-Bug Liman".

L. N. Bukhtiyarova detected *H. coffeiformis* in ephemeral freshwater bodies in the forest-steppe of Crimea, in mountain streams and freshwater springs near Serdolikovaya Bay in eastern Crimea [32].

This species is also found in hypersaline waters and has been detected in 16 out of 29 studied bodies of water with salinity ranging from 20 to 320 $g \cdot L^{-1}$ [34]. In Crimea, it is particularly abundant in two hypersaline bodies of water: Lake Chersonesskoye and Sivash Bay [24, 25, 35]. Furthermore, *H. coffeiformis* has been found in soda lakes [36] and in algal-bacterial mats in Kraternaya Bay of the Ushishir sea volcano (the Kuril Islands), at depths of 3–15 m and temperatures of 4–25°C [37].

Thus, the high ecological plasticity of *H. coffeiformis* and its wide distribution across the World Ocean make this species a promising candidate for experimental studies and biotechnological developments.

**Conclusion**

Analysis of the generalised long-term data on the occurrence of *H. coffeiformis* along the Crimean coast revealed its widespread distribution and high tolerance to a broad range of temperatures and salinities. A study of the seasonal dynamics of *H. coffeiformis* in the epizoon of cultivated mussels showed that during periods of maximum abundance and biomass, the contribution of the species to total community abundance exceeded its contribution to biomass due to the small size of its cells. Such species usually play an important ecological role, helping to maintain homeostasis in communities and colonise new substrates under extreme conditions.

A review of the literature revealed only one instance of domoic acid production by the species *H. coffeiformis*. Meanwhile, most authors who have not detected the toxin in its biomass point to the valuable biotechnological properties of the species.

---

[6)] Proshkina-Lavrenko, A.I., 1963. [*Diatoms of the Black Sea Benthos*]. Moscow, Leningrad: Nauka, 243 p. (in Russian).

Due to the widespread distribution of *H. coffeiformis* in the coastal waters of Crimea, its potential biotechnological significance and the challenges associated with taxonomic identification, it is recommended to isolate this species into an algologically pure culture. This would facilitate subsequent genetic analysis, as well as the study of its biochemical, toxicological and ecological properties. It would also enable the assessment of its biotechnological potential.

Appendix A

Quantitative indicators of *Halamphora coffeiformis* and characteristics of sampling points

| Study area | Date | Substrate | *h* | *t* | *S* | *d* | *N* | *B* |
|---|---|---|---|---|---|---|---|---|
| *Black Sea* | | | | | | | | |
| Artificial water area near Karantinnaya Bay | 22.08. 2011 | Experimental glass plates | 2 | 22 | 24 | – | – | – |
| Mussel farm, village of Katsiveli | 04.08. 2011 | Mussel shells | 4 | 24 | – | 26.4 × 17.6 | 5.5 | 0.0196 |
| Dzharylgach Lake | 01.08. 2011 | *Cladophora* sp. | 0.2 | 26 | 125 | 26.4 × 13 | Abun-dant | – |
| Mussel farm at the mouth of Karantinnaya Bay | 27.02. 2015 | Mussel shells | 6 | 9.7 | 17.9 | 23.5 × 10.3 | 4.9 | 0.0007 |
| | 19.03. 2015 | Mussel shells | 6 | 8.4 | 7.9 | 24.9 × 13.2 | 2.3 | 0.0009 |
| | | Sediments | 17 | 8.4 | 17.9 | 30.8 × 17.6 | 3.5 | 0.0010 |
| | 15.04. 2015 | Mussel shells | 6 | 10.3 | 17.9 | 33.4 × 15.0 | 2.5 | 0.0011 |
| | 20.05. 2015 | Mussel shells | 6 | 15.8 | 17.9 | 26.4 × 13.2 | 2.0 | 0.0004 |
| | | Sediments | 17 | 9.9 | 17.9 | 44.0 × 8.8 | 6.4 | 0.0013 |

*Continued*

| Study area | Date | Substrate | *h* | *t* | *S* | *d* | *N* | *B* |
|---|---|---|---|---|---|---|---|---|
| Mussel farm at the mouth of Karantinnaya Bay | 17.06. 2015 | Mussel shells | 6 | 19.2 | 17.9 | 33.7 × 13.2 | 2.7 | 0.0007 |
| | | Sediments | 17 | 16.2 | 17.9 | 52.8 × 13.2 | 6.9 | 0.0025 |
| | 15.07. 2015 | Mussel shells | 6 | 21.4 | 17.9 | 32.3 × 13.2 | 4.2 | 0.00007 |
| | | Sediments | 17 | 12.3 | 17.9 | 30.8 × 13.2 | 9.4 | 0.0020 |
| | 12.08. 2015 | Mussel shells | 6 | 25.5 | 17.9 | – | *Sp* | – |
| | | Sediments | 17 | 25.5 | 17.9 | 35.2 × 17.6 | 1.8 | 0.0006 |
| | 10.09. 2015 | Mussel shells | 6 | 23.7 | 17.9 | 31.9 × 13.2 | 0.4 | 0.0002 |
| | | Sediments | 17 | 23.4 | 17.9 | 35.2 × 13.2 | 3.1 | 0.0008 |
| | 16.10. 2015 | Mussel shells | 6 | 19.3 | 17.9 | 19.8 × 8.8 | 2.7 | 0.00003 |
| | | Sediments | 17 | 19.3 | 17.9 | 39.6 × 13.2 | 1.6 | 0.0004 |
| | 18.11. 2015 | Mussel shells | 6 | 12.9 | 17.9 | 19.8 × 11.0 | 0.1 | 0.00004 |
| | 16.12. 2015 | Mussel shells | 6 | 10.3 | 17.9 | 28.6 × 13.2 | 0.3 | 0.00015 |
| | 13.01. 2016 | Mussel shells | 6 | 9.5 | 17.9 | 28.6 × 13.2 | 0.2 | 0.00015 |
| | 15.02. 2016 | Mussel shells | 6 | 8.9 | 17.9 | 19.8 × 11.0 | 0.2 | 0.00007 |
| | | Mussel faeces | 6 | 9.5 | 17.9 | – | – | – |

*Continued*

| Study area | Date | Substrate | *h* | *t* | *S* | *d* | *N* | *B* |
|---|---|---|---|---|---|---|---|---|
| Artificial water area near Karantinnaya Bay | 26.08. 2016 | *Cladophora* sp. | 0 | 26.0 | – | – | – | – |
| Cape Feofan | 12.08. 2015 | Mussel shells | 4 | 25.4 | – | – | – | – |
| Sary-Bulatsky Lagoon | 30.10. 2015 | Rocks | 0.5 | – | 20.9 | 26.4 × 8.8 | 0.8 | 0.00009 |
| | 27.10. 2015<br>19.11. 2015<br>06.10. 2016 | Silt | 0.5 | – | 19.8 – 21.4 | – | – | – |
| Lebyazhi Islands | 20.05. 2016<br>06.10. 2016 | Sediments | 0.5 | 17.9 | – | – | – | – |
| Karkinit Bay | 29.03. 2017 | Sediments | 18<br>38 | 6.2 | 18.4 | 41 × 14 | *EF* | – |
| Kalamita Bay | 28.03. 2017 | Mussel shells | 20 | 8.3 | 18.4 | – | *EF* | – |
| Martynova Bay | 02.09. 2019 | Rocks | 1–2 | 22 | 16–18 | – | 3.3 | – |
| Inkerman Bay | | | | | | 16.3 × 7.4 | 7.1 | – |
| Yuzhnaya Bay | | | 6.0 | | | 31.1 × 9.5 | 0.1 | – |
| Lake Chersonesskoye | 30.03. 2018 | Intestines of *Eucypris mareotica* (Ostracoda) | до 0.3 | – | 35–120 | 16.8 × 3 | *Sp* | – |

*Finished*

| Study area | Date | Substrate | *h* | *t* | *S* | *d* | *N* | *B* |
|---|---|---|---|---|---|---|---|---|
| Lake Chersonesskoye | 29.05.2018 | Sediments | 0.3 | | | – | 11.2 | 0.006 |
| | 20.06.2018<br>13.09.2018 | *Cladophora* spp. | 0–0.3 | | | 17.6–39.6 × × 8.8–17.6 | 0.12–2.5 | 0.00001–0.0007 |
| Laspi Bay | 27.06.2023 | *Laurencia obtusa* | 0.5 | 17 | – | – | 0.8 | – |
| *Sea of Azov* | | | | | | | | |
| Gulf of Arabat<br>Cape Kazantip<br>Cape Fonar | 02.04.2017 | Sediments | 9–12 | 6–7 | 14–14.5 | – | *Sp* | *EF* |
| Sivash Bay | May–June 2018 | *Cladophora siwaschensis* | 0.2–0.6 | 19.5–26.0 | 30–82 | 12.5–35 × × 5–20 | 3.2 | 0.02292 |
| | | Sediments | | | | 30–37.5 × × 12.5–15 | 3.5 | 0.06988 |
| | 09.11.2018 | Sediments | | 10–14 | 100 | 16–27.5 × × 6–16 | 253.6 | 0.66116 |
| | 19.12.2020 | *Cladophora siwaschensis* | | 3–5 | 30–112 | 16.0–37.0 × × 8.5–14 | 0.37 | 0.00131 |
| | | Sediments | | | | 11.0–23.0 × × 7.7–11 | 38.5 | 0.03129 |
| | 16.07.2020 | *Cladophora siwaschensis* | 0–0.3 | 25–36 | 60–126 | 16.0–32.0 × × 6.0–16.0 | 0.12 | 0.00024 |
| | 03.08.2021 | *Cladophora siwaschensis* | 0–0.6 | 25.4–32.3 | 33.9–88.2 | 16.0–32.9 × × 6.0–15.8 | 0.1 | 0.00002 |
| | | Sediments | 0.2–0.6 | | | 9.3–29.0 × × 9.5–13.7 | 94.1 | 0.0147 |

Note: *N* – abundance, cells·cm$^{-2}$ (cells·cm$^{-3}$ in sediments); *B* – biomass, mg·cm$^{-2}$ (cells·cm$^{-3}$ in sediments); *h* – depth, m; *d* – dimensions, μm, *S* – salinity, g·L$^{-1}$; *t* – temperature, °C. The dash denotes that no measurements were taken. *Sp* – sporadically, *EF* – empty frustules.

REFERENCES

1. Glibert, P. M., Berdalet, E., Burford, M.A., Pitcher, G.C. and Zhou, M., eds., 2001. Global Ecology and Oceanography of Harmful Algal Blooms. Baltimor, Paris: SCOR & IOC, 2001. 86 p. https://doi.org/10.1007/978-3-319-70069-4
2. Ryabushko, L.I., 2003. *Potentially Harmful Microalgae of the Azov and Black Sea Basin*. Sevastopol: ECOSI-Gidrofizika, 288 p. (in Russian).
3. Orlova, T.Yu., 2014. Monitoring of Toxic Microalgae as the Basis of Biological Safety of Coastal Waters and Seafood. In: A. V. Adrianov, 2014. *Biological Safety of the Far Eastern Seas of the Russian Federation: Comprehensive Target Program of Oriented Fundamental Research of FEB RAS for 2007–2012*. Vladivostok: Dalnauka, pp. 354–369 (in Russian).
4. Anabtawi, H.M., Lee, W.H., Al-Anazi, A., Mohamed, M.M. and Aly Hassan, A., 2024. Advancements in Biological Strategies for Controlling Harmful Algal Blooms (HABs). *Water*, 16(2), 224. https://doi.org/10.3390/w16020224
5. Maranda, L., Wang, R., Musauda, K. and Shimizu, Y., 1990. Investigation of the Source of Domoic Acid in Mussels. In: Graneli, E., Sundstrom, B., Edler, L. and Anderson, D.M., eds., 1990. *Toxic Marine Phytoplankton: Proceedings of the Fourth International Conference on Toxic Marine Phytoplankton, Held June 26-30 in Lund, Sweden*. New York: Elsevier Sci. Publ. Co., Inc., p. 300–304.
6. Bates, S.S., 2008. Domoic-Acid-Producing Diatoms: Another Genus Added! *Journal of Phycology*, 36(6), pp. 978–983. https://doi.org/10.1046/j.1529-8817.2000.03661.x
7. Lundholm, N., Daugbjerg, N. and Moestrup, Ø., 2002. Phylogeny of the Bacillariaceae with Emphasis on the Genus *Pseudo-nitzschia* (Bacillariophyceae) Based on Partial LSU rDNA. *European Journal of Phycology*, 37(1), pp. 115–134. https://doi.org/10.1017/S096702620100347X
8. Shimizu, Y., Gupta, S., Masuda, K., Maranda, L., Walker, C. and Wang, R., 1989. Dinoflagellate and Other Microalgal Toxins: Chemistry and Biochemistry. *Pure and Applied Chemistry*, 61, pp. 513–516. 10.1351/pac198961030513
9. Sala, S.E., Vouilloud, A.A., Popovich, C.A., Sanchez-Puerta, M.V., Almandoz, G.O., Coy, B.M., Montoya, N.G. and Leonardi, P., 2021. Molecular, Morphological, and Toxinological Characterizations of an Argentinean Strain of *Halamphora coffeaeformis* with Potential Biotechnological Applications. *Journal of Applied Phycology*, 33, pp. 799–806. https://doi.org/10.1007/s10811-020-02353-4
10. Sala, S.E., Sar, E.A. and Ferrario, M.E., 1998. Review of Materials Reported as Containing *Amphora coffeaeformis* (Agardh) Kützing in Argentina. *Diatom Research*, 13(2), pp. 323–336. https://doi.org/10.1080/0269249X.1998.9705454.
11. Orlova, T.Y., Selina, M.S., Lilly, E.L., Kulis, D.M. and Anderson, D.M., 2007. Morphogenetic and Toxin Composition Variability of *Alexandrium tamarense* (Dinophyceae) from the East Coast of Russia. *Phycologia*, 46(5), pp. 534–548. https://doi.org/10.2216/06-17.1
12. Rajaram, M.G., Nagaraj, S., Manjunath, M., Boopathy, A.B., Kurinjimalar, C., Rengasamy, R., Jayakumar, T., Sheu, J.-R. and Li, J.-Y., 2018. Biofuel and Biochemical Analysis of Amphora coffeaeformis RR03, a Novel Marine Diatom, Cultivated in an Open Raceway Pond. *Energies*, 11(6), 1341. https://doi.org/10.3390/en11061341
13. El-Sayed, A.E.B., Aboulthana, W.M., El-Feky, A.M., Ibrahim, N.E. and Seif, M.M., 2018. Bio and Phyto-Chemical Effect of *Amphora coffeaeformis* Extract Against Hepatic Injury Induced by Paracetamol in Rats. *Molecular Biology Reports*, 45, pp. 2007–2023. https://doi.org/10.1007/s11033-018-4356-8

14. Popovich, C.A., Faraoni, M.B., Sequeira, A., Daglio, Y., Martín, L.A., Martínez, A.M., Damiani, M.C., Matulewicz, M.C. and Leonardi, P.I., 2020. Potential of the Marine Diatom *Halamphora coffeaeformis* to Simultaneously Produce Omega-3 Fatty Acids, Chrysolaminarin and Fucoxanthin in a Raceway Pond. *Algal Research*, 51, 102030. https://doi.org/10.1016/j.algal.2020.102030
15. Bilbao, P.G.S, Martín, L.A., Popovich, C.A., Almeyda, M.D., Chamorro, V. and Leonardi, P.I., 2020. Assessment of *Halamphora coffeaeformis* Growth and Biochemical Composition for Aquaculture Purposes. *Journal of Marine Science and Engineering*, 8(4), 282. https://doi.org/10.3390/jmse8040282
16. Shaban, N.S., Radi, A.M., Abdelgawad, M.A., Ghoneim, M.M., Al-Serwi, R.H., Hassan, R.M., Mohammed, E.T., Radi, R.A. and Halfaya, F.M., 2023. Targeting Some Key Metalloproteinases by Nano-Naringenin and *Amphora coffeaeformis* as a Novel Strategy for Treatment of Osteoarthritis in Rats. *Pharmaceuticals*, 16(2), 260. https://doi.org/10.3390/ph16020260
17. Jastaniah, S.D. and Albaqami, N.M., 2024. Dietary *Amphora coffeaeformis* Enhanced Growth Performance, Body Composition, Biochemical Parameters, Gene Expression on Red Tilapia (*Oreochromis niloticus* and *O. mossambicus*), and Resistance to *Saprolegnia* Infection. *Journal of Applied Phycology*, 36(6), pp. 3353–3366. https://doi.org/10.1007/s10811-024-03363-2
18. Martín, L.A., Popovich, C.A., Martinez, A.M., Damiani, M.C. and Leonardi, P.I., 2016. Oil Assessment of *Halamphora coffeaeformis* Diatom Growing in a Hybrid Two-Stage System for Biodiesel Production. *Renewable Energy*, 92, pp. 127–135. https://doi.org/10.1016/j.renene.2016.01.078
19. Lee, S.-H., Karawita, R., Affan, A., Lee, J.-B., Lee, K.-W., Lee, B.-J., Kim, D.-W. and Jeon, Y.-J., 2009. Potential of Benthic Diatoms *Achnanthes longipes*, *Amphora coffeaeformis* and *Navicula* sp. (Bacillariophyceae) as Antioxidant Sources. *Algae*, 24(1), pp. 47–55. https://doi.org/10.4490/ALGAE.2009.24.1.047
20. Pospelova, N.V., Balycheva, D.S. and Ryabushko, L.I., 2016. [Microalgae in the Diet of Cultivated Mussels (Crimea, Black Sea)] In: MSU, 2024. *Conference Proceedings of the V International Conference "Marine Research and Education" MARESEDU–2016. Moscow, 18–21 October 2016*. Moscow: Feoriya, pp. 308–318 (in Russian).
21. Anufriieva, E.V., Balycheva, D.S., Vdodovich, I.V. and Shadrin, N.V., 2018. Microalgae in the Diet of *Eucypris mareotica* (Crustacea, Ostracoda) in the Hypersaline Lake Chersonesskoye (Crimea). *Ecologica Montenegrina*, 17, pp. 100–104. https://doi.org/10.37828/em.2018.17.11
22. Ryabushko, L.I., 2013. *Microphytobenthos of the Black Sea*. Sevastopol: ECOSI-Gidrofizika, 416 p. (in Russian).
23. Balycheva, D.S. and Ryabushko, L.I., 2017. Benthos Microalgae of the Lebyazhy'i Ostrova Reserve in the Black Sea. *Nature Conservation Research*, 2(S2), pp. 9–18. https://doi.org/10.24189/ncr.2017.027
24. Shadrin, N., Balycheva, D. and Anufriieva, E., 2021. Spatial and Temporal Variability of Microphytobenthos in a Marine Hypersaline Lake (Crimea): Are There Some General Patterns? *Journal of Sea Research*, 177, 102121. https://doi.org/10.1016/j.seares.2021.102121
25. Shadrin, N., Balycheva, D. and Anufriieva, E., 2021. Microphytobenthos in the Hypersaline Water Bodies, the Case of Bay Sivash (Crimea): Is Salinity the Main Determinant of Species Composition? *Water*, 13(11), 1542. https://doi.org/10.3390/w13111542

26. Ryabushko, L., Balycheva, D., Kapranov, S., Shiroyan, A., Blaginina, A. and Barinova, S., 2023. Seasonal Dynamics of Microphytobenthos Distribution in Three Ecotopes on a Mussel Farm (Black Sea). *Journal of Marine Science and Engineering*, 11(11), 2100. https://doi.org/10.3390/jmse11112100
27. Levkov, Z., 2009. *Amphora* sensu lato. In: H. Lange-Bertalot, ed., 2009. *Diatoms of Europe: Diatoms of the European Inland Waters and Comparable Habitats*. Ruggell: A. R. G. Gantner Verlag K. G., 2009. Vol. 5. 916 p.
28. Stepanek, J.G. and Kociolek, J.P., 2019. Molecular Phylogeny of the Diatom Genera *Amphora* and *Halamphora* (Bacillariophyta) with a Focus on Morphological and Ecological Evolution. *Journal of Phycology*, 55, pp. 442–456. https://doi.org/10.1111/jpy.12836
29. Ryabushko, L.I. and Bondarenko, A.V., 2011. *Microalgae of the Sea of Azov (Checklist, Synonyms, Comment)*. Sevastopol: EKOSI-Gidrofizika. 211 p. (in Russian).
30. Bondarenko, A., Shiroyan, A., Ryabushko, L. and Barinova, S., 2024. Diatoms of the Macroalgae Epiphyton and Bioindication of the Protected Coastal Waters of the Kazantip Cape (Crimea, the Sea of Azov). *Journal of Marine Science and Engineering*, 12(7), 1211. https://doi.org/10.3390/jmse12071211
31. Stoermer, E.F. and Kreis, R.G., 1978. Preliminary Checklist of Diatoms (Bacillariophyta) from the Laurentian Great Lakes. *Journal of Great Lakes Research*, 4(2), pp. 149–169. https://doi.org/10.1016/S0380-1330(78)72180-5
32. Bukhtiyarova, L.N., 1999. *Diatoms of Ukraine. Inland waters*. Kyiv: M. G. Kholodny Institute of Botany, 134 p.
33. Genkal, S.I. and Eremkina, T.V., 2023. Diatom Algae of Reservoirs of Different Types in the Middle Urals (Sverdlovsk Oblast, Russia). *Inland Water Biology*, 16(3), pp. 385–393. https://doi.org/10.1134/S1995082923030082
34. Balycheva, D., Anufriieva, E., Lee, R., Prazukin, A. and Shadrin, N., 2023. Salinity-Dependent Species Richness of Bacillariophyta in Hypersaline Environments. *Water*, 15(12), 2252. https://doi.org/10.3390/w15122252
35. Prazukin, A., Shadrin, N., Balycheva, D., Firsov, Y., Lee, R. and Anufriieva, E., 2020. *Cladophora* spp. (Chlorophyta) Modulate Environment and Create a Habitat for Microalgae in Hypersaline Waters. *European Journal of Phycology*, 56(3), 231–243. https://doi.org/10.1080/09670262.2020.1814423
36. Ács, É., Bíró, T., Boros, E., Dobosy, P., Duleba, M., Földi, A., Kiss, K.T., Levkov, Z., Orgoványi, P., Szén, O.P., Trábert, Z., Vadkerti, E. and Grigorszky, I., 2023. *Halamphora* Taxa in Hungarian Soda Pans and Shallow Soda Lakes Detected via Metabarcoding and Microscopic Analyses. *Metabarcoding and Metagenomics*, 7, e111679. https://doi.org/10.3897/mbmg.7.111679
37. Ryabushko, L.I. and Tarasov, V.G. 1989. Qualitative Composition of Diatom Algae of Microphytobenthos in Kraternaya Bight. *The Soviet Journal of Marine Biology*, 15(3), 211–215. (in Russian).

Submitted 17.02.2025; accepted after review 21.03.2025;
revised 17.09.2025; published 30.12.2025

*About the author:*
**Daria S. Balycheva**, Senior Research Associate, A.O. Kovalevsky Institute of Biology of the Southern Seas of RAS (2 Nakhimov Av., Sevastopol, 299011, Russian Federation), PhD (Biol.), **ORCID ID: 0000-0001-9955-4182**, **Scopus Author ID: 56297496300**, **ResearcherID: C-5534-2016**, **SPIN-код: 2545-0169**, *balycheva@ibss.su*

*The author has read and approved the final manuscript.*

ISSN 2413-5577, Ecological Safety of Coastal and Shelf Zones of Sea, 2025, No. 4, pp. 133–146.

Original paper

# Laboratory-Based Estimation of Photosynthetic Performance in Dominant Macroalgal Species

**E. F. Vasechkina [1]*, I. P. Naumenko [1], T. A. Filippova [1], V. G. Shaida [2]**

[1] *Marine Hydrophysical Institute of RAS, Sevastopol, Russia*
[2] *Company "EcoService-A", Moscow, Russia*
* *e-mail: vasechkina.elena@gmail.com*

**Abstract**

The photosynthetic rate of macroalgae is well described by a logistic PE-curve, characterized by species-specific parameters (maximum photosynthetic rate, dark respiration rate, initial slope of the curve), which are primarily dependent on water temperature. The study is aimed to estimate these parameters for dominant macroalgal species under experimental conditions and to analyse their seasonal dynamics. In March and September 2024, several dominant species of brown, red and green macroalgae were sampled in the coastal waters of Sevastopol. The photosynthetic rates of the selected species were determined by the amount of released oxygen. A comparison of our results with previously published data showed that the obtained photosynthetic parameters for green algae of the genus *Ulva* fall within the ranges of intrageneric variability. The influence of water temperature on the photosynthetic rate was significant, with these species exhibiting considerable seasonal variation. The daily oxygen production resulting from photosynthesis in the species *G. barbata* and *E. crinita* was found to be higher than that in species from the more saline waters of the Mediterranean Sea and the North Atlantic. The obtained data provide additional information for quantitative assessments of carbon, oxygen, and nutrient fluxes in coastal ecosystems, where benthic phytocenoses play a significant role in biogeochemical processes. The results of this study can be applied in simulation models for biomass dynamics of benthic phytocenoses in the coastal zone of the Crimean Peninsula.

**Keywords:** photosynthesis, photosynthetic parameters, dark respiration rate, marine macrophytes, bottom phytocenosis, Black Sea, Crimean coast

**Acknowledgements**: the work was performed under state assignment of MHI RAS on topic no. FNNN-2024-0016 "Studies of spatial and temporal variability of oceanological processes in the coastal, near-shore and shelf zones of the Black Sea influenced by natural and anthropogenic factors on the basis of in situ measurements and numerical modelling".

**For citation**: Vasechkina, E.F., Naumenko, I.P., Filippova, T.A. and Shaida, V.G., 2025. Laboratory-Based Estimation of Photosynthetic Performance in Dominant Macroalgal Species. *Ecological Safety of Coastal and Shelf Zones of Sea*, (4), pp. 133–146.

# Определение параметров фотосинтетической активности массовых видов макроводорослей в лабораторных условиях

**Е. Ф. Васечкина [1] *, И. П. Науменко [1], Т. А. Филиппова [1], В. Г. Шайда [2]**

[1] *Морской гидрофизический институт РАН, Севастополь, Россия*
[2] *Общество с ограниченной ответственностью «ЭкоСервис-А», Москва, Россия*
* *e-mail: vasechkina.elena@gmail.com*

**Аннотация**
Скорость фотосинтеза макроводорослей хорошо описывается логистической *PE*-кривой, которая характеризуется видоспецифичными параметрами (максимальная скорость фотосинтеза, затраты кислорода на дыхание в темноте, начальный наклон кривой), зависящими главным образом от температуры воды. Целью работы является оценка этих параметров у массовых видов макроводорослей в экспериментальных условиях и анализ их сезонной динамики. В марте и сентябре 2024 г. в акватории г. Севастополя были собраны образцы нескольких массовых видов бурых, красных и зеленых макроводорослей. Скорость фотосинтеза отобранных макрофитов определяли по количеству выделяемого кислорода. Сравнение наших результатов с опубликованными ранее данными показало, что полученные значения фотосинтетических параметров для зеленых видов *Ulva* лежат в пределах интервалов внутриродовой изменчивости. Влияние температуры воды на скорость фотосинтеза существенно, у этих видов выявлена значимая сезонная изменчивость. Установлено, что суточная продукция кислорода в результате фотосинтеза у видов *G. barbata* и *E. crinita* выше, чем у видов из более соленых вод Средиземного моря и Северной Атлантики. Полученные данные дают дополнительную информацию для количественных оценок потоков углерода, кислорода, биогенных элементов в прибрежных экосистемах, где функционирование донных фитоценозов играет большую роль в биогеохимических процессах в системе. Результаты данного исследования могут быть применены в имитационных моделях динамики биомассы донных фитоценозов в прибрежной зоне Крымского полуострова.

**Ключевые слова**: фотосинтез, фотосинтетические параметры, темновое дыхание, морские макрофиты, донный фитоценоз, Черное море, Крымское побережье

**Благодарности**: работа выполнена в рамках государственного задания ФГБУН ФИЦ МГИ по теме FNNN-2024-0016 «Исследование пространственно-временной изменчивости океанологических процессов в береговой, прибрежной и шельфовой зонах Черного моря под воздействием природных и антропогенных факторов на основе контактных измерений и математического моделирования».

**Для цитирования**: Определение параметров фотосинтетической активности массовых видов макроводорослей в лабораторных условиях / Е. Ф. Васечкина [и др.] // Экологическая безопасность прибрежной и шельфовой зон моря. 2025. № 4. С. 133–146. EDN EZUNRP.

## Introduction

One of the key components of marine coastal ecosystems is macroalgae, which play an important role in the synthesis and transformation of organic matter and in the production of dissolved oxygen by absorbing solar energy and carbon dioxide during photosynthesis.

The photosynthetic rate of algae depends on light intensity and is well described by a logistic PE-curve. The shape of the curve is determined by photosynthetic parameters, which include the maximum photosynthetic rate, dark respiration rate, and the initial slope of the curve. A significant feature of these parameters is that they are species-specific and depend on external factors, primarily water temperature. Several parameterizations of the PE-curve are known [1–5]. Approximation of PE-curves for dominant macroalgal species of the Black Sea showed that the parameterization proposed by A. Jassby and T. Platt in 1976 [4] is the most suitable for the studied macrophytes.

Studies on oxygen production and consumption by macroalgae began as early as the 1950s and continue to the present day. It has been noted that the photosynthetic activity of aquatic plants is closely linked to their morphological characteristics and the temperature of the marine environment. High intraspecific and interspecific variability of photosynthetic parameters has been recorded [6]. We have compiled an archive of literature data on photosynthetic parameters of dominant macroalgal species and seagrasses obtained under experimental conditions at different temperatures and light intensities across various geographical regions [6]. However, information on macroalgae and seagrasses of the Black Sea region is absent from the literature.

In the present study, the photosynthetic rate as a light-response function was investigated under laboratory experimental conditions for dominant marine algal species collected in the coastal waters of Sevastopol. Regional estimates of photosynthetic parameters of macroalgae and seagrasses are necessary for adequate mathematical modeling of algal biomass dynamics throughout the year depending on environmental conditions.

One of the key components of Black Sea coastal ecosystems are phytocenoses of the perennial brown alga, represented by the species *Gongolaria barbata* and *Ericaria crinita*. These species with large bushy thalli grow on hard substrates (rocks, stones) at depths from 0.5 to 20 m; the peak of their vegetative period occurs in May – June. *Scytosiphon lomentaria* is a brown algal species with a tubular thallus 1–2 mm thick. It inhabits stones, rocks, and boulders. It is a seasonal species whose vegetative peak occurs in February – March.

The green algal species *Ulva intestinalis*, *Ulva linza* and *Ulva rigida* are widely distributed in the Black Sea. The species *U. intestinalis* has a tubular or laterally compressed to plate-like narrow thallus up to 20 cm long and attaches to stones, rocks, shells and hydraulic structures. The species *U. linza* has a flat plate-like or ribbon-like thallus with smooth or curled margins. The thallus of *U. rigida*, unlike the previous two species, appears as a broad plate with ruffled margins. All species are tolerant to environments polluted with wastewater and rich in nutrients; the peak of their vegetation occurs in spring and summer [7].

The red, branched, finely structured alga *Vertebrata subulifera* grows on stones, rocks and shells both in clean and polluted areas. It can occur from the water's edge down to a depth of 20 m and often settles on other algae, using them as a substrate. The red alga *Laurencia obtusa* has a thick, bushy, amber-yellow thallus and inhabits stones in clean areas at depths of 0.5–15 m. The widely distributed seasonal brown alga *Padina pavonica*, with a fan-shaped, whitish, calcified thallus, grows on rocky substrates at depths of 0.5–5 m, preferring unpolluted sites with intense water exchange. The perennial seagrass *Nanozostera noltei*, with flat leaves, forms extensive meadows in the shallow waters of bays, lagoons, and river estuaries [7].

**Materials and methods**

Samples of macroalgae were collected in the coastal zone of Sevastopol (Fig. 1) in the areas of Victory Park and Omega beaches at depths of 0.5–1 m and near the Aquamarine Complex at depths of up to 3 m.

The seawater temperature during sample collection was 12–13 °C in March and 25–26 °C in September. Algal samples were transported to the laboratory in plastic containers with seawater, where they were rinsed in fresh seawater and cleaned of epiphytes.

The photosynthetic rate was determined by measuring changes in the amount of dissolved oxygen in a hermetically sealed glass vessel filled with seawater and containing the algal sample. One of the factors capable of inhibiting plant photosynthesis is excess oxygen [8–10]. Oxygen inhibition occurs rapidly and is reversible [8]. In addition, excess oxygen forms small bubbles on the thalli and vessel walls, resulting in underestimated measurements of dissolved oxygen in the water. Since the water taken from the sea surface for the experiments was supersaturated with oxygen, it was preliminarily deaerated with sodium sulfite:

$$2Na_2SO_3 + O_2 \rightarrow 2Na_2SO_4. \quad (1)$$

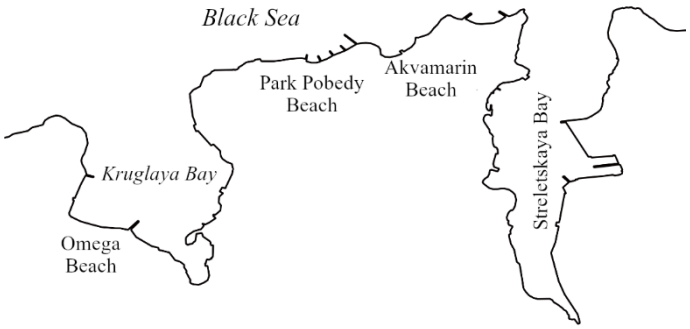


F i g . 1 . Sampling area

Seawater was supplemented with 80 and 53 mg/L of sodium sulfite in March and September, respectively, thoroughly mixed and then left for 24 hours. As a result, the initial oxygen concentrations in the experiments were 2–3 mg/L. Sodium sulfite is an oxygen scavenger that, when exceeding certain thresholds, can inhibit the growth of living organisms, including photosynthetic ones, and is used in experiments on biohydrogen production from algae [11]. In aqueous solutions, sodium sulfite fully dissociates into sodium cations and sulfite anions. Sulfite is rapidly oxidized to sulfate, with the reaction accompanied by the consumption of dissolved oxygen (formula (1)). The reaction produces sodium sulfate, which is highly soluble in water and fully dissociates.

The average sulfate concentrations in the surface layer of the Black Sea are 1445–1451 mg/L (15 mM) [12, 13]. The addition of sodium sulfite increases the sulfate concentration by 4%. Given the short-term nature of the experiments, we consider that the introduction of this additional sulfate source had no significant impact on the study objects.

Algal samples (apical plant parts 5 cm long and weighing 2–4 g wet weight) were placed in hermetically sealed 1 L glass flasks filled with deaerated seawater. Mixing in the flasks was performed using TAGLER magnetic stirrers. The water temperature in the flasks was maintained close to *in situ* values: 15 °C in March and 23 °C in September. For this purpose, the flasks were placed in a 22 L transparent glass aquarium with continuously cooled water. The water in the aquarium was stirred using aquarium aerators, and the temperature was monitored with a HANNA digital temperature thermometer for liquids.

The experiment was conducted at irradiances of 0, 44, 248 and 285 μmol photons $m^{-2} \cdot s^{-1}$. At each irradiance level, the experiment lasted 20–25 minutes, with instrument readings taken every five minutes. The vessels containing algal samples were illuminated by five 40-W LED panels with a colour temperature of 4000 K (white light). During measurements of dark respiration, the aquarium was covered with black opaque plastic. Irradiance control was performed using a TKA-LUX luxmeter. Dissolved oxygen concentrations were determined with Expert-001 liquid analysers equipped with DKTP-02 dissolved oxygen sensors with thermoelectric converters, and the photosynthetic rate $P$ ($mgO_2/(g\ DW \cdot h)$) was calculated using the formula

$$P = \frac{([O_2]_2 - [O_2]_1) \cdot V \cdot 60}{(t_2 - t_1) \cdot W_d}, \quad (2)$$

where $[O_2]_1$ and $[O_2]_2$ are the initial and final $O_2$ concentrations, respectively, mg/L; $V$ is the volume of water in the flask, L; $W_d$ is the dry weight of the algal sample, g; $t_1$ and $t_2$ are the start and end times of exposure at the given irradiance, min. Control experiments measuring oxygen concentration in seawater in the absence of algae showed no significant changes.

After completion of the experiments, excess liquid was removed from the samples, and wet weight $W_w$ was determined on VLTE-150S electronic laboratory scales, as well as volume in a 100 mL graduated cylinder. The samples were then dried at room temperature and subsequently in a drying oven at 60 °C to constant weight. For each algal sample, dry weight $W_d$ and the dry-to-wet weight ratio were determined. The obtained ratios for each algal species were averaged.

The measured photosynthetic rates $P_i(E_i)$ (formula (2)) at the irradiance levels specified above were used to construct the PE-curve of photosynthetic rate versus irradiance by the least-squares method. The parameterization proposed in [4, p. 541] was applied:

$$P(E) = (P_{\max} + R_d) \tanh\left(\frac{\alpha E}{P_{\max} + R_d}\right) - R_d, \quad (3)$$

where $P_{\max}$ is the maximum photosynthetic rate, $mgO_2/(g\ DW \cdot h)$; $R_d$ is the dark respiration rate, $mgO_2 / (g\ DW \cdot h)$; $E$ is the irradiance, μmol photons $m^{-2} \cdot s^{-1}$; $\alpha$ is the initial slope of the PE-curve, $(mgO_2/(g\ DW \cdot h)) / (\mu mol\ photons\ m^{-2} \cdot s^{-1})$.

From the fitted PE-curve, additional photosynthetic parameters can be derived: the saturation onset irradiance $E_k$, at which the photosynthetic rate reaches its maximum and the compensation irradiance $E_c$, at which respiratory oxygen consumption is exactly compensated by photosynthetic oxygen production [14].

**Results and discussion**

The dry-to-wet weight ratio $W_d / W_w$ of the studied macroalgal samples in March was below 20%. The highest recorded value was for *G. barbata* (19%) and the lowest for *U. intestinalis* (12%). Mean values for the investigated macrophyte species are given in the table. These values are lower than those we obtained earlier [14]. Differences in dry-weight ratios may be seasonal in nature [15, 16]. The $W_d / W_w$ ratios reported by other authors for algae growing in different geographical regions were close to ours: 17–18% for *U. intestinalis* [17, 18] and 18.3% for *G. barbata* [19].

Photosynthetic rates of marine plants is species-specific and strongly depends on water temperature, irradiance and salinity [6]. They differ markedly among macroalgal species and groups. They also exhibit pronounced seasonal variability (table). In March, the highest maximum photosynthetic rates $P_{\max}$ were recorded for the annual epiphytic green alga *U. intestinalis*, whereas the lowest were found in the seasonal winter brown alga *S. lomentaria*. The species *U. intestinalis* also showed the lowest respiratory costs, as well as the lowest saturation $E_k$ and compensation $E_c$ irradiances. Consequently, the growth rate of this epiphyte in March was the highest among the studied species. In September, the growth rates of *Ulva* species decreased noticeably. The species *G. barbata* and *E. crinita* exhibited nearly constant growth rates in both spring and autumn. It is noteworthy that the initial slope of the PE-curve $\alpha$, which characterizes photosynthetic efficiency at low irradiance, was higher in March than in September, while the saturation parameters were correspondingly lower. Higher dark respiration rates $R_d$ were also observed in March (Fig. 2). In our previous study [6], we identified clusters of macroalgae according to their photosynthetic performance. Notably, that in species belonging to cluster 3 (*Ulva*), which is characterized by the highest photosynthetic rates, and

Photosynthetic parameters of PE-curves of the studied macrophytes (mean) and dry to wet weight ratios $W_d / W_w$

| Species | Phylum | $P_{max}$ | $R_d$ | α | $E_k$ | $E_c$ | Number of experiments | $W_d / W_w$ |
|---|---|---|---|---|---|---|---|---|
| *March 2024, $T_{water} \approx$ 15 °C* | | | | | | | | |
| *G. barbata* | Brown | 9.94 | 4.57 | 0.230 | 63 | 20 | 5 | 0.180 |
| *S. lomentaria* | Brown | 7.28 | 3.68 | 0.175 | 59 | 21 | 2 | 0.166 |
| *U. intestinalis* | Green | 17.94 | 3.29 | 0.54 | 39 | 6 | 6 | 0.148 |
| *V. subulifera* | Red | 18.63 | 3.94 | 0.420 | 53 | 9 | 3 | 0.157 |
| *September 2024, $T_{water} \approx$ 23 °C* | | | | | | | | |
| *E. crinita* | Brown | 7.69 | 1.14 | 0.058 | 151 | 19 | 7 | 0.260 |
| *U. linza* | Green | 5.89 | 0.68 | 0.093 | 70 | 7 | 3 | 0.254 |
| *U. rigida* | Green | 7.91 | 0.82 | 0.107 | 82 | 8 | 3 | 0.259 |
| *L. obtusa* | Red | 9.52 | 1.42 | 0.070 | 156 | 20 | 2 | 0.134 |
| *P. pavonica* | Brown | 11.24 | 1.33 | 0.102 | 124 | 13 | 3 | 0.242 |
| *N. noltei* | Sea grasses | 11.83 | 1.84 | 0.070 | 192 | 26 | 2 | 0.195 |

Note: $P_{max}$ – maximum photosynthesis rate, $mgO_2$/(g DW·h); $R_d$ – dark respiration rate in the absence of light, $mgO_2$/(g DW·h); $E$ – irradiance, μmol photons $m^{-2}$ $s^{-1}$; α – initial slope of the P-E curve, ($mgO_2$ /(g DW·h)) / (μmol photons $m^{-2} \cdot s^{-1}$); $E_c$ – compensation point – value of irradiance, at which the costs of respiration are balanced by photosynthetic activity, μmol photons $m^{-2} \cdot s^{-1}$; $E_k$ – saturated irradiance – the point defined by the intersection of the initial slope of the P-E curve and the horizontal line representing the maximum photosynthetic rate, μmol photons $m^{-2} \cdot s^{-1}$.

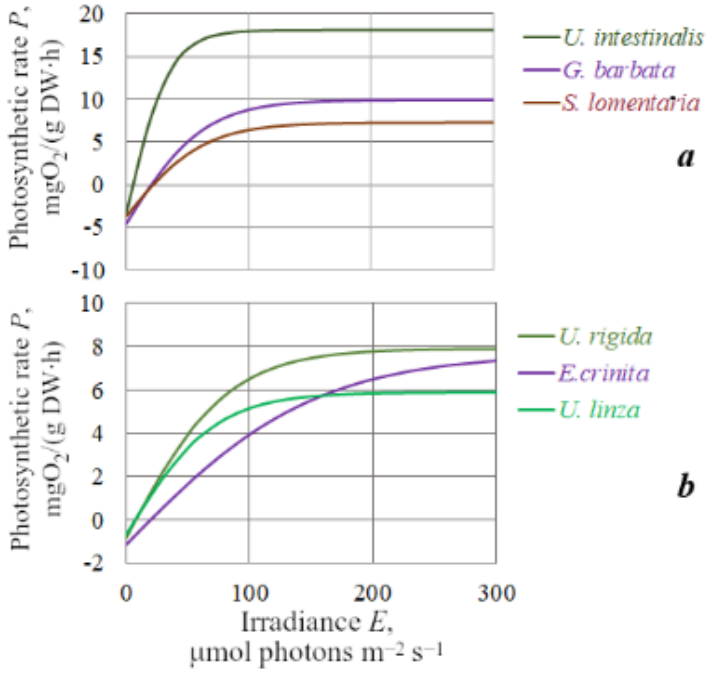


Fig. 2. PE-curves of the studied marine macrophytes at 15 °C in March (*a*) and 23 °C in September (*b*)

to cluster 2 (*Scytosiphon*), seasonal variability was recorded in our experiments. In contrast, algae of cluster 1 (*G. barbata*, *E. crinita*) exhibited nearly constant photosynthetic rates in both autumn and spring.

Further, we will analyze seasonal and intraspecific variability in two macroalgal groups for which sufficient literature data are available for comparison: the green *Ulva* species and the brown algae *G. barbata*, *E. crinita* and *S. lomentaria* (Fig. 2).

The photosynthetic parameters reported in the literature are highly heterogeneous (see Appendix A). Each geographical region has unique environmental conditions that affect physiological differences even among individuals of the same species or genus. Intraspecific variability is further compounded by temperature fluctuations, making direct comparison of our data with published values rather difficult. For example, the oxygen consumption rates in darkness that we obtained for *U. intestinalis* at 15 °C are higher than those reported by other authors. The $P_{max}$ and $R_d$ values measured in our experiments at 15 °C for *G. barbata* exceed those reported for the same species along the French coast, whereas the $E_k$ and $E_c$ parameters are similar [20].

Given the high variability of published photosynthetic parameters, daily oxygen production and consumption graphs (Fig. 3) provide a convenient way to assess interspecific differences in photosynthetic performance. These graphs were constructed using the three key photosynthetic parameters $P_{max}$, α and $R_d$. A model of daily irradiance variation (day/night = 14/10) available at a depth of 3–5 m was applied. Oxygen production during the light period and oxygen consumption during the dark period were compared using daily curves constructed from our own data (blue curves in the diagrams) and from data published by other authors (Fig. 3).

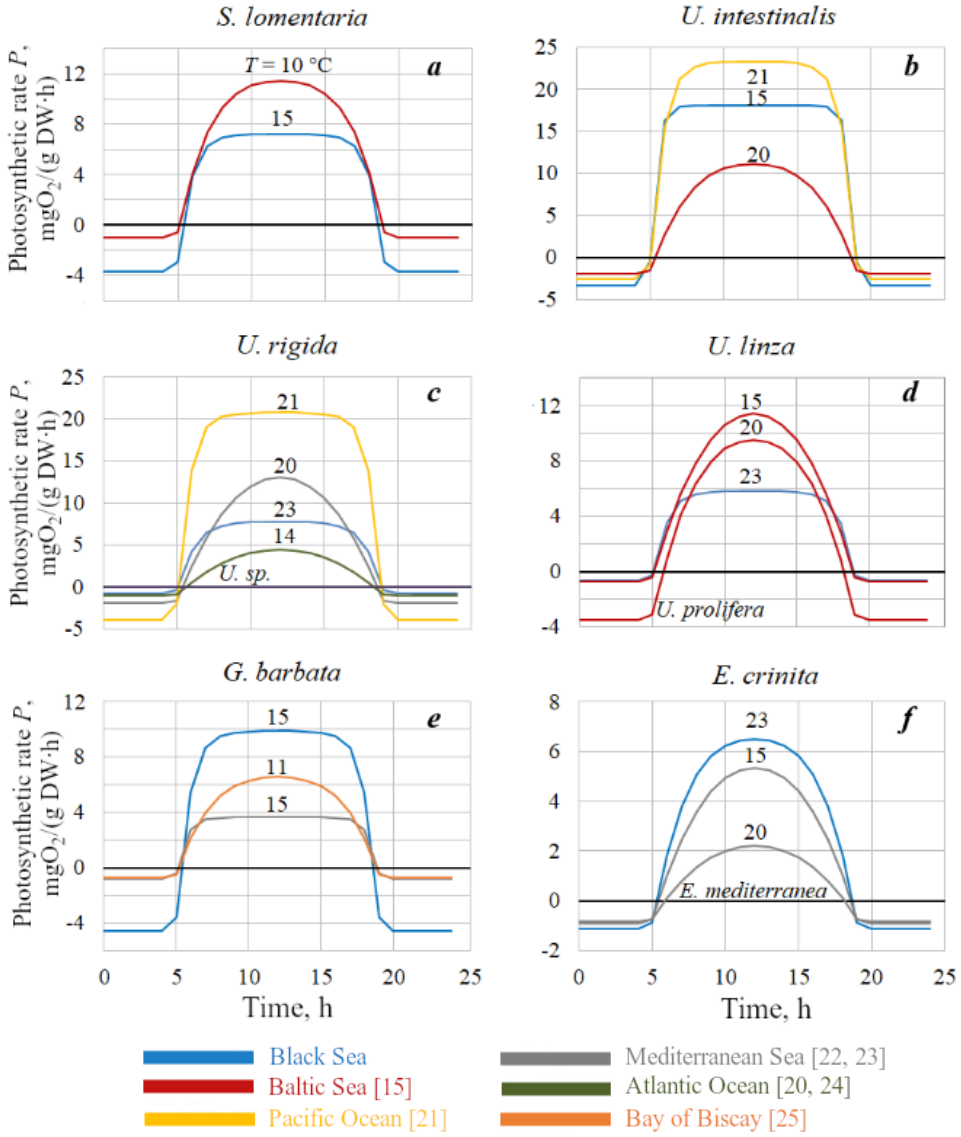


Fig. 3. Daily oxygen production by dominant species of macroalgae at different water temperatures according to literature data in comparison with experimentally obtained values

The daily oxygen production curve for the winter cold-tolerant brown alga *S. lomentaria* (Fig. 3, *a*) lies below that obtained for the same species in the Baltic Sea. However, given the 5 °C temperature difference, our data can confidently be considered consistent with the values reported in [15]. The daily production curves constructed from our results for different *Ulva* species (Fig. 3, *b*, *c*, *d*) fall within the variability corridor defined by the numerous published data on photosynthetic activity of *Ulva*; these green algae have been intensively studied since the 1980s. As with all annual macroalgae, the photosynthetic rate of *Ulva* exhibits a clearly pronounced seasonal pattern. It should be noted that the interspecific variability shown in the graphs in Fig. 3 is also influenced by seasonal fluctuations driven by water temperature. Further experiments are required to determine which *Ulva* species in the Black Sea exhibits the highest photosynthetic activity. The maximum photosynthetic rate obtained for *U. intestinalis* at 15 °C is consistent with known data indicating that the peak of vegetative growth of green algae, particularly of the genus *Ulva*, occurs in late spring and early summer [26].

Daily oxygen production by the community-forming macroalgae *G. barbata* and *E. crinita*, which occur in mass in the coastal waters of Crimea, changed only slightly when the temperature increased from 15 °C in March to 23 °C in September. Notably, compared with values reported for algae from the Mediterranean Sea and the Atlantic, these species exhibit higher photosynthetic rates, at least during the warm seasons of the year (Fig. 3, *e*, *f*).

**Conclusion**

For several dominant macrophyte species of the Sevastopol coastal zone, the photosynthetic curve parameters ($P_{max}$, $R_d$, α, $E_c$, $E_k$) were experimentally determined at water temperatures of 15 and 23 °C. In addition, the dry-matter content of the thalli was measured. Comparison of our results with published data showed that the photosynthetic parameters obtained for green algae of the genus *Ulva* fall within the ranges of intrageneric variability. The influence of water temperature on photosynthetic rate is substantial, with these species exhibiting pronounced seasonal variability.

In contrast to *Ulva* species, spring and autumn photosynthetic activity in the species *G. barbata* and *E. crinita* differed only slightly. Their daily oxygen production resulting from photosynthesis exceeds that of congeners inhabiting the more saline waters of the Mediterranean Sea and the North Atlantic.

The obtained data complement existing information and enable more accurate quantitative assessments of carbon, oxygen, and nutrient fluxes in coastal ecosystems, where benthic phytocenoses play a key role in biogeochemical processes. The regional estimates of photosynthetic parameters presented here are used in mathematical models of biomass dynamics of benthic vegetation phytocenoses.

**Appendix A**

Photosynthetic parameters of the studied macrophytes, published in the literature

| Species | *T*, °C | $P_{max}$ | $R_d$ | α | $E_k$ | $E_c$ | Location | Source |
|---|---|---|---|---|---|---|---|---|
| *E. crinita* | 15 | 9.6 | 0.9* | 0.036** | 290** | 25* | Mediterranean Sea, Algeria | [23] |
| *G. barbata* | 15 | 3.66 | 0.8 | 0.091 | 57 | 12 | Mediterranean Sea, France | [20] |
| *G. nodicaulis* | 11 | 7.8 | 0.7** | 0.054** | 156 | 13 | Bay of Biscay, Spain | [25] |
| *G. nodicaulis* | 20 | 3.648 | 0.59** | 0.018** | 242 | 33.7 | | |
| *E. mediterra-nea* | 20 | 4.15 | 0.83 | 0.018 | 288** | 51 | Mediterranean Sea, Spain | [22] |
| *S. lomentaria* | 10 | 12.96* | 1* | 0.1** | 137** | 9.8* | the Baltic | [15] |
| *Enteromorpha sp.* | 17.5 | 11.56 | 0.78 | – | – | – | North-eastern coast of New Zealand | [27] |
| *Ulva sp.* | 17.5 | 15.78 | 1.25 | – | – | – | | |
| *Ulva sp.* | 14 | 12.99 | 0.99 | 0.029 | 465 | 34.4 | Atlantic Ocean, USA | [24] |
| *U. linza* | 15 | 22.2* | 0.72* | 0.068** | 338** | 11* | the Baltic | [15] |
| *U. compressa* | 20 | 26.85 | 1.76 | 0.086 | 333** | 21 | Mediterranean Sea, Spain | [22] |
| *U. prolifera* | 20 | 14.04* | 3.51* | 0.084** | 208** | 41.7* | the Baltic | [15] |
| *U. intestinalis* | 20 | 14.4* | 1.9* | 0.09** | 183** | 21* | | |
| *U. intestinalis* | 21 | 23.4** | 2.6** | 0.42 | 56 | 6 | Pacific Ocean, USA | [21] |
| *U. rigida* | 21 | 20.8** | 3.912** | 0.416 | 50.3 | 9.4 | | |
| *U. rigida* | 20 | 26.43 | 1.95 | 0.083 | 341** | 24 | Mediterranean Sea, Spain | [22] |

Note: $P_{max}$ and $R_d$ (mg $O_2$ /(g DW·h)) are maximum photosynthesis and respiration rates; α – initial slope of the P-E curve, (mg$O_2$ (g DW·h)) / (μmol photons $m^{-2} \cdot s^{-1}$); $E_c$ – compensation point – value of irradiance, at which the costs of respiration are balanced by photosynthetic activity, μmol photons $m^{-2} \cdot s^{-1}$; $E_k$ – saturated irradiance – the point defined by the intersection of the initial slope of the P-E curve and the horizontal line representing the maximum photosynthetic rate, μmol photons $m^{-2} \cdot s^{-1}$.

* Values read off the graphs of the dependence of photosynthetic rate on irradiance.

** Values calculated from the data given in the works.

REFERENCES

1. Baly, E.C.C., 1935. The kinetics of photosynthesis. *Proceedings of the Royal Society of London. Series B, Biological Sciences*, 117(804), pp. 218–239. https://doi.org/10.1098/rspb.1935.0026
2. Steele, J.H., 1962. Environmental Control of Photosynthesis in the Sea. *Limnology and Oceanography*, 7(2), pp. 137–150. https://doi.org/10.4319/lo.1962.7.2.0137
3. Web, W.L., Newton, M. and Starr, D., 1974. Carbon Dioxide Exchange of *Alnus rubra*: A Mathematical Model. *Oecologia*, 17(4), pp. 281–291. https://doi.org/10.1007/BF00345747
4. Jassby, A.D. and Platt, T., 1976. Mathematical Formulation of the Relationship Between Photosynthesis and Light for Phytoplankton. *Limnology and Oceanography*, 21(4), pp. 540–547. https://doi.org/10.4319/lo.1976.21.4.0540
5. Aalderink, R.H. and Jovin, R., 1997. Estimation of the Photosynthesis/Irradiance (P/I) Curve Parameters from Light and Dark Bottle Experiments. *Journal of Plankton Research*, 19(11), pp. 1713–1742. https://doi.org/10.1093/plankt/19.11.1713
6. Vasechkina, E.F. and Naumenko, I.P., 2023. Variability of Photosynthetic Parameters of Macroalgae and Seagrasses Based on Laboratory Experiments. *Ecological Modelling*, 486, 110512. https://doi.org/10.1016/j.ecolmodel.2023.110512
7. Milchakova, N., 2011. *Marine Plants of the Black Sea. An Illustrated Field Guide*. Sevastopol: DigitPrint, 144 p. https://doi.org/10.21072/978-966-02-5801-3
8. Turner, J.S., Todd, M. and Brittain, E.G., 1956. The Inhibition of Photosynthesis by Oxygen. I. Comparative Physiology of the Effect. *Australian Journal of Biological Sciences*, 9(4), pp. 494–510. https://doi.org/10.1071/BI9560494
9. Downton, W.J.S., Bishop, D.G., Larkum, A.W.D. and Osmond, C.B., 1976. Oxygen Inhibition of Photosynthetic Oxygen Evolution in Marine Plants. *Australian Journal of Plant Physiology*, 3(1), pp. 73–79. https://doi.org/10.1071/pp9760073
10. Gordon, D.M. and Sand-Jensen, K., 1990. Effects of $O_2$, pH and DIC on Photosynthetic net-$O_2$ Evolution by Marine Macroalgae. *Marine Biology*, 106(3), pp. 445–451. https://doi.org/10.1007/BF01344325
11. Sudha, N.R., Varaprasad, D., Riazunnisa, K., Prasanna, V.A., Reddy, P.R. and Chandrasekhar, T., 2022. Effects of Oxygen Scavengers (Sodium Sulfite, sodium Bisulfite, Sodium Dithionite, and Sodium Metabisulfite) on Growth and Accumulation of Biomass in the Green Alga *Asterarcys quadricellulare*. *Journal of Applied Biology and Biotechnology*, 10(4), pp. 136–140. https://doi.org/10.7324/JABB.2022.100418
12. Dubinin, A.V., Rimskaya-Korsakova, M.N. and Semilova, L.S., 2022. Sulfate-Chlorinity Ratio in the Black Sea Water and its Variability over the Last 70 Years. *Physical Oceanography*, 29(5), pp. 508–523.
13. Eremeev, V.N. and Bezborodov, A.A., 1992. Hydrogen Sulphide in the Deep-Water Part of the Black Sea: Origin, Distribution, Sources and Discharge. In: MHI, 1992. *Hydrophysical and Hydrochemical Studies of the Black Sea.* Sevastopol: MHI, pp. 31–57 (in Russian).
14. Vasechkina, E.F., Rudneva, I.I., Filippova, T.A., Naumenko, I.P., Parkhomenko, A.V. and Shaida, V.G., 2023. Photosynthetic Parameters of the Seaweeds Widely Spread near the Crimean Coast. *Regional Studies in Marine Science*, 66, 103170. https://doi.org/10.1016/j.rsma.2023.103170
15. King, R.J. and Schramm, W., 1976. Photosynthetic Rates of Benthic Marine Algae in Relation to Light Intensity and Seasonal Variations. *Marine Biology*, 37(3), pp. 215–222. https://doi.org/10.1007/BF00387606

16. Harlin, M.M. and Craigie, J.S., 1978. Nitrate uptake by *Laminaria longicruris* (Phaeophyceae). *Journal of Phycology*, 14(4), pp. 464–467. https://doi.org/10.1111/j.1529-8817.1978.tb02470.x
17. Thomas, T.E. and Harrison, P.J., 1978. Rapid Ammonium Uptake and Nitrogen Interactions in Five Intertidal Seaweeds Grown Under Field Conditions. *Journal of Experimental Marine Biology and Ecology*, 107(1), pp. 1–8. https://doi.org/10.1016/0022-0981(87)90118-3
18. Villares, R. and Carballeira, A., 2004. Nutrient Limitation in Macroalgae (*Ulva* and *Enteromorpha*) from the Rías Baixas (NW Spain). *Marine Ecology*, 25(3), pp. 225–243. https://doi.org/10.1111/j.1439-0485.2004.00027.x
19. Orfanidis, S., Iveša, L., Gounaris, S., Tsioli, S., Devescovi, M. and Papathanasiou, V., 2017. *Cystoseira* Scale-Based Biometric Relationships. *Botanica Marina*, 60(3), pp. 285–295. https://doi.org/10.1515/bot-2017-0024
20. Baghdadli, D., Tremblin, G., Pellegrini, M. and Coudret, A., 1990. Effects of Environmental Parameters on Net Photosynthesis of a Free-Living Brown Seaweed, *Cystoseira barbata forma repens:* Determination of Optimal Photosynthetic Culture Conditions. *Journal of Applied Phycology*, 2(3), pp. 281–287. https://doi.org/10.1007/BF02179786
21. Arnold, K.E. and Murray, S.N., 1980. Relationships Between Irradiance and Photosynthesis for Marine Benthic Green Algae (Chlorophyta) of Differing Morphologies. *Journal of Experimental Marine Biology and Ecology*, 43(2), pp. 183–192. https://doi.org/10.1016/0022-0981(80)90025-8
22. Enriquez, S., Duarte, C.M. and Sand-Jensen, K., 1995. Patterns in the Photosynthetic Metabolism of Mediterranean Macrophytes. *Marine Ecology Progress Series*, 119, pp. 243–252. https://doi.org/10.3354/meps119243
23. Tremblin, G., Coudret, A. and Baghdadli, D., 1986. Photosynthèse Apparente et Installation Chez Deux Cystoseires Mediterranntennes: *Cystoseira stricta* et *Cystoseira crinita* (Phèophycèes, Fucales). Effets de la Lumière, de la Temperature et de la Salinitè. *Cryptogamie, Algologie*, 7(4), pp. 291–300. https://archive.org/details/biostor-261735/page/292/mode/2up
24. Rosenberg, G. and Ramus, J., 1982. Ecological Growth Strategies in the Seaweeds *Gracilaria foliifera* (Rhodophyceae) and *Ulva sp*. (Chlorophyceae): Photosynthesis and Antenna Composition. *Marine Ecology Progress Series*, 8, pp. 233–241. https://doi.org/10.3354/meps008233
25. Rico, J.M., Fernández, C., 1997. Ecology of *Sargassum muticum* on the North Coast of Spain. II. Physiological Differences Between *Sargassum muticum* and *Cystoseira nodicaulis. Botanica Marina*, 40(1–6), pp. 405–410. https://doi.org/10.1515/botm.1997.40.1-6.405
26. Gladyshev, M.I. and Gubelit, Y.I., 2019. Green Tides: New Consequences of the Eutrophication of Natural Waters (Invited Review). *Contemporary Problems of Ecology*, 12(2), pp. 109–125. http://doi.org/10.1134/S1995425519020057
27. Taylor, M.W., Taylor, R.B. and Rees, T.A.V., 1999. Allometric Evidence for the Dominant Role of Surface Cells in Ammonium Metabolism and Photosynthesis in Northeastern New Zealand Seaweeds. *Marine Ecology Progress Series*, 184, pp. 73–81. https://doi.org/10.3354/meps184073

Submitted 26.02.2025; accepted after review 05.06.2025;
revised 17.09.2025; published 30.12.2025

*About the authors:*

**Elena F. Vasechkina**, Deputy Director for Research, Methodology and Education, Head of Laboratory of Simulation Modeling of Coastal Marine Ecosystem Dynamics of Department of Computational Technologies and Mathematical Modeling, Marine Hydrophysical Institute of RAS (2 Kapitanskaya St., Sevastopol, 299011, Russian Federation), Dsc (Geogr.), **ORCID ID: 0000-0001-7007-9496, Scopus Author ID: 6507481336, ResearcherID: P-2178-2017,** *vasechkina.elena@gmail.com*

**Inga P. Naumenko**, Research Associate, Marine Hydrophysical Institute of RAS (2 Kapitanskaya St., Sevastopol, 299011, Russian Federation), PhD (Phys.-Math.), **ORCID ID: 0000-0002-0182-4074, Scopus Author ID: 57215354221, ResearcherID: U-1807-2018,** *ingaingatm@gmail.com*

**Tatiana A. Filippova**, Junior Research Associate, Marine Hydrophysical Institute of RAS (2 Kapitanskaya St., Sevastopol, 299011, Russian Federation), **ORCID ID: 0000-0001-5762-5894, Scopus Author ID: 56190548500, ResearcherID: AAO-5512-2020**, *deryabina1993@yandex.ru*

**Valentin G. Shaida**, Researcher Engineer, Company "EcoService-A" (17A Verkhnyaya Krasnoselskaya Str., Bldg. 1Б, Of. 8, Moscow, 107140, Russian Federation), *svg1841@mail.ru*

*Contribution of the authors:*

**Elena F. Vasechkina** – study task statement, sampling and conducting laboratory experiments, processing and analysis of the results, article text preparation

**Inga P. Naumenko** – sampling and conducting laboratory experiments, processing and analysis of the results, literature data preparation, article text and graphic materials preparation

**Tatiana A. Filippova** – sampling and conducting laboratory experiments, article text preparation

**Valentin G. Shaida** – conducting laboratory experiments, preparation and calibration of experiment equipment, article text preparation

*All the authors have read and approved the final manuscript.*

ISSN 2413-5577, Ecological Safety of Coastal and Shelf Zones of Sea, 2025, No. 4, pp. 147–156.

Original paper

# Density Dynamics of Mussel Larvae *Mytilus galloprovincialis* Lamarck, 1819 and Hydrological and Hydrochemical Parameters on a Marine Farm in the Waters of Sevastopol (the Black Sea)

**D. S. Borisova, E. V. Lisitskaya *, V. I. Ryabushko**

*A.O. Kovalevsky Institute of Biology of the Southern Seas of RAS, Sevastopol, Russia*
* *e-mail: e.lisitskaya@gmail.com*

**Abstract**
In 2023, a comprehensive study was performed near the mussel and oyster farm in the outer roadstead of Sevastopol to monitor the hydrological, hydrochemical and hydrobiological characteristics of seawater. The study aims to investigate the seasonal dynamics of hydrological and hydrochemical parameters of seawater and the density of *Mytilus galloprovincialis* Lamarck, 1819 mussel larvae in the plankton. Meroplankton samples were collected monthly from the 0–10 m layer using a Juday net. The live material was processed by counting pelagic larvae of benthic invertebrates in a Bogorov chamber under MBS-9 and Micmed-5 light microscopes. At the same time, water samples were taken in the surface water layer to determine the temperature, salinity, dissolved oxygen concentration, BOD5, permanganate index in an alkaline medium, concentrations of nitrites, nitrates, phosphates and ammonium. In 2023, the surface water temperature was minimum in February (8.1 °C) and maximum in August (26.5 °C). The water salinity was 17.70–18.50‰ with an average value of 18.23‰. The oxygen saturation of the waters varied from 93 to 126.6%, and hypoxia was not observed throughout the year. During the study period, the maximum density of mussel larvae (82 ind.·m$^{-3}$) was recorded in March at a water temperature of 9°C, whereas the autumn peak was not observed. The results of the monitoring showed moderate correlation (0.51) between water temperature and the number of bivalve larvae in the plankton. The effect of nutrients on the density of *Mytilus galloprovincialis* larvae was not established. The results confirm that the conditions in the farm's waters are favourable for shellfish cultivation and underscore the need for continued monitoring.

**Keywords**: mariculture, nutrients, meroplankton, Bivalvia, Black Sea

**Acknowledgments**: We thank S. V. Shchurov for his help in collecting the material. This work was carried out under IBSS state research assignment "Comprehensive study of the functioning mechanisms of marine biotechnological complexes with the aim of obtaining bioactive substances from hydrobionts" (no. 124022400152-1).

**For citation**: Borisova, D.S., Lisitskaya, E.V. and Ryabushko, V.I., 2025. Density Dynamics of Mussel Larvae *Mytilus galloprovincialis* Lamarck, 1819 and Hydrological and Hydrochemical Parameters on a Marine Farm in the Waters of Sevastopol (the Black Sea). *Ecological Safety of Coastal and Shelf Zones of Se*a, (4), pp. 147–156.

# Динамика плотности личинок мидии *Mytilus galloprovincialis* Lamarck, 1819 и гидролого-гидрохимических показателей на морской ферме в акватории Севастополя (Черное море)

**Д. С. Борисова, Е. В. Лисицкая *, В. И. Рябушко**

*ФГБУН ФИЦ «Институт биологии южных морей им. А. О. Ковалевского РАН», Севастополь, Россия*

* *e-mail: e.lisitskaya@gmail.com*

**Аннотация**

Комплексный мониторинг гидрологических, гидрохимических и гидробиологических показателей был проведен в 2023 г. в акватории мидийно-устричной фермы, расположенной на внешнем рейде г. Севастополя. Цель работы – изучение сезонной динамики гидролого-гидрохимических показателей морской воды и плотности личинок мидии *Mytilus galloprovincialis* Lamarck, 1819 в планктоне. Пробы мезопланктона отбирали ежемесячно в слое 0–10 м сетью Джеди. Материал обрабатывали в живом виде путем тотального подсчета пелагических личинок донных беспозвоночных в камере Богорова под световыми микроскопами МБС-9 и «Микмед-5». Одновременно отбирали пробы воды в поверхностном слое для определения температуры, солености, содержания растворенного кислорода, биохимического потребления кислорода за пять суток, перманганатной окисляемости в щелочной среде, концентрации нитритов, нитратов, фосфатов, аммония. В 2023 г. температура воды на поверхности была минимальной в феврале (8.1 °C) и максимальной – в августе (26.5 °C). Соленость воды составляла 17.70–18.50 ‰ при среднем значении 18.23 ‰. Насыщаемость вод кислородом изменялась от 93 до 126.6 %, гипоксию в течение всего года не наблюдали. В 2023 г. максимальная плотность личинок мидий (82 экз.·м$^{-3}$) зарегистрирована в марте при температуре воды 9 °C, осенний пик не отмечен. Результаты комплексных исследований показали умеренную корреляцию (0.51) между температурой воды и количеством личинок двустворчатых моллюсков в планктоне. Прямого влияния биогенных элементов на плотность личинок мидии *Mytilus galloprovincialis* не установлено. Результаты подтверждают, что условия в акватории фермы благоприятны для выращивания моллюсков и подчеркивают необходимость продолжения мониторинга.

**Ключевые слова**: марикультура, биогенные элементы, мезопланктон, Bivalvia, Черное море

**Благодарности**: выражаем благодарность научному сотруднику ФИЦ ИнБЮМ С. В. Щурову за помощь в сборе материала. Работа выполнена в рамках государственного задания ФИЦ ИнБЮМ по теме «Комплексное исследование механизмов функционирования морских биотехнологических комплексов с целью получения биологически активных веществ из гидробионтов» (№ гос. регистрации 124022400152-1).

**Для цитирования**: *Борисова Д. С., Лисицкая Е. В., Рябушко В. И.* Динамика плотности личинок мидии *Mytilus galloprovincialis* Lamarck, 1819 и гидролого-гидрохимических показателей на морской ферме в акватории Севастополя (Черное море) // Экологическая безопасность прибрежной и шельфовой зон моря. 2025. № 4. С. 147–156. EDN QEZZHL.

## Introduction

Artificial reproduction of aquatic biological resources (aquaculture) provides food for millions of people worldwide [1]. To ensure the sustainable development of aquaculture, it is important to assess the consequences of environmental changes. In order to reduce the risk of shellfish mortality on farms and obtain high yields, it is necessary to comprehensively study the factors affecting the functioning of benthic and planktonic communities [1, 2]. Currently, mariculture of bivalves is intensively developing in the coastal areas of Crimea and the Caucasus. One of the main cultivated species is mussel *Mytilus galloprovincialis* Lamarck, 1819. The biotechnology of mussel cultivation in the Black Sea is based on the natural settlement of pelagic larvae onto artificial substrates. The foundation of the future harvest has already been established at the initial stage, during spat collection [3], which requires taking into account material and surface quality of collectors, depth of their immersion, timing of their placement in the sea, water temperature and turbulence to be successful.

Concentration of mussel larvae in the plankton at the veliconcha stage ("with an eye spot") is one of the main factors influencing the intensity of shellfish settlement on collectors. Seasonal and interannual variations in many abiotic and biotic factors, as well as food availability, affect shellfish spawning timing and larval density dynamics [3, 4]. Thus, commercial shellfish cultivation is impossible without monitoring water quality and state of biota in the waters of marine farms. Comprehensive environmental monitoring enables tracking seasonal dynamics of mussel larvae density as well as hydrological and hydrochemical parameters [5–7].

The present study aims to investigate the seasonal dynamics of the density of *Mytilus galloprovincialis* mussel larvae and to analyse its relationship with hydrological and hydrochemical parameters in the waters of a marine farm cultivating bivalves.

## Material and methods

Comprehensive studies were carried out monthly throughout 2023 in the waters of a mussel and oyster farm located in the outer roadstead of Sevastopol, between Karantinnaya Bay and the south pier (Fig. 1). The 4-hectare farm is located at depths of 10–16 m. Meroplankton samples were collected 1–2 times per month on average in the 10–0 m layer using a Juday net. A total of 69 samples were collected. The live material was processed through a complete count of pelagic larvae of benthic invertebrates using a Bogorov chamber under MBS-9 and Micmed-5 light microscopes [5, 6, 8]. Mussel larvae and total benthic invertebrate larvae densities

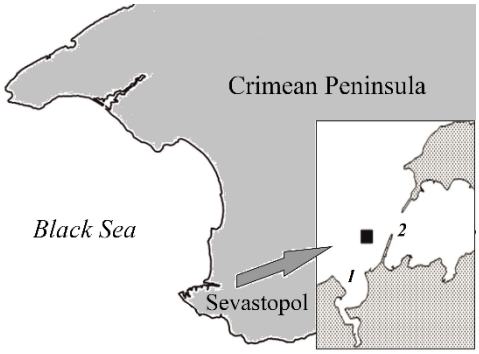


F i g . 1 . South-western region of the Crimean peninsula. The inset shows the western part of Sevastopol Bay: *1* – Karantinnaya Bay, *2* – south pier. The research area is marked with a black rectangle

were counted separately. Literature data [1)] were used to identify shellfish larvae [9].

Simultaneously, water samples were taken in the surface layer to determine salinity, temperature, dissolved oxygen concentration, biochemical oxygen demand over five days (BOD5), permanganate index in an alkaline medium as well as concentrations of ammonium, nitrites, nitrates, phosphates and silicon using standard techniques [2), 3)]. Dissolved oxygen content was determined by the Winkler method, and nutrients were measured photometrically. Phosphates were measured using the Murphy–Riley method, nitrites using the Bendschneider–Robinson method (with a "single" colour reagent), nitrates by reduction of nitrates to nitrites using copper-coated cadmium, ammonium nitrogen using the Grasshoff-Johansen method and silicon using the Korolev method. A total of 475 hydrological and hydrochemical analyses were performed.

## Results and discussion

*Hydrological and hydrochemical characteristics*

In 2023, new data on the hydrological and hydrochemical characteristics of seawater in the mussel and oyster farm waters were obtained (Table 1). Surface water temperature ranged from a minimum in February (8.1 °C) to a maximum in August (26.5 °C). Dissolved oxygen concentration varied from 7.51 mg/L in August to 10.42 mg/L in June and oxygen saturation of the water ranged from 93 to 126.6%. Hypoxia was not recorded throughout the year. High oxygen concentration in the farm waters in March and April coincided with the spring phytoplankton bloom [10].

---

[1)] Zakhvatkina, K.A., 1972. [Larvae of Bivalvia]. In: V. A. Vodyanitskiy, 1972. [*Field Guide for the Black Sea and the Sea of Azov*]. Kiev: Naukova Dumka. Vol. 3, pp. 250–270 (in Russian).

[2)] Sapozhnikov, V.V., 1988. [*Methods for Hydrochemical Studies of Main Nutrients*]. Moscow: VNIRO, 119 p. (in Russian).

[3)] *On the Approval of Water Quality Standards for Water Bodies of Fishery Importance, Including Standards for Maximum Permissible Concentrations of Harmful Substances in the Waters of Water Bodies of Fishery Importance*: Order of the Federal Agency for Fisheries (Rosrybolovstvo) No. 20 of January 18, 2010 (in Russian).

Table 1. Thermohaline and hydrochemical parameters in the surface layer of the water area of the mussel and oyster farm in 2023

| Month | *T*, °C | *S*, ‰ | $O_2$ | | Content, μg/L | | | | | Permanganate index, mgO/L |
|---|---|---|---|---|---|---|---|---|---|---|
| | | | mg/L | % | $NO_2^-$ | $NO_3^-$ | $NH_4^+$ | $PO_4^{3-}$ | Si | |
| January | 9.5 | 18.5 | 10.14 | 99.2 | 2.9 | 16.1 | 5.9 | 4.2 | 83.8 | 3.62 |
| February | 8.1 | 18.5 | 9.71 | 93.0 | 2.2 | 21.5 | 3.1 | 7.0 | 43.5 | 3.19 |
| March | 9.0 | 18.3 | 10.14 | 98.3 | 0.8 | 0.4 | 8.7 | 2.4 | 34.1 | 2.64 |
| April | 11.8 | 18.3 | 10.28 | 107.2 | 0.9 | 16.6 | 9.4 | 2.7 | 76.2 | 3.61 |
| May | 15.2 | 18.2 | 9.71 | 107.5 | 1.0 | 7.7 | 7.0 | 3.0 | 85.6 | 3.62 |
| June | 19.6 | 17.7 | 10.42 | 126.6 | 1.1 | 42.7 | 24.0 | 2.1 | 174.4 | 4.43 |
| July | 24.0 | 18.2 | 8.71 | 103.7 | 1.4 | 56.0 | 31.0 | 6.4 | 158.3 | 4.93 |
| August | 26.5 | 17.7 | 7.51 | 101.2 | 0.5 | 22.6 | 10.5 | 3.8 | 35.1 | 4.13 |
| September | 24.2 | 17.7 | 8.01 | 105.9 | 2.4 | 219.8 | 4.7 | 1.3 | 89.4 | 5.97 |
| October | 18.2 | 18.5 | 9.31 | 110.4 | 0.4 | 4.2 | 6.8 | 1.3 | 60.9 | 2.77 |
| November | 16.3 | 18.4 | 8.45 | 96.53 | 2.2 | 8.1 | 60.9 | 4.4 | 87.4 | 3.01 |
| December | 12.1 | 18.4 | 9.34 | 97.57 | 3.0 | 87.9 | 20.5 | 6.3 | 160.3 | 7.86 |

The water salinity throughout the year ranged from 17.70 to 18.50‰. The decrease in salinity observed in summer was likely caused by the influence of municipal wastewater due to increased anthropogenic load.

Concentrations of mineral nitrogen forms in the water were low. Nitrite content varied from 0.4 μg/L in October to 3.0 μg/L in December, and nitrate content ranged from 0.4 μg/L in March to 219.8 μg/L in September. The reduced nitrate concentrations in March were apparently due to their consumption during the spring phytoplankton vegetation [11]. Elevated nitrate concentrations during the summer were caused by seasonal intensification of anthropogenic load on the waters [4].

Ammonium nitrogen concentration ranged from 3.1 µg/L in February to 60.9 µg/L in November, which characterizes the studied waters as unpolluted. Mineral phosphorus content ranged from 1.3 to 7.0 µg/L. Maximum permissible concentrations (MPC) of nutrients in water are as follows: $NO_2^-$ – 20 µg/L, $NO_3^-$ – 9000 µg/L, $NH_4^+$ – 390 µg/L, permanganate index shows 4.0 mgO/L. All the indicated nutrient concentrations were significantly below the MPC (Table 1). Exceedances of the permanganate index standard were recorded during the summer and, unexpectedly, in December. Thus, all the thermohaline and hydrochemical parameters of seawater presented in the table were typical for the area and close to long-term seasonal average values [4].

*Meroplankton*

Pelagic larvae of benthic invertebrates constitute meroplankton, which is a temporary component of zooplankton. In the waters of the marine farm, larvae of bivalves (Bivalvia) are one of the permanent components of meroplankton. These larvae are present in the plankton year-round though their species composition and abundance vary seasonally. During the hydrological winter, larvae of bivalves accounted for 25 to 69% of the total meroplankton density. When the water temperature reached 15.2 °C, the density of these larvae did not exceed 5 ind.·m$^{-3}$ and they accounted for 1% of the total meroplankton only. In the summer–autumn period, the proportion of Bivalvia larvae was 20–30% of the total meroplankton, reaching 80% only in September at a water temperature of 24.2 °C. The most common bivalves in the plankton belong to the family Mytilidae, which includes the mussel *M. galloprovincialis*. Since this mussel is one of the main species cultivated on the marine farm, we investigated the density dynamics of its pelagic larvae in relation to season and water temperature (Fig. 2). Mussel larvae dominated the plankton from autumn to spring and were practically absent in summer.

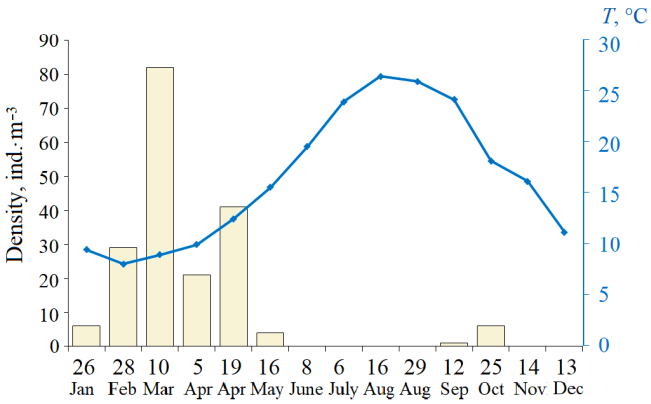


Fig. 2. Dynamics of the density of *Mytilus galloprovincialis* mussel larvae depending on the water temperature

During the winter, the abundance of mussel larvae did not exceed 29 ind.·m$^{-3}$; all of them were at the veliconcha stage ("with an eye spot"). Since the eye spot in veliconchas appears only on the 30th day [9] and that they remain in the plankton for a long time, it is reasonable to assume that these were the autumn generation larvae. The maximum density of mussel larvae (82 ind.·m$^{-3}$) was recorded in March at a water temperature of 9 °C. It was during this period that the minimum content of nitrites and nitrates was noted (Table 1). In terms of hydrological characteristics, March can be attributed to the winter season. At the veliconcha stage, the larval density was 15 ind.·m$^{-3}$, while at the later veliconcha stage "with eye spot" it reached 67 ind.·m$^{-3}$. In April, when the water temperature reached 11.8°C, the larvae density did not exceed 41 ind.·m$^{-3}$, and in May, at a water temperature of 15.2°C, it was only 4 ind.·m$^{-3}$. During the summer months, *M. galloprovincialis* larvae were not found in the plankton. The autumn peak in mussel larval abundance was not recorded, with a maximum of 6 ind.·m$^{-3}$.

The density of mussel larvae varies by season and year. Thus, in January 2014, the density of veliconchas reached 100 ind.·m$^{-3}$ at a water temperature of 8.9 °C. An autumn peak in larval abundance was recorded at the end of September 2016 (more than 500 ind.·m$^{-3}$) [8]. However, our results in 2023 align well with long-term research data, which show that the abundance of mussel larvae in the coastal waters of Crimea is on average higher in spring than in autumn, with the maximum density typically occurring in April [12]. Changes in water hydrological and hydrochemical conditions, as well as the state of the food base, can affect larval density in the plankton significantly. Thus, monitoring the state of the ecosystem and trends in its variability is necessary for the marine farm to function optimally [5, 7].

To identify the relationship between hydrological and hydrochemical parameters and the abundance of Bivalvia larvae at the mussel and oyster farm, we calculated the Pearson's pairwise correlation coefficient (Table 2). The results show that water temperature influenced the density of bivalves larvae to a certain extent (correlation coefficient 0.51). Water temperature is known to determine the timing of shellfish reproduction and consequently the appearance of their larvae in the plankton [3, 9]. In the waters of the marine farm, an increase in water temperature was recorded from June to August (Table 1). At these temperatures, *M. galloprovincialis* mussels do not reproduce [9], which explains the absence of their larvae in the plankton.

Significant negative correlation coefficients were found for the abiotic parameters of water temperature and salinity (−0.77), as well as for dissolved oxygen content (−0.73). These results reflect an inverse statistical relationship. As temperature rises, the concentration of dissolved oxygen in water typically decreases. The relationship between water temperature and salinity is a rather complex process influenced by numerous factors. In 2023, in the waters of the marine farm, the minimum salinity values (less than 17.7‰) were recorded in June, August and September (Table 1). According to literature data, salinity values in the summer period were also lower, which was explained by the inflow of less saline waters from the north-western part of the Black Sea, as well as increased runoff from local rivers due to higher precipitation [7]. The variability range of thermohaline parameters

T a b l e 2 . Pearson's pairwise correlation coefficient matrix

| Parameter | *T*, °C | *S*, ‰ | $O_2$, mg/L | Content, µg/L | | | | Bivalvia, ind.·m$^{-3}$ | Permanganate index, mgO/L |
|---|---|---|---|---|---|---|---|---|---|
| | | | | $NO_2^-$ | $NO_3^-$ | $PO_4^{3-}$ | Si | | |
| *T*, °C | | −0.77 | −0.73 | −0.31 | 0.46 | −0.28 | 0.15 | 0.51 | 0.25 |
| *S*, ‰ | −0.77 | | 0.39 | 0.30 | −0.45 | −0.45 | −0.13 | −0.51 | −0.24 |
| $O_2$, mg/L | −0.73 | 0.39 | | −0.03 | −0.43 | −0.07 | 0.15 | −0.61 | −0.61 |
| $NO_2^-$, µg/L | −0.31 | 0.30 | −0.03 | | 0.44 | 0.18 | 0.32 | −0.42 | 0.52 |
| $NO_3^-$, µg/L | 0.46 | −0.45 | −0.45 | 0.44 | | −0.29 | −0.29 | −0.07 | 0.71 |
| $PO_4^{3-}$, µg/L | −0.28 | 0.65 | −0.07 | 0.18 | −0.29 | | 0.06 | 0 | 0.04 |
| Si, µg/L | 0.15 | −0.13 | 0.15 | 0.32 | −0.29 | 0.06 | | −0.29 | 0.65 |
| Bivalvia, ind.·m$^{-3}$ | 0.51 | −0.51 | −0.61 | −0.42 | −0.07 | 0 | −0.29 | | 0 |
| Permanganate index, mgO/L | 0.25 | −0.24 | −0.61 | 0.52 | 0.71 | 0.04 | 0.65 | 0 | |

in the waters of the marine farm was optimal for bivalves cultivation for most of the year [4, 7], which is also confirmed by our studies. High correlation between permanganate index and nitrate content (0.71) can probably be explained by anthropogenic influence: the higher the pollution of waters (e. g., from stormwater runoff or emergency discharge of municipal wastewater), the higher the nitrate content and oxidizability. According to the 2023 data, no direct relationship was found between the shellfish larvae density and the content of nutrients; Pearson's correlation coefficients did not exceed −0.42 (Table 2). The minimum nitrate content recorded in March (Table 1) can limit the growth of microalgae, which serve as the food source for mussels, during the spring.

## Conclusion

The obtained data show that the meroplankton structure in the mussel and oyster farm waters changed significantly throughout the year. In winter, Bivalvia larvae accounted for up to 70% of the total meroplankton, while in summer and autumn, their share reached up to 30%. Larvae *Mytilus galloprovincialis* dominated during the winter and spring. The maximum density of mussel larvae was recorded in March (82 ind.·m$^{-3}$), with no autumn peak observed. We analyzed the relationship between the density of mussel larvae *Mytilus galloprovincialis* and the hydrological and hydrochemical parameters in the waters of the marine farm. A moderate positive correlation (0.51) was found between water temperature and the number of larvae in the plankton. Based on the 2023 research results, no direct influence of nutrients on the density of larvae *Mytilus galloprovincialis* was revealed. These results confirm the optimal location for the mussel and oyster farm, since nutrient concentrations never exceeded the maximum permissible concentrations (MPC) during the study period. The minimum recorded nitrate content in March is not directly related to the density of mussel larvae. Because hydrological, hydrochemical and hydrobiological conditions in the waters of the marine farm can vary by season and year, comprehensive environmental monitoring of shellfish cultivation areas is necessary.

REFERENCES


1. Reverter, M., Sarter, S., Caruso, D., Avarre, J.-C., Combe, M., Pepey, E., Pouyaud, L., Vega-Heredía, S., de Verdal, H. and Gozlan, R.E., 2020. Aquaculture at the Crossroads of Global Warming and Antimicrobial Resistance. *Nature Communications*, 11, 1870. https://doi.org/10.1038/s41467-020-15735-6
2. Suplicy, F.M., 2020. A Review of the Multiple Benefits of Mussel Farming. *Reviews in Aquaculture*, 12(1), pp. 204–223. https://doi.org/10.1111/raq.12313
3. Holodov, V.I., Pirkova, A.V. and Ladygina, L.V., 2017. *Cultivation of Mussels and Oysters in the Black Sea*. Voronezh: OOO "IZDAT-PRINT", 508 p. (in Russian).
4. Kapranov, S.V., Kovrigina, N.P., Troshchenko, O.A. and Rodionova, N. Yu., 2020. Long-Term Variations of Thermohaline and Hydrochemical Characteristics in the Mussel Farm Area in the Coastal Waters off Sevastopol (Black Sea) in 2001–2018. *Continental Shelf Research*, 206, 104185. https://doi.org/10.1016/j.csr.2020.104185
5. Ryabushko, V.I., Shchurov, S.V., Kovrigina, N.P., Lisitskaya, E.V. and Pospelova, N.V., 2019. A Comprehensive Environmental Study of Coastal Area of Western Crimea as Justification of Selection of Marine Farming Sites (Black Sea). *Ecological Safety of Coastal and Shelf Zones of Sea*, (2), pp. 67–77. https://doi.org/10.22449/2413-5577-2019-2-67-77 (in Russian).
6. Ryabushko, V.I., Shchurov, S.V., Kovrigina, N.P., Lisitskaya, E.V. and Pospelova, N.V., 2020. Comprehensive Research of the Environmental Status of Coastal Waters of Sevastopol (Western Crimea, Black Sea). *Ecological Safety of Coastal and Shelf Zones of Sea*, (1), pp. 104–119. https://doi.org/10.22449/2413-5577-2020-1-104-119 (in Russian).
7. Troshchenko, O.A., Subbotin, A.A. and Eremin, I.Yu., 2019. Variability of Main Limiting Environmental Factors in the Process of Bivalve Mollusk Cultivation at the Mussel Farm in Sevastopol. *Scientific Notes of V.I. Vernadsky Crimean Federal University. Geography. Geology*, 5(2), pp. 308–321 (in Russian).

8. Lisitskaya, E.V., 2017. Taxonomic Composition and Seasonal Dynamics of Meroplankton in the Area of Mussel-Oyster Farm (Sevastopol, Black Sea). *Marine Biological Journal*, 2(4), pp. 38–49. https://doi.org/10.21072/mbj.2017.02.4.04
9. Pirkova, A.V. and Ladygina, L.V., 2024. Morphometric Features of Larvae of the Mussel *Mytilus galloprovincialis* (Lamarck, 1819) (Bivalvia: Mytilidae) in Ontogenesis. *Ruthenica, Russian Malacological Journal*, 34(3), pp. 127–138. https://doi.org/10.35885/ruthenica.2024.34(3).4 (in Russian).
10. Stelmakh, L.V., 2024. *Patterns of Phytoplankton Growth Rate and Its Consumption by Microzooplankton in the Black Sea*. Simferopol: IT ARIAL, 194 p. (in Russian).
11. Stelmakh, L.V., Mansurova, I.M., Farber, A.A., Kovaleva, I.V. and Borisova, D.S., 2024. Structural and Functional Parameters of the Black Sea Phytoplankton During the Summer Bloom of the Coccolithophore *Emiliania huxleyi*. *Regional Studies in Marine Science*, 76, 103594. https://doi.org/10.1016/j.rsma.2024.103594
12. Kazankova, I.I., 2014. Peculiarities of Seasonal Dynamics of *Mytilus Galloprovincialis* Larvae Numbers in the Coastal Zone of the Crimea (based on long-term data). *Hydrobiological Journal*, 50(3), pp. 13–20. https://doi.org/10.1615/HydrobJ.v50.i3.20

Submitted 05.03.2025; accepted after review 11.08.2025;
revised 17.09.2025; published 30.12.2025

*About the authors:*

**Diana S. Borisova,** Postgraduate Student, A.O. Kovalevsky Institute of Biology of the Southern Seas of RAS (2 Nakhimov Av., Sevastopol, 299011, Russian Federation), **Scopus AuthorID: 59141486300**, *borisova_ds@ibss.su*

**Elena V**. **Lisitskaya,** Senior Researcher Associate, A.O. Kovalevsky Institute of Biology of the Southern Seas of RAS (2 Nakhimov Av., Sevastopol, 299011, Russian Federation), PhD (Biol.), **ORCID ID: 0000-0002-8219-4616**, **Scopus AuthorID: 57211271270**, **ResearcherID: T-1970-2017**, *e.lisitskaya@gmail.com*

**Vitaly I. Ryabushko,** Chief Research Associate, A.O. Kovalevsky Institute of Biology of the Southern Seas of RAS (2 Nakhimov Av., Sevastopol, 299011, Russian Federation), DSc (Biol.), **ORCID ID: 0000-0001-5052-2024**, **Scopus AuthorID**: **7801673501**, **ResearcherID: H-4163-2014**, *rabushko2006@yandex.ru*

*Contribution of the authors:*

**Diana S. Borisova** – collection and processing of the material, carrying out hydrochemical analyses, preparation of the graphic materials

**Elena V. Lisitskaya** – processing of meroplankton samples, analysis of the meroplankton composition and abundance, formation of the article.

**Vitaly I. Ryabushko** – setting the research task, editing the manuscript.

*All the authors have read and approved the final manuscript.*